Modelling and Evaluation of Laminated Windings

Direct Cooling

Rasmus Kjellstrand
Ville Akujärvi

Division of Industrial Electrical Engineering and Automation
Faculty of Engineering, Lund University

ABSTRACT

Electrical machines in electrical vehicles are sometimes put under a lot of stress when for example climbing an uphill road. In order for the machine to cope with the heat generation that comes of running extended periods of time near or at peak power one needs a highly developed cooling system. At the division of Industrial Electrical Engineering and Automation (IEA), located at Lunds Tekniska Högskola (LTH), a new and innovative winding design is developed which make cooling the machine more efficient. The winding consists of a laminated sheet which is rolled in a spiral. There is a small space between each winding turn making it possible for an air stream to flow through cooling the conductive sheets.

The cooling capabilities of such design are evaluated throughout this thesis. Measurements are performed on two prototype winding built at IEA. The measurement rig are built solely for this purpose mainly in order to maintain the right measurement, a great deal of time during the thesis is put on perfecting the rig.

Beside measurements are numerical models of the winding built in Comsol Multiphysics, both in 2 and 3 dimensions. Besides numerical modeling is an analytical model built with help of Matlab. The analytical model is used, among else, to simulate transient conditions and drive cycle analysis of an electrical machine suited for a bus.

Results from simulations and measurement show that the laminated winding is able to cope with high amounts current without harm due to the effective cooling. Simulations show an ability to use current densities in the winding stretching towards 30 A/mm^2 and still are able to keep tolerable temperatures. Results also point out weaknesses in the winding construction in form of sensitivity to winding geometries of certain type as well as unevenly spaced winding turns. Ways to improve the cooling performance of the winding by altering the geometry and improving the construction process are discussed in this thesis.

The electrical machines used today are often oversized in order to thermally handle the periods of excessive power need. The effectiveness of such a machine is best during these short stretches of high power output even if they nominally are driven at a much lower power where the effectiveness is worse. The laminated winding design enables the use of smaller machines with peak efficiency at nominal drive that still are able to cope the periods of extreme power need due to the effective cooling.

ACKNOWLEDGEMENTS

CONTENTS

1. INTRODUCTION

1.1 BACKGROUND

Traditionally there are two types of designs for cooling an electric motor: Totally Enclosed, Fan Cooled (short TEFC) and Open Drip Proof (short ODP).

The TEFC is, as the name reveals, totally enclosed from the outer environment. The cooling of this type of machine is by fans located on the outside of the enclosure. The fans blow air through ducts on the enclosure, which serves as a heat sink. This method protects the inside, i.e. the winding and mechanical parts, from the elements and pollutions, such as dust and other particles. The heat generated inside, such as conductor losses and core losses, have to travel through the motor enclosure before it's blown away by the fans. This isn't an imminent response to the heat generated, leaving the TEFC quite vulnerable to runaway heating.

On the other end of the scale there's the ODP motor design. The ODP draws the outside air directly in to the enclosure. The advantage with this is that the cooling in applied more directly, giving a more rapid response to the heat generation. The open design of the cooling leaves the interior of the motor quite vulnerable to the pollutions of the outside air. A build-up of pollution over time might cause severe damage to the machine or in worst case leave the machine inoperable.

The application of the electric motor sets the terms for which design should be chosen. If the application is in an inside and relatively dust free environment then the ODP is a preferable design, while the TEFC is preferable if the machine is used outside.

Electric machines in electric vehicles are sometimes put under a lot of stress, i.e. the machine has to work close to peak power for longer periods of time when for instance climbing an uphill road. This puts a lot of weight on the thermal design in order for the machine to be able to cope with the heat generation.

Conventionally cooled machines, i.e. air, water jacket, oil jacket or oil spray, are thermally designed close to peak power. These are oversized on purpose to be able to handle the strain.

By using a more extreme way of cooling the machine it can be thermally designed for average power, but because of the cooling still be able to handle the strain from longer periods at peak power. This gives a significantly smaller machine with the same performance as the one previously mentioned.

An extreme way of cooling the machine can be achieved by using a laminated winding and forcing the cooling medium between the winding turns. By applying the cooling directly where the most of the heat is generated it is possible to increase the efficiency of cooling the machine.
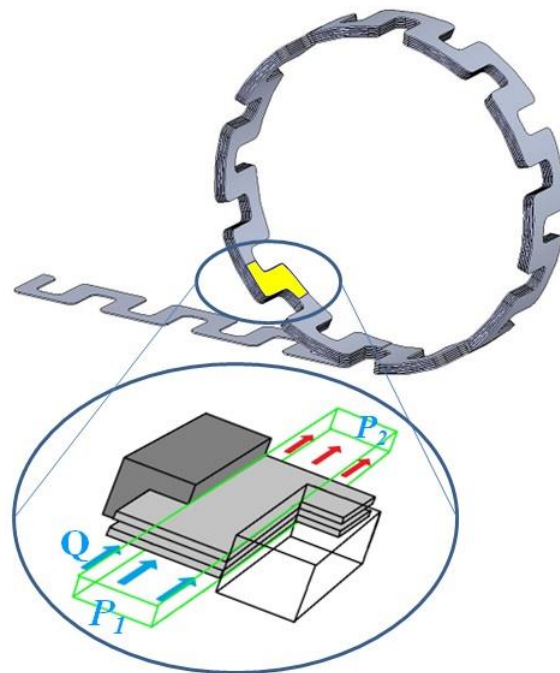
Fig 1.1.1. A laminated winding with the cooling channel enhanced.

The department of Industrial Electrical Engineering and Automation (IEA) at Lund University has built two laminated winding prototypes and a third is under construction during this thesis. The aim of this thesis is to examine these and also investigate the thermal possibilities of the laminated winding technique.

1.2 OBJECTIVES

The main objective of the thesis is to examine the thermal capabilities of laminated windings based on experience drawn from thermal modeling and measurements executed on the two prototype windings available at IEA.

Both analytical and numerical modeling is to be executed on the three winding prototypes. The model should consist of a single winding slot of the laminated winding, see figure 1.1.1 for clarification. The theory used to build the analytical model is retrieved from literature studies and the numerical model is to be made in Comsol Multiphysics.

Experimental verification of the models is to be made in first hand with measurement on the first prototype called M1 but also with measurements executed on the second prototype called M2. The test rig should consist of a cylindrical channel with air inlet at one end and free air outlet at the other. The air flow and heat loss in the winding should be controllable and winding temperature is to be measured.

The experience drawn from simulations and measurement should be used to evaluate the cooling performance of the three prototype windings as well as suggestions of cooling system designs.

1.3 WORK DIVISION

The work during this thesis has been divided among the two writers. The main areas of reasonability are divided according to table 1.3.1 and the writing of the thesis according to table 1.3.2. Even though the work is being divided are both writers greatly involved in each other's responsibilities.

Table 1.3.1. Division of responsibilities.

Ville's responsibilities	Rasmus' responsibilities	Joint responsibilities
	Air cooling theory.	
	Implementation of the air cooling theory into an analytic model in Matlab.	
	Numerical model simulations in Comsol Multiphysics.	
		Analysis of simulation results.
Background investigation of "traditional flow meter design".	Background investigation of "pressure drop based flow meter design".	Building of flow meters.
Background investigation of temperature sensors.		
		Building of experimental setup.
Conducting measurement series.		
Ir-camera footage analysis.		
Measurement data processing.		
		Analysis of measurement results.
		Assessment of measurement and simulation results.

Table 1.3.2 Division of writing.

Chapter	Ville	Rasmus
1.1 Background	X	X
1.2 Objectives	X	X
1.3 Work Division	X	X
1.4 Prototype description	X	X
2.1 Heat sources		X
2.2 Natural cooling		X
2.3 Forced cooling		X
3.1 System description	X	
3.2 Test object	X	
3.3 Control of heating power	X	
3.4 Traditional flow meter design	X	
3.5 Pressure drop flow meter		X
3.6 Contact temperature sensors	X	
3.7 Temperature sensor: IR-camera	X	
4.1 Analytical model in Matlab		X
4.2 Numerical models in Comsol Multiphysics		X
4.3 Analytic and 2D model comparison		X
4.4 Conslusions from the models		X
5.1 Resistivity	X	X
5.2 Natural cooling	X	
5.3 Forced cooling	X	
5.4 Directed forced cooling	X	
5.5 Comparison to Matlab model		X
6.1 Cooling maps	X	X
6.2 Drive cycle analysis	X	X
7 Conclusions	X	X
7.1 Further work	X	X
Appendix A		X
Appendix B	X	
Appendix C	X	X
Appendix D	X	X

1.4 PROTOTYPE DESCRIPTION

This section intends to give a short description of the three prototype machines.

M1 is the machine which winding is being used in most of the experimental measurements. The winding is built for educational purposes and are originally designed to work as a generator. During measurements the winding will be enhanced with spacers that intend to give a uniform distance between every winding turn.

M2 is going to be used as a wheel motor on an electrically driven wheel chair with a maximum power of 200W. A short measurement series is being made on M2 during the thesis. The possibility to air cool M2 is investigated mainly through simulations.

M3 is not finished during the writing of this thesis but the performance of M3 is being analyzed with the help of simulation models. M3 is going to be placed in a city bus and have a nominal power of 80kW. The intention with M3 is to air cool it and therefore be able to stay at higher powers than nominal for an extent period for example during an uphill climb.

The winding dimensions are presented in table 1.4.1. Figure 1.4.1 and the following list explains the meaning of the winding parameters presented in table 1.4.1.

- N_p = Number of poles (teeth).
- R_i = Inner radius of the winding.
- R_o = Outer radius of the winding.
- H_w = Height of the winding.
- H_e = Height difference between teeth and winding.
- W_s = Width of the teeth.
- d_c = Thickness of the winding laminates.
- N_t = Number of winding turns.
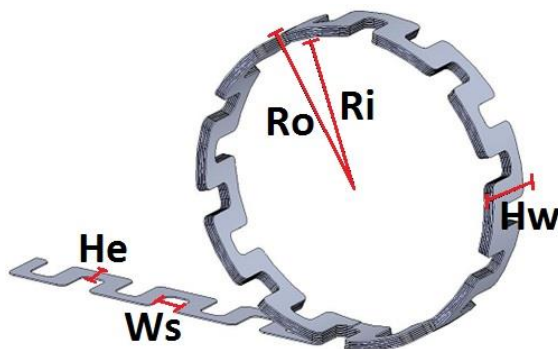
Fig. 1.4.1 Illustration of some of the winding parameters.

Table 1.4.1 The winding parameters describing the three prototype machines.

Machine	Prototype	Specification
M1		Np=20-pole Ri=58 mm Ro=69 mm Hw=25 mm He=9 mm Ws=9 mm dc=0.5 mm Nt=12 turns
M2		Np=22-pole Ri=66 mm Ro=79 mm Hw=28 mm He=3.5 mm Ws=11 mm dc=0.5 mm Nt=17 turns
M3		Np=6-pole Ri=63 mm Ro=76mm Hw=100 mm He=22 mm Ws=42.4-48.0 mm dc=0.8 mm Nt=12 turns

2. THEORY

2.1 HEAT SOURCES

2.1.1 POWER LOSS IN WINDING (COPPER LOSSES)

When current is forced through a winding it gives rise to resistive heat losses. The resistance of the winding depends on the geometrics and resistivity of the material in use. Resistivity is dependent on the temperature of the material and most materials used as conductors (e.g. aluminum and copper) have a resistivity that rises with temperature. The resistance of a given geometric can be determined from the resistivity (φ) of the material, length (L) and cross section area (A) of the conductor by:

$$R = \varphi \frac{L}{A} \qquad\qquad 2.1.1[1]$$

As mentioned above the resistivity is temperature dependent and one model for describing the temperature dependency is presented as:

$$\varphi(T) = \varphi_0\big(1 + \alpha(T - T_0)\big) \qquad\qquad 2.1.2[1]$$

Where φ_0 is the resistivity at temperature T_0 and α is a material specific temperature coefficient.

If the geometrics, resistivity and temperature coefficient of the winding material is known one can describe the heat developed in the conductor from Ohm's law as:

$$P_{conductor\ loss} = I^2_{RMS} * R \longrightarrow$$

$$P_{conductor\ loss} = I^2_{RMS} * \varphi_0\big(1 + \alpha(T - T_0)\big) * \frac{L}{A} \qquad\qquad 2.1.3$$

Determining the resistance analytically becomes more difficult when the cross section area changes along the length of the conductor. Since this is the case with the concept studied in this thesis a numerical model is used to determine the resistance of an arbitrary winding geometry.

---

[1][1] [*Physics For Scientists and Engineers,* P. A. Tipler, G. Mosca, W. H. Freeman & Co., 2008, *p. 845-847*]

In some results presented below the heat losses are mapped to current density rather than current. The current density changes along the winding due to its geometry and when presenting current density in upcoming results it refers to the average value across the whole winding. The winding heat losses are evaluated from average current density analytically by manipulating equation 2.1.3:

$$P_{conductor\ loss} = I_{RMS}^2 * \varphi_0\big(1 + \alpha(T - T_0)\big) * \frac{L}{A} \rightarrow$$

$$[I_{rms} = J_{rms} * A] \rightarrow$$

$$P_{conductor\ loss} = J_{RMS}^2 * \varphi_0\big(1 + \alpha(T - T_0)\big) * L * A \rightarrow$$

$$P_{conductor\ loss} = J_{RMS}^2 * \varphi_0\big(1 + \alpha(T - T_0)\big) * Vol \qquad 2.1.4$$

Where J_{RMS} is the RMS value of the current density and Vol is the winding volume.

2.1.2 OTHER HEAT LOSSES[2]

Since this thesis concentrate on the cooling capability of the winding no measurements or simulations are done in order to determine heat losses which might arise in other places of the machine than the winding. But in a real application other than resistive heat losses are present nonetheless and this chapter aims to present the basic facts of some commonly apparent heat losses.

One of the other heat sources present is the iron core. The heat losses in the core can be divided into two main groups, hysteresis and eddy currents.

If the iron core is magnetized into one direction it would not relax when the magnetic field is removed but instead it will stay magnetized. The only way to change the direction of the magnetization in the core back is to force it with the help of another magnetic field oriented in the opposite direction. This give rise to a magnetization loop which is called a hysteresis and the losses is evaluated by integrating the area of the loop.
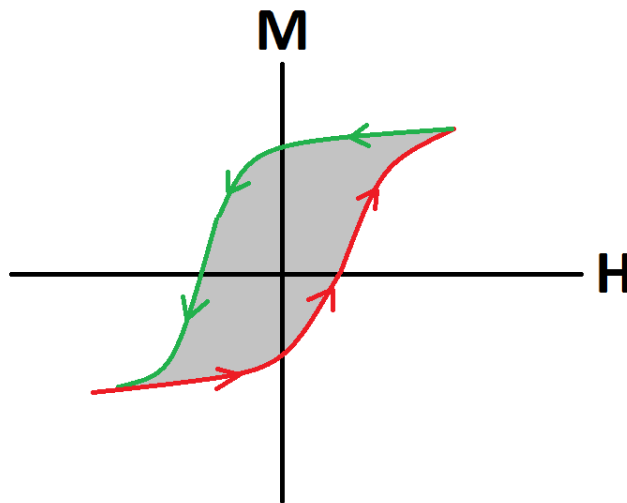
Fig. 2.1.1. M stands for the magnetization of the material (iron core in this case) and H is the intensity of the applied field from the winding. When changing direction of the magnetic field one loses energy that equals the grey area as a result from the hysteresis.

The varying magnetic field induced to the core will be surrounded by an electric field according to Faraday's law of induction. Due to the resistivity of the core material and electrical field are eddy currents starting to flow

---

[2] [2] [*Design of Powder Core Inductors,* H. Skarrie, Lic. Thesis, IEA, 2001, *chapter 3*]

through the core which gives rise to resistive heat losses within the material itself.

The impact from the core heat losses on the winding temperature is strongly dependent on the surroundings, such as the design of the casing, where it is mounted etcetera. Since the core in an inner rotor machine is pressed to the casing and therefore is mostly influenced by the natural heat transfers (see chapter 2.2) the natural cooling capability of the winding will be reduced if the core heat losses increase. If the core losses get high enough during forced cooling are heat going to start to travel from the core to the winding rather than the opposite. The natural cooling capability of the winding is both measured and modeled during the thesis and therefore the core losses are indirectly taken into account but as mentioned above are not investigated any further.

Further there are heat losses in the rotor of an electrical machine, there are heat losses due to friction in the air gap between stator and rotor. There are also some mechanical heat losses in bearings, gaskets etcetera. None of these heat losses are investigated during this thesis.

2.2 NATURAL COOLING

The heat energy that is being generated in the winding will be transferred to the surroundings through conduction, convection and radiation even without applying an active cooling system. The efficiency of the natural cooling of a machine depends on placement, geometrics, surrounding temperature, air humidity etcetera. The natural heat transfer from the winding layers can be divided into two groups, natural convection and conduction to the iron core. The impact from radiation is ignored since it is very small in comparison to the other two.

The winding layer temperature resulting from heat losses and natural convection can in its simplest form be described with a one dimensional model. The model[3] consists of a single semi-infinite plane representing a winding turn where energy is evenly generated within the center of the winding. The heat can only travel directly toward the edges of the plane where convection will take place. The surrounding room temperature is considered constant.
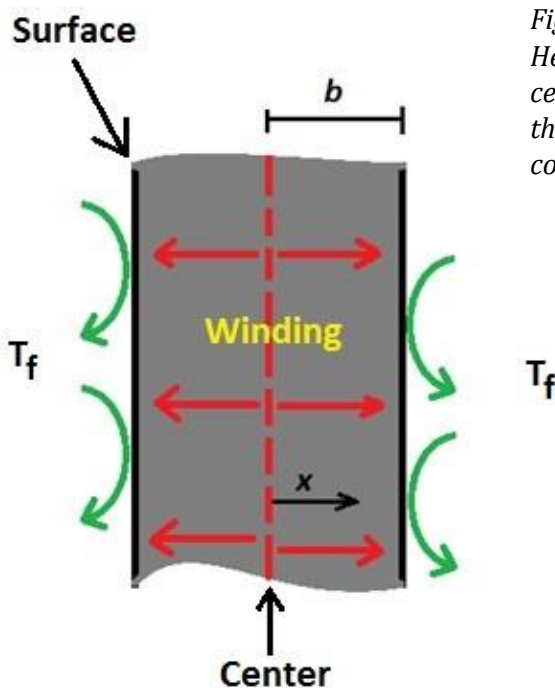
Fig. 2.2.1. A winding turn. Heat is generated in the center and travels toward the edges were convective cooling will take place.

---

[3] [3] [*Värmeöverföring,*B. Sundén, Studentlitteratur, 2006, *p. 33-34*]

The temperature at distance x from the winding center can be described as:

$$\Delta T(x) = \left(T(x) - T_f\right) \qquad\qquad 2.2.1$$

$$\frac{d^2 \Delta T}{dx^2} + \frac{\dot{Q}}{\lambda} = 0 \qquad\qquad 2.2.3$$

Where T_f [K] is the surrounding temperature, $\dot{Q}$ [W/m³] is the heat source and λ [W/mK] is the heat conductivity of the winding material.

With the following boundary conditions:

$$x = 0 : \frac{d\Delta T}{dx} = 0$$

Which means that the temperature difference between the winding center and the surrounding is stationary.

$$x = b : -\lambda \frac{d\Delta T}{dx} = h\Delta T$$

Which means that the change in temperature difference (energy flow) at the surface of the winding depends on the convection constant h [W/m²K] and the temperature difference.

The solution to the first order differential equation system is:

$$\Delta T(x) = -\frac{\dot{Q}}{2\lambda}x^2 + Cx + D$$

With help of the boundary conditions the solution becomes:

$$\Delta T = \frac{\dot{Q}}{2\lambda}(b^2 - x^2) + \frac{\dot{Q}b}{h} \qquad\qquad 2.2.4$$

The maximum temperature is reached at the center of the winding (x=0) and the temperature at the surface (x=b) is expressed as:

$$\Delta T = \frac{\dot{Q}b}{h} \qquad\qquad 2.2.5$$

This model assumes that the natural convection (h) taking place at the winding surface is known. The natural convection is dependent on a large number of variables such as placement with respect to gravity, surrounding temperature, air humidity etcetera. Since this change not only with different surrounding but also between every winding turn and teeth placement will the natural heat convection later be approximated by experiments and simulations rather than analytically determined.

The second natural heat transfer from the winding is that of conduction to the iron core. The conductive heat transfer from the winding is limited since the contact surface between the layers and the core is small. There will occur heat transfer to the iron core not only by conduction but also by two way convection. Air that is being heated by a winding layer will if possible dissipate heat to the iron core by convection. The core has a large contact surface with the casing and heat losses generated and transferred to the core will be conducted to the casing. Heat will be transferred from the casing by convection.

The following model[4] tries to explain the fundamentals of conductive heat transfer between different materials. The model consists of a wall with different layers and an energy flow taking place due to a temperature difference between the edges of the wall.
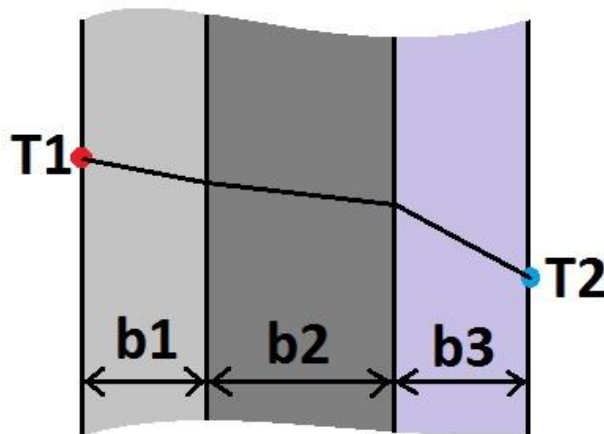
Fig. 2.2.2. Illustration of a wall consisting of three different layers. An energy flow through the wall is present due to the temperature difference between T1 and T2.

$$\dot{Q} = \frac{T1 - T2}{\frac{b_1}{\lambda_1 A} + \frac{b_2}{\lambda_2 A} + \frac{b_3}{\lambda_3 A}} \qquad 2.2.6$$

Where A [m^2] is the cross section area of the wall.

The conductive heat transfer in the machine is mainly occurring between the iron core and the casing but also from the winding to the iron teeth. No deeper investigation will be done in order to analytically determine the heat conductive capabilities of the machines which are to be investigated.

---

[4] [1] [*Värmeöverföring,* B. Sundén, Studentlitteratur, 2006, *p. 27*]

Figure 2.2.3 illustrates the expected heat energy flow through the winding.
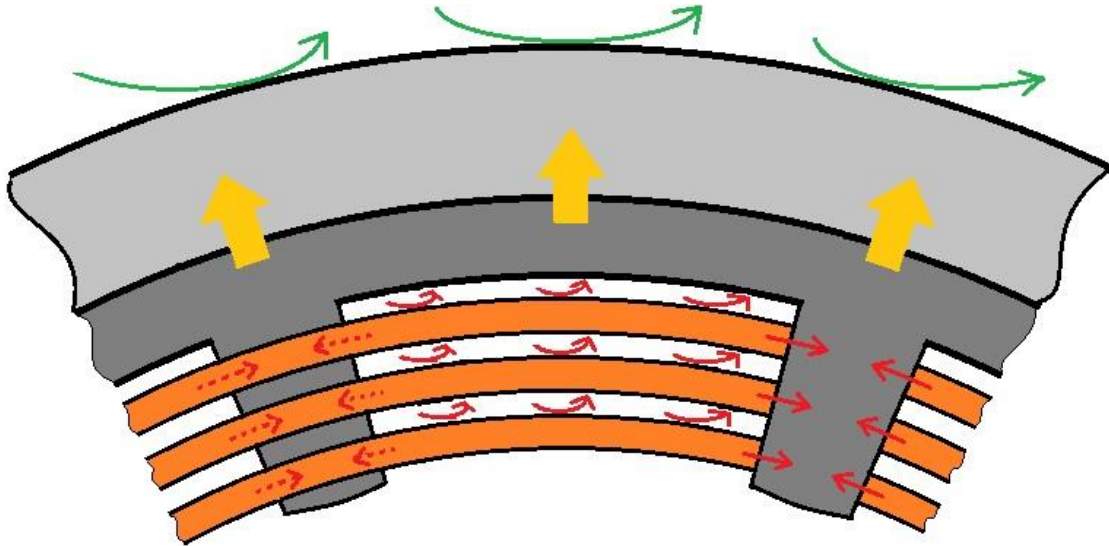
Fig 2.2.3. Illustration of the different heat transfer ways from the winding and the iron core. Heat is dissipated by both convection and conduction from the winding layers. The iron core absorbs heat from the winding and conducts it to the casing. The casing dissipates heat through convection to the surrounding air.
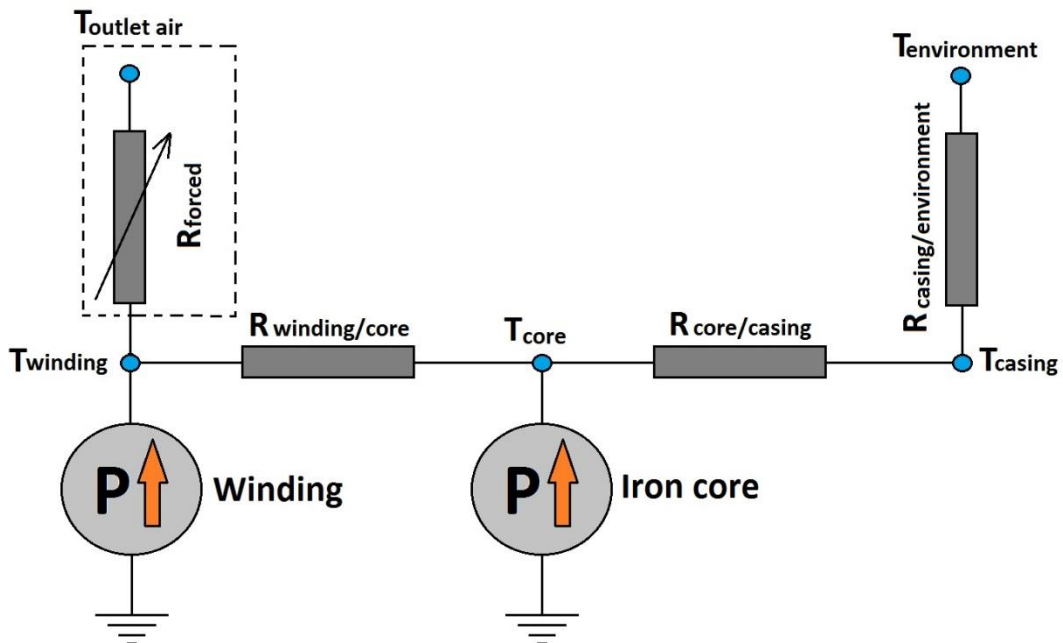
Fig. 2.2.4. Schematic of the heat transfer ways in the electrical machine.

Figure 2.2.4 shows the heat generation and dissipation that takes place in the winding and iron core. The natural heat transfers that take place will not be deeply examined in this thesis since they change between applications and properties of the surroundings. But measurements are done on prototype M1 in order to get an idea of the magnitude of the total natural cooling capabilities. A simplified equation is used in simulations and measurement results to describe the total effect from the natural cooling on the winding. The equation builds on the description of heat transfer between two solids or stationary fluids, the equation is:

$$\dot{Q}_{natural} = h_{natural} * A * (T_{winding} - T_{surrounding}) \quad 2.2.7^5$$

A [m^2] represent the area which is exposed to the heat transfer $h_{natural}$ [W/m^{2}K].

As both A and $h_{natural}$ are treated as design parameters it was chosen to use the area of the winding as A and change the magnitude of the natural cooling by varying $h_{natural}$.

The reader should note that since only the winding will be examined during this thesis no core losses are present during measurements or simulations. The dashed square in figure 2.2.4 represents an alternative forced air cooling way that will be used to enhance the cooling capabilities of the machine.

---

[5] [1] [*Värmeöverföring,* B. Sundén, Studentlitteratur, 2006, *p. 3*]

2.3 FORCED COOLING

In order to have a better cooling in a system one can use forced convective heat transfer, i.e. forcing a cooling fluid through ducts or channels of the application one wishes to cool. The forcing of the coolant is often done by external machines, such as pumps or fans. In any case of forced convection there is always some amount of natural convection present, giving a mixed convection situation.

Forced cooling can be applied in different ways. For instance one could let the fluid flow distribute itself freely or one could concentrate the flow to areas where the cooling fluid is of greater use.

When forcing a fluid through a channel there is a build-up of a boundary layer along the channels inner surface. It's assumed that the velocity of the fluid at the entrance to the channel is uniform across the width of the channel. The boundary layer acts as a blocker to the fluid, reducing the velocity of the fluid to zero at the inner surface and at the edge of the boundary layer the core region velocity is achieved.
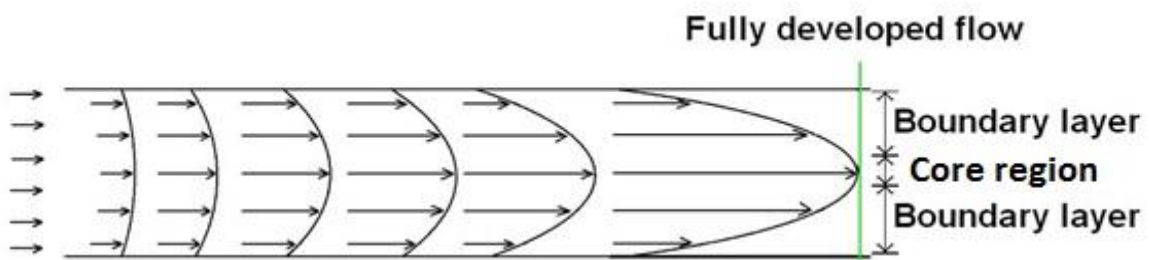
Fig. 2.3.1. Illustration of how the boundary layer affects the flow through a channel.

The deceleration of the fluid at the boundary layers is the cause for the development of a velocity perpendicular to the fluid velocity. In order to maintain the balance of the mass flow the velocity of the fluid must increase in the core region (see fig. 2.3.1). The boundary layers are gradually merging as their thickness grows. At the point when they are merged the velocity field of the fluid is said to be fully developed.

The boundary layer can rarely be treated as a laminar boundary layer. In cases with wide channels, high fluid velocities or fluids with small kinematic viscosities there may occur a transition to turbulent flow before the flow is fully developed, i.e. giving a turbulent velocity profile. Viscosity is the property of a fluid that causes the resistance to flow, for example honey has a higher viscosity than water.

2.3.1 FLOW CHARACTERSISTICS

By evaluating the Reynolds number one could determine the type of flow occurring in the winding slot. The Reynolds number is evaluated as:

$$Re = \frac{U * D_h}{\nu}$$
2.3.1[6]

Where U [m/s] is the mean velocity of the fluid, D_h [m] is the hydraulic diameter of the winding slot and ν [m²/s] is the kinematic viscosity of the fluid.

The critical Reynolds number for channel flows is 2300[5] and therefore the flow is surely laminar for Reynolds numbers below 2000 and turbulent for flows over 3000. Reynolds numbers between 2000 and 3000 indicates that the flow is in a transition state being nor completely laminar or turbulent.

The flow is typically laminar for the winding application studied in this thesis, stretching from Reynolds numbers from approximately 50 to 2000. But in order to model the more extreme cases it was chosen to include the turbulent theory as well as the laminar.

---

[6] [1] [*Värmeöverföring,*B. Sundén, Studentlitteratur, 2006, *p. 161*]

2.3.2 INLET STRETCH

The flow characteristics in a channel do not develop instantly at the inlet but needs to travel a certain distance before the velocity profile has converged to a steady value. The distance that the fluid has to travel along the channel until the flow characteristics is fully developed is called inlet stretch. During this inlet stretch the flow characteristics and heat distribution of the fluid is different from the fully developed case.

During the development of the velocity and heat profiles one would have higher heat convection than in the fully developed profile. When considering fluid flows in channels where the entrance region constitute a large part of the total length one can not ignore the impact of the inlet stretch as normally when dealing with longer channels. The inlet stretch for laminar flows is given by:

$$L_V = 0.05 Re D_h \qquad 2.3.2^{[7]}$$
$$L_t = 0.05 Re Pr D_h \qquad 2.3.3^{[7]}$$

Where L_v [m] is the velocity inlet stretch and L_t [m] is the thermal inlet stretch.

Both the velocity and the thermal inlet stretch is much shorter for turbulent flows; both of them are approximately 10 times the hydraulic diameter.[2]
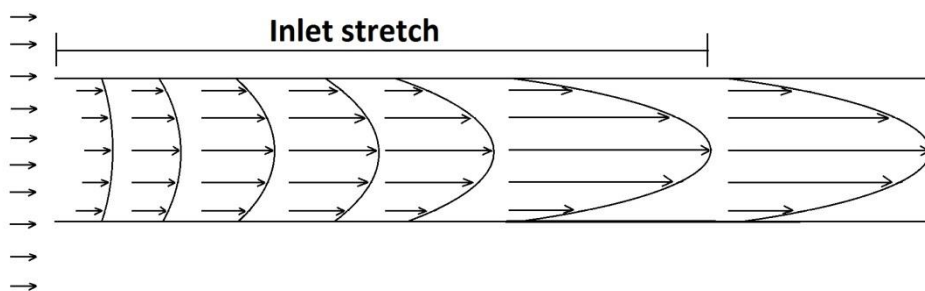
Fig 2.3.2. Illustration of the velocity inlet stretch and how the air speed distribution develops along it. After the inlet stretch the flow is fully developed and has a stationary flow distribution.

---

[7] [4] [*Heat and Mass Transfer: A Practical Approach, 3/e*, Y.A Cengel, McGraw-Hill, 2007, *p.449*]

2.3.3 NUSSELTS NUMBER

Nusselts number (Nu) is used to determine the magnitude of the convection between a surface and the surrounding fluid. Empirical equations for deciding Nusselts number is often only valid within a given interval of Reynolds and Prandtl number. Prandtl number (Pr) is dimensionless and tells the quota between momentum and thermal diffusivity.

Nusselts number in its raw form is given by:

$$Nu = \frac{hD_h}{k}$$
$$\text{2.3.4}$$

Where k is the thermal conductivity of the fluid and h is the convection coefficient.

Since the Nusselts number depends on the convection and no simple analytical description of that exists the number is often determined empirically and the formulas used change for different applications. One equation for determining the mean Nusselt number including inlet stretch for a parallel plate channel during laminar flow conditions is:

$$Nu = 7.55 + \frac{0.024\left(\frac{L}{D_h RePr}\right)^{-1.14}}{1+0.0358Pr^{0.17}\left(\frac{L}{D_h RePr}\right)^{-0.64}} \qquad \text{2.3.5}[8]$$

The equation is valid for laminar flow conditions and for 0.1 < Pr < 1000.

For turbulent flows one could use Gnielinskis equation for determining the Nusselt number. Gnielinskis equation does not take the inlet stretch into account and will therefore give a slightly lower convection than a measured one. It was chosen anyway since the turbulent inlet stretch is short in comparison to the total channel length in our applications.

$$Nu = \frac{\frac{f}{8}(Re-1000)Pr}{1+12.7\sqrt{\frac{f}{8}}\left(Pr^{\frac{2}{3}}-1\right)} \qquad \text{2.3.6}[9]$$

Valid in for 2300 ≤ Re ≤ 10[6], 0.5 < Pr < 2000. f is the friction factor of the channel.

---

[8] [5] [*Journal of Heat Transfer*, Y. S. Muzychka, M. M. Yovanovich, ASME, Vol. 126 2004, *p. 55, Eq. 16*]

[9] [6] [*A heat transfer textbook,* J.H. Lienhard IV, J.H. Lienhard V, Phlogiston Press, 2008 *p. 359*]

2.3.4 PRESSURE DROP

When air is forced through the channel it will give rise to a pressure drop. The magnitude of the pressure drop depends on the speed of the incoming air, the friction of the channel walls and the profile of the flow etcetera. Being able to minimize the pressure drop with regard to the heat dissipation is crucial since it reduces the pump power needed to transport the air through the system.

When determining the pressure drop in the application, the problem was divided the problem into two parts. First treat the channel as a piece of a longer channel of the same dimension assuming the flow to be fully developed and determine the pressure drop over a determined length of the channel. Then treat the inlet of the channel as an "inlet area reduction" and calculate the pressure drop produced from the shock loss.
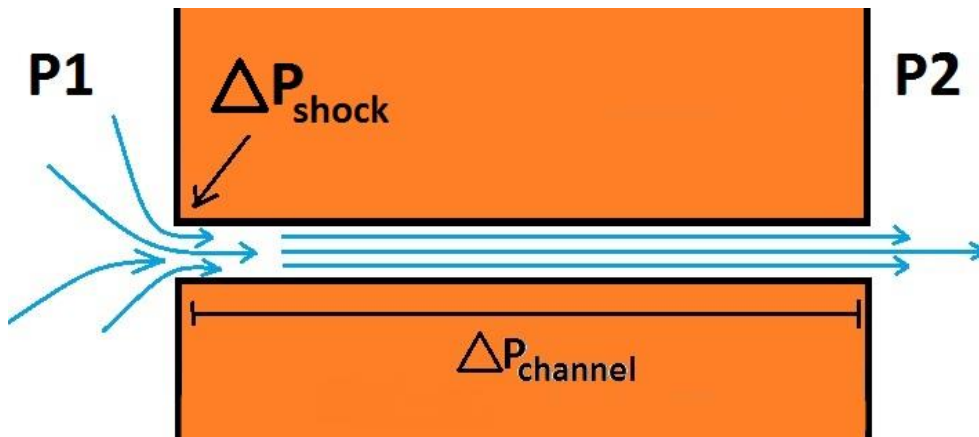
Fig. 2.3.3. Illustrates the difference between shock and channel pressure drop, P1>P2.

The channel pressure drop is given by:

$$\Delta p = f * \frac{L}{D_h} * \frac{\rho U^2}{2}$$
  2.3.7[10]

The shock loss is given by:

$$\Delta p_{shock} = \zeta * \frac{\rho U^2}{2}$$
  2.3.8[10]

The application resembles with a "sharp cornered outlet" and therefore the specific loss coefficient (ζ) is approximated to 0.5[11].

[10] [7] [*Tillämpad termodynamik,* I. Ekroth, E. Granryd, Studentlitteratur 2006, *p. 373*]
[11] [7] [*Tillämpad termodynamik,* I. Ekroth, E. Granryd, Studentlitteratur 2006, *p. 388*]

The friction factor (f) for turbulent and laminar flows can be determined from the following empirically determined formulations:

Turbulent flow:

$$f = \frac{1}{(0.79 \ln(Re) - 1.64)^2} \qquad \qquad 2.3.9\,[12]$$

Laminar flow (only valid if the layer spacing << inlet width):

$$f = \frac{96}{Re} \qquad \qquad 2.3.10\,[13]$$

---

[12] [6] [*A heat transfer textbook,* J.H. Lienhard IV, J.H. Lienhard V, Phlogiston Press, 2008 *p. 359*]
[13] [3] [*Värmeöverföring,*B. Sundén, Studentlitteratur, 2006, *p. 146*]

2.3.5 AIR DISTRIBUTION BETWEEN PLATES

The air that hits the stack of slots is assumed to have a flat profile and therefore will a stack of evenly distributed slots have the same amount of air travelling between every pair of plates. But what if the layer spacing is not evenly distributed? Since different slot sizes give rise to different pressure drops it is chosen to distribute the mass flow in a way that all slots had the same pressure drop. Let us assume that the total air mass flow that hit the stack of slots is known as well as the individual layer spacing of each slot. If the flow through the slot is laminar then the mass flow distribution can be determined by the following reasoning:

The total pressure drop over one slot is the sum of equations 2.3.7 and 2.3.8. From these equations it is possible to determine the mass flow for a certain pressure drop and slot geometrically by the following calculation, note that only the positive solution to the second degree polynomial is of interest since the mass flow can not be negative.

$$\Delta p_{Tot} = \Delta p + \Delta p_{shock} = f * \frac{L}{D_h} * \frac{\rho U^2}{2} + \zeta * \frac{\rho U^2}{2} =$$

$$\left[f = \frac{96}{Re} = \frac{96\mu A}{\dot{m}_{slot} D_h}, U = \frac{\dot{m}_{slot}}{\rho A}, \rho = \frac{\Delta p_{Tot} + p_{abs}}{2R_{air}T} \right] =$$

$$\frac{\dot{m}_{slot}^2}{\rho^2 A^2} * \left(\frac{96\mu A}{\dot{m}_{slot} D_h} * \frac{L}{D_h} * \frac{\rho}{2} + \zeta * \frac{\rho}{2} \right) = \frac{48\dot{m}_{slot}\mu L}{\rho A D_h^2} + \frac{\zeta \dot{m}_{slot}^2}{2\rho A^2} \rightarrow$$

$$\rightarrow \dot{m}_{slot}^2 + \dot{m}_{slot} * \frac{96\mu L A}{\zeta D_h^2} - \Delta p_{Tot} A^2 * \frac{\Delta p_{Tot} + p_{abs}}{\zeta R_{air}T} = 0 \rightarrow$$

$$\dot{m}_{slot}(\Delta p_{Tot}) = -\frac{48\mu L A}{\zeta D_h^2} + \sqrt{\left(\frac{48\mu L A}{\zeta D_h^2}\right)^2 + \Delta p_{Tot} A^2 * \frac{\Delta p_{Tot}+p_{abs}}{\zeta R_{air}T}} \qquad 2.3.11$$

From the equations describing the mass flow in each slot one can decide the total mass flow as a function of the total pressure drop as

$$\dot{m}_{tot}(\Delta p_{Tot}) = \sum_{i=1}^{nbrOfSlots} \dot{m}_i(\Delta p_{Tot})$$

If the total mass flow that hits the stack is known one can write a function $g(\Delta p_{Tot})$ such as

$$g(\Delta p_{Tot}) = -\dot{m}_{tot} + \sum_{i=1}^{nbrOfSlots} \dot{m}_i(\Delta p_{Tot})$$

Since the sum $\sum_{i=1}^{nbrOfSlots} m_i(\Delta p_{Tot})$ has a derivative that is strictly positive for all $\Delta p_{Tot} > 0$ and that $\dot{m}_{tot}$ is constant will there only be one solution to $g(\Delta p_{Tot}) = 0$ for $\Delta p_{Tot} > 0$. Δp_{Tot} that solves $g(\Delta p_{Tot}) = 0$ is the total pressure drop over the stack of slots matching the value of $\dot{m}_{tot}$ The reader should note that if the mass flow distribution is to be evaluated for turbulent flow conditions one would have to use equation 2.3.9 instead of 2.3.10 when determining the friction factor.

When the total pressure drop is known one can evaluate the mass flow for each individual slot in the stack by equation 2.3.11.
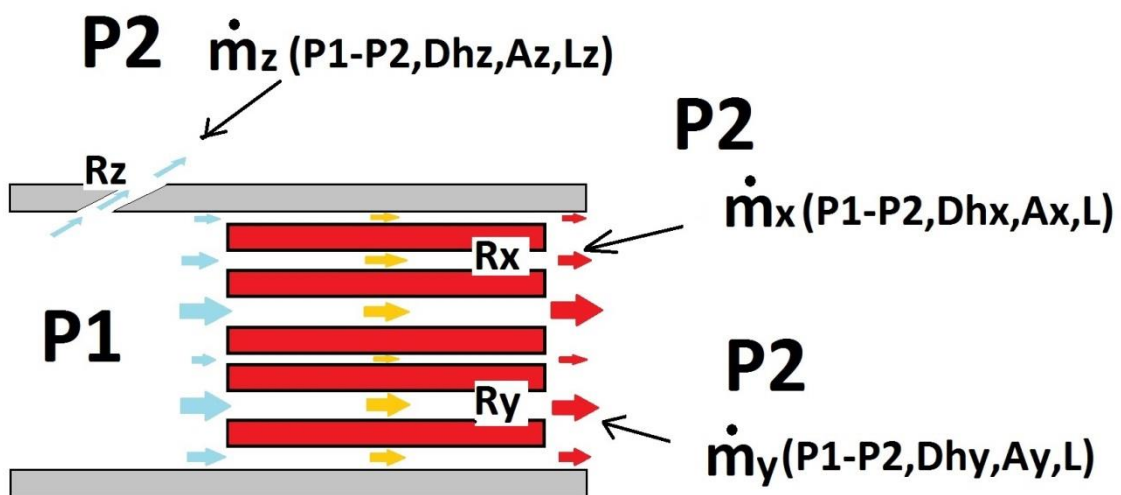
Fig. 2.3.4. Illustration of how the mass flow is distributed across unevenly spaced winding layers. A leakage is treated in the same way as a winding slot. Every leakage or slot has its own resistance towards air flow which makes it more or less hard for the air to pass through. The pressure drop (P1-P2) is the same for all slots/leakage paths.
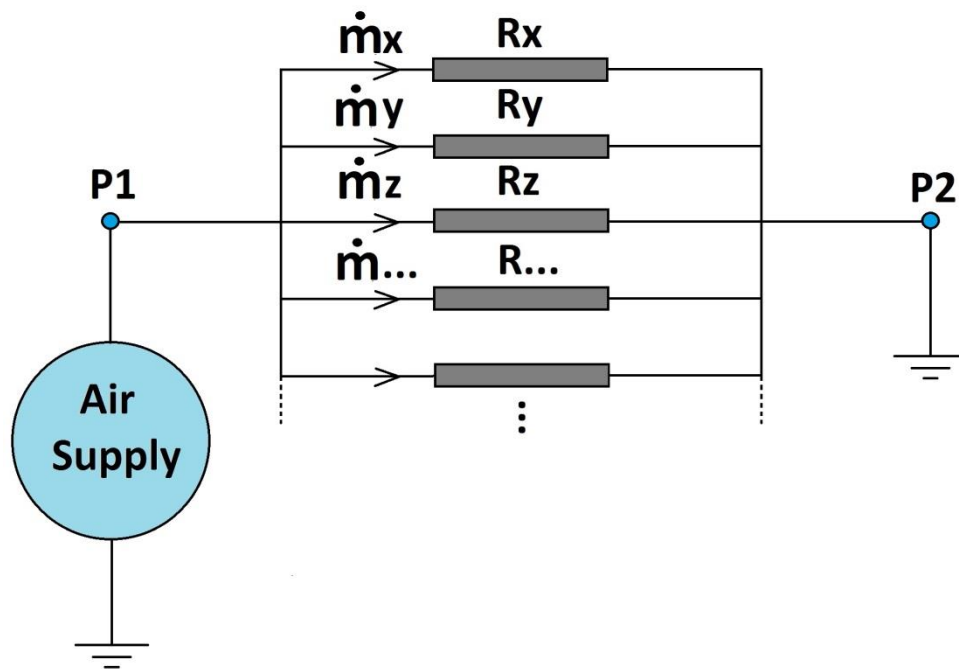
Fig. 2.3.5. Illustration of a flow network which describes the air distribution between slots. The air supply is considered as the power source which creates the potential P1. The drop in potential (pressure) is the same for all resistances (slots/leakage paths) but they will give rise to different mass flow magnitudes through them. The mass flow magnitude through each resistance is determined by equation 2.3.11.

One could use the same reasoning for simulations when the total mass flow is not known. Let us say that one would use a regulator to make sure that no slots exceed a predefined reference temperature. Then the regulator would determine the mass flow through the hottest slot in the stack and one could thereby determine the pressure drop over that slot. Since the pressure drop across the laminated winding in flow direction has to be equal for all slots in the stack one could use the pressure drop over the hottest slot as the total pressure drop and thereby determine the mass flow through the rest of the slots by equation 2.3.11. Then the mass flow that has to hit the stack is simply the sum of all mass flows through the slots in that stack.

2.3.6 DETERMINE THE COOLING EFFICIENCY

Based on the high thermal conductivity of an electrical conductor the energy is assumed to distribute itself instantly throughout the winding slot, and an assumption of constant surface temperature can be used. Under the assumption of constant surface temperature the air outlet temperature (T_E) is approaching the surface temperature (T_S) along the channel length (x) exponentially. The speed of which the outlet air temperature approaches the surface temperature is dependent on the inlet air temperature (T_I), convection (h), air wetted perimeter (P_W), specific heat capacity of air (C_p) and mass flow rate ($\dot{m}$). One can determine the air temperature at any place along the length of the slot by equation 2.3.12.

$$T_E(x) = T_S - (T_S - T_I) * \exp\left(-\frac{hP_W x}{\dot{m}C_p}\right) \qquad 2.3.12^{14}$$

If the dimensions of the plates, convection constant, mass flow, air inlet temperature are known one could decide the air outlet temperature for a certain surface temperature. Since all energy is used to heat the air (at steady state conditions) one could determine the energy dissipation by the following expression:

$$\dot{Q} = \dot{m}C_p * (T_E - T_I) \qquad 2.3.13^{15}$$

By combining these two expressions and equation 2.3.4 and 2.3.5 one could determine how much energy that is being dissipated by the air for a certain surface temperature, air inlet temperature and mass flow rate.

---

[14] [4] [*Heat and Mass Transfer: A Practical Approach, 3/e*, Y.A Cengel, McGraw-Hill, 2007, *p.429*]
[15] [1] [*Physics For Scientists and Engineers,* P. A. Tipler, G. Mosca, W. H. Freeman & Co., 2008, *p. 592*]

By equation 2.3.7 to 2.3.10 one can determine the pressure loss for any given motor geometry and mass flow rate. If also the mean temperature of the outlet air and mass flow rate also is known one can determine the volumetric air flow. From the pressure drop and volumetric flow one can determine the ideal pump power needed to force the air through the winding and thereby determine the cooling efficiency at steady state.

$$\rho_{air} = \frac{\left(p_{abs} + \frac{1}{2}\Delta p_{Tot}\right)}{R_{air}(T_I + T_E)}$$

where R_{air} is specific gas constant for air.

$$Vol_{flow} = \frac{\dot{m}_{tot}}{\rho_{air}}$$

$$PumpPower_{ideal} = Vol_{flow} * \Delta p_{Tot} \qquad\qquad 2.3.14$$

2.3.7 TRANSIENTS

The transient state of the winding can be determined from the same methodology as above except one would have to determine the first order differential equation describing the transients of the event. In order to do this one would need an expression for the temperature rise taking place in the winding. The winding is assumed to be fixed and hold shape and phase and therefore the increase in temperature is:

$$\Delta T = \frac{\Delta E}{mC_p} \rightarrow \left[\Delta E = \left(\dot{Q}_{HL} - \dot{Q}_{Air} \right) * t \right] \rightarrow \qquad 2.3.15$$

$$\Delta T = t * \frac{\dot{Q}_{HL} - \dot{Q}_{Air}}{mC_p}$$

$$T_{new} = T + \Delta T$$

Where E is the internal energy of the winding and m is the winding mass.

Under the same assumptions stated above and a time step of k seconds one could solve the transient problem numerically by the following algorithm:

```
┌─────────────────────────────────────┐
│   Determine motor dimensions,        │
│   convection constant, air inlet     │
│   temperature and mass flow rate.    │
│   Determine an initial value of Ts.  │
└─────────────────────────────────────┘
```

$$T_{E(k)} = T_{S(k)} - \left(T_{S(k)} - T_I \right) * \exp\left(-\frac{hP_W L}{\dot{m}C_{pAir}} \right)$$

$$\dot{Q}_{Air(k)} = \dot{m}C_{pAir} * \left(T_{E(k)} - T_I \right)$$

$$k = k + 1$$

$$\Delta T_S = k * \frac{\dot{Q}_{HL} - \dot{Q}_{Air(k)}}{m_{Al}C_{pAl}}$$

$$T_{S(k+1)} = T_{S(k)} + \Delta T_S$$
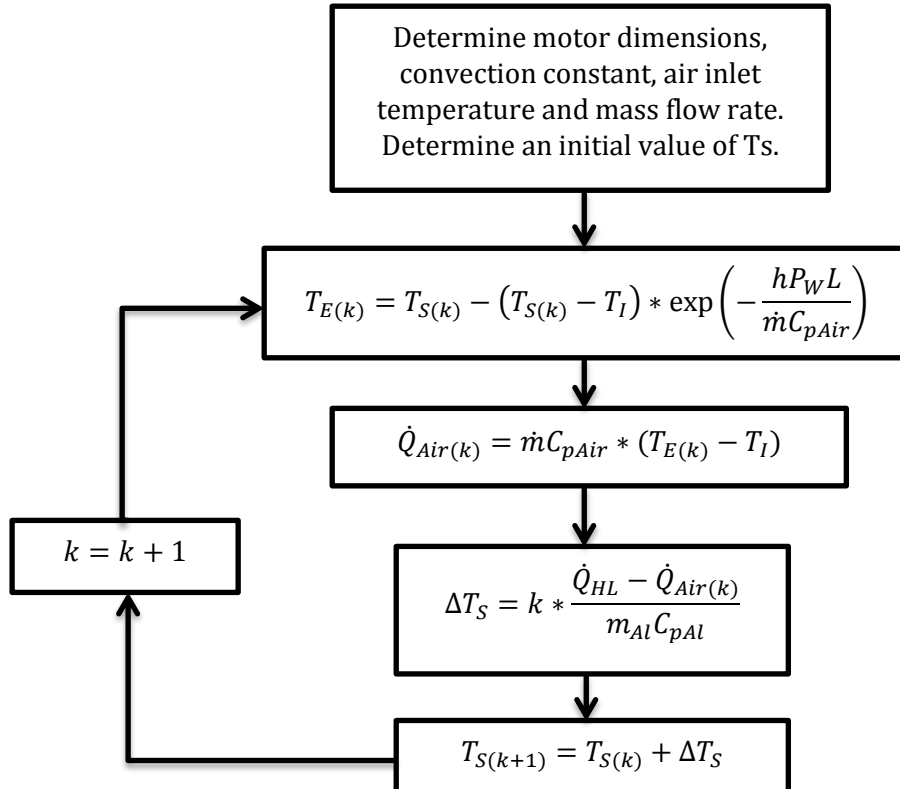
One can easily add the influence of other heat conduction paths by adding a negative energy flow term into the equation of ΔT_S. This gives the opportunity to build a more complex model where i.e. heat conduction through the casing is taken into account. The algorithm also gives an opportunity to improve the approximation of the convection constant h. By letting the air properties change with temperature and pressure it is possible to describe the transient behavior of the inlet stretch and flow characteristics during the heating process and therefore get a more accurate picture of reality.

3. EXPERIMENTAL SETUP

The purpose of doing measurements is to study the effects of the cooling on a real winding in order to compare it to the theoretical results given from the simulations. For this to happen, it is necessary to have a good experimental setup.

3.1 SYSTEM DESCRIPTION

3.1.1 TEST METHOD

In order to study the effect of how well the forced air cooling works on a real laminated winding several tests are made for different flow rates and currents through the winding. The test method works as
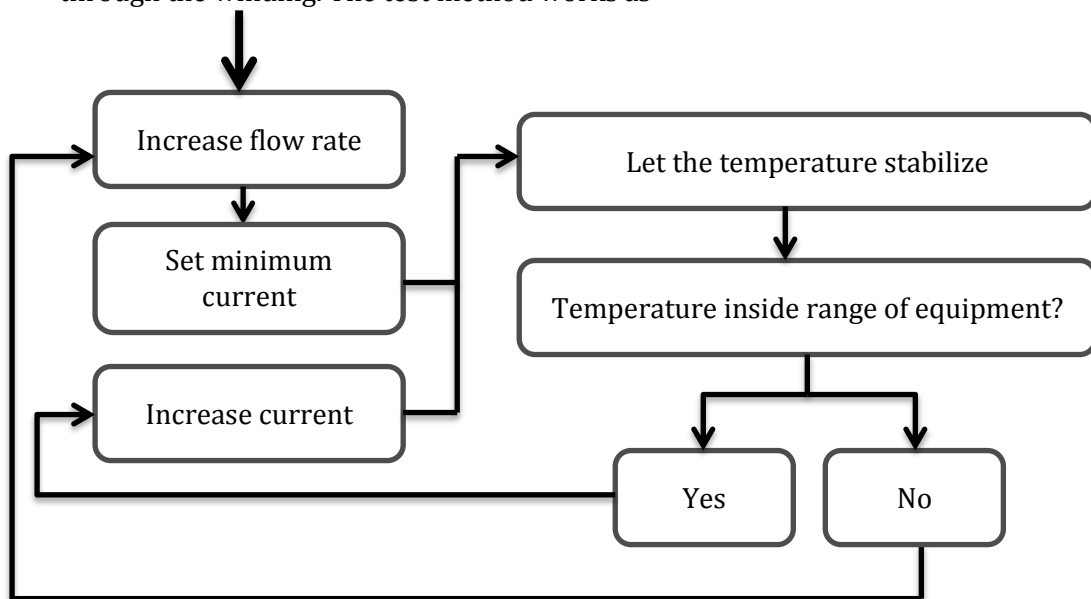
Fig. 3.1.1. Illustration of the test method in a flow chart.

This is also applied to the same winding but with a more directed cooling approach, in order to investigate the possibility of concentrating the flow of the coolant. While restricting the total area of where the air can be transported through the winding it is expected that the pressure should increase inside the housing. The increase in pressure in the housing translates to an increase in the work needed for a pump to supply the air flow needed. The investigation is made in order to see if this increase in pump power is compensated for with more efficient cooling.

A minor investigation about the effects of other sources of heat dissipation is also made. Even with the insulation it is expected that some of the heat generated in the winding will find its way out through the insulation.

This investigation is made by applying quite small amount of current through the winding and letting the temperature reach stationary without any airflow. With this method it is possible to estimate how large the heat transfer coefficient is without forced convection applied, and can then later on be taken into account when studying the forced convection.

In order to measure and control all necessary variables in the tests a bunch of equipment is needed, these are described below.

3.1.2 TEST BENCH

The test bench was quite big with cables, wires and pipes running everywhere. A picture of it would only be hard to comprehend; hence a smaller schematic overview of it is shown below.
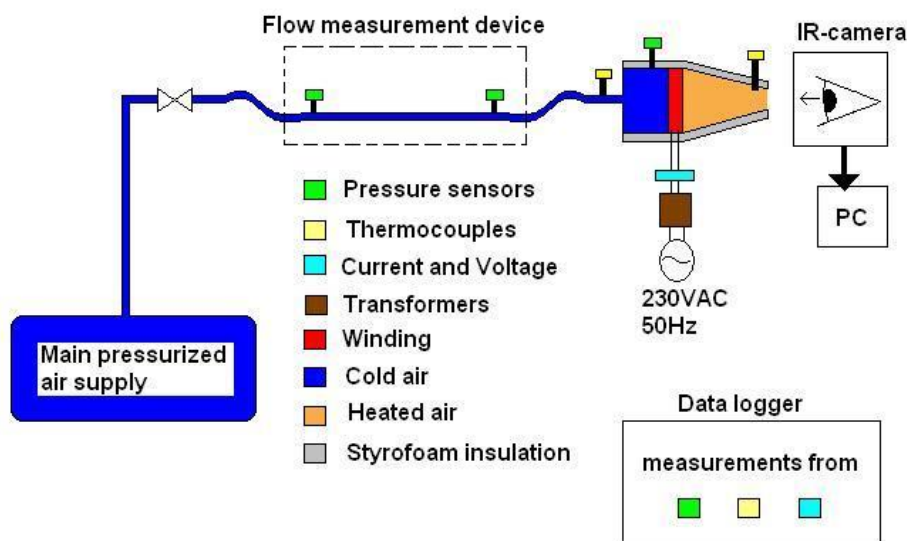

Fig. 3.1.2. An illustration of the setup of the test bench.

The test bench consisted of the winding mounted into a housing. The housing with the winding is covered in a styrofoam insulated funnel. The purpose with the funnel is to collect the hot air that has passed the winding into a smaller opening in order to measure the temperature of the air. The purpose with the

insulation covering the funnel is to reduce the natural cooling paths and therefore to increase the significance of the forced cooling through the conductors in the laminated winding.

On the backside of the housing a pipe is connected that supplies the air for the cooling. The air is taken from the main air supply of the building and on its way to the housing the air passes through the flow measurement device.

The heat in the winding is generated from a current passing through it. The current is taken from the 230 VAC grid. On the way to the winding the current passed through a couple of transformers to get a high current but keep the voltage low. The frequency of the current was the standard of the grid, i.e. 50 Hz. The schematic of the power supply is shown in section 3.3.

The winding temperature can be measured in many ways with different types of sensors. For instance one could use contact temperature sensors, such as thermocouples or RTDs (Resistance Temperature Detectors), by inserting these into the winding. For a less invasive approach an IR-camera is used. Temperature sensing is discussed in more detail in sections 3.6 and 3.7.

3.1.3 MEASUREMENT EQUIPMENT

Most of the measurement data is logged with Agilent 34972A. With this it is possible to connect and sample 20 channels continuously and save the data to a USB memory stick. The number of channels in use limits the maximum sample rate, with ten channels in use the sample rate is limited to once each 4.5 seconds. With these ten channels it is possible to sample 5 voltages (3 from pressure sensors, 1 for the voltage and 1 for the current) and 5 temperatures (1 at the inlet air, 2 at the outlet air and 2 on the housing).

Since the current through the winding need to be high it is not directly possible to measure the current without damaging the data logger. Instead a shunt with known resistance is placed in series with the winding. With the known conversion factor of the shunt the current could later be calculated from the measured voltage drop.

The pressure sensors used are *Smartec SPD015G*. These are gauge pressure sensors, measuring up to 1 bar in relative air pressure. One of the pressure sensors are used for determining the pressure inside the housing. The other two sensors measure the pressure drop for the flow measurement equipment.

The thermocouples of type J are placed so that the inlet and outlet air temperatures can be measured in order to calculate how much of the heat that's drawn away by the forced air cooling.

The IR-camera *(FLIR Systems ThermaCam T360)* is used to measure and monitor the temperature in the winding. It makes it easy to detect if there are any short circuits in between the winding turns. The movies from the measurements have to be analyzed in Matlab in order to extract the temperatures.

3.2 TEST OBJECT

3.2.1 DIMENSIONS

The test object is a laminated winding from a small 20 pole machine (M1). The material of the winding laminates is aluminium with a thickness of 0.5 mm.
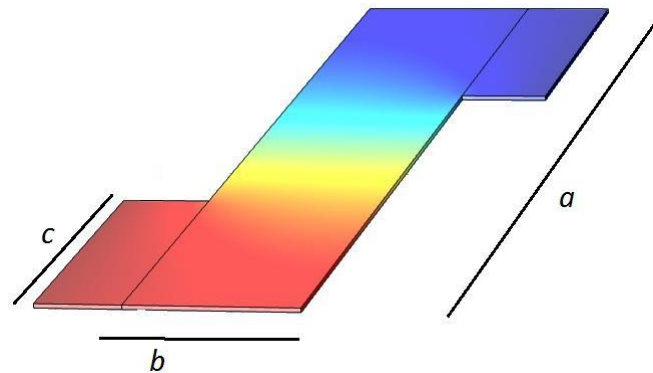
Fig. 3.2.1. Illustration of a winding segment. a= 25 mm, b =10 mm, c =5 mm.

The dimensions of the winding are written in the description of fig. 3.2.1. It should be noted that cooling width (b in the figure) is the average cooling width of the winding, i.e. the cooling width depends on which turn that is measured since the winding is wrapped into a spiral of 12 layers. The layer spacing, i.e. the radial distances between each layer of the laminated winding, is designed to be 0.2 mm. Future mentions of layer spacing refers to this layer spacing, if not otherwise stated.

3.2.2 IMPROVEMENTS

As the winding was already made there is little that could be done to influence the layout of the winding. Never the less, some improvements are made mainly to ensure more even layer spacing. Previously made measurement (Appendix B) left some notions of what could be improved to get more accurate results, such as thermocouple placement. The placements of thermocouples are discussed in section 3.6.6.

The layer spacing between each turn is fitted with pieces of 0.2 mm thick wires in order to keep the layer spacing the same size throughout the winding. The spacing between layers is still not exactly the same size, as seen in fig. 3.2.2 in area A.

The thermocouples had in the previous measurements made the winding very uneven, giving larger layer spacing in those places where they were placed. Because of that the thermocouples are not used, in an effort to keep the layer spacing more even.

Larger layer spacing is obstructed with some insulation as well as the inner and outer part of the winding, giving the air less alternative routes to flow. That said, by confining the air flow to take place in the layer spacing in between the winding turns, the utilization of the air as coolant should increase.
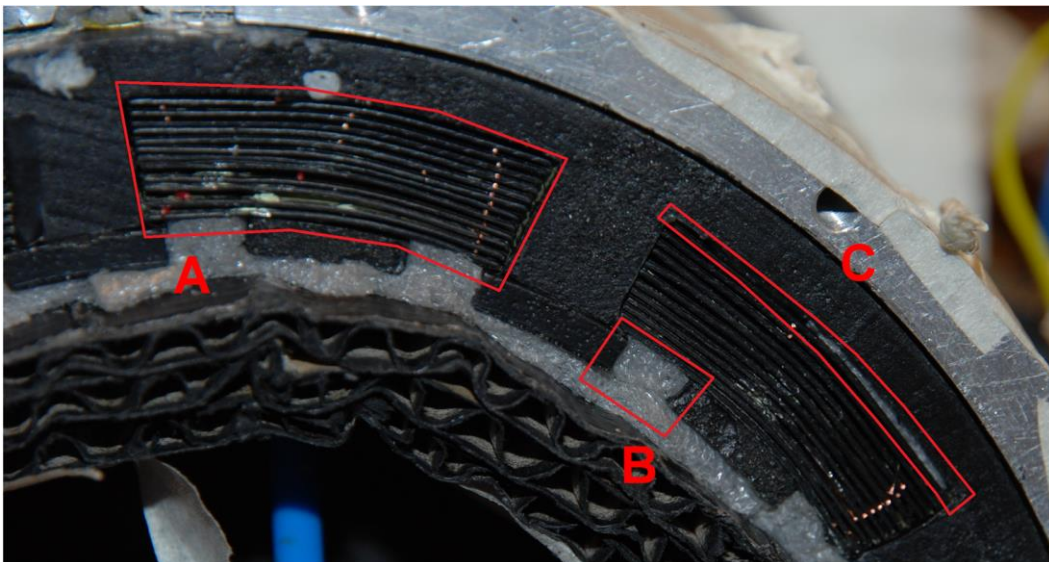
Fig. 3.2.2. Illustration of problem areas in the winding and what was done about it. A shows an example of uneven layer spacing. B and C shows insulation of suspected air leakage.

The areas marked with red in fig. 3.2.2 shows the problem areas of the winding, although already amended. The largest area to the left (A) shows an example of how the layer spacing between the winding turns hasn't the same size throughout the whole winding. The small brighter dots in the same area are spacers which are placed to prevent too great inequality of the layer spacing. The small red rectangle (B) shows where it was suspected to flow larger amounts of air without giving any cooling effect. The last red area (C) shows another insulated area where the air could previously escape.
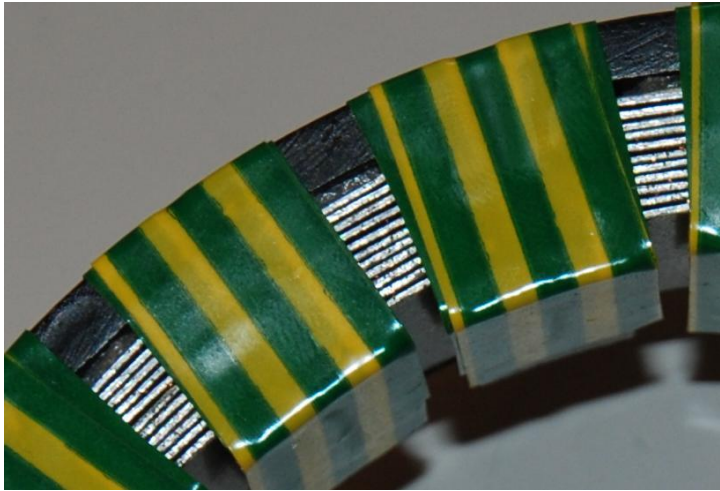

Fig. 3.2.3. Illustration of directed cooling approach.

The figure above shows a simple approach to the directed cooling idea. Portions of the backside of the winding (the side that is exposed to the incoming cool air) was taped. The width of an inlet sector is approximately 4.3 mm.

3.3 CONTROL OF HEATING POWER

The heating power is caused by a current running through the winding. A schematic circuit of the setup is shown below.
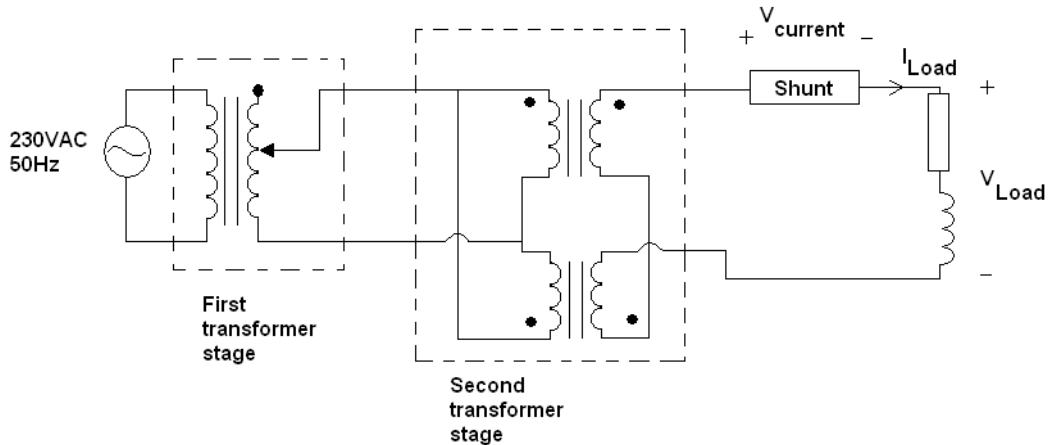
The power is drawn from the 230 VAC 50 Hz grid. From this the current passes through two transformer stages. The first is a variable transformer, i.e. the point at which the heating power is controlled. The first transformer stage has a fuse that limits the current to 4 A at this stage. After this the current passes yet another transformer stage, consisting of two in series coupled transformer. These transformers increase the current 20 times. This configuration gives a high current through the load, i.e. the winding, while keeping the voltage quite low. The maximum the setup can be loaded with is around 350 W at 80 A through the load.

The $V_{current}$ marked in the figure is where the current through the load is measured. By measuring the voltage drop over a shunt the current through it can be determined. A shunt is used because of that they generally have low voltage drops for quite high currents, in order not to affect the whole system all that much. The shunt has a voltage drop of 60 mV at 200 A, which is more than enough for this setup since the current cannot be higher than 80 A without blowing a fuse. The voltage over the winding is quite simply measured over the terminals of the winding.

The current has to be carefully monitored during measurements since the resistivity of an object is directly dependent on the temperature of the object, i.e. the current decreases with increasing resistivity. For this reason the current set point in the variable transformer has to be adjusted during measurements in order to keep the desired set point of constant heating power.

3.4.1 THEORY

The volume flux is described by Q = dV/dt. If the volume dV passes through a part of a tube with the cross-section area A then the volume flux can be described by Q = A*dx/dt, given that the volume moves the distance dx during the time dt.

If the tube is assumed to be leakage free and the flow is incompressible, then the volume flux will be the same everywhere in the tube independent of changes in the cross-section area of the tube. This gives

$$Q = A_1 \frac{dx_1}{dt} = A_2 \frac{dx_2}{dt} \qquad\qquad 3.4.1$$

where dx_1 and dx_2 is the distance covered during the time dt in the parts with cross-section areas A_1 and A_2.

The speed is known to be U = dx/dt giving that the speed difference between the different part of the tube is given by

$$U_2 = U_1 \frac{A_1}{A_2} \qquad\qquad 3.4.2$$

Assume that there is two pressure-zones in a tube filled with a fluid with no leakages. The net force is described by

$$F = dpA \qquad\qquad 3.4.3$$

Assume also that the fluid moves a distance of dx, meaning that the fluid is exposed for the work

$$W = Fdx = dpAdx = dpdVol \qquad\qquad 3.4.4$$

dVol is a small volume that has a kinetic energy, described by

$$E_{kin} = \frac{dm}{2} U_2^2 - \frac{dm}{2} U_1^2 = \frac{dm}{2} (U_2^2 - U_1^2) \qquad 3.4.5$$

Where the mass dm is a subject to a kinetic energy change. dm can be described as

$$dm = dx_1 A_1 \rho = dx_2 A_2 \rho = dVol\rho \qquad\qquad 3.4.6$$

Since there are no leakages in the tube the law of conservation of energy states that

$$dpdV = \frac{dVol\rho}{2}(U_2^2 - U_1^2)$$

$$dp = \frac{\rho}{2}(U_2^2 - U_1^2) \qquad\qquad 3.4.7$$

When combining eq. 3.4.7 with 3.4.2

$$U_1 = \sqrt{\frac{2dp}{\rho(\frac{A_1^2}{A_2^2}-1)}} \qquad\qquad 3.4.8$$

This statement is not only true for incompressible fluids (such as most liquids) but also for compressible fluids (gases) for speeds ranging in low Mach numbers. The Mach number[16] is defined as ratio of the source speed (U1) and the speed of sound of the fluid.

---

[16] [1] [Physics for Scientists and Engineers Sixth Edition, P. Tipler, G. Mosca, W.H. Freeman and Company 2008, p. 523]

3.4.2 VENTURI METER

The above stated eq. 3.4.8 can be used to calculate the volume flow with two similar methods: the Venturi meter and the orifice meter.

The Venturi meter consists of a tube that is contracted to a certain radius for a short length and then returning to the original radius of the tube. Given that the pressures p1 and p2 can be measured one can calculate the velocity v1, and hence even the volume flow, of the fluid flowing in the tube.
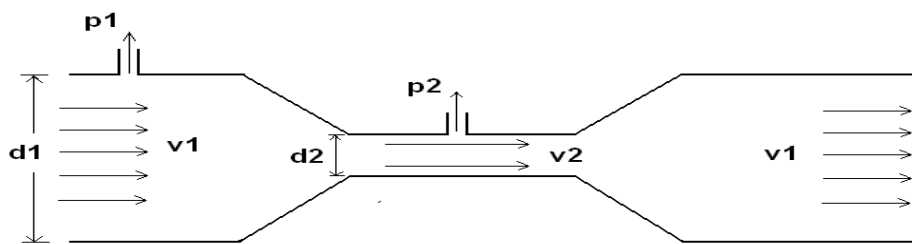

Fig. 3.4.1. An illustration of the principal behind the contruction of a Venturi meter.

Using equation eq. 3.4.8 for the Venturi meter the velocity of the flow is:

$$U_1 = \sqrt{\frac{2dp}{\rho(\frac{d_1^4}{d_2^4}-1)}} \qquad\qquad 3.4.9$$

3.4.3 ORIFICE METER

The orifice meter is of similar construction, the difference is that the orifice has a small disc with smaller inner radius than that of the pipe. By measuring the pressure one tube diameter d1 before the orifice and a half tube diameter after the orifice one can calculate the velocity v1 and the volume flow through
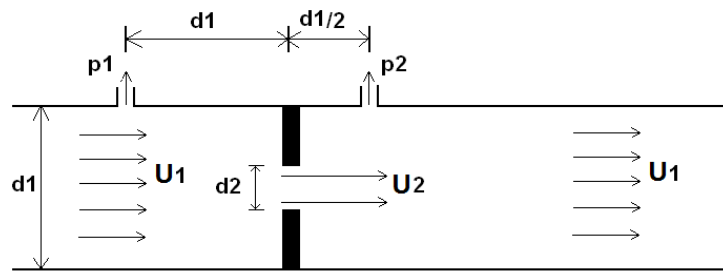
the tube.

Fig.3.4.2. An illustration of the principal behind the construction behind the orifice meter. The orifice is the thicker wall inside the pipe with an opening diameter d2.

With the notations in the figure 3.4.2, eq. 3.4.8 would yield:

$$U_1 = \sqrt{\frac{2dp}{\rho(\frac{d_1^4}{d_2^4}-1)}} \qquad\qquad 3.4.10$$

3.4.4 PITOT-PIEZOMETER

The Pitot-Piezometer is based on two different measurement techniques, see fig. 3.4.3. The first is a Pitot tube (B) which measures the total pressure created by the airflow, i.e. a tube with its opening directed toward the incoming airflow (A). The second is a Piezometer tube (C) which measures the static pressure of the airflow, by having a tube with one end plugged shut and tiny holes located perpendicular to the airflow.
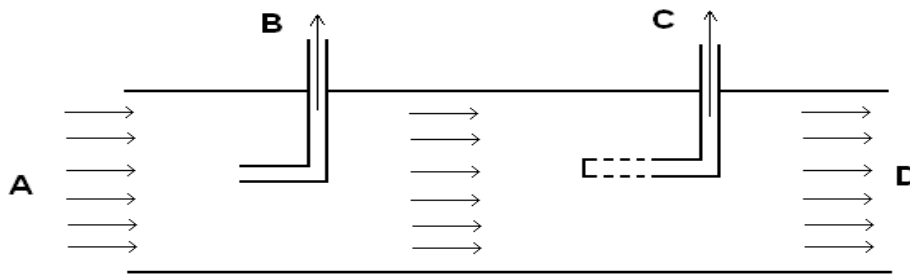

Fig. 3.4.3 A incoming airflow, B pressure from the Pitot tube, C pressure from the Piezometer tube, D outgoing airflow.

Bernoulli's equation states that the total pressure is equal to the sum of the dynamic pressure and the static pressure, i.e. the dynamic pressure is given by:

$$p_d = \frac{\rho * U^2}{2} = p_t - p_s \qquad\qquad 3.4.11$$

giving that the velocity of the airflow is:

$$U = \sqrt{\frac{2*(p_t - p_s)}{\rho}} \qquad\qquad 3.4.12$$

3.4.5 TESTING AND VERIFICATION

In comparison to the Venturi and orifice meter, the Pitot-Piezometer has a very simple design. The simple design comes for the cost of accuracy. With a Venturi or orifice meter the accuracy is determined by the design, i.e. if the design is poor the measurements become poor. Since our combined knowledge in building stuff with great accuracy is quite limited the Pitot-Piezometer seemed as a good place to start.

The Pitot-Piezometer tube had a very crude design (see fig. 3.4.4), consisting of a plastic tubing through which the air will flow. The pressure sensors were placed outside of plastic tubing connected to smaller plastic tubes which in turn was inserted into the larger tube and fixated in the right orientation.
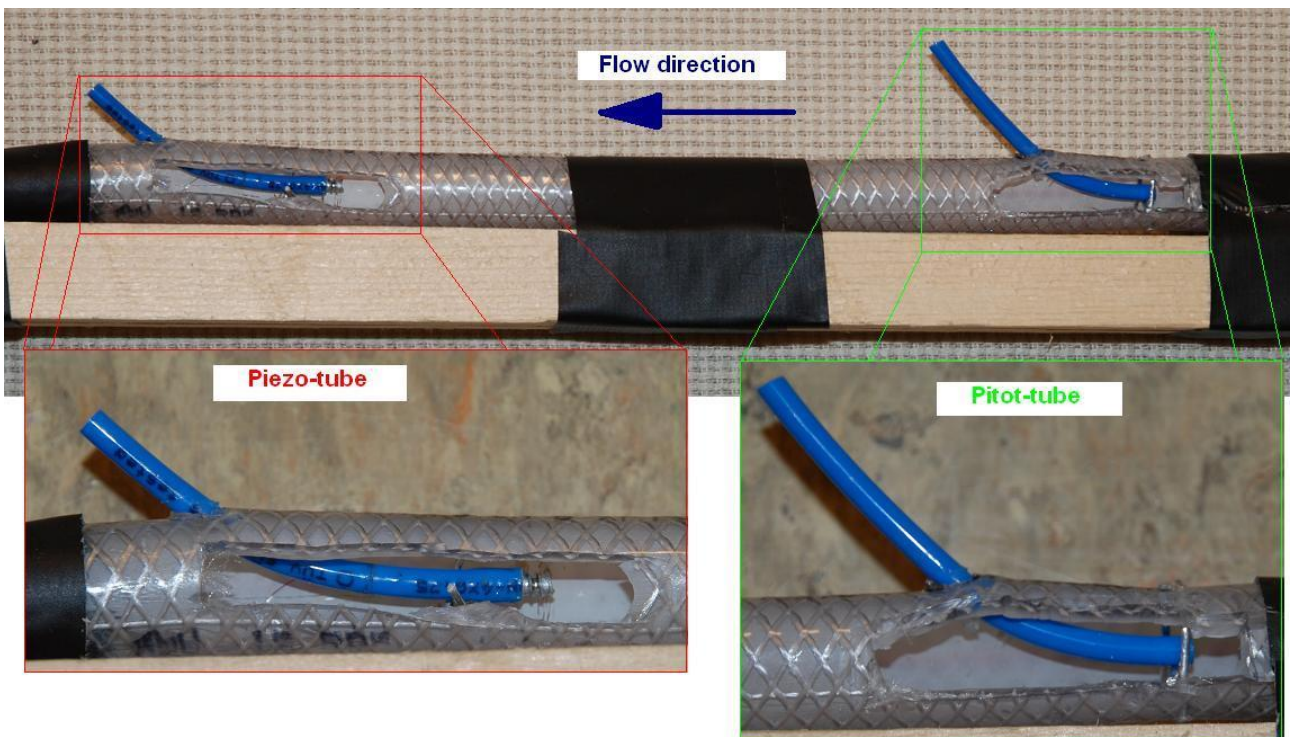
Fig. 3.4.4. Illustrates how the Pitot-Piezometer was built. The Pitot- and Piezo-tube placement and orientation is shown in the cross-sections.

In order to test the Pitot-Piezometer, the pressure sensors had calibrated and evaluated if they would react to the pressure in the flowing air with different flow rates.

The next thing is to determine the quantity of the air flow. With a simple fill test one can measure the time it took to fill an object, i.e. a large ball, with a known volume. As known from earlier theory the volume flow is equal to the quota of the change in volume and the change in time. This fill test is performed many times in order to get a more accurate mapping between the pressures measured in the tube and the time it took to fill the known volume, i.e. mapping between the "measured" dynamic pressure and the volume flow. The dynamic pressure is not directly measured, rather calculated from the difference between the total pressure and the static pressure measurements.

It should be noted that the "known" volume is not actually a hundred percent known, since the object is an elastic ball that will stretch a bit when it's being filled. For that reason the pressure inside the ball was monitored so that the ball was filled to a predetermined amount of pressure. This ensures that the volume of air inside the ball will be the same throughout all the tests.

To determine the quality of the measurements, i.e. the accuracy of the measurements, one would have to calibrate it against another flow meter. Since there were no flow meters at disposal, the Pitot-Piezometer would only give a rough estimate of how much airflow there is and cannot really be regarded as the absolute truth within a tolerable error boundary.

Below some of the possible inaccuracies are listed:

1. leakage in tube

2. poor workmanship

3. calibration of pressure sensors

4. noisy signal

3.5.1 THEORY

When a fluid is transported through a channel the roughness of the channel's inner surface gives rise to a pressure drop. The pressure drop is not only dependent of the roughness but also to the characteristics of the flow, the temperature, the viscosity of the fluid, the mass flow rate and the length and hydraulic diameter of the channel. When a compressible gas such as air is flowing through a channel the gas speed will increase due to the change in static pressure (and therefore density) along the length of the channel. But as the speed increases the density of the gas decreases accordingly which makes the mass flow through the channel constant. The mass flow will also induce a change in temperature of the gas along the channel. The change in temperature is very small for speeds under 0.3 Mach and for simplification purposes the flow is considered isothermal[17].

By measuring the pressure drop along a channel with known length, hydraulic diameter and absolute roughness the mass flow rate can be calculated by the formulas 3.5.1 to 3.5.3 assuming that:

- The process is both isothermal and adiabatic.
- The airspeed never exceeds 0.3Mach.
- No mechanical work is added or done by the gas along the channel.
- The frictions factor is constant along the channel.
- The flow is turbulent with a fully developed profile.
- The hydraulic diameter is constant along the channel.
- The channel is not induced to any changes in elevation.
- The pressure drop is linear along the length of the channel (no sharp corners).

[17] See appendix A for proof

In order to determine the characteristics of the flow the Reynolds number has to be evaluated. By manipulating the equation for Reynolds number, equation 2.3.1, one can determine the flow characteristics from the mass flow rather than the air speed.

$$Re = \frac{Ud}{v} \rightarrow \left[U = \frac{\dot{m}}{A\rho}, v = \frac{\mu}{\rho} \right] \rightarrow$$

$$Re = \frac{\dot{m}d}{A\mu} \qquad\qquad 3.5.1$$

For a smooth and circular pipe the flow characteristics is laminar for Re<2300 and turbulent for Re>2300[12]. The Reynolds number for the pipe and hose used to measure the mass flow stretches from approximately 4000 to 85000 and therefore has a turbulent profile.

The friction factor of the channel is not only dependent of the absolute roughness of the inner walls but depends also upon the flow characteristics (Reynolds number). In order to approximate the friction factor for different flow characteristics one could use the Colebrook's formula[13] which state as follows.

$$\frac{1}{\sqrt{f}} = -2 * log10 \left(\frac{2.825}{Re\sqrt{f}} + \frac{k_r/d}{3.72} \right) \qquad\qquad 3.5.2\text{[18]}$$

Colebrook's formula is only valid in the transition zone which stretches from the limit of laminar flow at Reynolds numbers of approximately 3000 to the "fully rough flow" region.

---

[18] [8] [*Applied Mathematics Letters Vol. 24 Issue 8,* D. Brkić, August 2011, *p. 1379-1383*]
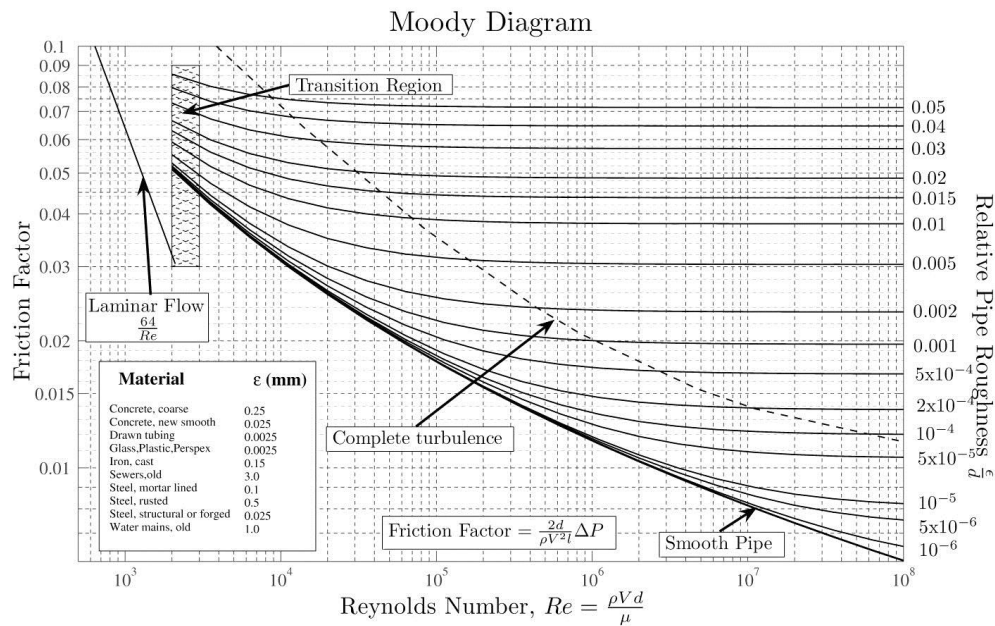
Fig. 3.5.1 Illustration of the friction factor versus Reynolds number for different absolute roughness's. Colebrook's formula is applicable from the transition region to the border of complete turbulence. Graph retrieved from Wikipedia.

When the friction factor is known for a certain chosen mass flow the downstream pressure (p_2) can be determined for a series of upstream pressures (p_1) by the equation 3.5.3. For a constant friction factor and mass flow the pressure drop will depend on the length and diameter of the channel that is below the upstream sensor and the total mean pressure will depend on what happen to the channel after the downstream sensor as well. Equation 3.5.3 is originally used for pressure drop calculations of large lengths of natural gas pipe lines where the pressure drop exceeds 40% of the upstream pressure.

$$p_1^2 - p_2^2 = Z_m R_{air} T_{air} \left(\frac{\dot{m}}{A}\right)^2 * \left(f\frac{L}{d} + 2 * \ln\left(\frac{p_1}{p_2}\right)\right) \qquad 3.5.3[19]$$

Where Z_m is the mean compressibility factor of air.

---

[19] [9] [*Compressible gas flow,* Pipe flow Calculations, *Retrieved 06-03-2013 at http://www.pipeflowcalculations.com/pipe-valve-fitting-flow/compressible-gas-flow.php*]

3.5.2 IMPLEMENTATION

The static pressure difference is measured by inserting small tubes at two different locations on the hose/tube that is transporting air to the winding. In the end of each smaller tube a pressure sensor is mounted.
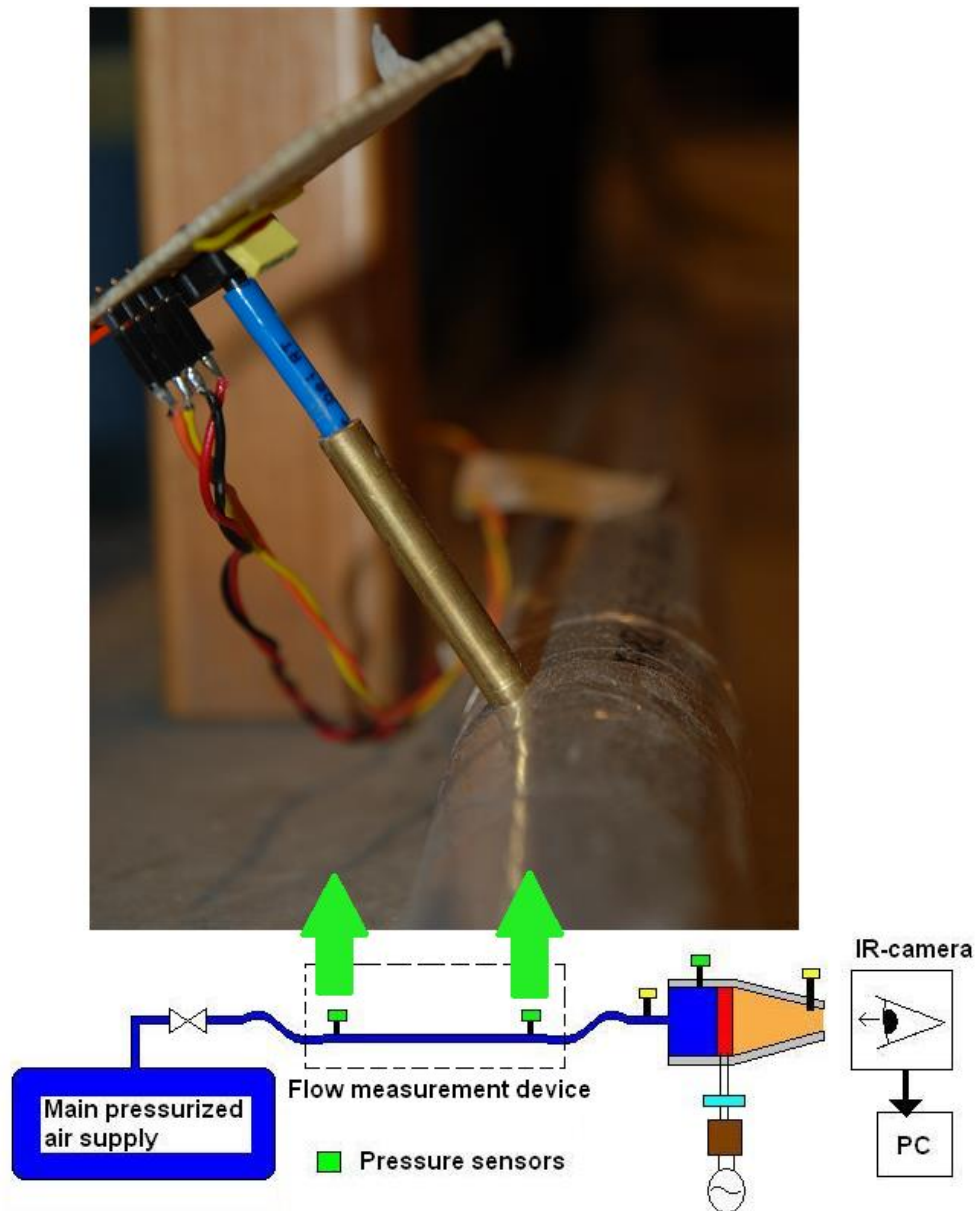
Fig. 3.5.2 Illustration of the placement of the pressure sensors in order to measure the pressure drop over the hose/tube that is transporting air to the winding.

Since equation 3.5.2 is implicit and that equations 3.5.1 through 3.5.3 are all dependent on the results from one another, one need to use iterative numerical methods in order to determine the mass flow from the measured pressure drop. The mass flow has to be determined for every sample in the recorded data and in order to save computation time it was chosen to evaluate the mass flow for a range of possible pairs of up- and downstream pressures and then store the data in a three dimensional matrix. The matrix can be used later to retrieve the mass flow corresponding to a certain measured pressure drop.

Since the geometrics of the pipe do not change and the process is considered isothermal the Reynolds number is linearly dependent on the mass flow rate, see equation 3.5.1. When building the matrix one needs to decide how large error one can accept. Since a tight mass flow grid gives good resolution but cost in computation time one has to find a balance. It was chosen to use every 50th Reynolds number is the range from 3000 to 84500, the range stretches from the transition region to a mass flow that gives a velocity of 0.3 Mach in the hose. This gives a resolution of 3.1mg/s or 0.05 l/minute @ 6bar and a reasonable computation time.

For every Reynolds number in the measuring range the friction factor of the hose were evaluated by Newton iteration of equation 3.5.2. When determining the friction factor by Colebrook's formula one need to know the absolute roughness of the hose/tube. In the following table some different values of the absolute roughness coefficient are presented.

Type according to source	Absolute roughness [mm]
PVC pipe[20]	0.005
Hose (rough estimate)[20]	0.0187
Flexible rubber tubing – smooth[21]	0.006-0.07
Drawn Tubing, glass, plastic[21]	0.0015-0.01
Reinforced PVC[22]	0.14
Rigid PVC[22]	0.005
Neoprene[22]	0.0818
Copper pipe (new)[23]	0.0015

Table 3.5.1 Absolute roughness for different materials.

When the friction factor of the hose is determined (for a chosen absolute roughness factor) a series of possible upstream pressures is chosen. For every

---

[20] [10] [Norsok standard P-001 "Process Design", Edition 5, September 2006, p.9]
[21] [11][Absolute Roughness of pipe materials, Native Dynamics, May 26th 2012, Retrieved 06-03-2013 at http://nativedynamics.com.au]
[22] [12] [Pipe flow wizard v1.12, PipeFlow®, Daxesoft Ltd.]
[23] [13] [Fluid Mechanics, Binder, R.C. , Prentice-Hall, Inc. (Englewood Cliffs, NJ), 1973]

combination of mass flow, friction factor and upstream pressure a downstream pressure is evaluated by Newton iteration of equation 3.5.3. These values are mapped into the three dimensional matrix.

In order to determine the absolute roughness of the hose used as flow meter some experimental measurements is made. The experiments are done by letting the air flow at a steady pace trough the hose and fill an elastic ball with known volume until it reaches a predetermined pressure. The air mass of the ball is therefore known (the air temperature is considered constant at 18°C). By dividing with the time it took to fill the ball the mass flow rate is determined. The measured flow rate and pressures gives a dot in a three dimensional space. In order to determine the absolute roughness of the hose different pressure-mass flow planes are created from equations 3.5.1-3, each for a specific absolute roughness. The absolute roughness of the plane that is closest to the measured values is used as the parameter for determining the mass flow rate in the hose. In order to determine if the absolute pressure in the hose would influence the results three different measurement series is carried out. One with a long piece of hose left after the downstream pressure sensor, one with a nozzle attached to the end of the hose and at last a test where the hose were cut shortly after the downstream pressure sensor.
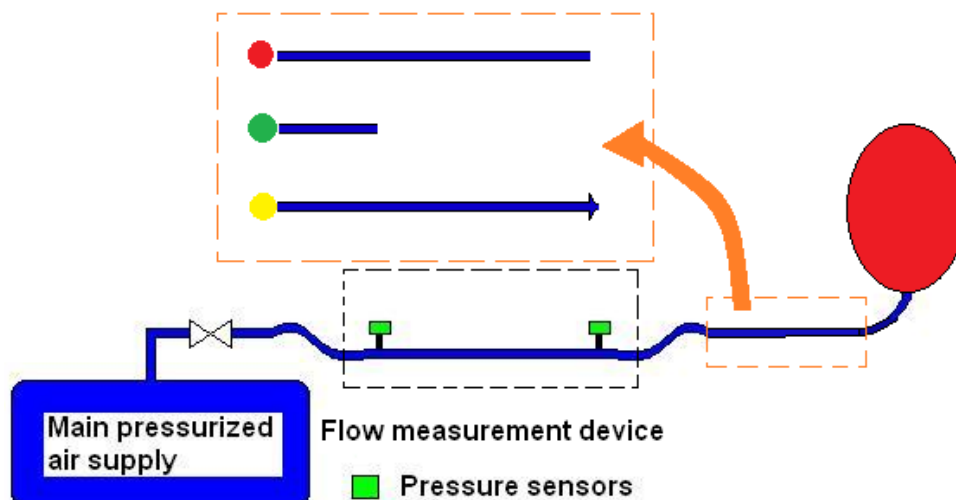
Fig. 3.5.3. Illustration of the ball measurement set up, the three different hose endings change the absolute pressure inside the hose.

To get a second opinion regarding the absolute roughness of the hose another experimental measurement is made as well. A copper pipe is connected in series with the hose. The absolute roughness of copper is better documented and therefore a relatively small interval from where the real roughness of the pipe should lay within is narrowed down. By measuring the pressure drop over both the copper tube and plastic hose the mass flow rate could be evaluated from data derived from the copper tube and thereof the absolute roughness of the plastic hose.

3.5.3 RESULTS

Figure 3.5.4 shows the mean percentage difference between the mass flow measurements done with the elastic ball and theoretical mass flow for different absolute roughness coefficients. The difference between measured and theoretical mass flow reaches a minimum when the absolute roughness coefficient has a value of 0.001915mm. With this absolute roughness the mean difference between measured and theoretical mass flow value is less than one percent under the assumption that the air mass of the ball is correct.
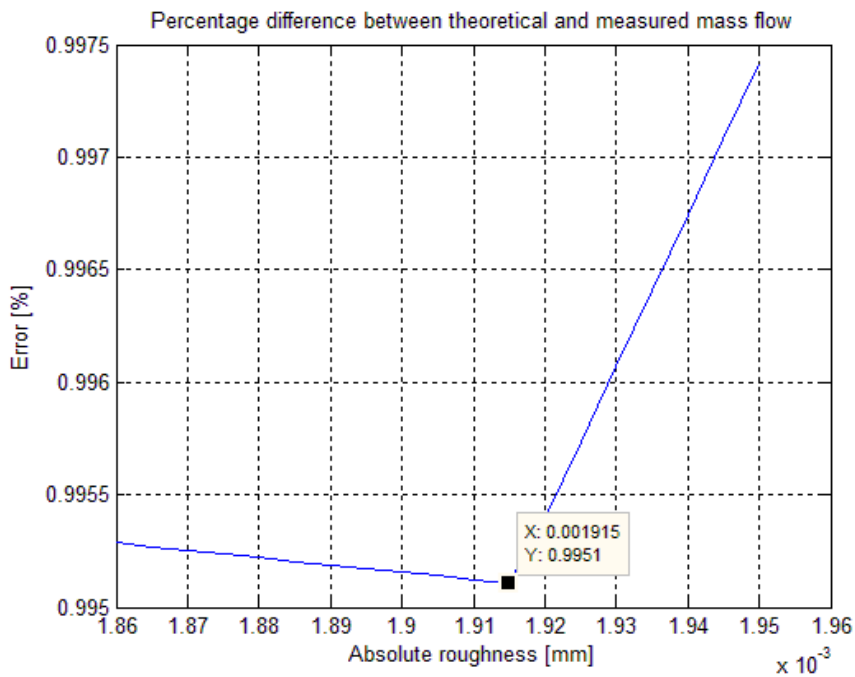

Fig. 3.5.4. Illustration of the mean difference between measured and theoretical values of the mass flow for different absolute roughness coefficients.

The theoretical mass flow plane for different up- and downstream pressures is illustrated in figure 3.5.5. The absolute roughness used for this plane is 0.001915 mm. The green, yellow and red dots represent measured values from the different measurement series, the color coding is the same as in figure 3.5.3.
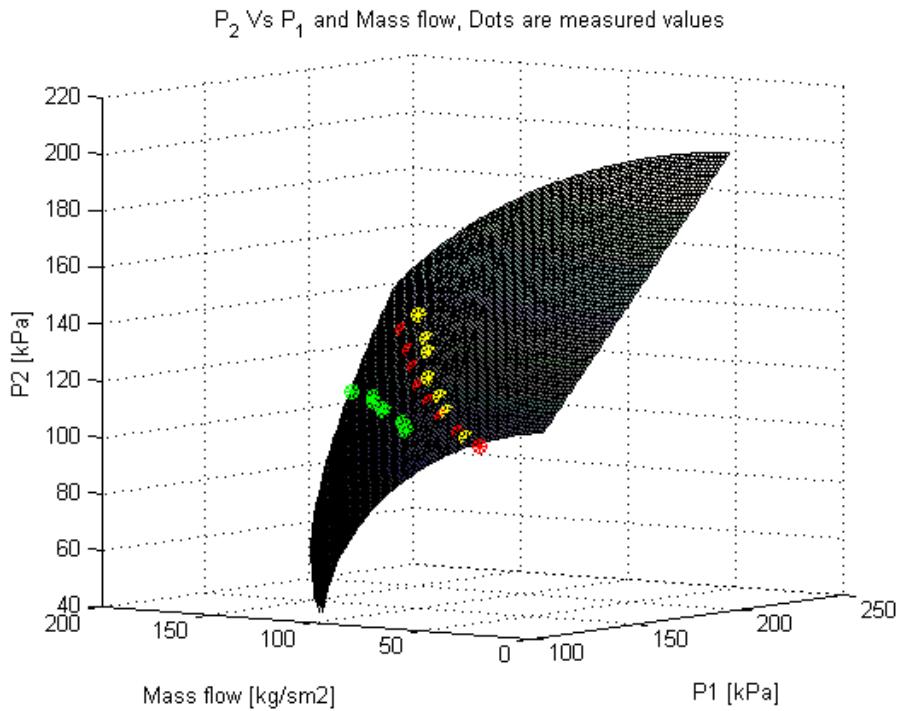
Fig. 3.5.5. Illustration of the theoretical "mass flow plane" for an absolute roughness of 0.001915 mm as well as measured values (colored dots) from the ball measurement series. The lower right corner of the plane is closest to the reader.

The absolute roughness coefficient of the copper pipe is assumed to lie between 0.001 mm and 0.002 mm. Figure 3.5.6 show measured mass flow and absolute roughness of the plastic hose, both mean and instantaneous values if the copper pipe has an absolute roughness of 0.0015 mm.
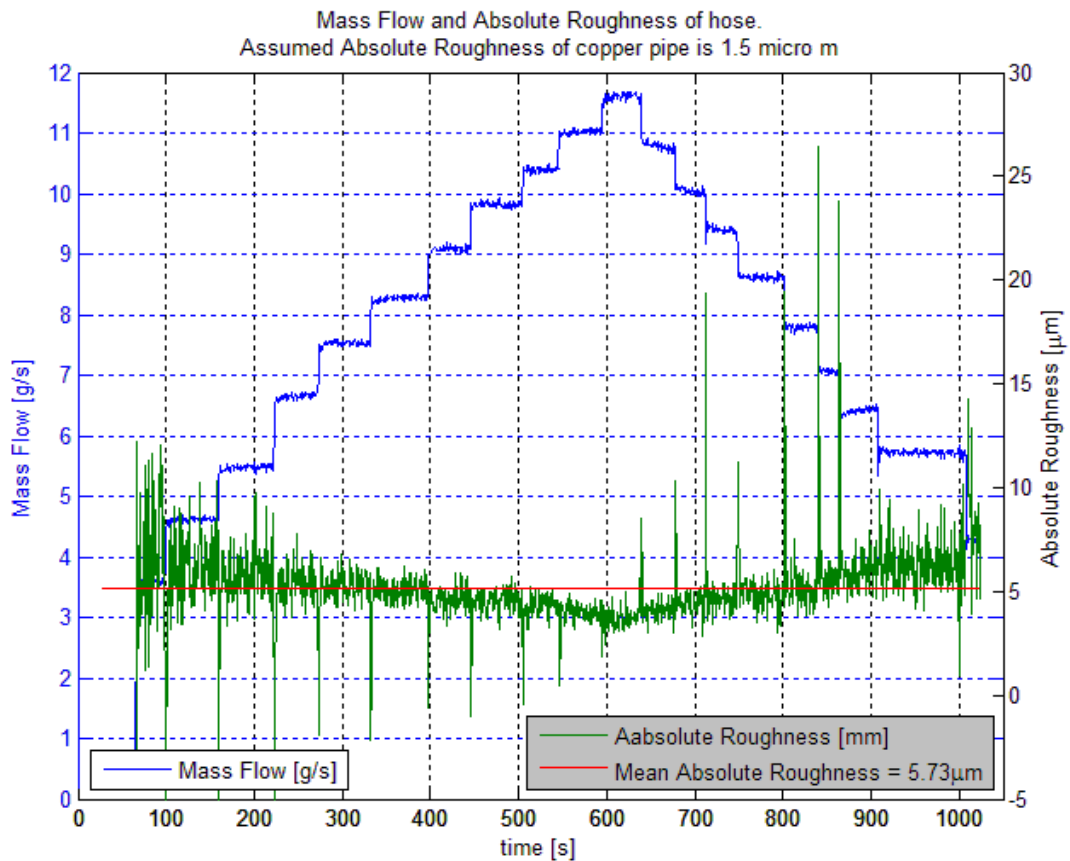

Fig. 3.5.6. Illustration of the absolute roughness of the hose and mass flow under the assumption that the copper pipe has an absolute roughness of 0.0015 mm.

If the absolute roughness of the copper pipe lays between 0.001 and 0.002 mm, the measured value of the absolute roughness of the hose is somewhere between 0.00511 mm and 0.00632 mm.

3.5.4 CONCLUSIONS AND EVALUATION

The measurements done with the ball indicates that the plastic hose ought to have a really low absolute roughness value in comparison to those presented in table 3.5.1. This value is strongly connected to the size of the ball as well as the precision when measuring the time it took to fill it. Since the test shows a very small absolute roughness for the hose it gives an indication that the ball size is overestimated. When examining the impact of the ball diameter on the absolute roughness it shows that an error of 5 mm when measuring the ball diameter of 700 mm gives an absolute roughness error of nearly 100%. The time measurement which also is of importance is sampled with a rate of 4 Hz which gives an error of half a second in worst case. Because of the reasons mentioned above the ball measurements are not to be trusted when determining the absolute roughness of the hose. Even if the ball measurements can not be used for accurate determination of the absolute roughness of the hose it show that the theoretical formulas and assumptions holds since it is possible to fit all the measured points into one theoretically determined plane, see figure 3.5.5.

A copper pipe has a well-documented absolute roughness since it is a very common component in regular water pipe installations. Therefore it is decided to build a second flow meter of the copper pipe and use that in series with the hose. The absolute roughness of the copper pipe can be considered known and therefore it is possible to decide the roughness of the hose since they are connected in series. The results from the measurements with copper pipe show an absolute roughness of approximately 6μm which also is confirmed by the documentation available on PVC coated hoses. This result also confirms the absolute roughness of the copper pipe since both values match the literature. Since a second flow meter in copper is built it will be used instead of the hose flow meter. The reason for determining the absolute roughness of the hose even though it after this point in time will not be used any more is to be able to determine the mass flow rate in the old measurements which were executed with the hose flow meter in operation.

The main sources of error concerning the flow measurement are:

- The precision of the pressure sensors which has a maximum absolute error of $\pm$ 0.5% of measured value.
- The assumption that the process is isothermal which in the worst case scenario would give an error in pressure reading of $\pm$ 0.7%. (Appendix A)
- The assumption of known and uniformed absolute roughness of the copper pipe. The friction factors impact on the results change with the type of flow and has to be determined for every individual case. But the trend is that the error increases as the flow becomes "more turbulent".
- That the processes is adiabatic, meaning that no heat is transferred to or from the pipe or hose that the air is travelling through. This has somewhat been helped by isolating the copper pipe. At air speeds under 0.3 Mach this source of error is small and it has been chosen to neglect it.
- Pressure changes due to elevation and turns in the hose or pipe. The layout of the hose/pipe has been done to avoid turns and elevations and therefore has no concern been taken to this source of error.

The precision is evaluated for the case of a mass flow of 9 g/s (which is in the top range of used mass flows) and an absolute roughness of 15 μm for the copper pipe flow meter. If the upstream pressure sensor would show 1.2% too much and the downstream sensor 0.5% too low and the real absolute roughness would be as low as 10 μm then the mass flow error would be 4.5%.

Another way of evaluating the precision of the flow meter is made from the heat measurements done with the funnel and air temperature measurement equipment in use. Since the law of conservation of energy has to be fulfilled and the air temperature rise and mass flow is known it is possible to determine the amount of energy that is being dissipated by the air. Since the heat loss in the winding can be considered known it would be enough to be able to determine all other heat transfers taking place in the winding in order to determine the precision of the flow meter. Since it is hard to accurately determine the impact of conduction and natural convection one could try to determine the trends that the different error sources would give to the measured results. When describing the trends one can use the conservation of energy as base and therefore try to explain what impact, i.e. a misguiding flow meter will have on the dissipated energy. If all sensors are measuring correct and the heat transfers executed by natural convection and conduction as well as heat loss in the winding is known one would be able to subtract heat losses by dissipated energy and get the answer zero.

The energy being dissipated by the forced convection is dependent on the mass flow rate and air temperature rise, see equation 2.3.13. The outlet air temperature is measured by thermocouples and the reading error from them is assumed to be stochastic. The error from the flow meter should rise with mass flow magnitude since the friction factor becomes more dependent on the absolute roughness as the Reynolds number increase, se figure 3.5.1. That means that it becomes more critical to have an accurately known absolute roughness as the mass flow inside the hose/pipe increases. If the flow meter is correct over a range of mass flows the amount of dissipated energy would according to equation 2.3.13 be the same regardless of mass flow rate (if the heat losses are held constant) since the rise in air temperature will increase when the mass flow decreases. Figure 3.5.7 show the difference between heat losses and energy being dissipated by air.
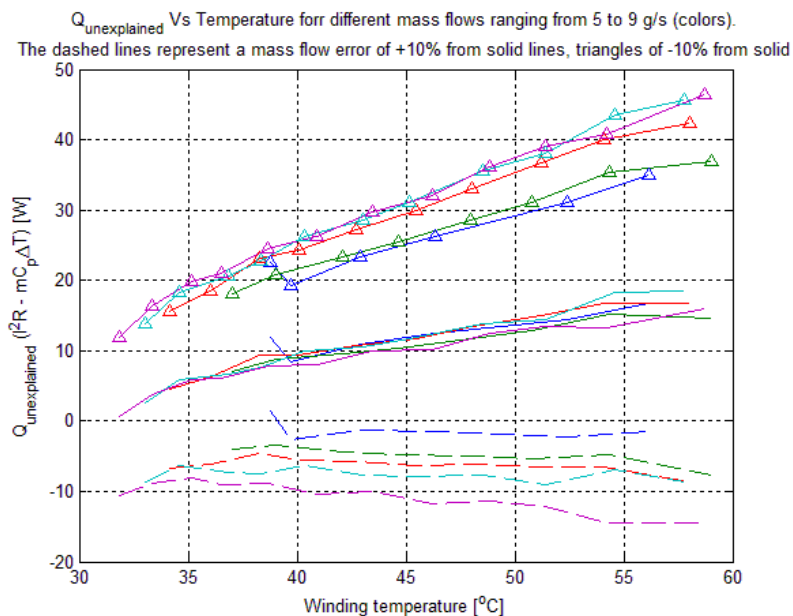

Fig. 3.5.7. Illustration of the energy left when withdrawing heat carried away by air from the total heat losses versus winding temperature. The solid lines are measured values, the dashed lines are measured values with a mass flow error of 10%, and the triangles have an error of -10%. The colors represent different measurement series where the mass flow has been held constant and the heat losses been increased in steps from 100 to 300W. The mass flow in the different measurement series is ranging from 5 to 9g/s in steps of approximately 1g/s.

In figure 3.5.7 one can see that the energy error from the different measurement series seem to be dependent on the winding temperature rather than the flow rate. This conclusion comes from the fact that the solid lines which are measured values lay close to each other even if the mass flow changes between them. If the mass flow meter would show a large error a greater scatter between the measurement series would be expected. As the triangle and dashed lines in figure 3.5.7 show, the scattering of the lines is increased when an error is intentionally induced on the measurement results.

Since the energy left after withdrawing forced convection from heat losses seems to be dependent on the temperature in the winding rather than the mass flow it indicates that the natural convection and conductive heat transfers has a noticeable impact on the results even if great effort has been made in order to isolate the measurement setup. The conductive and natural convection heat transfers is not dependent of the mass flow and depend on the temperature difference between winding and surrounding, see equation 2.2.7. Since the convection coefficient (h) and area is hard to analytically determine it is chosen to use the total winding surface area and increase the convection constant stepwise and study the impact on the measurement results. The area exposed for convection and convection constant is seen as design parameters and it is chosen to use the surface area of the winding and try different convection constants. Figure 3.5.8 show the energy left with and without other heat conduction ways than forced convection present.

$Q_{unexplained}$ Vs Temperature for different mass flows (colors)
The dashed lines represent "unexplained" energy with no other heat transfer ways present.
The solid lines represent "unexplained" energy with a natural heat transfer of 2.6 W/Km^2.
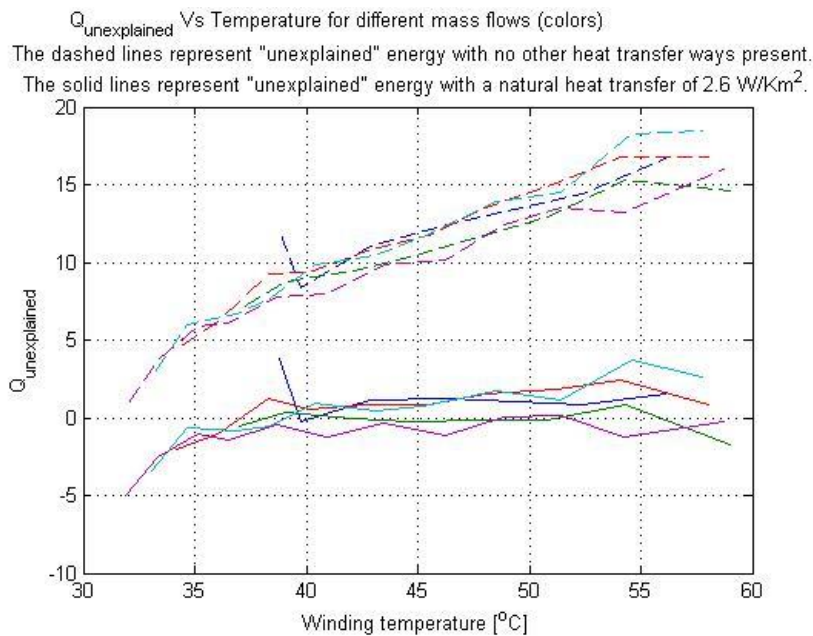
Fig. 3.5.8. Illustration of the energy left when withdrawing forced convection (dashed lines) and both forced convection and other heat transfer ways (solid lines) from total heat losses. The colors represent different measurement series using different mass flows.

In figure 3.5.8 one can see that adding a heat transfer coefficient of 2.6 W/Km^2 over the total winding surface area centers the measurement series and the results seems to fulfill the energy conservation law in a better way. The scatter that still exists in solid lines in figure 3.5.8 is considered measurement insecurities due to sensor misreading.

If the air temperature measurements are perfect and the conductive and natural convective heat transfers is accurate is the mean absolute error of the mass flow meter 0.6%.

3.6 CONTACT TEMPERATURE SENSORS[24]

There are several types of contact temperature sensors to choose from. The two most well-known are the thermocouple and the resistance temperature detector (short RTD). In this section some of the basics of these sensors are briefly examined. These sensors are then compared to each other in some aspects to ease the decision in which to use.

In order to measure the winding temperature the sensors have to be placed somewhere within the winding. Possible placements and things to consider before placing the sensors are briefly discussed.

3.6.1 THERMOCOUPLE THEORY

A thermocouple is a simple device for measuring temperature. The thermocouple is made up of two wires of different metals. The wires are soldered or welded together at one end, called the junction end or measuring end, and left free at the other end, called the tail end or reference end. The junction end is inserted to the environment in which the temperature shall be determined, while the tail end remains in ambient temperature connected to the measurement equipment.
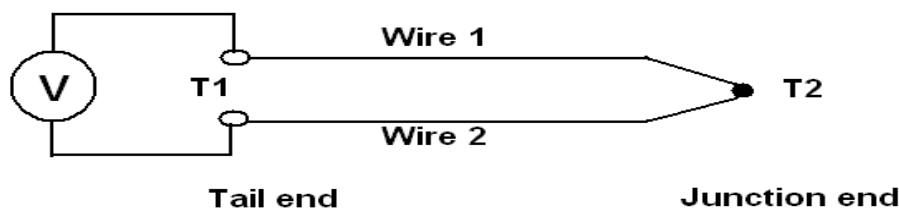
Fig. 3.6.1. A schematic sketch of the thermocouple.

As the junction end is heated, a voltage difference can be measured at the tail end between the two thermo elements. This means that the thermocouple is a temperature-voltage transducer.

The relation between the temperature and voltage is described by:

$$Emf = \int_{T_1}^{T_2} S_1 - S_2 \, dT \qquad\qquad 3.6.1$$

---

[24] [14] [*Temperature Sensors,* The Watlow Educational Series Book Four, Watlow St. Louis, 1995, *retrieved at 2013-05-31 from http://www.m-r-c.co.il/Media/Doc/TechnicalInformation/Temp_Measuring1.pdf*]

where Emf is the electromotive force across the reference end, S_1 and S_2 are the Seebeck coefficient for the two metals and T_1 and T_2 are the temperature at the reference end and measuring end.

From the equation one can conclude that if both wires are made of the same material the Emf will be zero, i.e. the thermocouple must have wires of different materials for it to become a temperature sensing unit. Also if both the junction end and the tail end is located in the same environment, i.e. in the same temperature, it will yield zero voltage. In order to measure the temperature the junction end and the tail end must be located in environments with different temperatures, making the thermocouple a differential measurement sensor rather than an absolute temperature sensor. In order to get an accurate absolute temperature measurement the temperature at the tail end must be known.

3.6.2 PROS AND CONS WITH THERMOCOUPLE

Pros with thermocouple:

- The temperature ranges: The thermocouple can be used from -200°C to +2500°C, depending on which thermo elements are used.
- Rapid response: The low thermal capacity of the thermo elements gives the thermocouple a rapid   response to temperature changes, especially so if the junction end is left exposed, given that the environment allows this without affecting the wires.
- No self-heating: Since the thermocouple does not require any external power source for excitation, the thermocouple will not t self-heat.

Cons with thermocouple:

- The inherent inaccuracies in the thermo elements due to their metallurgical properties.
- The quality of the tip at the junction end. If the soldering or welding is not done properly it can change the property of the thermocouple, yielding in inaccurate measurements.
- The precision of the cold junction compensation is said traditionally to be between 1°C and 2°C. This makes that the measurements are only as accurate as the temperature at the reference end can be measured.
- Corrosion over time may occur, largely depending on the environment where the thermocouple is used, resulting in deterioration of the materials and hence the accuracy.
- Since the voltage measurements are at μV-level the susceptibility to noise, from stray electrical and magnetic fields, can be an issue.

3.6.3 RTD THEORY

The Resistance Temperature Detector measures the temperature by correlating it to the resistance of the RTD-element, i.e. the RTD is a electrical resistance to temperature transducer. Since RTD measures the resistance in order to determine the temperature they need excitation power in order to operate. When adding excitation power the RTD-element will self-heat which means that in order to retrieve accurate temperature readings the self-heating has to be compensated for.

The RTD-element is in most cases a finely coiled wire wrapped inside ceramic or glass casing. The RTD-elements are usually placed inside a protective sheet because they are quite fragile. The wire is made of pure material with predictable temperature behavior, such as platinum, nickel or copper. Predictable temperature behavior refers to that the resistance of the pure material has a near linear increase with the temperature.

Fig. 3.6.2 shows the simplest configuration of a RTD circuit, i.e. a 2-wire bridge connection. By measuring V_b and knowing the values of R1, R2 and R3 the resistance of the RTD-element can be determined. This RTD configuration is the least accurate, but is used to demonstrate how the temperature measurements work. For more accurate measurements, one could use a 3-wire or a 4-wire bridge connection instead.
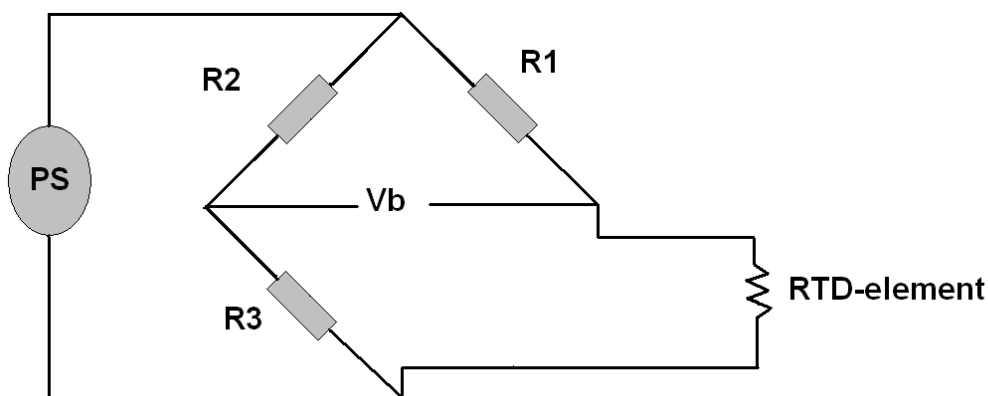
Fig. 3.6.2. A schematic sketch of the simplest resistance temperature detector configuration, i.e. a 2-wire RTD.

3.6.4 PROS AND CONS WITH RTD

Pros with the RTD:

- Accuracy: RTDs are usually very accurate, but the accuracy is temperature dependent. The accuracy is described by ±(0.15 + 0.002*T)°C or ±(0.3 + 0.005*T)°C , depending on if the RTD is class A or B. T is the temperature at which the accuracy needs to be determined, i.e. if T = 100°C then the accuracy of class A and B is ±0.35°C and ±0.80°C respectively.
- Stability: The RTDs are very stable, i.e. they drift very little over time, making the RTDs   accurate over a longer period of time.
- Temperature range: Depending on which material the RTD-element is made of the temperature ranges varies. For platinum the range is usually -200°C – 650°C. For others the range is less than that.

Cons with the RTD:

- Cost: The complexity of the manufacturing techniques and the price of the RTD-element make the RTDs quite expensive.
- Response time: The response time of RTDs is quite slow, usually measured in seconds. There are two reasons for the slow response time of the RTD. The first is that the heat has to be transferred through the casing which surrounds the RTD-element. The second reason is that the entire RTD-element must reach the same temperature in order to give a accurate temperature reading.

3.6.5 THERMOCOUPLE VS RTD

Cost: The more advanced RTD have a 2 times or higher price-tag than a comparable thermocouple assembly.

Temperature range: RTD has a range of -200°C to 500°C, while thermocouple goes up to 2500°C. If temperatures are higher than 500°C then thermocouple is the only choice.

Response time: If it's important to determine fast changes in the temperature, i.e. in fractions of a second rather than seconds, then thermocouple has the advantage over RTD.

Accuracy and stability: Thermocouple has a quite poor accuracy, usually between one and two degrees Celsius, making the thermocouple a good choice if the accuracy is not of outmost importance. Adding to that the thermocouple is more prone to drift over time, leading to more inaccurate readings if the

drift is not compensated for. If the stability and accuracy is important for the application then the RTD is the better choice.

Size: Protective sheet makes the RTD quite bulky, ranging from 3 to 6mm, while the thermocouples are much smaller, about 1.6mm with a protective sheet. With the less fragile thermocouple it is also possible to use it without the protective sheet, making it as compact as the thermo elements (wires).

As the sample rate of the data logger was limited to one sample each 4.5 seconds and that the temperature of the test object would never exceed 500°C, the RTD is the better choice in every aspect except for the size, and size do matter. It would be hard to fit a bulky RTD in the layer spacing, or in any other place for that matter, giving back the advantage to the thermocouple.

3.6.6 SENSOR PLACEMENTS

There are some things that should be considered before using contact temperature sensors when measuring the winding temperature which has to do with the placement of these. The main concern is that the sensors would interfere somehow with the winding or that the winding would interfere with the sensors. The latter concern is not really any problem in this case since the test object was not influenced by any magnetic fields or high frequencies. But when using this type of sensors in a complete machine, EMC type of interference should be considered. Some of the possibilities are illustrated in fig. 3.6.3.
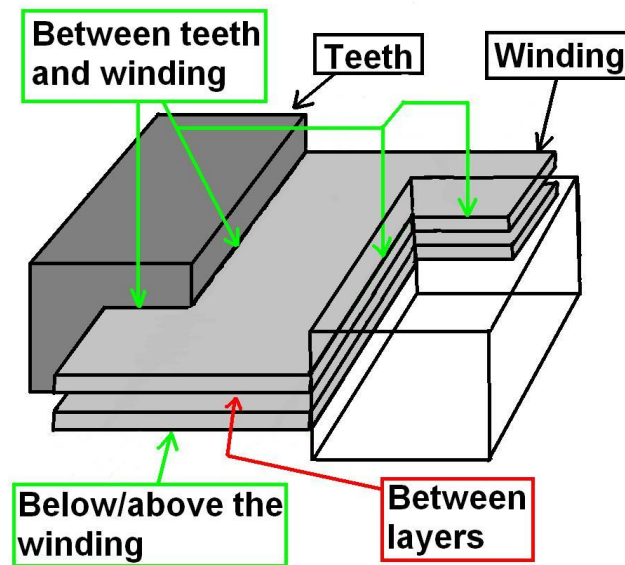
Fig. 3.6.3. An illustration of possible placements (green) and where the thermocouple has been used (red).

The obvious place, i.e. in between the winding turns, was proven to be a poor idea (see appendix B.2). This because of that it affected the geometry of the winding. But if the winding would be less tightly wound, i.e. the size of the layer spacing was greater than the size of the sensor, and then it would not matter.

One could also place these below or above the winding, i.e. below and above refers to outside of the innermost and outermost layer of the winding. At these places the sensors would not interfere with the geometry of the winding.

The third alternative is to place the sensors between the teeth and winding, if there is room for the sensors. The sensor at the short side of the teeth should

be placed at the opposite side of the air inlet, since it is possible that the temperature measurements would be a bit misleading if the cool air is directly blown on the sensor.

3.6.7 CONCLUSIONS

Thermocouples are good temperature sensors. They react fast for changes in temperature, have a wide range where they can be used and are quite accurate. But the placement of these should be considered before using them. The test object has not really any room for trying out the other thought of placements than that between the layers, and was proven to be a bad spot for this winding.

3.7.1 FINDING THE SLOTS

Previously the analyzed areas of the IR-camera footage were picked out by hand. It worked well for a couple of movies, when the movement of the camera was minimal. Trying to make a new measurement the next day, after removing the camera the day before, results most likely in that the areas has to be readjusted. This will in the long term be a very tedious process.

This is where a quite simple but very time efficient script comes in to play. The scripts main purpose is to provide the locations to where in the movies the temperatures should be analyzed. By supplying a reference frame to the script with some color restriction it will find the exact positions of where the slots are located.
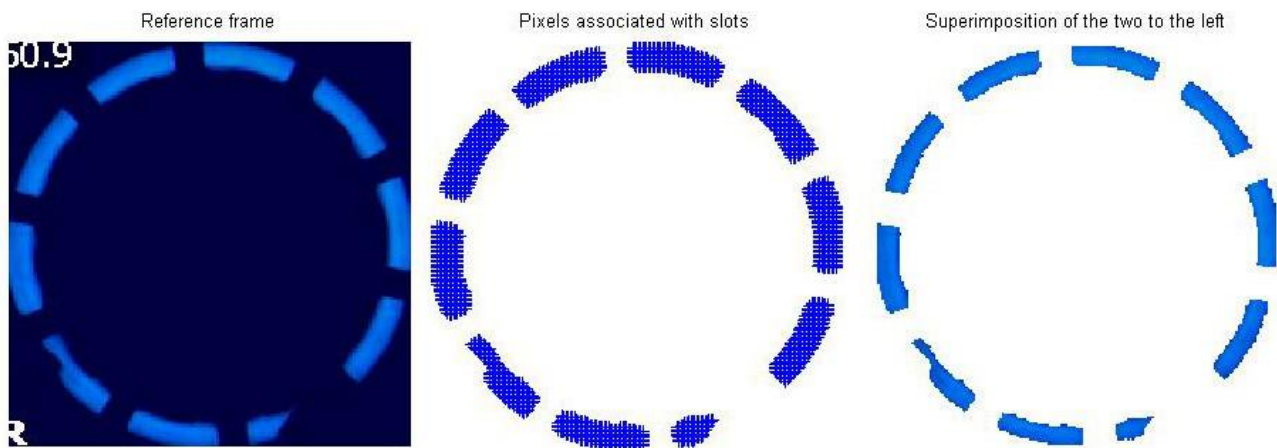
Fig 3.7.1. Above the figures are, starting from the left; the reference frame, the pixels associated with the slots and the superimposition of the two previous figures. The slots which are missing some of its pixels are due to that the power cables are connected to the winding at these spots, and hence obstructing the view.

Unlike the "background" color the boundary layer of pixels surrounding the slots are widely varying in RGB color although they look as they have the same. This means that these pixels cannot be specified with a specific RGB color code when searching for the pixels associated with the slots. For this reason the script also peel away the outermost boundary layer with pixels around the slots to prevent that any unwanted pixels showing up in the calculations.

As seen from figure 3.7.1 to the far right the boundary of the slots are almost completely without the dark blue "background" color of the figure to the left, meaning that the script has successfully found the right pixels associated with the slots.

3.7.2 CONVERTING COLORS TO TEMPERATURES

The main problem occurring in the conversion between decoded images and numeric temperature is that the reference temperature scale only contains 117(!) different color codes while the decoded image has the possibility of containing any combination of the 24 bit RGB color spectrum, i.e. over 16 million colors.
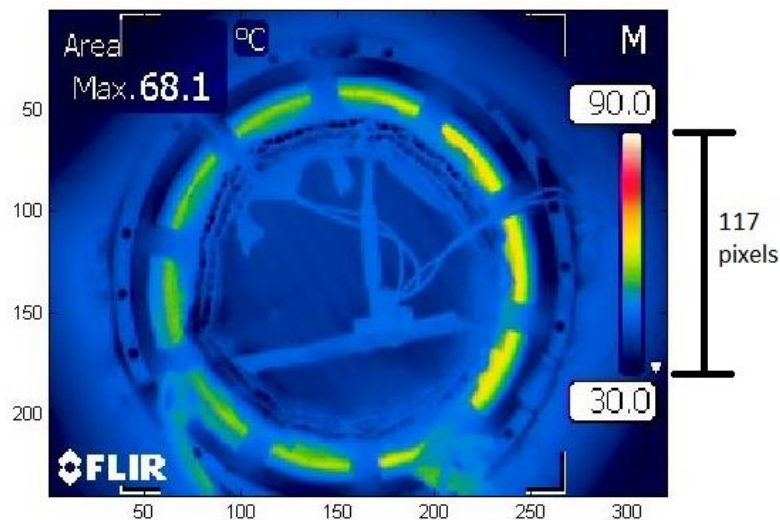
Fig 3.7.2. Showing a random frame form the IR-camera footage, enhancing the size of the temperature scale.

The resolution is wherein the problem originates. The resolution of 320x240 limits the amount of pixels that the camera can supply for the temperature scale. Unfortunately the temperature scale must also be fixated, i.e. the upper and lower limits cannot change with time since it would be too hard to extract the temperature with a Matlab script.

In order to grasp the problem at hand, one can think of the RGB colors in 3-dimensional space, with 255 variations of red, green and blue on the axis. All the combinations of the color spectrum form a cube in the Cartesian

coordinate system, with black in the origin a white opposite of the origin (see fig. 3.7.2). It is quite obvious that the possibility of a vast amount of the analyzed RGB colors will never hit any of the color codes in the references temperature scale.

If the temperature scale was a straight line confined within the RGB cube it would be simple to determine the temperatures associated with a color. The gray scale is an example of a straight line, running from black to white. Simply by slicing the cube into planes with the straight line as the normal to the planes, one can check which plane a pixels color belongs to or is closest to and from that the temperature is known. Unfortunately this is not possible with this temperature scale as it is very non-linear, as illustrated in fig. 3.7.3. The figure illustrates also how small the part of the RGB cube consists of the temperature scale.
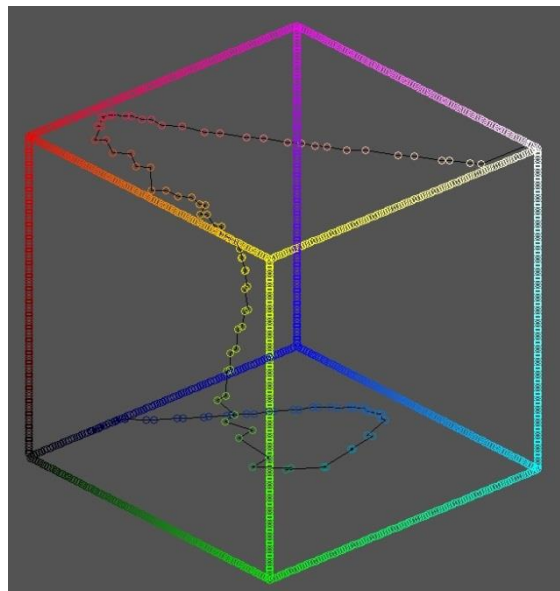
Fig. 3.7.3. Illustration of the outline of the RGB space as a cube. Inside the cube the temperature scale is plotted.

The simplest way of determining the position of an object that is confined within a cube is to measure the distances from three fixed points inside that cube. By mapping each point of the temperature scale with the distances from the three fundamental colors of RGB space (Red, Green and Blue) the result is another 3-dimensional space, shown in fig. 3.7.4.
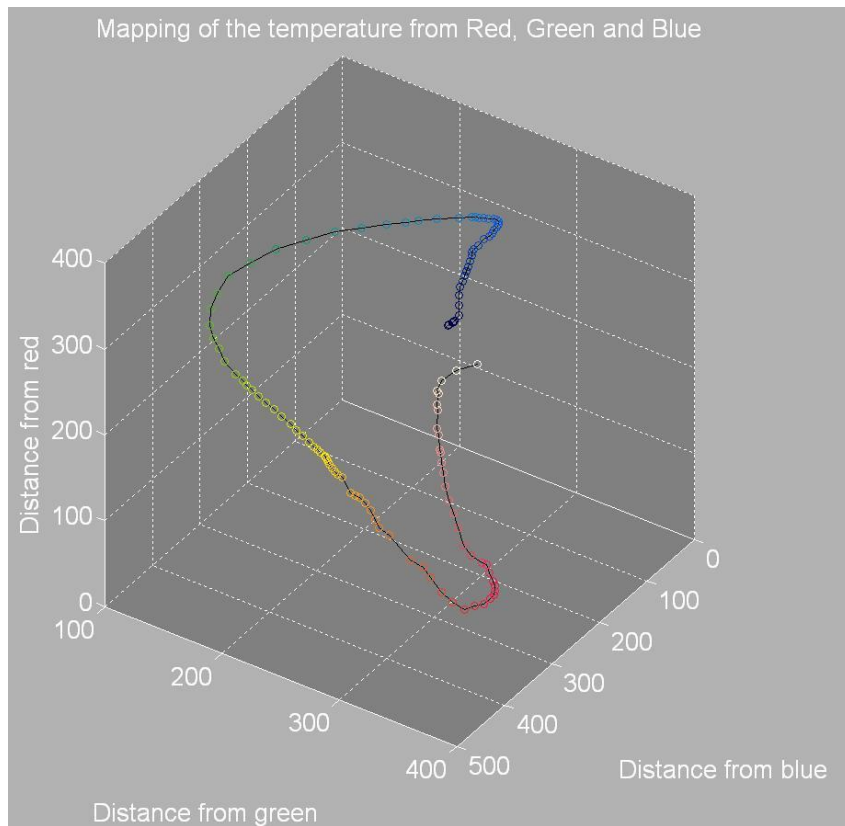
Fig. 3.7.4. Temperature scale remapped as the distances from Red, Green and Blue.

By having this as a reference when converting the colors of the pixels to temperatures, one can map the pixels one by one and taking the Euclidean distances from each point in the reference temperature scale to the pixel. The minimum of the distances corresponds in most cases to the right temperature. In some of the more rare cases the pixels maps to a place that is somewhere inside of the U-turn in the lower part of fig. 3.7.4**.** These temperatures may show up as larger spikes when plotting the analyzed temperatures vs. time, i.e. a sort of disturbance.

The problem is that there are some colors inside the U-turn that are closer to the pink (higher temperature) but should actually be mapped towards the lighter orange to get rid of the larger spikes. This can be achieved by comparing the result from the distance mapping in fig. 3.7.4 with distance between the actual color of the pixel and the temperature scale, as in fig. 3.7.3.

69

The temperature is chosen from the result of the minimum distance between a pixel and the different mapping. In order to distinguish between good and bad temperatures the following set of rules are used:

1. If both the RGB mapping and distance mapping give the same temperature,

2. else if the temperature from the distance mapping is within specified tolerance,

3. else if the temperature from the RGB mapping is within specified tolerance,

4. else choose the temperature in between the RGB and distance mapping.

The mentioned tolerance must in this case be quite big, since the number of possible colors is much greater than the temperature scale contains. This of course presents a problem in the already mentioned U-turn. If the tolerance is to big the problem will not disappear, but with the proper choice of tolerance the problem will be attenuated to a tolerable degree.
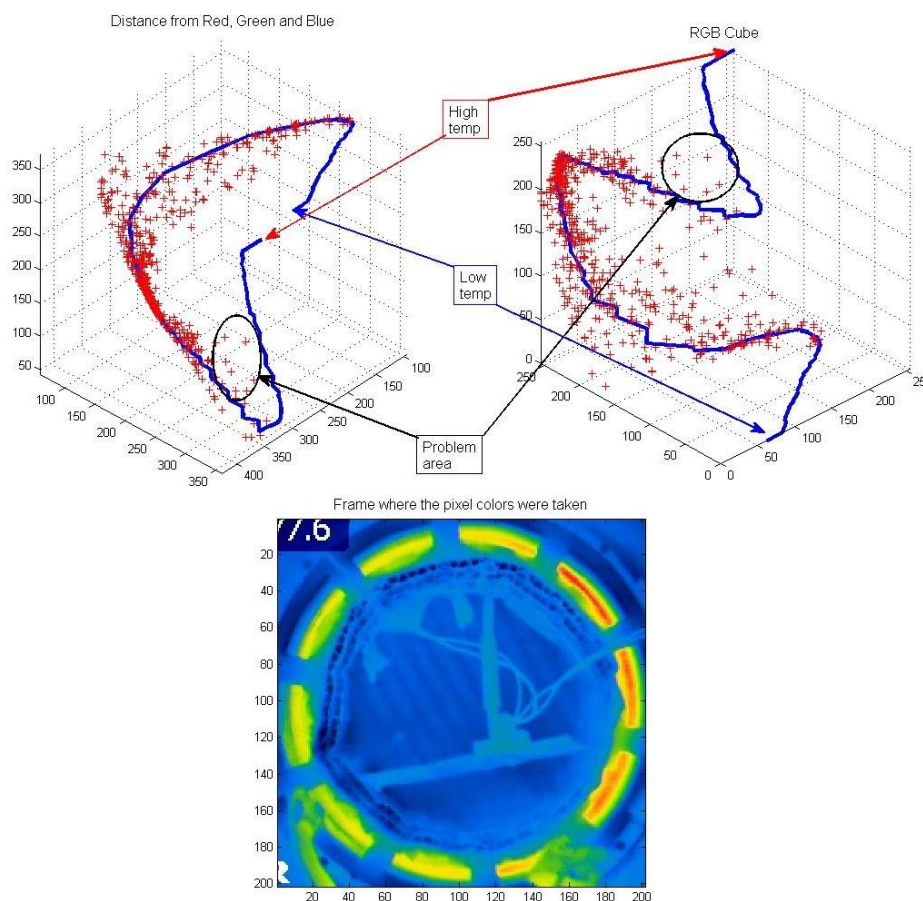
Fig. 3.7.5. Pixels mapped from a frame (bottom) to distance form Red, Green and Blue (top left) and the RGB cube (top right). The circular areas mark the problem pixels.

Fig. 3.7.5 shows a mapping of every five pixels of a frame. The circular areas in the figure show the problem pixel colors. Just by looking at where the other pixels are mapped with the picture of the frame in mind, one can easily notice that no pixels should be mapped to the right side of the U-turn. This because of that the hottest colors in the frame are ranging from orange to red which are located on the left side to the bottom of the U-turn.

Although the mapping algorithm sorts out some of the problems, there are still some problems left, especially when finding the maximum temperature of the frame. These are tackled by finding how many of the pixels that share the same maximum temperature. If it is just a small percentage of the pixels that is within 10°C of the maximum temperature then that maximum is regarded as a disturbance and hence neglected.

3.7.3 DISTURBANCES

The cameras built-in measurement functions are of great use. The "max of an area" function was used in order to see that the temperature was not to high or that a short circuit was present. But, as later realized, it came with a cost. The information field in the top left corner in the video that displays the temperature would randomly grow in size and cover the top part of the winding (see fig. 3.7.6). In that information field were some random letters written in white with a dark blue background.
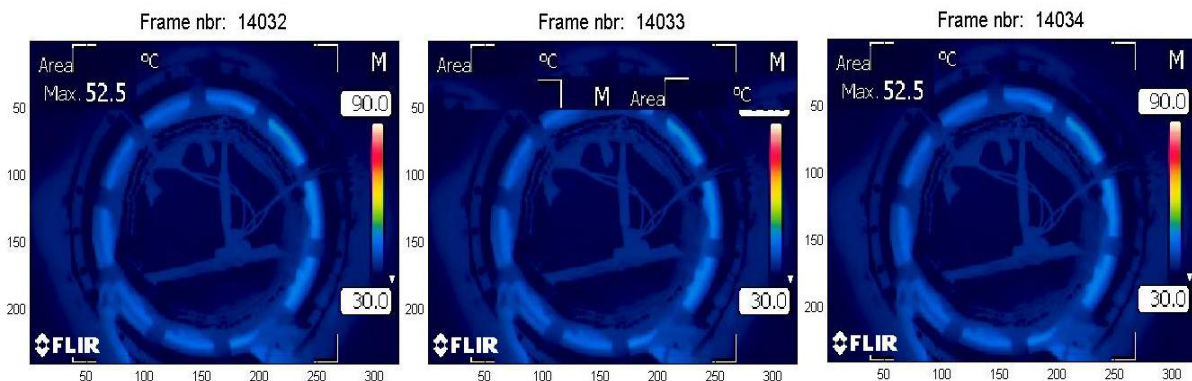
Fig. 3.7.6. Illustration of three consecutive frames where the middle one is affected by the random behavior of the information field in the top left corner.

Fortunately this went almost unnoticed in the calculation of the mean temperature, lucky in the sense that the white (high temperature) was canceled out by the dark blue (low temperature). Unfortunately the maximum temperatures are greatly disturbed by this, since white is the maximum

71

temperature that in the temperature scale. As the figure below illustrates the mean temperature remains almost completely unaffected by the disturbance but the max temperature skyrockets.
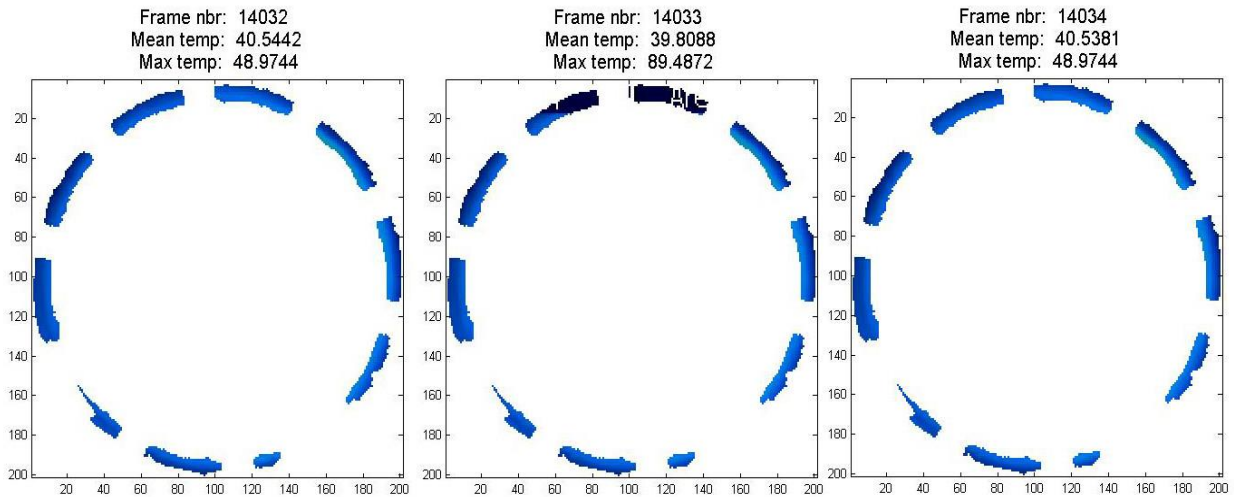
Fig. 3.7.7. Illustration of the disturbance of the the maximum temperature when the information field randomly grows. The middle frame is affected by the the disturbance.

With some smart filtering the effect of these disturbances could be minimized. The figure below shows the effect of the filtering; the max temperature is returned to its original value.
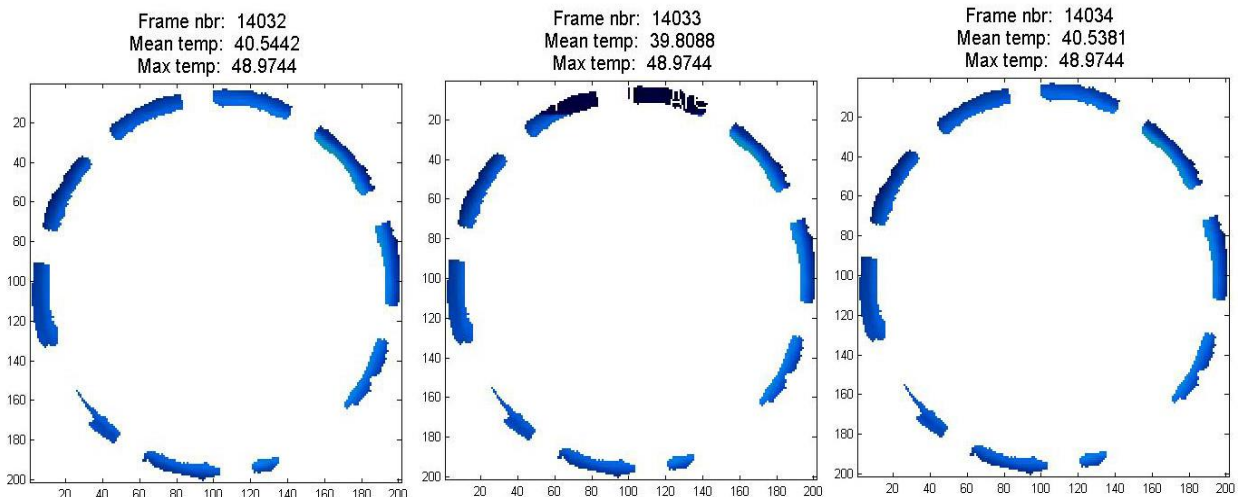
Fig. 3.7.8. Illustration of the same frames as in figure 3.7.7 but with the filtering active.

3.7.4 ACCURACY AND RESOLUTION

The inherent accuracy of the camera, which is printed in the technical specifications of the product, is ±2°C. This accuracy can be achieved when the emissivity is set to the right value of the object that the camera is pointed at. The emissivity is a material constant that relates to the ability of said material to emit thermal energy. The emissivity is expressed as a percentage which the camera uses in the correction of its measurements. The winding was spray painted with a matt black color under the assumption that the emissivity of that was close to 0.98. Industrial grade spray paints, manufactured for just this purpose, is often very expensive which was the reason for this more crude solution. Even if the emissivity is chosen correctly the camera has worse accuracy than the thermocouples, which usually is ±1°C. But since the thermocouples interfere with the winding the better accuracy becomes negligible.

The resolution of the temperature scale is quite bad. The temperature interval ranges from 30 to 90°C with 117 steps gives 60/117 = 0.5128°C/step. This is arguably bad, but on the other hand the temperature interval can not be much narrower in order not to compromise the calculation of the mean temperature and as explained earlier the amount of pixels in the temperature scale is limited. In other words, this resolution is just something that one has to live with and deem is as relatively good.

3.7.5 CONCLUSIONS

In hindsight the choice of having rainbow representation of the thermograph was not really a good idea. Confining the thermograph to the gray scale (black to white) would take away lots of problems. But since all the videos was already recorded before this problem was encountered it seemed easier to work around the problem within the data already at hand than re-record all of it.

4. EVALUATION MODELS

4.1 ANALYTICAL MODEL IN MATLAB

4.1.1 SIMPLIFICATIONS AND ASSUMPTIONS

When analyzing the cooling characteristics of the winding it was decided for simplification purposes to analytically model the cooling capability of two parallel plates. When scaling measured values into the analytical model two important assumptions are made. The first is that all air travels directly into the slot opening and no air hit the tooth and is pressed into the opening. The second assumption is that all heat that is generated in the parts of the winding where no movement of air exists according to the first assumption is evenly distributed over the air wetted parts of the winding. The model is built under the same mathematical equations and simplifications as those presented in chapter 2.
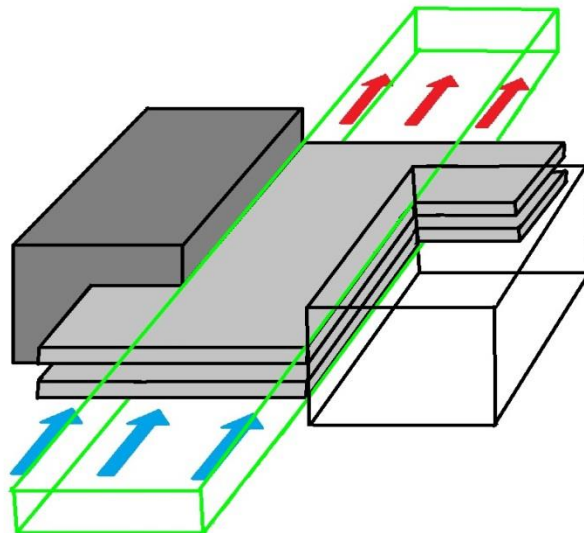
Fig. 4.1.1. Illustration of a winding segment, the green box is the part that is analytically examined.

4.1.2 FLOW AND HEAT DITRIBUTION ACROSS SLOTS

The analytical model is using the formulas made for one single slot and repeats the procedure in order to build a stack of slots. But since there will occur heat conduction between turns as well one need to model the connection between slots in order to simulate for a whole stack.
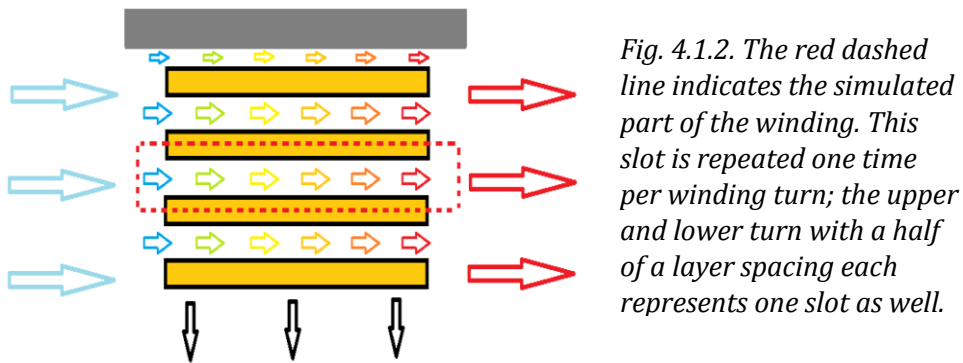
Fig. 4.1.2. The red dashed line indicates the simulated part of the winding. This slot is repeated one time per winding turn; the upper and lower turn with a half of a layer spacing each represents one slot as well.

The flow distribution between slots is based on the technique presented in chapter 2.3.5 which distributes the mass flow in order to achieve equal pressure drop.

The heat distribution model is built upon two assumptions. The first assumption is that energy will distribute itself faster in the conducting plate than to the air. This means that it is possible to use the mean temperature when describing the temperature of each turn even though the heat convection differs from top and bottom.

The second assumption is that the air between turns is continuously mixed along the length of the slot, necessary in order to use the air bulk temperature at every point x along the length of the slot even though the heat transfer differs from top and bottom laminate. This assumption makes it possible for heat to transfer itself through the air from a hotter plate to a cooler one. This is done by dividing the length of the plates into smaller pieces and use equations 2.3.10 and 2.3.11 to determine energy flow and outlet temperature for each piece along the length of the plates. The outlet temperature from one piece is used as inlet temperature to the next.
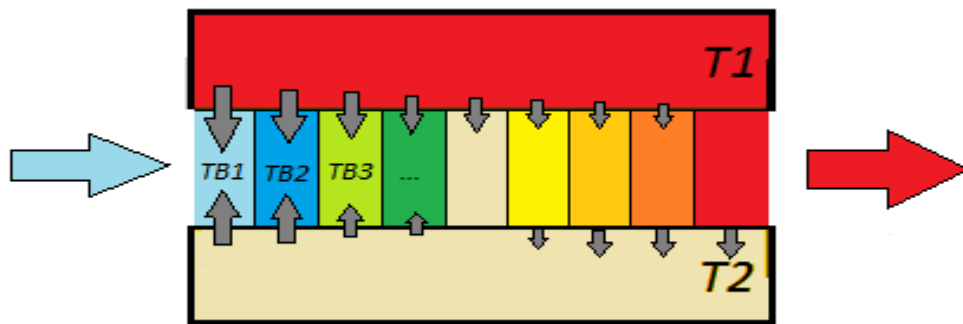
Fig. 4.1.3. Illustration of the energy flow from a hotter plate to a cooler (T1>T2). The air bulk temperature (TB...) and energy flow (grey arrow) is revaluated in every piece along the length of the plate. The total energy flow from each plate is the sum of energy flow from the individual pieces.

4.1.3 MODEL STRUCTURE

The model is used to simulate both ideal layer spacing and randomly distributed spacing within a chosen tolerance. The magnitude of the natural heat transfer from the winding has to be set by the user. One can chose either to set a constant or prerecorded mass flow value or let a PI controller decide continuously in order to keep a certain winding temperature.

The input in terms of machine power and efficiency is fetched from external .mat files which holds total simulation time and vectors containing machine power and efficiency. These files can either be built manually but are preferably fetched from a drive cycle recording.

After initiation is a mass flow value fetched from either a predetermined vector or from the PI controller. If the mass flow is set by the PI controller it gives a value for the mass flow in a predetermined slot, this could for example be the first slot in the layer spacing vector or the hottest or smallest slot.

The mass flow distribution calculations can be made more effective if the regulator sets the mass flow in one of the slots instead of determining the total mass flow. The mass flow is distributed according to chapter 2.3.5.

The convection and energy flow from both top and bottom of the winding is evaluated for every turn as well as air outlet temperature from each slot. When the energy flow from each turn is known one can update the surface temperature accordingly. From the total mass flow and pressure drop one can evaluate the ideal pump power needed. Then the algorithm starts over and evaluates the winding values for time k+1.

```
┌─────────────────────────────────────┐
│            Initiation                │
│      •   Winding geometrics          │
│      •   Natural convection          │
│      •   Mass flow                   │
│      •   Power vector                │
└─────────────────────────────────────┘
                    │
                    ▼
┌─────────────────────────────────────┐
│            Mass flow                 │
│   •  K(r − y + 1/Ti ∫₀ᵗ r − y dτ)    │
│         or Manually                  │
└─────────────────────────────────────┘
```

Mass flow

$$ K\left(r - y + \frac{1}{T_i}\int_0^t r - y \, d\tau\right) $$

or Manually

Update mass flow?

YES!

NO!

Mass flow distribution

Heat and energy distribution

Update parameters
- Pressure drop
- Surface temperature
- Ideal pump power
- Air outlet temperature

k = k+1
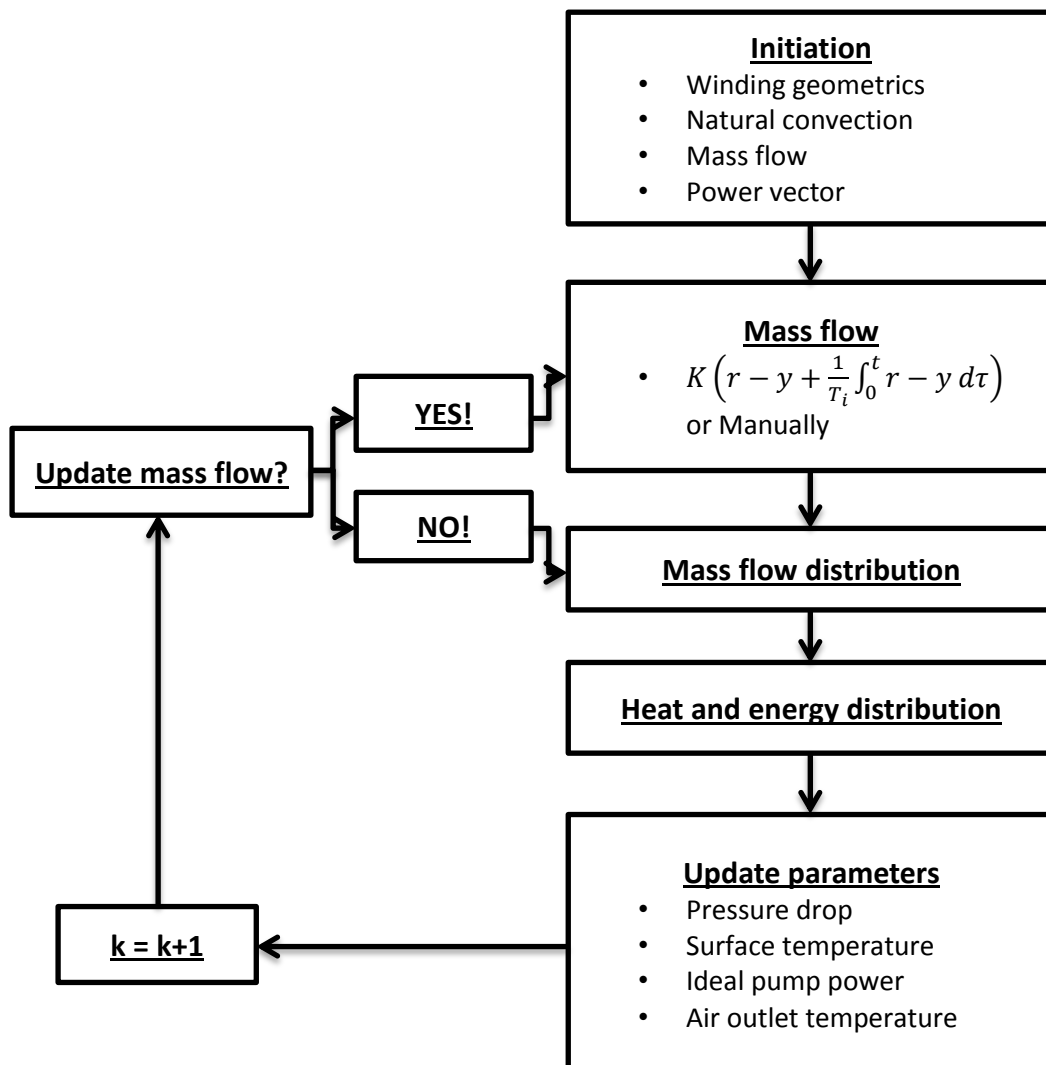
Fig. 4.1.4. Illustration of the overall structure of the transient model of a stack of slots.

The model is used in this thesis to determine the cooling capability of the three prototype windings. The results regarding pump power, pressure drop and mass flow rate can be used to dimension a pump or pressurized air system which will be able to run the machine under a certain amount of heat losses. One can also determine the margins with regard to temperature control of the winding.

The ability to load recorded traction or drive cycles makes it possible to design a more application oriented cooling system. If a traction/drive cycle exists that describes a typical working scheme for a laminated winding one can use the model to design a cooling system accordingly. One can for example determine the needed size of the compressor and air tank as well as maximum heat losses that can be tolerated in an application were the laminated machine are to be cooled with a pressurized air system. One can also try different options regarding isolation and geometry of the winding and get a sense of direction regarding design of such.

4.1.4 MASS FLOW DISTRIBUTION FUNCTION

The mass flow is distributed according to chapter 2.3.5. The distribution is determined under the assumption of even pressure in the space directly in front of the stack of slot. Pressure drop and air exit temperature at time k-1 is used to approximate the air density at time k.

Inputs
- Mass flow in slot X.
- Individuall geometrics of each slot.
- Pressure drop @ time k-1.
- Air exit temperature @ time k-1.

Pressure drop of slot number X
- Reynolds number.
- Friction factor.
- Mean air velocity.
- *Gives pressure drop over slot X.*

for i=1:number_of_turns

Decide mass flow in slot i
- Geometrics(i)
- Pressure drop
- Air exit temperature(i,k-1)
- *Gives mass flow through slot i.*

i = i+1

Output
- Mass flow for each slot.
- Pressure drop

Fig. 4.1.5. Illustration of the structure of the mass flow distribution function.

4.1.5 HEAT AND ENERGY DISTRIBUTION FUNCTION

The heat exchange between winding turns has to go through the air that flows between them. One way of approximate the energy exchange taking place between turns is presented below.
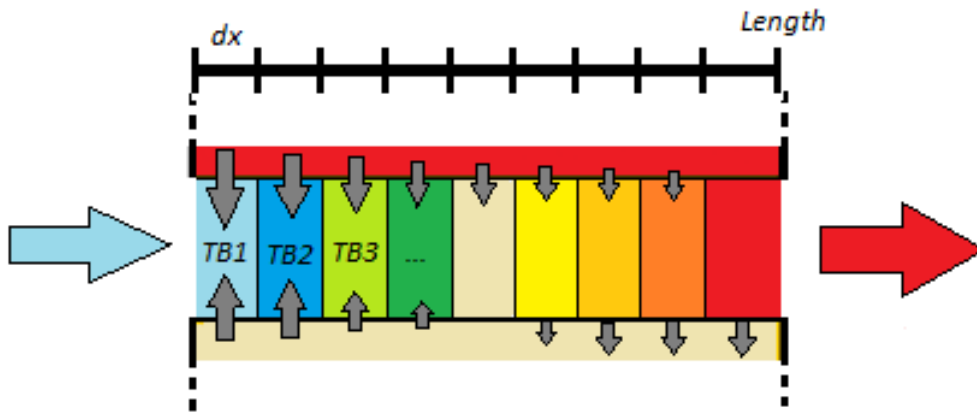
Fig.4.1.6. Illustration of how to discretize the slot in order to determine the total energy exchange between each plate and air.

- Determine air temperature at distance x+dx as if the slot consisted of two upper parts and two lower parts respectively. Eq 2.3.12, use air bulk temperature at distance x and upper and lower surface temperature respectively as input.
- Determine mean energy exchange between winding and air over distance x to x+dx for both upper and lower case. Eq 2.3.13, use upper and lower surface temperature as input.
- Determine air bulk temperature at distance x+dx by taking the mean value of the air temperature at distance x+dx from upper and lower part.
- Repeat until x+dx equals the slot length. The total energy exchange of the upper respectively lower turn is the sum of the energy exchange of each part.
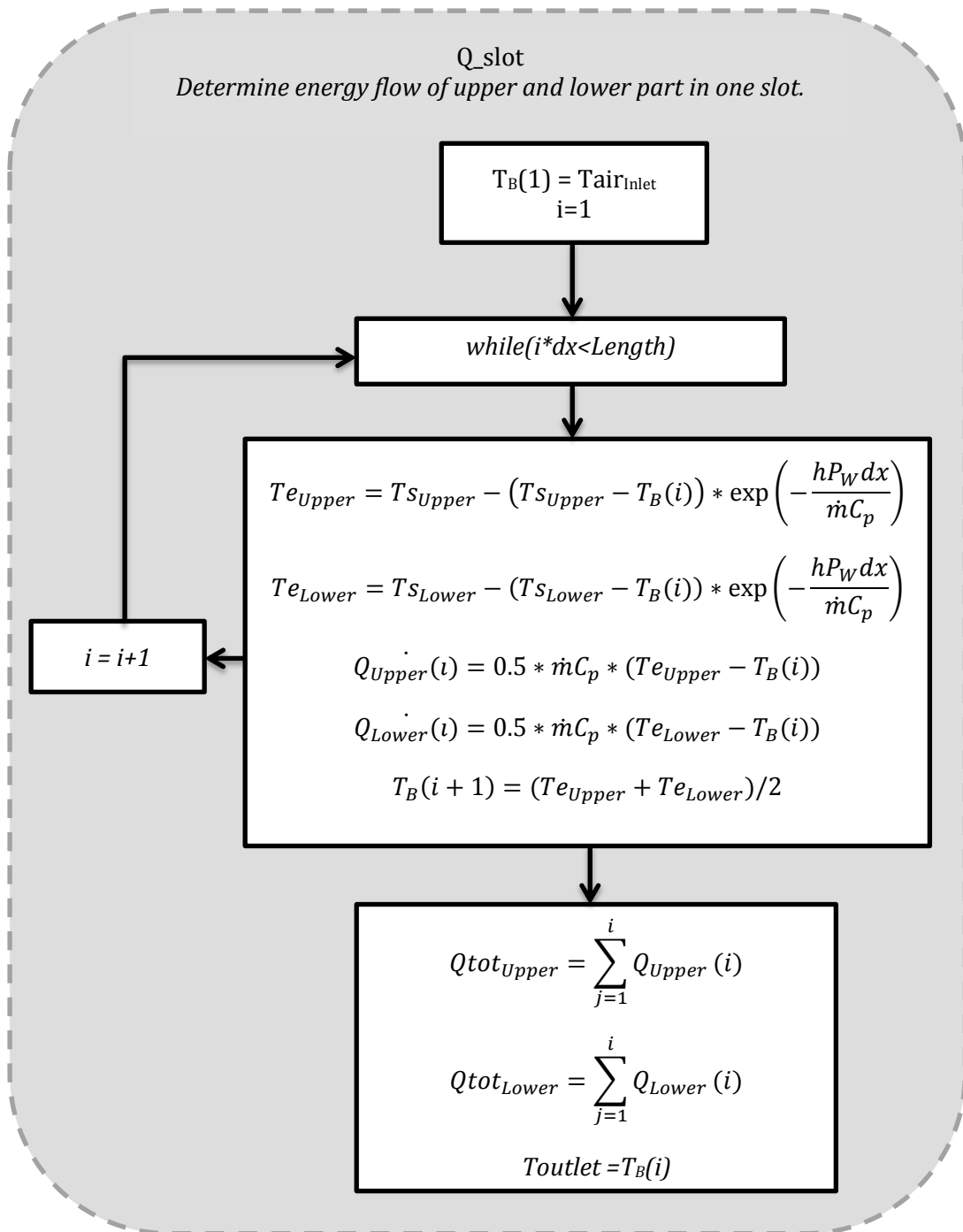
Fig. 4.1.7. Illustration of a flow scheme of how to mathematically estimate the energy flow between air and each plate in a winding slot.

When it is possible to determine the energy exchange for the upper and lower part in each slot one can determine the total energy dissipation to air for every turn in the stack of slots. By using the function "Q_slot" for every slot in the stack and then add the vectors Qtot_upper and Qtot_lower one get the total energy dissipation from every winding turn.
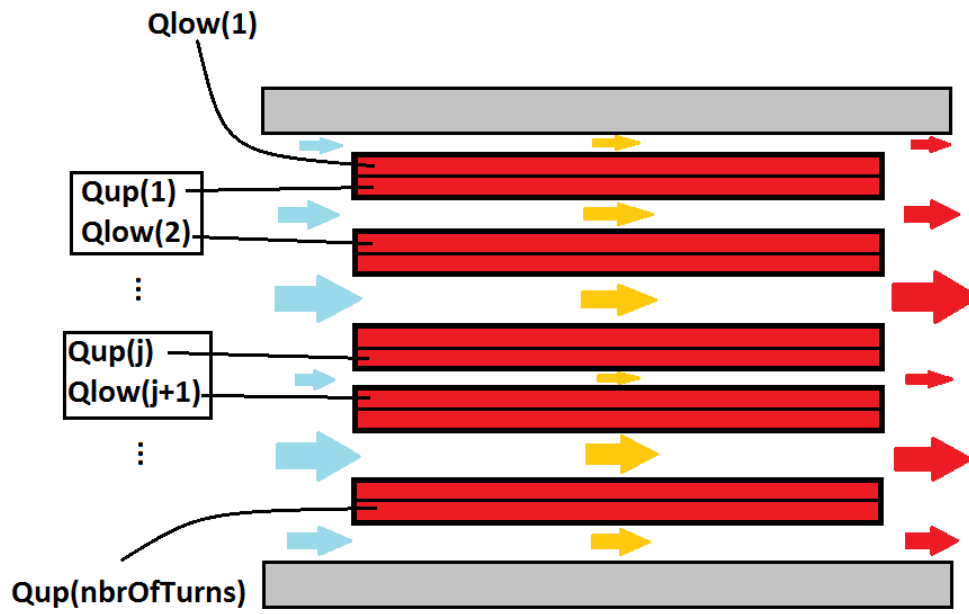
Fig. 4.1.8. Illustration of how to add the results from "Q_slot" in order to get the energy dissipation to air from each individual winding turn.

When the energy dissipation from each turn is known it is possible to determine the change in surface temperature for each turn by equation [2.3.12]. Since it is assumed that heat travel infinitely fast inside the plate the change in temperature for turn number i is simply given by:

$$\Delta T(i) = t * \frac{Q_{HL} - Q_{Upper}(i) - Q_{Lower}(i)}{mC_p} \qquad 4.1.1$$

Inputs
- Mass flow distribution vector.
- Surface temperature @ time k-1.
- Individual geometrics of each slot.
- Inlet air temperature.
- Pressure drop @ time k-1
- Air outlet temperature @ time k-1

Determine convection for each slot
- Reynolds number
- Nusselts number
- *Gives mean convection. (h)*

Function Q_slot
- T_surface(1) and T_surface(nbrOfTurns)
- h(1) and h(nbrOfTurns+1)
- *Gives Qup(nbrOfTurns), Qlow(1), T_outlet(1,k) and T_outlet(nbrOfTurns+1,k)*

for i=1:nbrOfTurns-1

i=i+1

Function Q_slot
- T_surface(i) and T_surface(i+1=
- h(i+1)
- *Gives Qup(i), Qlow(i+1) and T_outlet(i+1,k)*

Output
- The vectors Qup and Qlow.
- Air outlet temperature @ time k

Fig.4.1.9. Illustration of the structure of the heat and energy distribution function.

83

4.2.1 RESISTIVITY, NATURAL COOLING

The model consists of a single piece of a winding turn. It is built with the joule heating package in Comsol Multiphysics. It simulates a current flowing through the piece giving rise to conductive heat losses. On the top and bottom of the piece is a natural convection boundary condition applied which lets the heat dissipate from the plate. The model let the user determine material properties such as resistivity; one can also choose geometrics of the winding piece.

The model can be used to determine current density, voltage drop (resistance) and temperature rise for an arbitrary winding geometry, current and natural convection.
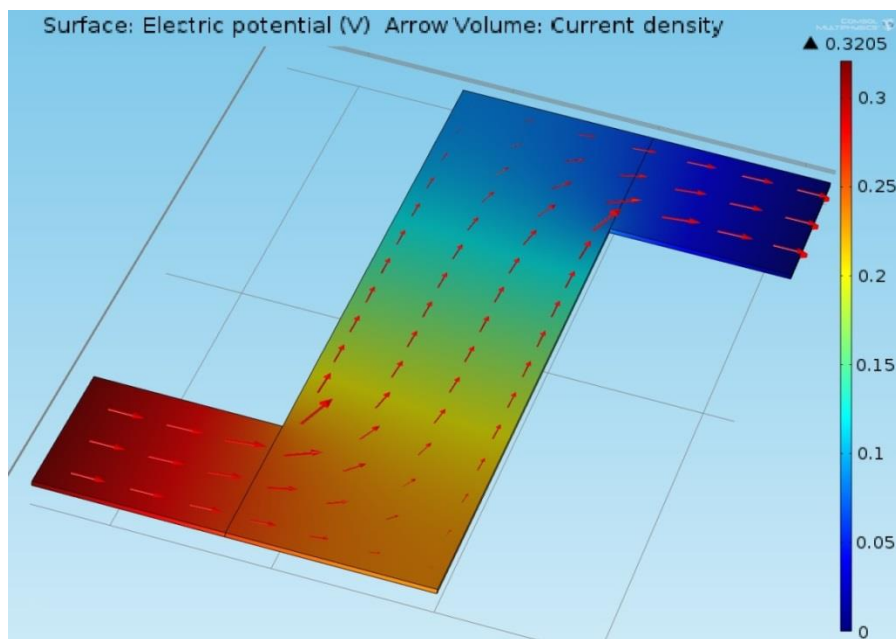
Fig. 4.2.1. Illustration of a model of a winding piece, the voltage drop, current density and temperature rise can be evaluated for an arbitrary winding geometry, current and natural convection.

The resistivity model is used during evaluation of measurement data in order to determining the temperature coefficient of aluminum as well as approximates a value of the natural heat convection taking place during no active cooling. The model is also used to build polynomials which maps current and current density/heat losses for an arbitrary winding geometry.

4.2.2 2D LAYER SPACING

The model consists of a single winding slot, since the model only has 2 dimensions it is not possible to simulate the impact of the teeth. The assumptions regarding air flow and heat distribution are similar to those of the analytical model. It is assumed that no air hits the teeth and that all heat losses generated in front of a tooth is instantly and lossless transported to the air wetted part of the slot, see figure 4.1.1 for clarification. The biggest difference between the 2D layer spacing model and the analytical model is that the heat is not assumed to distribute itself instantly across the length of the slot. This means that the numerical model takes the difference in surface temperature along the length of the winding into account; the analytical model assumes constant surface temperature along the whole length of the winding. The heat loss of this model is not tied to a resistive loss as in the model described in 4.2.1 but is instead set by the user. The reason for not connecting the two models is that of increased simulation time and problem with divergence. Instead the model in 4.2.1 is used to map heat loss and current for a certain winding geometry and temperature. The 2d layer spacing model can then be used to determine mass flow rate for the heat losses generated by model 4.2.1. Since this disables the ability for resistivity and thereby heat loss to change with temperature the precision of the model is impaired. When using the model the resistivity is evaluated for the maximum allowed winding temperature and the results for lower winding temperatures will thereby be more pessimistic. As mentioned above the reason for using both models separately is that of saved simulation time and it also gives better stability and the models is less keen to diverge.
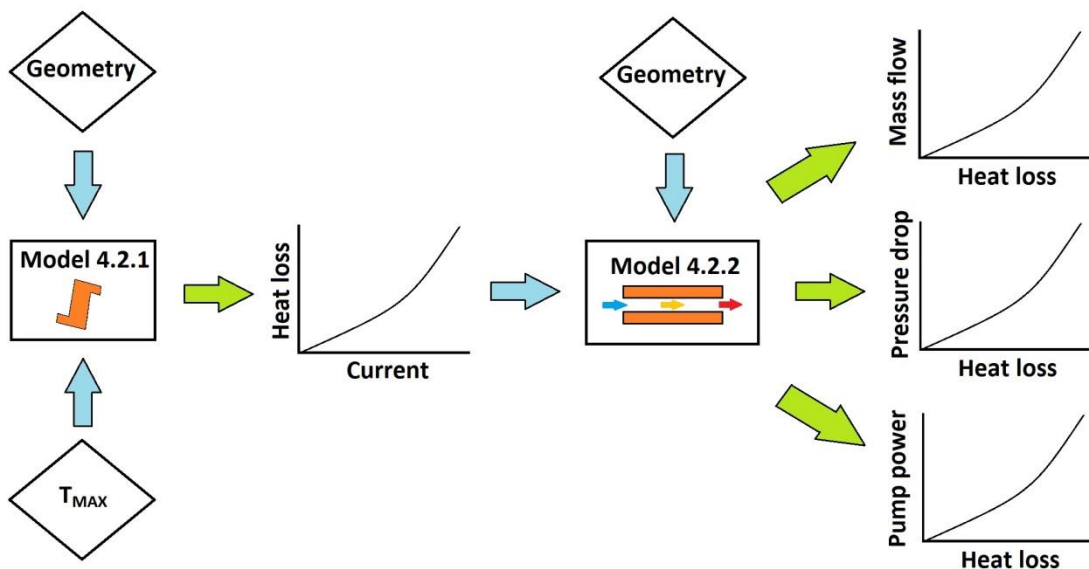
Fig. 4.2.2. Illustration of one way to use the models described in chapter 4.2.1-2.

The model is built with the "Conjugate heat transfer" package in Comsol Multiphysics. Since only a small part of the winding is simulated it is built under the same rule of repetition as presented in figure 4.1.2. In the 2d layer spacing model all slots are assumed to be uniformly spaced and therefore heat and flow distribution rules are not needed since exactly the same conditions are repeated along the whole stack. The heat generated in the two parallel plates presented in the 2d layer spacing model is assumed to travel towards the layer spacing and no concern to natural heat conduction ways is taken into account.
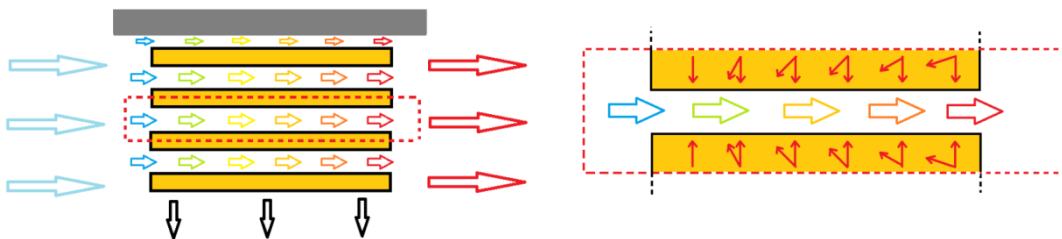
Fig. 4.2.3. Illustration of the repetitive rule that the 2d layer spacing model is built upon. The heat generated in the slot will only travel towards the space between layers.

The model has an out of plane depth which corresponds to the distance between teeth in the winding; this makes air flow scaling from one slot to the whole winding easier. The inlet boundary conditions that can be set are air mass flow magnitude and air inlet temperature. At the end of the simulation channel two outlet boundary conditions are set, that both heat energy and air mass is allowed to exit the model. The laminate walls have a non-slip boundary condition which states that a viscous fluid will have zero velocity at the boundary between solid and fluid. The walls which not consist of aluminum laminates have a slip-wall boundary condition which let the air travel freely at the boundary.
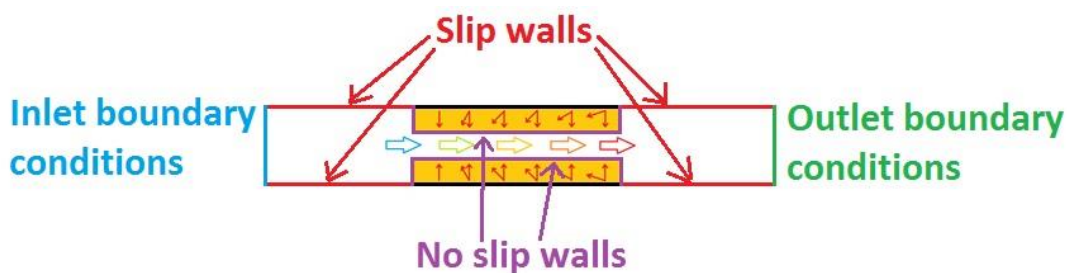
Fig. 4.2.4. Illustration of the structure of the 2d layer space model.
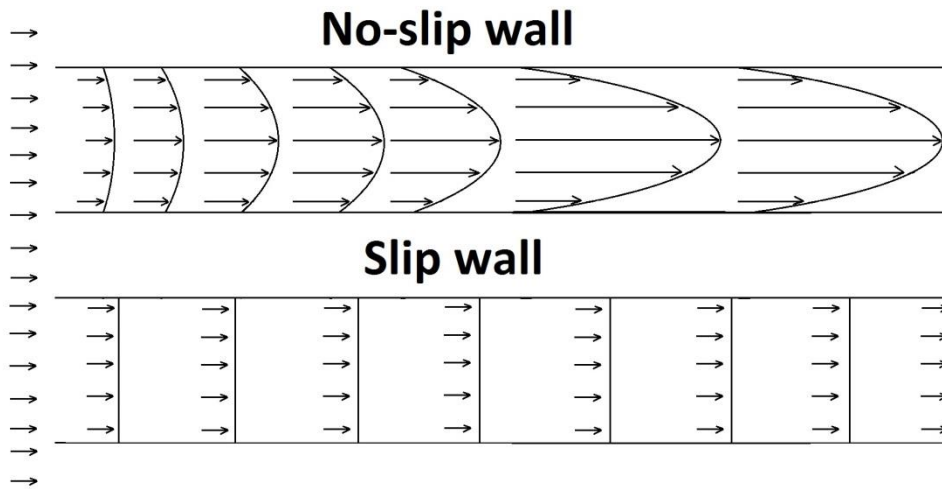
Fig. 4.2.5. Illustration of the difference in air flow characteristics between the slip and no-slip wall boundary conditions.

The result from the model is strongly dependent on the ability to describe the heat transfer taking place at every step along the length of the winding as well as how the air mixes inside the channel. A too coarse mesh will give a faulty value of these parameters and makes the result untrustworthy. An easy first check to see if the results seem reasonable is to calculate the energy dissipated by air and the heat generated in the winding layers. In steady state these two should have the same value and if not the model is suggesting that energy is either created or destroyed during the cooling process. Both cases are impossible at least according to the knowledge about physics that has been discovered to this day.

The mesh used in the 2d layer spacing model is custom build and have an increasing accuracy (finer mesh) at the air wetted surfaces.
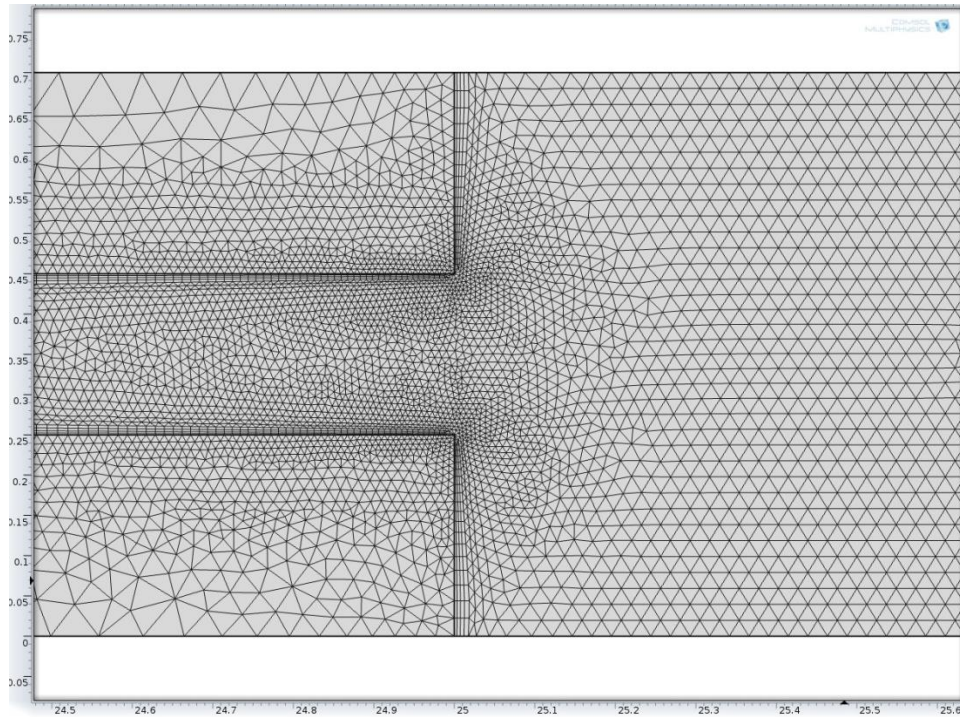
Fig. 4.2.6. Illustration of the mesh at the outlet of the 2d layer spacing model.

The 2d layer spacing model is used to try to estimate the mass flow needed for an arbitrary winding geometry and heat loss. The biggest flaw with this model is the simulation time in relation to the information collected. Since it is not possible to simulate for the flaws in the winding one can only receive the result under ideal conditions. If the temperature increase along the plate is not of big interest the analytical model can be used to receive the same results but at a fraction of the time. This is often the case since the winding will burn off at the hottest place anyway. A closer comparison between the analytical and 2d layer spacing model will be executed in chapter 4.3.

4.2.3 3D LAYER SPACING

The model consists of a single winding slot. The model is built in three dimensions and therefore simulates the teeth impact on the cooling process. It uses the "Conjugate heat transfer" as well and has the same inlet, outlet and wall boundary conditions as the 2d layer spacing model. By using a 3d representation of the slot it is possible to see the impact of the teeth and one can also use different kind of inlet nozzles. One could also extend the model to include a more than one slot along the winding turn; this enables the possibility to simulate for different mass flow directions in to the winding. In example could every even teeth opening be cooled from the opposite direction than the odd ones. The disadvantage of using a 3d model is the computation time and memory needed to execute the simulation. When building the 3d layer spacing model it was chosen to use the finest possible mesh which did not need more memory than the computer could offer and had a reasonable computation time. The computational time of the first simulation series made with the 3d layer spacing model was approximately 48 hours and included 144 different simulations. But the mesh was not good enough as the heat losses and energy dissipated by air did not match up. The model shows the steady state conditions and in our case are the heat losses bigger than the energy being dissipated by air. Since no other heat transfer ways are present in the model are the results suggesting that energy magically disappears from the winding piece which obviously is not the case. A number of attempts were made to reduce the magnitude of the model in order to be able to use a finer mesh. But problems with convergence and misleading results were always present. One attempt to improve the model was made by manually divide the mesh into subareas and only use fine mesh at air wetted areas of the model. One simulation with the improved mesh were initiated but canceled since it still had not converged after 48 hours.
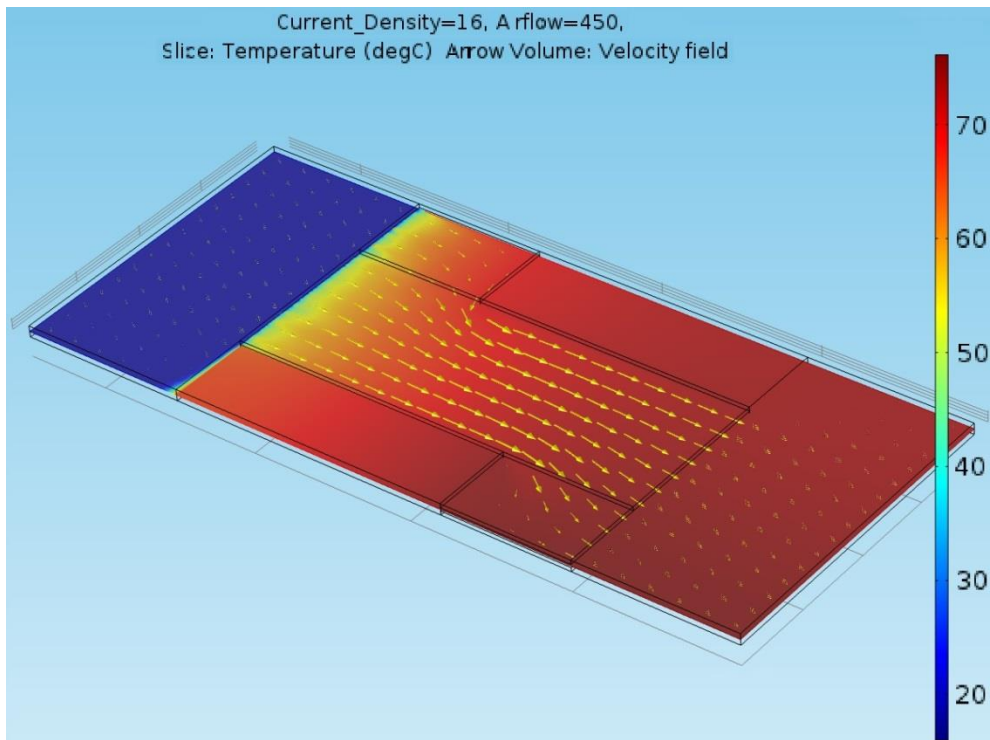
Fig. 4.2.7. Picture of the 3d layer spacing model, color represent temperature in degrees Celsius and arrows velocity field.

The attempts of creating a 3d model of the winding slot were eventually stopped mainly due to the problems mentioned above but also since the analytical and 2d model gave results which matched good with measurements. We are confident that it is possible to use Comsol Multiphysics to create an accurate 3d model of the winding slot but we simply did not have the time and competence to make it happen.

The 2D model made in Comsol Multiphysics and the analytical model created in Matlab hold the same dimensions and they also make the same assumptions regarding the parts of the slot which is not included in the model (the parts covered by teeth). The biggest difference between the models is that the analytical model only uses equations under the assumption of constant plate surface temperature. The Comsol model on the other hand has a numerical approach which gives a more precise picture of the surface temperature along the length of the slot.

The following figure shows the change in air bulk temperature and surface temperature for the two different models.
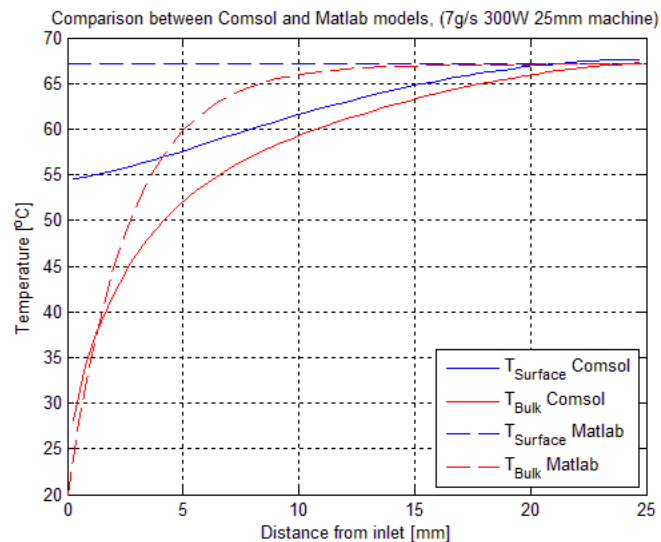
Fig. 4.3.1 Plate and air temperature along the length of the plates.

In the figure above one can see the consequence of the assumption constant surface temperature. Since the Comsol model does not assume that the heat distributes itself infinitely fast along the plate (as it does under the constant surface temperature assumption) one can see an increase in surface temperature toward the end of the slot channel. Even if the Comsol model is more complex both models have to reach the same outlet air temperature in order to have a correct energy balance. Since the plate will hold the same or a lower temperature at a distance closer to the inlet than at the outlet one could use the constant surface temperature simplification to simulate for the worst case temperature along the length of the plate. If a cooling design were to be made under the constant surface approximation one would always have a temperature along the length of the winding slots that is the same or lower than the temperature designed for.

The following figure shows a comparison between the 2D model made in Comsol and the analytical model made in Matlab. The temperature that is used for comparison is taken from the end of the plates in the Comsol model.
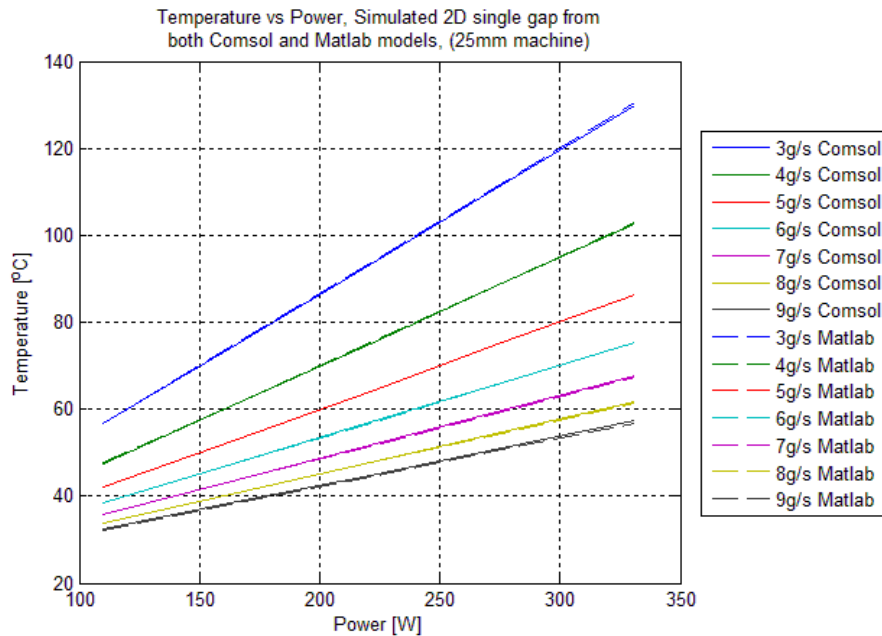
Fig 4.3.2. A comparison between the results from the Matlab and 2d Comsol models.

As shown in the graph there is nearly no difference between the Comsol and Matlab models when investigating the highest temperature along the length of the plate.

Both models comes with pros and cons and the biggest advantage of using the Matlab model is that it is easily coupled with other simulations such as that of a predetermined drive cycle, it has a much faster simulation time and can easily be transformed into a transient model. The disadvantage of the model is that of loss in accuracy when describing more complex parts of the system such as the heat distribution along the plate.

The big advantage of the Comsol model is the ability to numerically describe more complex parts of the process such as the impact of the teeth (in a 3D model) and if for example one would use different air inlet directions for different slots. One could also decide what would happened if the air would be sprayed at the slots through a nozzle with smaller outlet area than the stack of slots. One disadvantage of the Comsol model is the simulation time which in the case of a complex 3D model could stretch into days. Another disadvantage is the difficulty and time that has to be spent in order to build a mesh that is good enough to correctly model the flow. The mesh could be built as fine as

possible in order to ensure reliability but it has to be weighed against the increased simulation time which comes with it.

The results that is being compared in the figure above is a series made for 5 different heat loss magnitudes, each one is simulated for 7 different mass flows which gives a total of 35 simulations. The Comsol model is a 2D model with custom made mesh that is tested to be reliable; the total simulation time for the Comsol model is 4 hours and 22 minutes. The Matlab model is analytical and uses the simplification of constant surface temperature; it will therefore only give the largest temperature of the plate and not take the heat distribution along the length of it into consideration. The total simulation time of the Matlab model is 0.54 seconds.

4.4 CONCLUSIONS FROM THE MODELS

4.4.1 LAYER SPACING OPTIMIZATION

The layer spacing is defined as the radial distance between winding layers. During this chapter it is assumed that the space between casing and rotor is fixed which means that the thickness of the laminates is considered variable and will change with the fill factor. As the thickness of the laminates is changed the layer spacing will change accordingly. The definition of fill factor in this chapter is:

$$Fill\ factor = \frac{Thickness_{laminate} * NumberOfTurns}{Stack\ height}$$
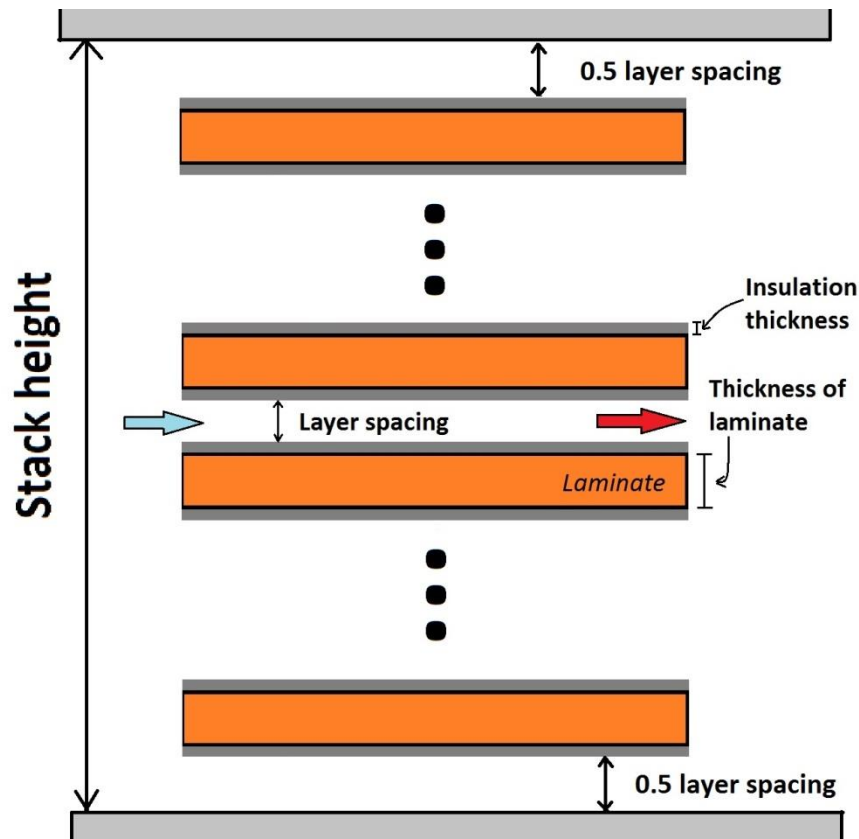
Fig. 4.4.1. Illustration of a cross section of a winding stack.

Further on when referring to stack current density it means current density in one of the laminate layer conductors times the fill factor. This will give the current density to space ratio in a cross section of the stack.

When assuming constant surface temperature one have a convection constant that mainly dependent on the inlet dimensions. The mass flow has an impact on the increased convection during the inlet stretch but this contribution is rather small in comparison (see equations 2.3.5-6). The gain of using small layer spacing, i.e. thick laminates, is that of increased convection and fill factor. The convection increases since the hydraulic diameter is in the nominator of the raw formula for Nusselts number (see equation 2.3.4). The loss of using a small layer spacing is that the pressure drop increase, the pressure drop increases approximately with a factor 8 for every time one halves the layer spacing. Since the increased pressure drop give rise to an increased pump power one would like to get as much heat transportation out of the winding at the lowest possible pressure drop.

As the air that is being forced through the winding channels is heated up it absorbs less heat from the layer and if the convection is high enough one would get a near zero heat flux at the end of it. The air will hold nearly the same temperature as the layer at the outlet. On the other hand if the convection is too low, i.e. too big layer spacing, the difference between layer and air outlet temperature will increase. This results in a higher winding temperature for the same amount of mass flow and therefore degrades the performance of the system.

If the length of the machine, number of teeth, number of turns, stack height, maximum heat losses and maximum allowed winding temperature is known one could optimize the laminate thickness. Since the pressure drop decreases with a factor 8 when the layer spacing halves but the convection decreases only with approximately a factor two. One would get the best cooling performance with increasingly larger layer spacing, within reasonable ranges. Even though the magnetic performance of the motor will not be treated in this thesis it is understood that keeping a high fill factor is crucial to the machine performance. Since the pump power increases potentially with layer spacing one will find a limit when the increase in fill factor will not be worth the gain in pump power. This point changes with the motor dimensions and mass flow through the winding.

The following three cases try to illustrate the fill factors impact on the needed pump power and dissipated heat. The pump power is ideal and therefore one have to add some sort of pump efficiency factor as well as if one have other pressure drops in the system except the machine.

Table 4.4.1 Specifications for the three different winding prototypes used in the layer spacing optimization simulations.

Case	M1	M2	M3
Channel Length	25 mm	28 mm	100 mm
Channel width	9.63 mm	8.8 mm	15.5 mm***
Plate thickness	0.5 mm	0.5 mm	0.7 mm
Insulation thickness	25 μm[25]	25 μm[24]	25 μm[24]
Number of teeth	20	22	6
Number of turns	12	17	12
Surface temperature	70°C	120°C	140°C
Air inlet temperature	18°C	18°C	18°C
Air density friction loss	1.1171 kg/m³	1.0475 kg/m³	1.0 kg/m³
Air density shock loss	1.2 kg/m³	1.2 kg/m³	1.2 kg/m³
Air thermal conductivity	0.0285 W/mK	0.0328 W/mK	0.0343 W/mK
Prandtl number	0.7120	0.7106	0.7080
Air dynamic viscosity	19.41e-6 Pa s	20.409e-6 Pa s	20.940e-6 Pa s
Air Cp	1001 J/kgK	1001 J/kgK	1001 J/kgK
Conductivity of aluminum @ Surface temperature	2.7958e+007 S/m	2.4340e+007 S/m	2.3142e+007 S/m

---

[25] [15] [*Laminated Winding with a Rapid Cooling Capability for Electrical Machines,* C. Högmark, A. Reinap, K. Frogner, M. Alaküla, *International Conference for Inductive and Electromagnetic Components, Systems and Devices including Manufacturing and Processing (INDUCTICA 2012)*, Berlin, Germany, June 26-28, 2012]
***The edges of the winding in M3 are taped and thereby reduce the effective cooling area.

Case M1
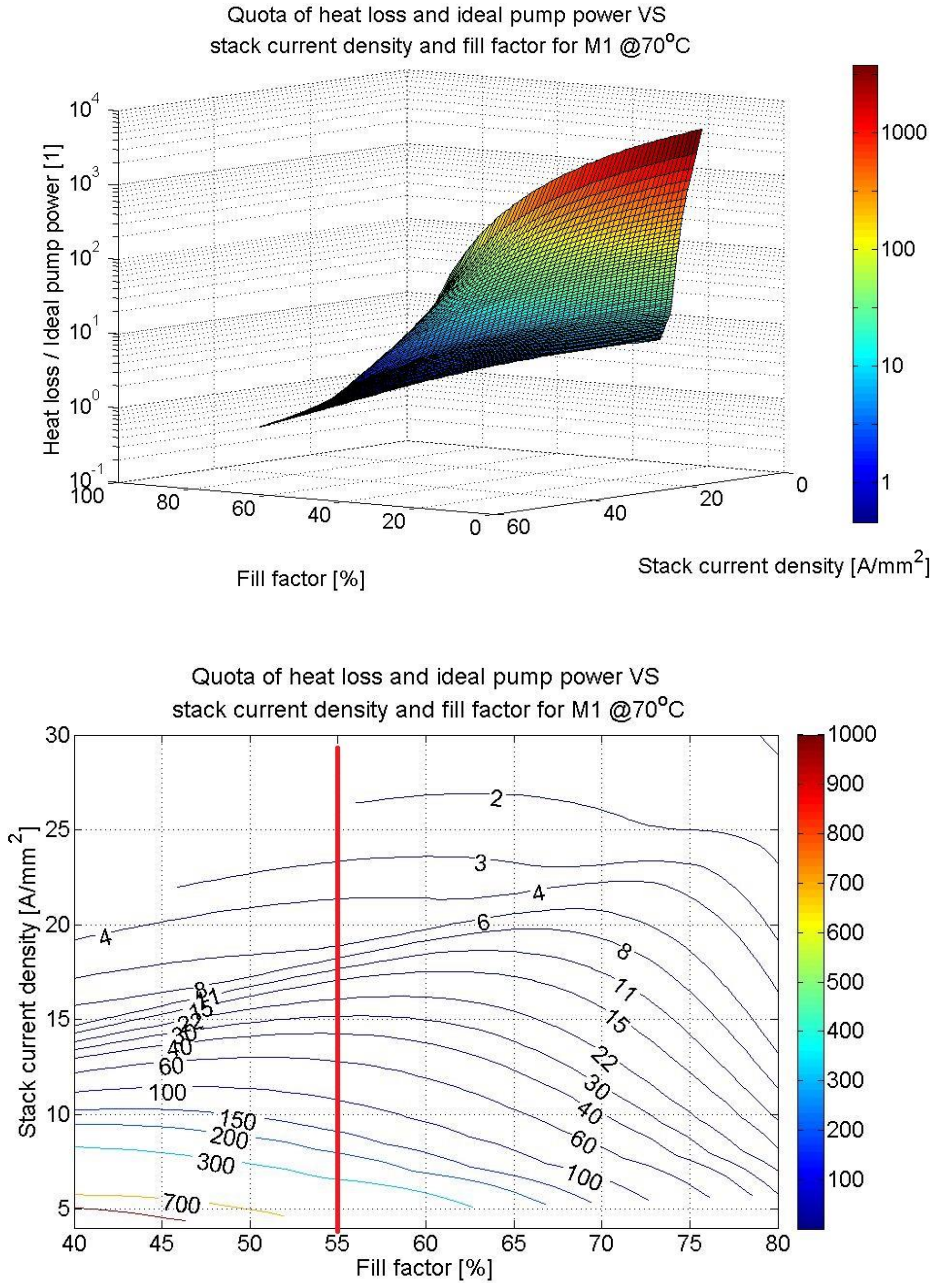
Fig. 4.4.2. Illustration of the quota between ideal pump power and heat losses versus fill factor and stack current density. The same plot is illustrated both as surface and contour plots. The red line indicates a laminate thickness of 0.5mm which is that of prototype M1.
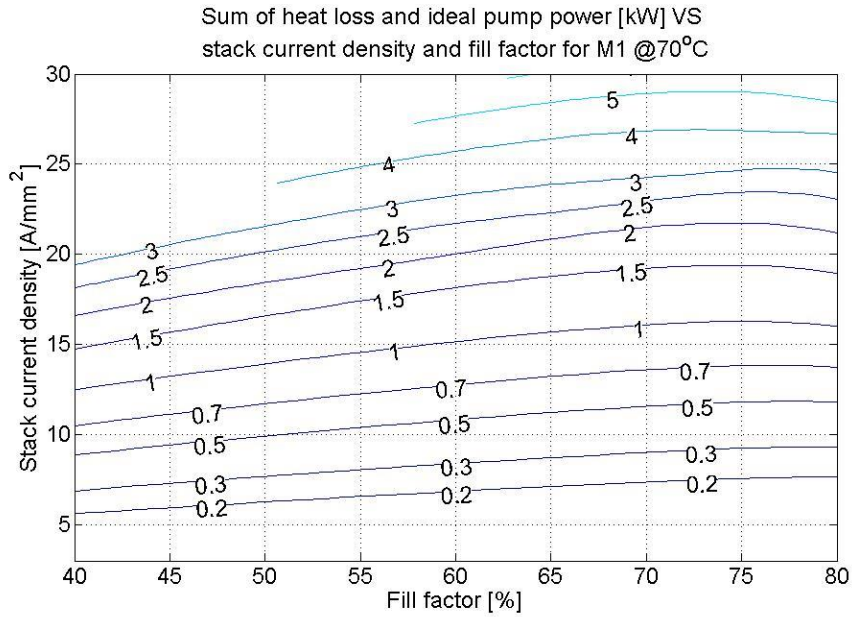
Fig. 4.4.3. Total power loss, i.e. heat loss and ideal pump power, plotted against the stack current density and fill factor for M1.
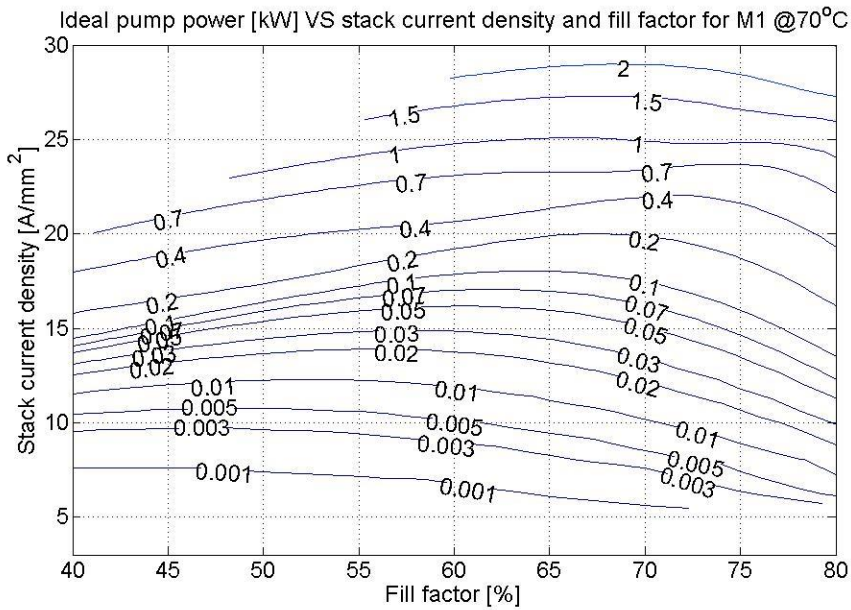
Fig. 4.4.4. Ideal pump power plotted against stack current density and fill factor for M1.

Case M2
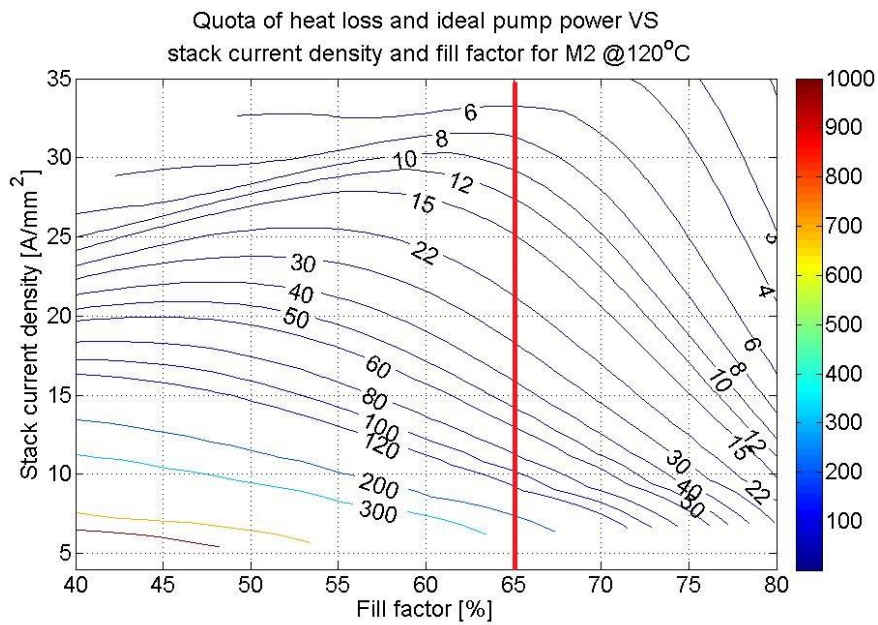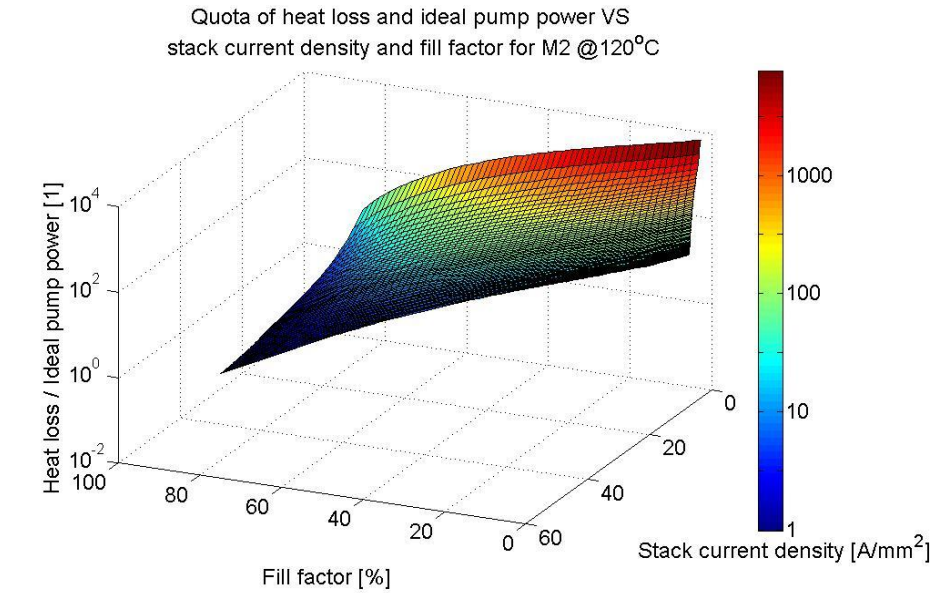
Fig. 4.4.5. Illustration of the quota between ideal pump power and heat losses versus fill factor and stack current density. The same plot is illustrated both as surface and contour plots. The red line indicates a laminate thickness of 0.5 mm which is that of prototype M2.
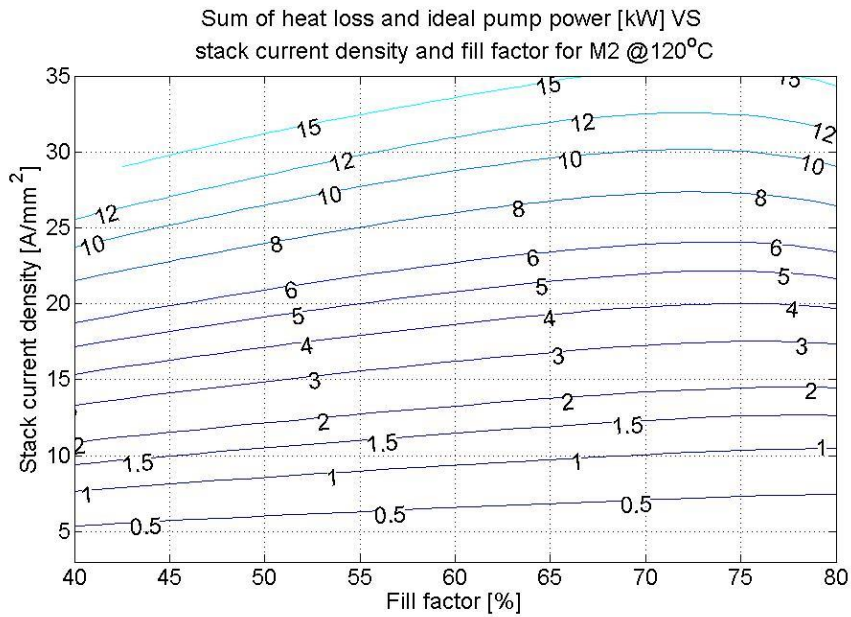
Fig. 4.4.6. Total power loss, i.e. heat loss and ideal pump power, plotted against the stack current density and fill factor for M2.
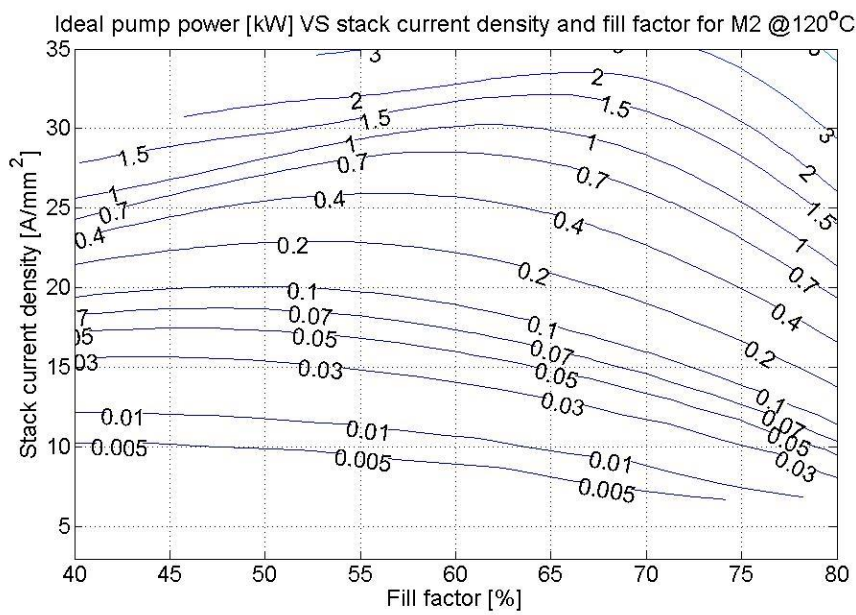
Fig. 4.4.7. Ideal pump power plotted against stack current density and fill factor for M2.

Case M3
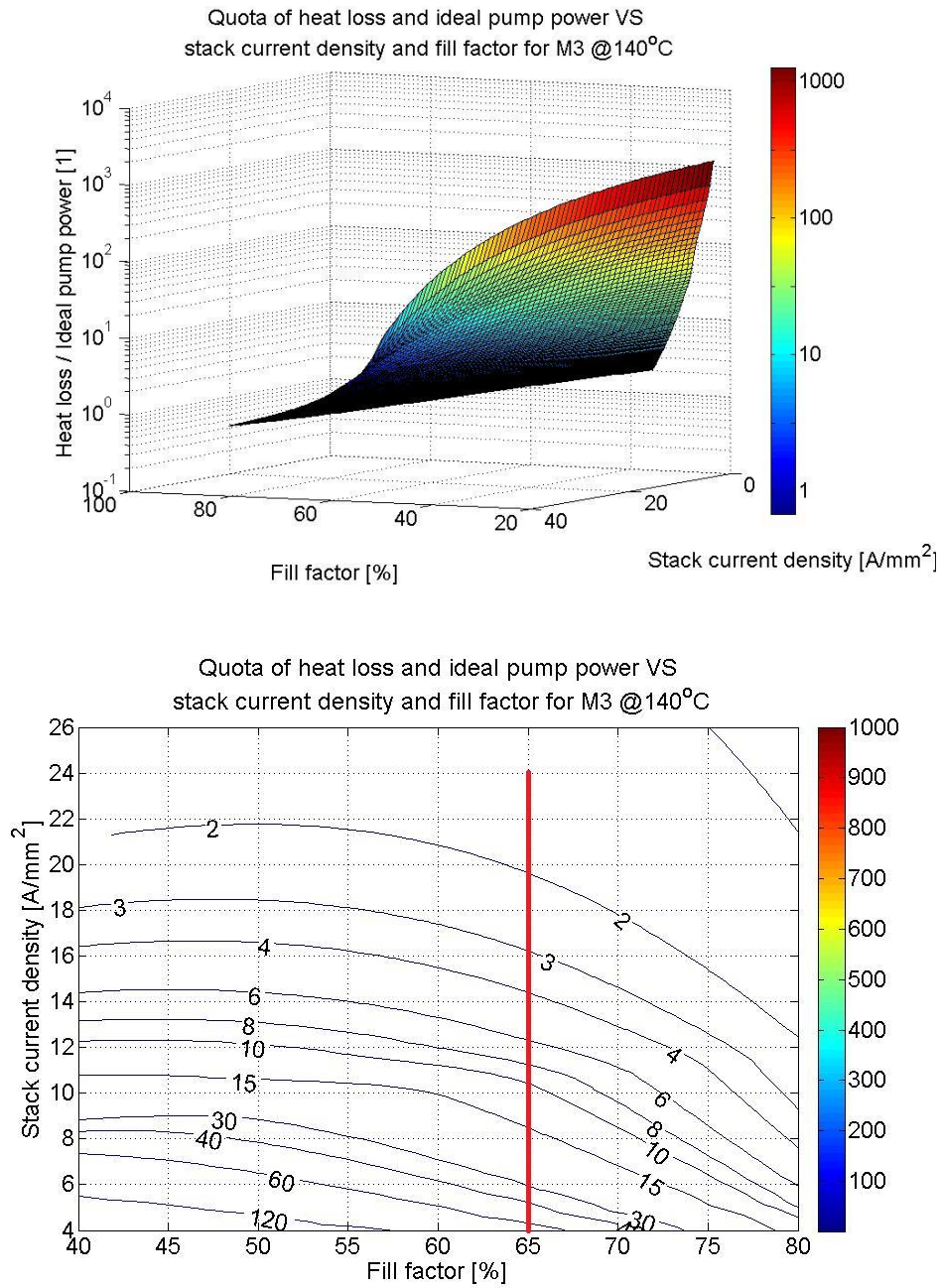
Fig. 4.4.8. Illustration of the quota between ideal pump power and heat losses versus fill factor and stack current density. The same plot is illustrated both as surface and contour plots. The red line indicates a laminate thickness of 0.7mm which is that of prototype M3.
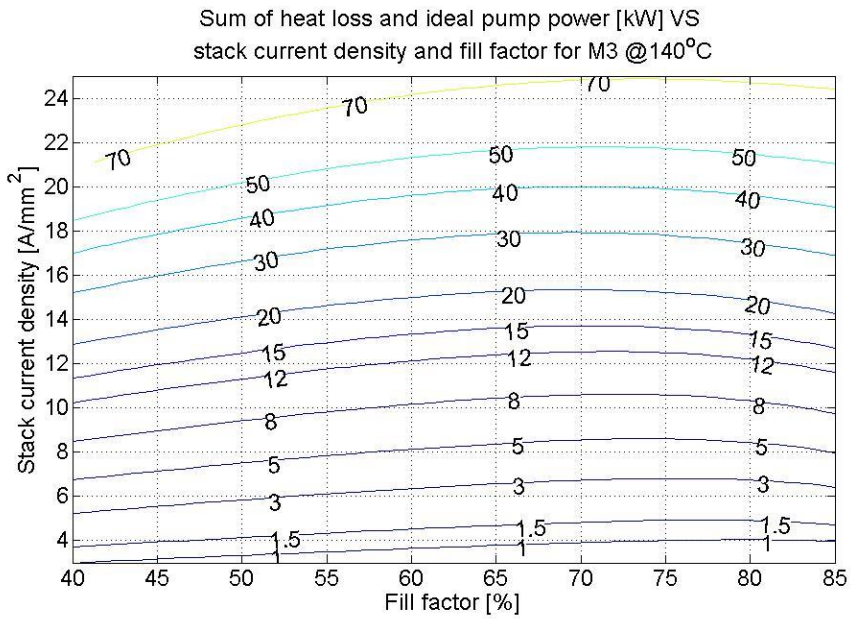
Fig.4.4.9. Total power loss, i.e. sum of heat loss and ideal pump power, plotted against the stack current density and fill factor for M3.
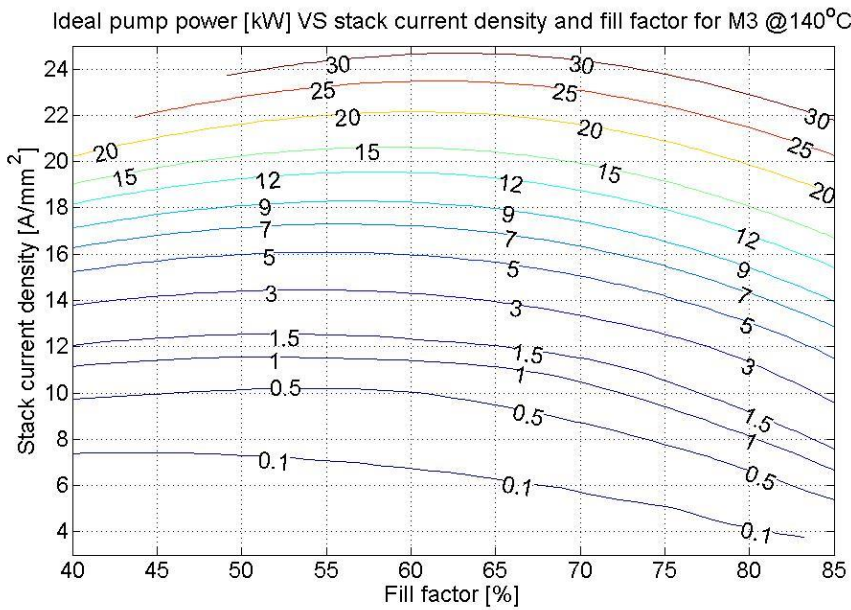
Fig. 4.4.10. Ideal pump power plotted against stack current density and fill factor for M3.

The cooling efficiency, i.e. the quota of heat loss and ideal pump power, is easily evaluated by looking at the contour plots in figures 4.4.2, 4.4.5 and 4.4.8. The fill factor which M2 is design for is near optimum cooling efficiency if it was to run at a very high stack current density. Since the figures mentioned above give a heat loss to ideal pump power ratio it is quite unclear how much ideal pump power is actually needed for a given heat loss. For this reason the total power loss and ideal pump power are plotted within reasonable limits for M1, M2 and M3 in figure 4.4.3-4, 4.4.6-7 and 4.4.9-10.

When designing a laminated winding with the intention of forced air cooling these kinds of contour plots as in fig. 4.4.2, 4.4.5 and 4.4.8 should be considered. Let us take a hypothetical example for M3: the variation of fill factor can be between 40 and 65% and the maximum stack current density is allowed to be 14A/mm². By looking in the contour plot in fig. 4.4.8 one can see that the optimal cooling performance for the two criterias stated is achieved at a fill factor of 45%.

Optimizing the fill factor only by cooling efficiency does not mean that the overall performance is optimized. Instead the optimization of the fill factor should be a weight between the overall efficiency of the machine and the cooling efficiency.

All of the results above are dependent of a predetermined machine length. But what will happen if the length of the machine is changed? The pressure drop increases linearly with the length of the channel but in the same time there is an increase in air wetted area in which heat can be transferred into the air. When the air travels through the channel it will raise faster in temperature at the beginning of the channel and at some point it will have almost the same temperature as the plate. Beyond this point the air's capability to receive any more heat energy is very limited and the cooling of the plate at this length along the channel will be greatly reduced.

Figure 4.4.11 shows the dissipated energy and ideal pump power for different machine lengths, the results are fetched from the Matlab model.
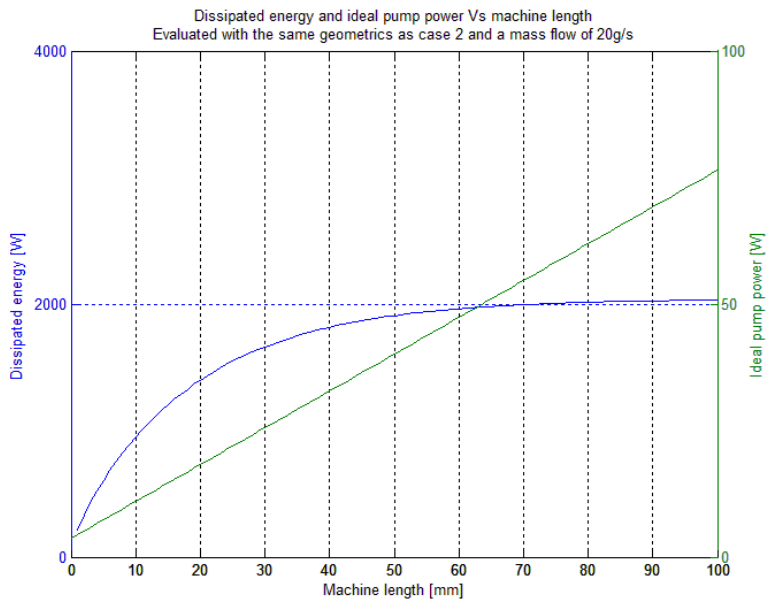
Fig 4.4.11. Ideal pump power and dissipated energy versus machine length. Other parameters are fetched from case 2 above and the simulation is done for a mass flow of 20g/s.

In order to optimize the length of the machine with respect to the cooling efficiency of the system it was chosen to maximize the quota between dissipated energy and needed pump power with respect to the length of the machine.
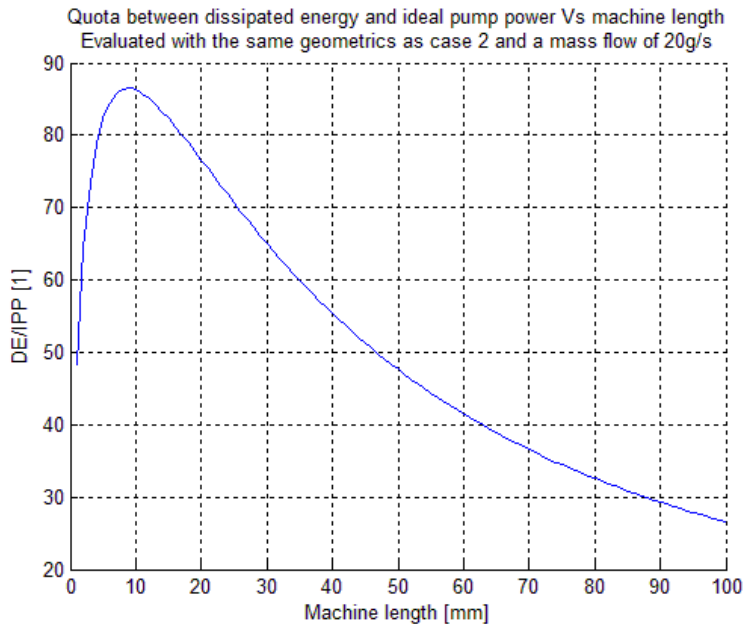
Fig 4.4.12. Cooling efficiency versus machine length, evaluated for case 2 and with a mass flow of 20g/s.

The results show that the optimum machine length would be rather short, but one should keep in mind that in a real application one has to optimize the machine length with respect to magnetic and torque capabilities as well. From fig. 4.4.11 one can evaluate the critical length of the machine for a mass flow of 20g/s. With critical length it is meant the length when the dissipated energy curve has converged, any machine which is longer than the critical length will have a higher pressure drop but will not gain any more in dissipated energy.

The width of the slot channel also has an impact on the pressure drop and cooling capabilities. Figure 4.4.13 illustrates the width and length of the channels impact on the quota between dissipated energy and ideal pump power.
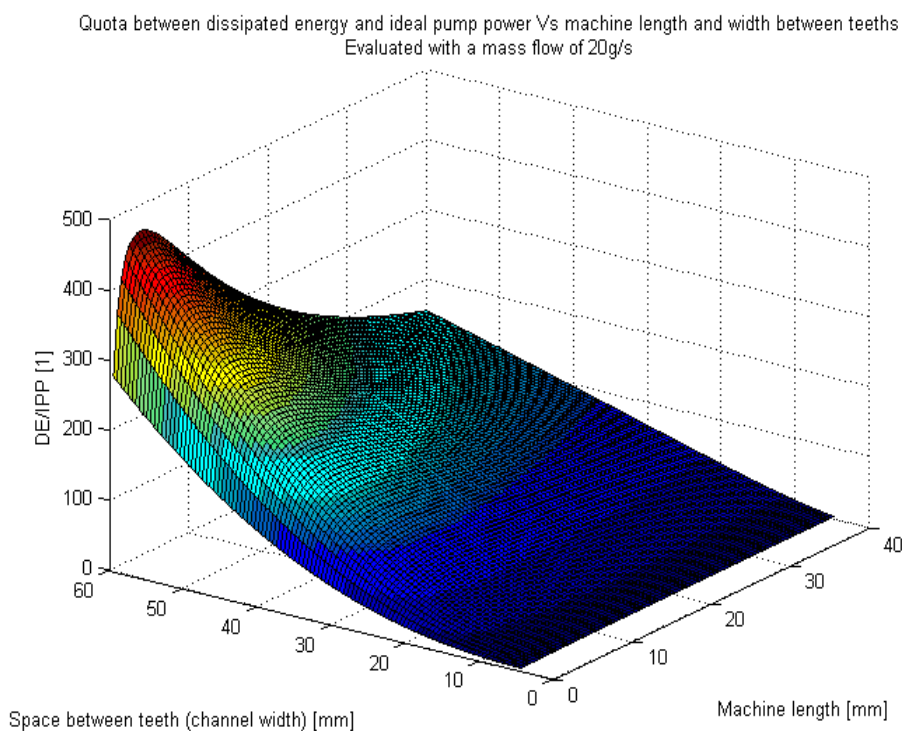
Fig 4.4.13. Cooling efficiency versus machine length and distance between teeth's, evaluated for M3 and with a mass flow of 20g/s.

The results show that the efficiency of the cooling system increases with the width of the layer spacing. As the width increases the pressure drop and thereby pump power is reduced. The results show that the best cooling capabilities are found in a short machine with wide layer spacing. But as mentioned before the cooling performance has to be weighed against the torque capabilities of the machine, one might find an optimal geometry that differs from the results in the test above when taking these properties into account when solving the optimization problem.

It should be noted that for the results to be valid one has to have uniformly spaced layers and no air flow leakages in the system. It is almost impossible to accomplish this in a practical application and therefore one would have to use some sort of degradation factor that describes the faulty formations and leakages in the system.

4.4.2 MASS FLOW DISTRIBUTION IN AN UNEVEN STACK

When the spacing between the layers is not evenly distributed one will obviously experience an increase in mass flow in the broader slots in comparison to the smaller ones. The reason for this is that the air will strive to distribute itself evenly in the space directly in front of the stack of slots, which leads to a uniform air pressure in the area in front of the slots. Since the slot layer spacing's are unevenly distributed the mass flow through each slot will be a function of the slots unique geometric and the pressure in the area directly in front of the stack of slots.

The stack mass flow distribution can be likened with a group of parallel coupled resistances. Each resistance has its own ohm value but nonetheless will the voltage across all of them be uniformly distributed, just as the pressure in the stack example. But the current through each resistance has to distribute itself according to Ohm's law in order to keep the balance of the system. In the same way the mass flow is forced to distribute itself across the slots in order to keep the system in balance. The mass flow distribution is dependent on a large number of variables and in order to keep it to a level which is manageable it is chosen to use the same simplifications as in the analytical model. A description of the formula used to calculate the mass flow distribution is presented in chapter 2.3.5.

The biggest different from the metaphor with the electrical system is that for most pressure drops the mass flow will not distribute itself linearly across the slots as the current would. The non-slip phenomenon which occurs at the laminate walls makes it harder for the air to pass through a smaller slot. The impact of the slow-speed-air-layer nearest to the laminates will be reduced as the pressure increases and as the pressure in front of the stack goes towards infinity the mass flow distribution will go toward the linear case. The term "linear distribution" refers to a mass flow distribution which is even with respect to layer spacing. In a linearly distributed mass flow system a slot with twice as large layer spacing as the rest of the slots in the same stack would get twice as much air mass flow as well, independent of the magnitude of the pressure drop.

In the figure 4.4.9 which is taken from a Comsol simulation it is possible to see the impact of the non-slip phenomena on the mass flow distribution in a stack of slots. Note that if the mass flow would be linearly distributed, as the electrical circuit the air speed would be the same through all slots.
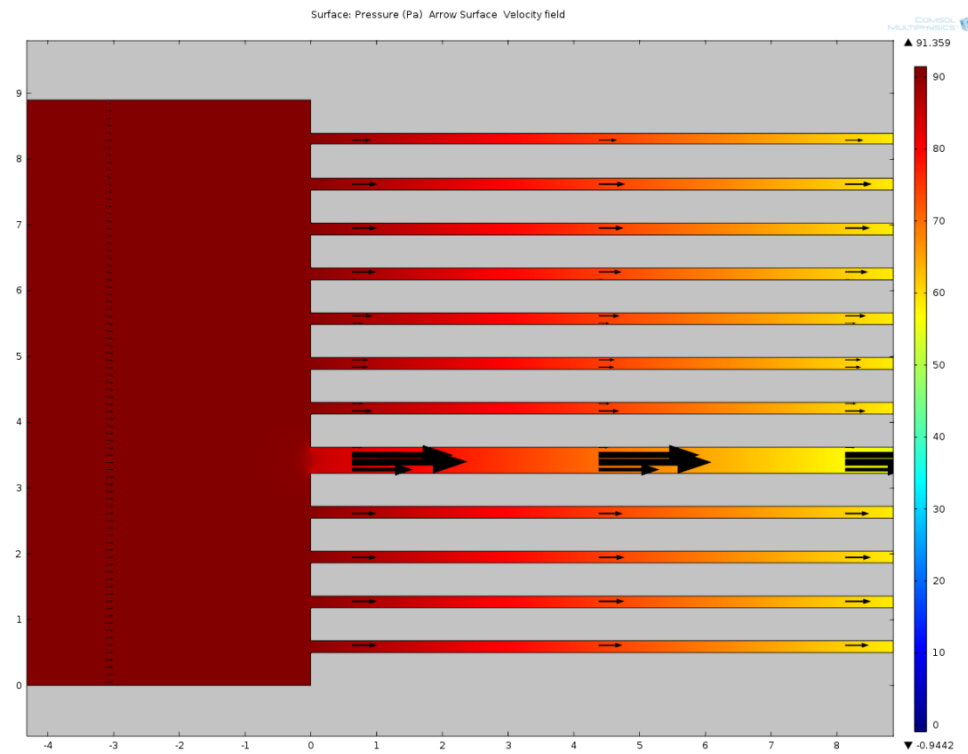
Fig. 4.4.9. Illustration of the pressure and air velocity for a stack of slots where one slot is twice as large as the rest of the slots. (The arrow size represent air speed, color represent gauge pressure.)

The picture illustrates the impact on the mass flow resulting from an uneven layer spacing. In the simulation above the inlet air speed is set to 0.5m/s and the length of the slots is 25mm. The layer spacing sizes are 0.2 and 0.4 mm respectively. Nearly 50% of all air is traveling through the broad slot which leaves less than 5% of the total mass flow to each of the smaller ones. That means that ten times more air flows through the broad channel in comparison to the small one, in a linear distribution would the ratio be 2:1. Since it's harder for the heat to travel between slots than to the air directly and the fact that a wider channel has a lower convection constant the temperature is bound to rise in the smaller channels in order to compensate for the smaller amount of available air. As the temperature in the smaller slots rises the mean temperature (and max) will rise which leads to an increased use of air in order to hold the winding under a functioning temperature. In order to force a larger amount of air through the stack will one be forced to use more pump power and the effectiveness of the cooling system will degrade.

The Matlab model was used to illustrate the mass flow distribution versus total pressure drops for different layer spacing in the same stack. The following plot shows the air distribution for a winding consisting of three turns with a layer spacing of 0.4, 0.6 and 0.8mm respectively, the width of the slot channel (distance between teeth) is 25mm. The three different symbols represent machine lengths of 50, 100 and 200mm.
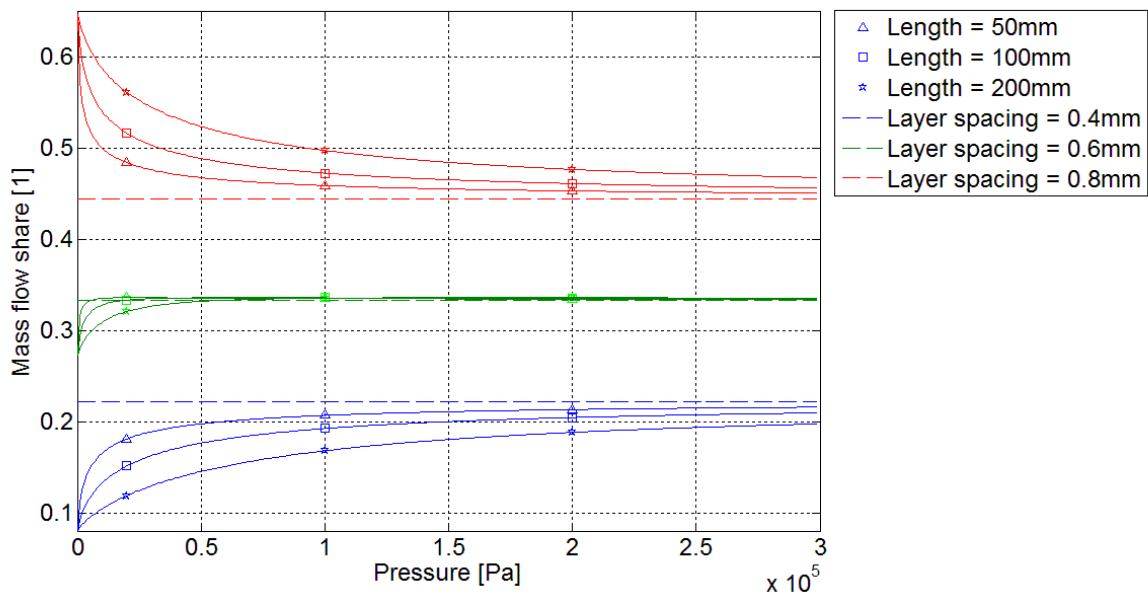
Fig 4.4.10. Illustration of the mass flow distribution between the layers in the winding. The three different symbols represent different machine lengths. The dashed lines represent what the mass flow ratio would be if the distribution would be linear towards the layer spacing.

The results from the simulation show that the mass flow distribution is more even among the winding turns for shorter machines with high pressure drop. The problem with unevenly spaced winding turns can therefore in some extent be helped by keeping the machine short and increase the inlet pressure with the help of a nozzle. The increased inlet pressure has to be weighted by the increase in pump power that it induces. When trying to compensate for an unevenly spaced winding one should keep in mind that the distribution can never be better than the linear case and the best way to resolve the problem is to try to keep a low error margin in the building process of the winding.

4.4.3 TOLERANCES TO LEAKS AND UNEVEN LAYER SPACINGS

In order to optimize the cooling performance one must strive for uniformity with regard to the distance between winding layers. The results of uneven layer spacing gives an uneven air distribution between slots and will also reduce the convection in the larger ones. If the airflow that hits the inlet sector is assumed to be uniformly distributed along the inlet area one will experience an increase of temperature in the smaller slots. Even if the convection increases with decreasing slot size the effects from decreased air flow rate will impact the temperature in greater extent. If one or a few slots are bigger than the rest one will get less effective use of the air throughput and be forced to increase the mass flow and therefore lose in pump effectiveness.

Figure 4.4.11 presents the temperature increase when having one slot that is 50, 100 and 150% bigger than the other slots in the stack. The same motor dimensions and assumptions as case 1 from layer spacing optimization are used but with an specified layer spacing of 0.2mm (0.71 in theoretical fill factor) and a mass flow of 8g/s. Since this example is executed with a transient solver it has changing air property parameters. The heat loss in the winding is 600W and no natural convection is taken into account. The air flow and heat development are both considered to start instantly at time zero.
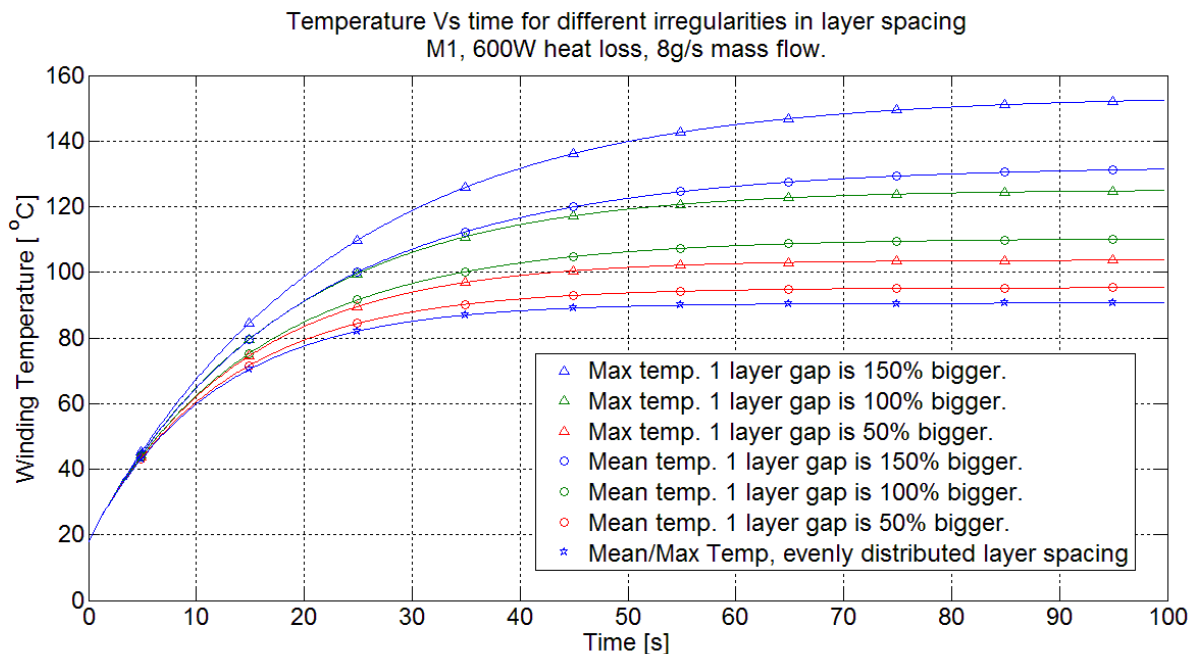
Fig. 4.4.11. Illustration of how the mean temperature of the winding changes with uneven layer spacing.

When examining the example above one should have in mind that similar effects rise from one slot shrinking to a much smaller size than the others as well. The mean convection of the whole winding for the different cases with unevenly distributed radial distance between winding layers is evaluated by using the mean surface temperature and outlet air temperature. The mean convection decreases as the slots become more uneven and if one slot has 50% bigger gap size one would get a degradation of 65% from the case of evenly distributed layer spacing. For 100 and 150% bigger gap size the degradation is 81% and 88% respectively. The reader should note that the temperature or efficiency is not degraded in the same rate as the convection and therefore it might seem as a bad way to present the efficiency loss from the uneven spacing. But since the convection can be used to describe the mean properties of the winding one could use the degradation factor to sum up all the flaws in a real application and consider them when building a model. The example above is made in order for the reader to get a picture of the magnitude of the winding flaws that correspond to a certain degradation factor.

The same effect as in the problem formulation above could rise from leakage due to margins between winding and casing/rotor. In order to optimize performance one should try to keep these margins as small as possible. This certainly states a problem since these margins are there to keep the rotor spinning freely, reducing the risk of voltage breakdowns to the motor casing.

One solution to the problem could be to seal of the winding in some way that not only makes it leakage free but also meet the other physical requirements. This could be both costly and hard to realize especially if the absolute pressure in the system is high since this will increase the risk of leakages as the machine starts to wear down. An alternative to seal off the winding can be to direct the air instead, making sure that no air could pass in openings between winding and casing/rotor. The directed air approach would not only reduce the problem with margins to casing/rotor but also improve the performance due to a better air distribution as a result of the increased pressure that hit the stack of slot. If for example a nozzle could be used to direct the air at the stack of slots one would not have to worry about the safety margins to casing/rotor. One could also manipulate the shape of the nozzle to for example get a larger part of air directed to the middle part of the winding where the effect of other heat conducting ways is lowest. The loss of using directed air through a nozzle is that it induces a higher pressure drop which will increase the pump power and it also reduces the actively cooled area of the winding since the air would not be able to reach as big part of the winding as it normally would.

5. MEASUREMENT RESULTS

Several measurements were made during the course of this project. Below are the final one presented and analyzed.

For the sake of clarity the notation of *Added power* refers to the heat loss power created when a current is sent through the winding, i.e.

$$P = UI = I^2 R \qquad\qquad 5.1$$

Further the notation of *Air cooling power* refers to the power that is transported to the air as it travels through the winding, i.e.

$$\dot{Q} = \dot{m}C_p(T_{exit} - T_{inlet}) \qquad\qquad 5.2$$

Furthermore the notation of *Ideal pump power* is calculated from difference of the measurements of the pressure from inside the housing and atmospheric pressure, i.e.

$$P_{pump} = \Delta p \dot{Vol} = p_{meas}\dot{V} = p_{meas}\frac{\dot{m}}{\rho} \qquad 5.3$$

5.1 RESISTIVITY

In order to accurately model the heat losses generated in the winding the resistivity of the winding has to be known. The resistivity of aluminum differs depending on the purity of the material. For that reason the resistivity was measured on a reference piece of the same aluminum used in the winding. Unlike the winding the reference piece has a much more simple geometric shape, which will help in the calculation of the resistivity. By measuring the temperature and the resistance of the reference piece φ_0 and T_0 will become known in eq. 2.1.2, where φ_0 is calculated from eq. 2.1.1. The temperature was measured with thermocouples and the resistance was measured with four-terminal sensing.

As the resistivity is temperature dependent the temperature coefficient α must also be approximated. By measuring the winding temperature, current through the winding and voltage over the winding the temperature coefficient can be calculated from a combination of eq. 2.1.1 and 2.1.2 together with the result from the previous measurement, i.e.

$$\alpha = \frac{\frac{\rho}{\rho_0}-1}{T-T_0} = \frac{\frac{R\frac{A}{L}}{R_0\frac{A}{L}}-1}{T-T_0} = \frac{\frac{R}{R_0}-1}{T-T_0}$$

where R = U/I and T is the measured winding temperature.

The resistivity of the reference piece was measured to 30.557 nΩm at 20°C. For pure aluminum the resistivity is 28 nΩm[26].

The temperature coefficient was measured with three independent measurement series. Figures 5.1.1-3 shows the results of these.

---

[26] [1] [Physics for Scientists and Engineers Sixth Edition, P. Tipler, G. Mosca, W.H. Freeman and Company 2008, p. 847]
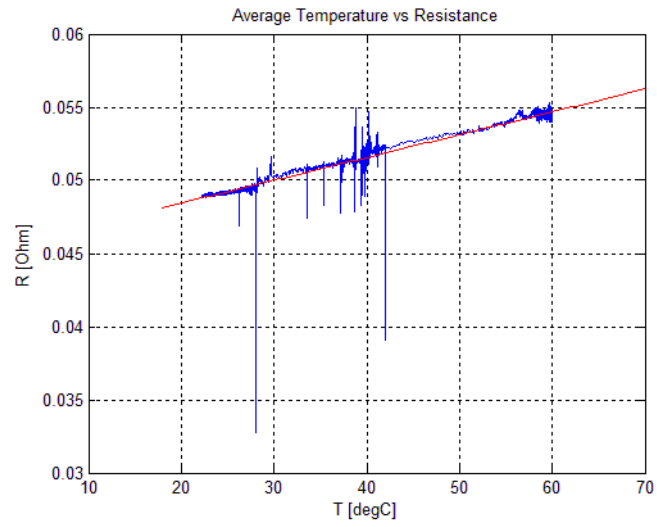
Fig. 5.1.1. First measurement series (blue) with a first order trend curve (red) of the temperature coefficient.
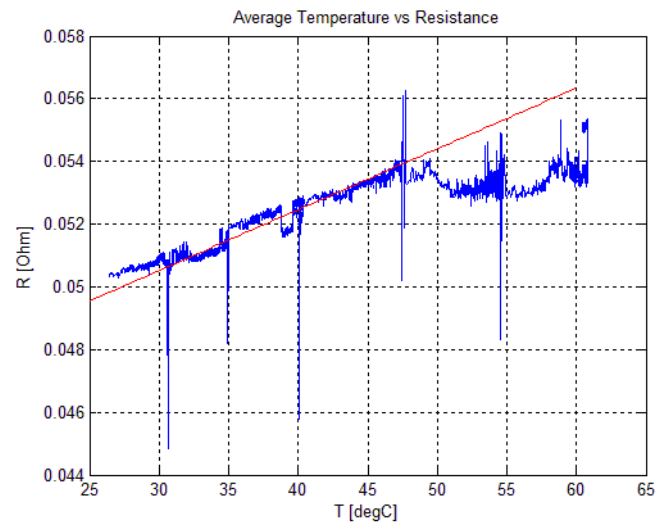
Fig. 5.1.2. Second measurement series (blue) with a first order trend curve (red) of the temperature coefficient.
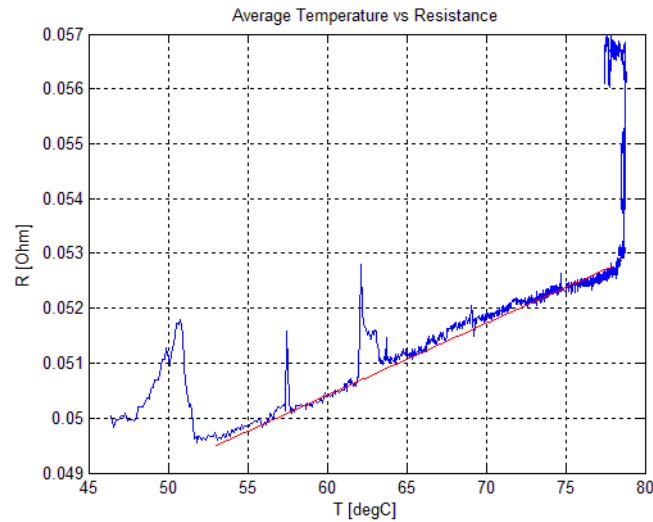
Fig. 5.1.3. Third measurement series (blue) with a first order trend curve (red) of the temperature coefficient.

It was expected that the three independent measurements should show similar results, but when comparing the red curves in the fig. 5.1.1-3 one will notice that they have different coefficients, i.e. different temperature coefficients.

Table 5.1.1. Temperature coefficients for the three independent measurement (coefficients of the red curves in fig. 5.1.1-3).

Measurement serie	Temperature coefficient α [1/K]
First	0.0032
Second	0.0039
Third	0.0026

As seen in table 5.1.1 the temperature coefficients from the independent measurements are widely varying, resulting in that no real conclusions can be drawn from these measurements. Instead the temperature coefficient is approximated by simulating for different currents through the winding. The simulation is made by using the same currents as in the measurements and altering the convective heat transfer coefficient until the same temperature as for the measurement is achieved. When the temperatures are the same the thermal properties of the pure material in the simulation are altered until the voltage is the same as in the measurements. The result of this approximated the temperature coefficient to 0.00348 K^{-1}.

The natural cooling was studied by applying a small current through the winding. The winding is surrounded by an iron core which in turn is surrounded by a casing. The housing is encapsulated by a styrofoam insulation. Fig. 5.2.1 shows an illustrative cross-section of the setup.
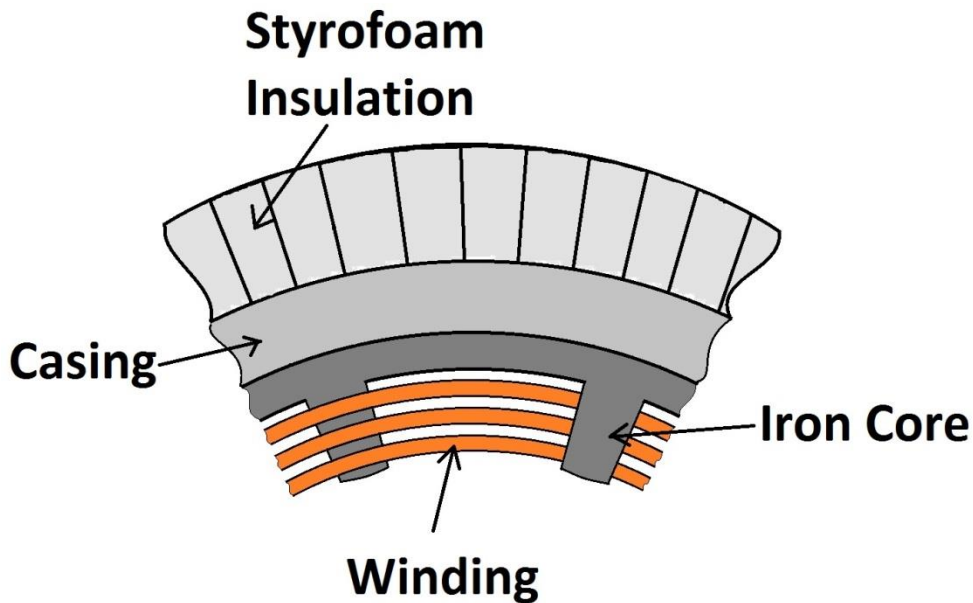
Fig. 5.2.1. Illustration of what is surrounding the winding.

After hours of letting the winding and housing reach their stationary temperature, the natural heat transfer coefficient could be calculated. Note that even after almost 8 hours of waiting the temperature of the winding was not completely at stationarity. The heat transfer coefficient looks as if it would not move much more even if the test would be prolonged, i.e. this measurement is regarded as a success. These are used to calculate the natural cooling over the surface area of the winding, i.e. the top and bottom of the winding if it was uncoiled to a long strip. It should be noted that the whole setup is located in a room with a temperature of approximately 20°C, which was used in the calculation of the heat transfer coefficient. The heat transfer coefficient is used as a measure of how much heat energy that is dissipated through other means than forced cooling.

5.2.1 NATURAL COOLING OF M1

The fig. 5.2.2 shows that the heat transfer coefficient converges around 1.5W/m²K as the temperature for a given added power reaches stationarity. This means that the winding dissipates heat to its surroundings via conduction, radiation and natural convection. The largest contributor to this heat transfer coefficient is most likely the conduction from the winding through the housing and styrofoam to the free air.
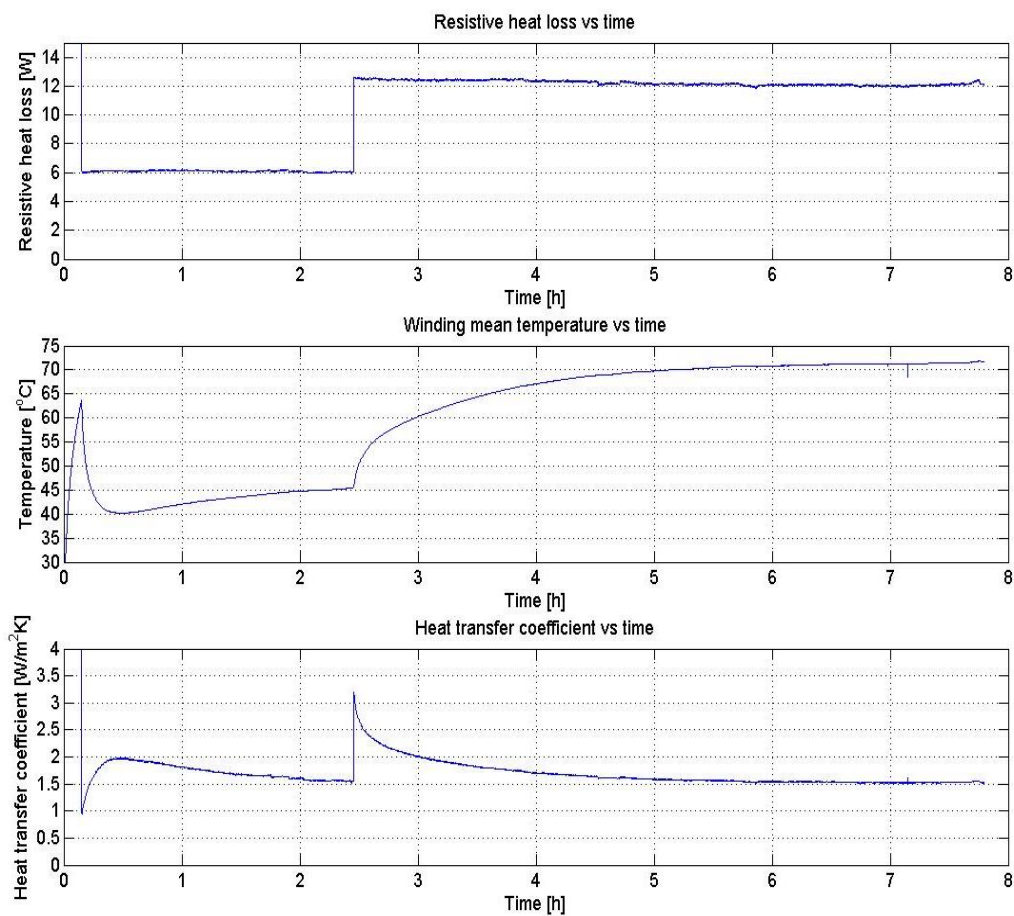
Fig. 5.2.2. Three plots from the measurements made during the investigation of natural cooling of M1.

Also seen in fig. 5.2.2 is that the heat transfer coefficient converges towards the same value, independent of the temperature and added power, which is consistent with theory.

5.2.2 NATURAL COOLING OF M2

The procedure of the natural cooling measurement for M2 was made the same way as with M1. Since the IR-camera was used to measure the winding temperature it was chosen to not record the whole sequence, as an effort to save time when converting the recording to numerical temperatures. It should also be noted that the winding was encapsulated directly by the styrofoam funnel, i.e. there was no casing for this winding.
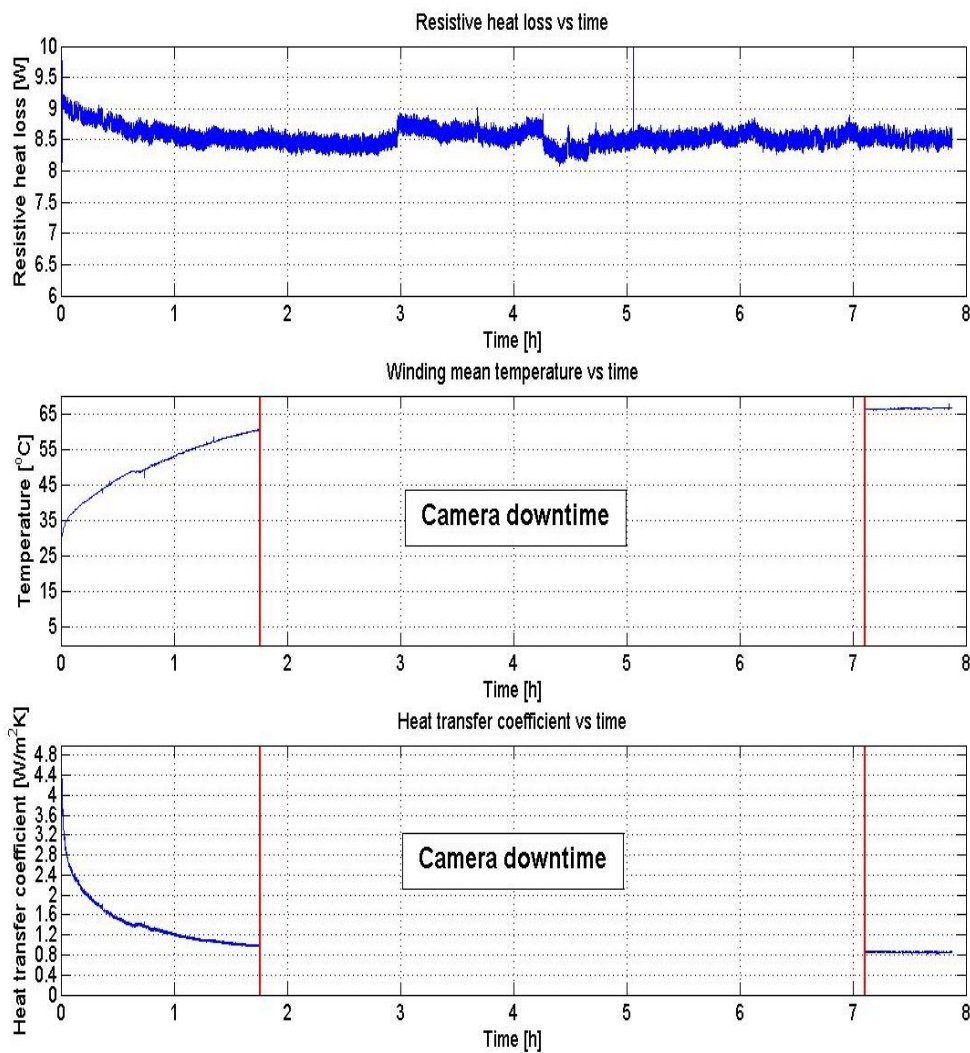
Fig. 5.2.3. Three plots from the measurements made during the investigation of natural cooling of M2.

The heat transfer coefficient converges toward 0.8W/m²K. There could be numerous reasons for measuring a lower natural heat transfer coefficient than that from M1. It is believed that this is due to the lack of casing, which in M1's case gives a good conductive path for the heat transfer.

5.3.1 M1

The forced cooling is investigated in several stationary points. The current density is varied from 9 up to 14.5 A/mm^2 in increments of 0.5 A/mm^2. The air flows used in the measurements was 5.8, 6.6, 7.7, 8.4 and 9.5 g/s, which corresponds to 41, 47, 55, 60 and 68 l/min at 6 bar air gauge pressure. The result of this is shown in fig. 5.3.1.
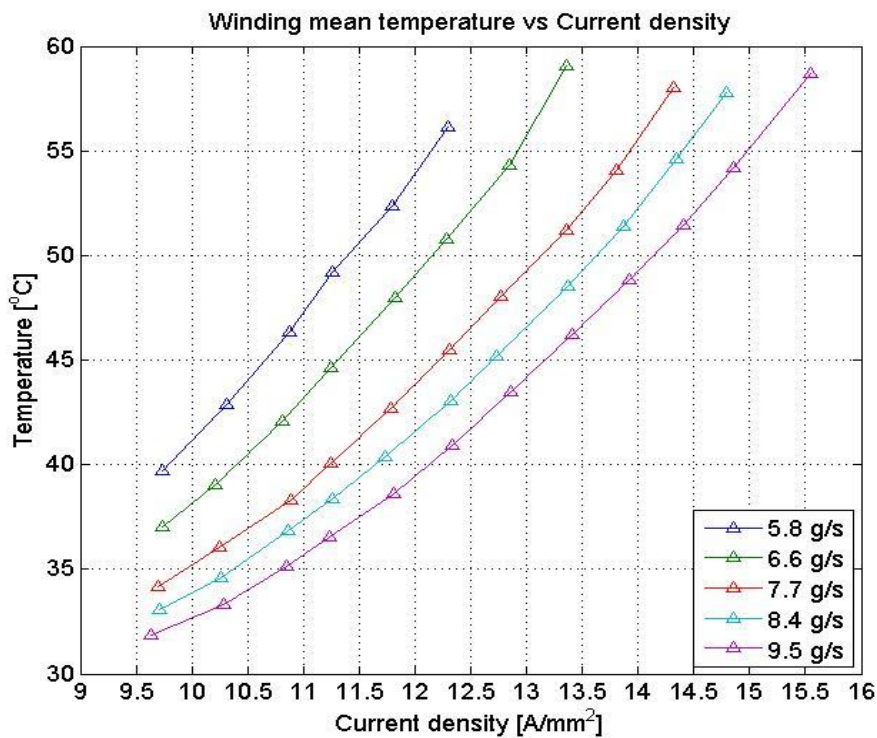

Fig. 5.3.1. The mean winding temperature plotted against the current density for different mass flow rates for M1.

Note that the temperatures, in particular for higher current densities, are lower for these measurements than the previously made (see Appendix B). This shows that less of the air is wasted and is now used in the cooling

process. The second order behavior (fig. 5.3.1) of the current density, i.e. current since the area is constant, vs. temperature can be derived from eq. 5.1 and 5.2. Fig. 5.3.2 illustrates the correlation between the added power and air cooling power for different mass flow rates. The reader might notice that the figures are the same except for the slight shift in the x-direction, i.e. $P = c\dot{Q}$ where c is a constant larger than 1. While keeping a constant air flow and assume that the variation of the inlet temperature is minimal, i.e. almost constant, the eq. 5.1 and 5.2 yield

$$I^2R \geq c_1(T_{exit} - c_2) \qquad\qquad 5.3.1$$

where $c_1 = c\dot{m}C_p, c_2 = T_i$. The relation between T_{exit} and T_s (surface temperature of the winding) is described by

$$T_{exit} = T_s - (T_s - T_i)e^{\frac{-hA_s}{\dot{m}C_p}} \qquad\qquad 5.3.2$$

Every variable except T_s in eq. 5.3.2 can be considered constant for a constant mass flow, i.e. $T_e \propto c_3 T_s$ where c_3 is less than one since the temperature of the air cannot be larger than the temperature of the winding surface without breaking the law of conservation of energy.
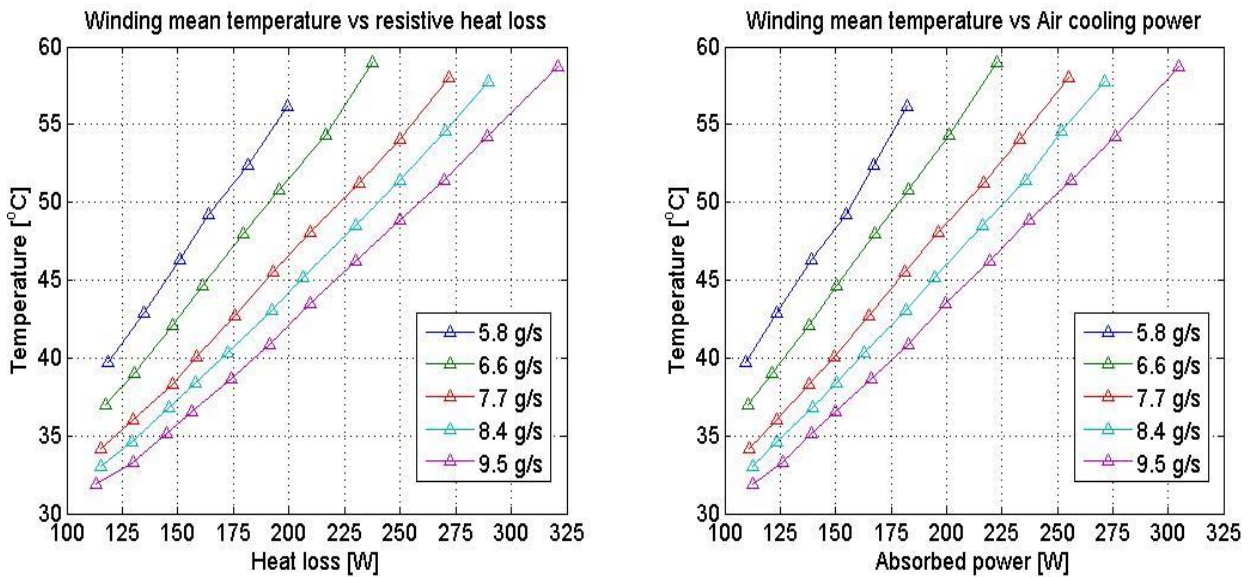
Fig. 5.3.2. The mean winding temperature plotted against the Added power (left) and Air cooling power (right) for different mass flow rates for M1. The mean percentage difference between heat losses and absorbed power is 5% without natural heat transfers and 2% with.

The ideal pump power required to supply the air flow is quite low, as seen in *fig. 5.3.3.* As the figure shows it is required to increase the power as temperature increases. Eq. 2.3.7 states that the pressure drop over a channel is

$$\Delta p = 0.5 f \frac{L}{D_h} \rho U^2$$

where $U = \frac{\dot{m}}{A\rho}$. With this added to the equation the result is

$$\Delta p = 0.5 f \frac{L}{D_h} \frac{\dot{m}^2}{A\rho} \qquad\qquad 5.3.3$$

Since density of air decreases with increasing temperature, the pressure drop over the channel will also increase, hence the increasing pump power for a constant air flow as seen in fig. 5.3.3.
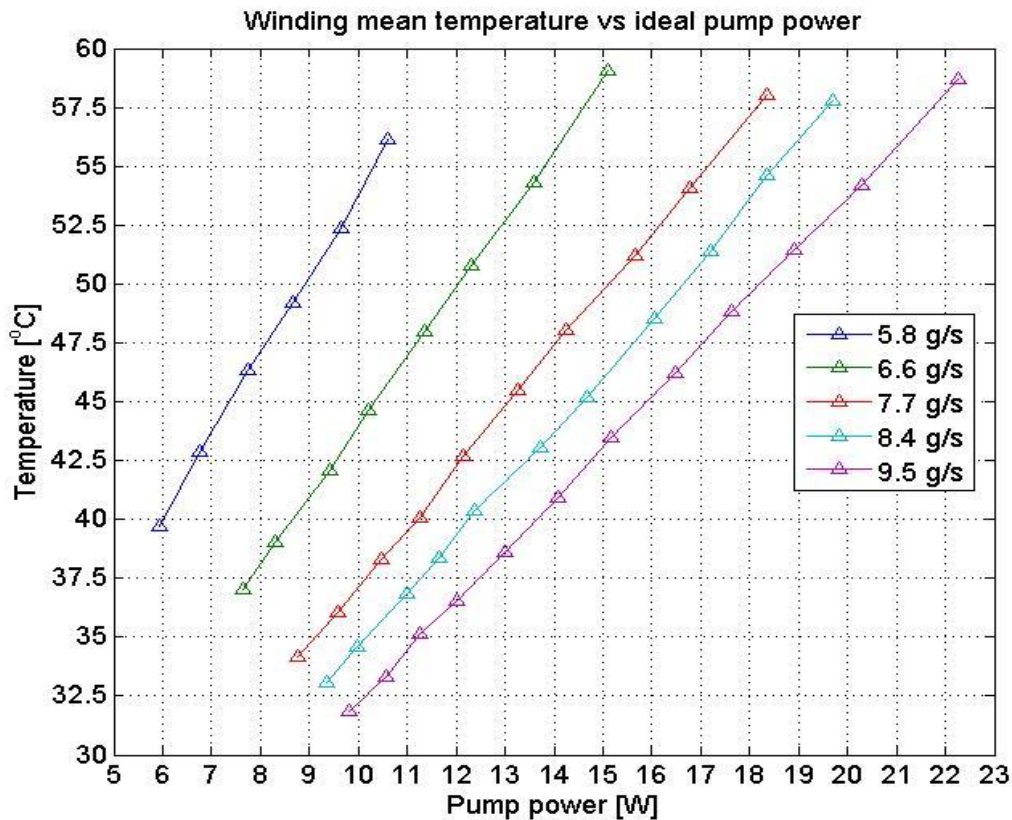
Fig. 5.3.3. The mean winding temperature plotted against the Ideal pump power required for different mass flows M1.

Fig. 5.3.4 shows a performance curve of how much ideal pump power one must use in order to keep the winding at a desired temperature for different heat losses. For instance if the heat loss is 190W there are a wide variety of ideal pump power that can be chosen from, depending on what is a tolerable winding temperature is for that application.
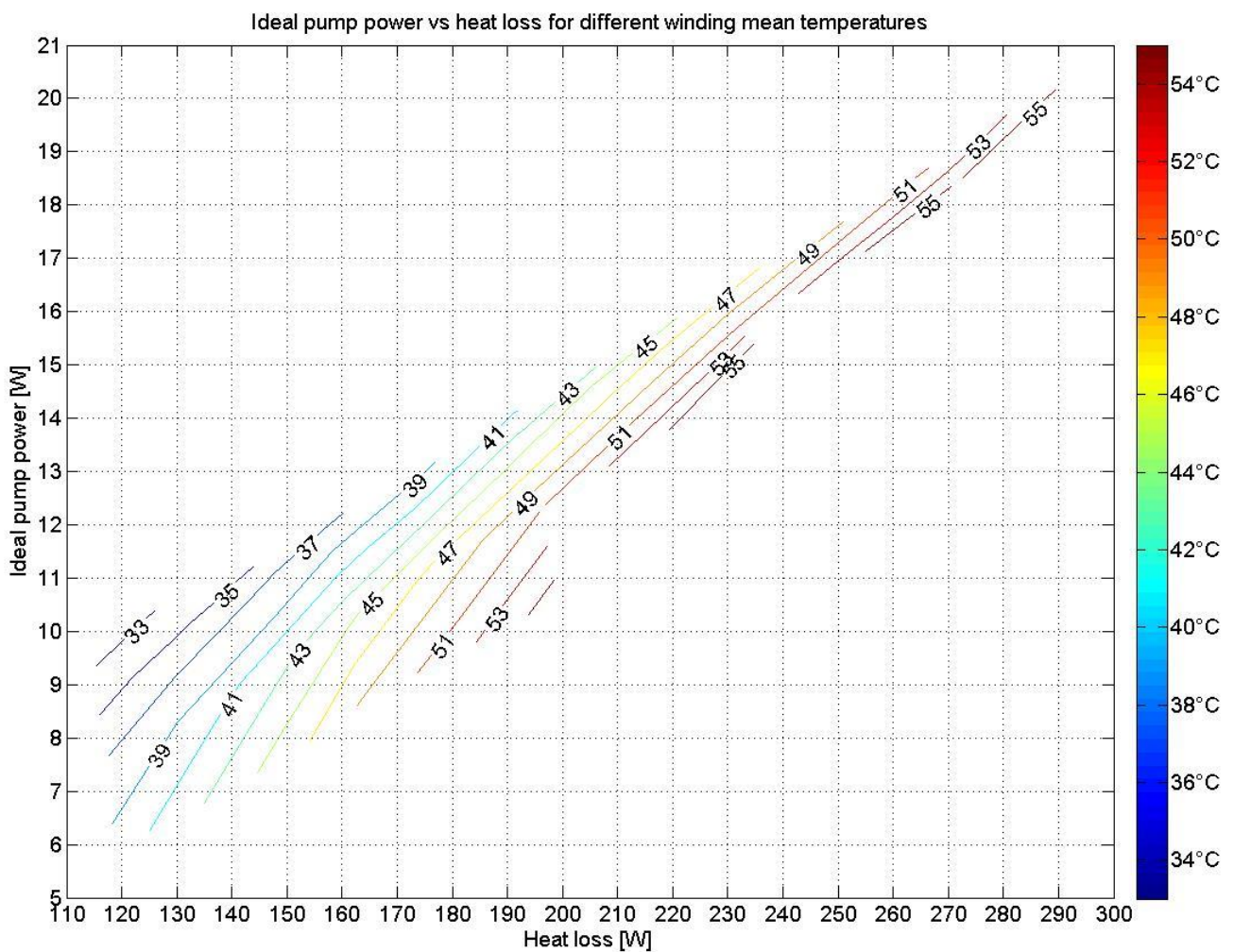
Fig. 5.3.4. The of Ideal pump power against heat loss for different mean winding temperatures.

5.3.2 M2

The forced cooling for M2 is done in a similar fashion as for M1. The current density is varied from 8 to 12.5 A/mm² and the air flow is varied from 5 to 9 g/s. The result from this is presented in fig. 5.3.5.
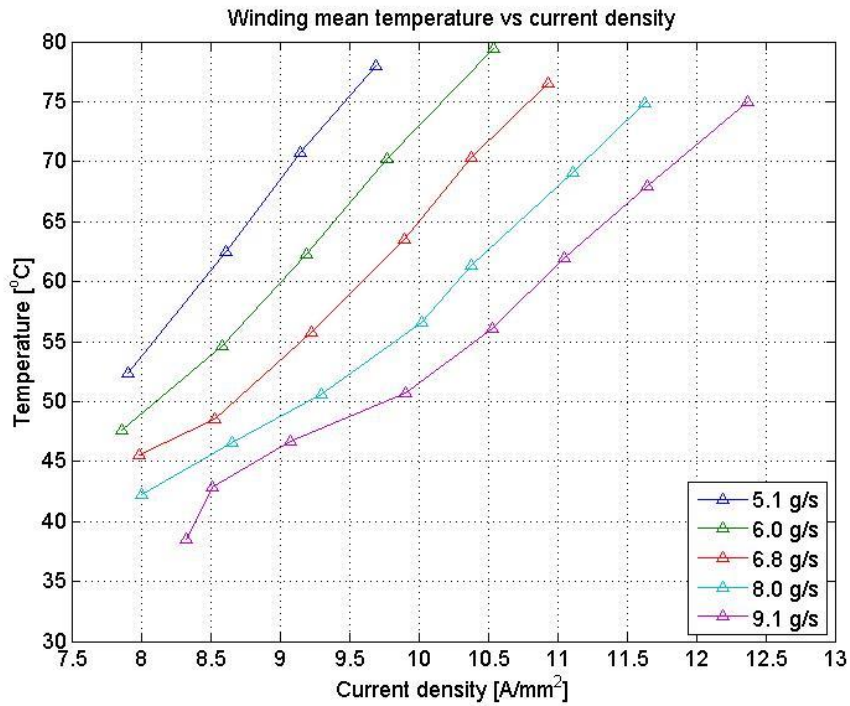

Fig. 5.3.5. The mean winding temperature plotted against the current density for different mass flow rates for M2.

The heat loss from these current densities are presented in fig. 5.3.6, as well as the air cooling power needed for achieving the winding temperatures.
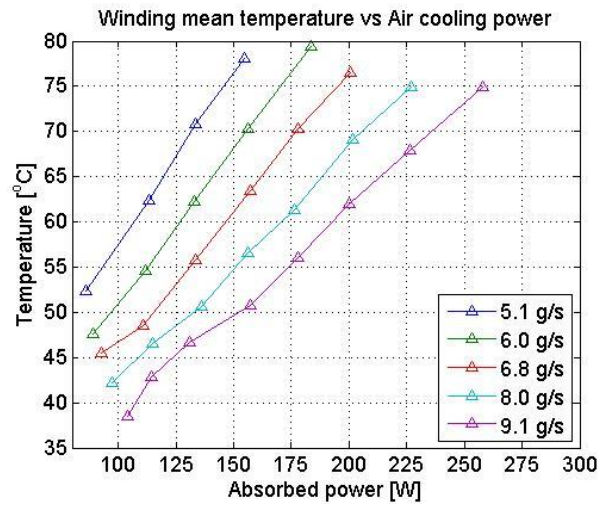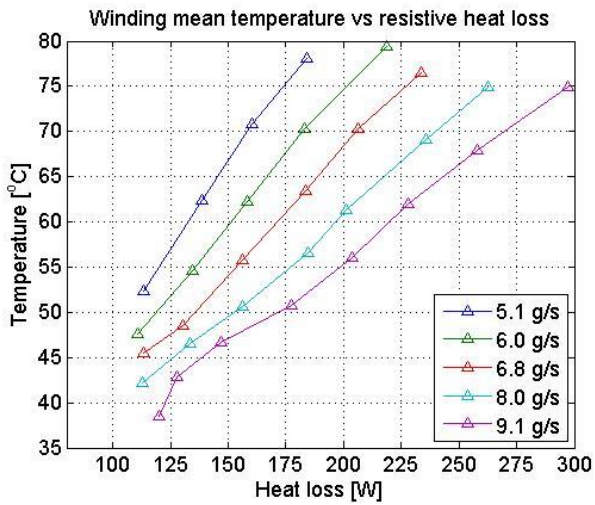
Fig. 5.3.6. The mean winding temperature plotted against the Added power (left) and Air cooling power (right) for different mass flow rates for M2.

Figure 5.3.6 show a rather large different between heat losses and absorbed power. Some of the difference is explainable through natural heat transfers leading heat out through the styrofoam cover. Some of it cannot be explained with theory and is probably a cause of leakages in the setup and misreading's from the flow meter and air temperature sensors. The mean difference between heat loss and absorbed power are 15% without adding natural heat transfers and 9% with it.
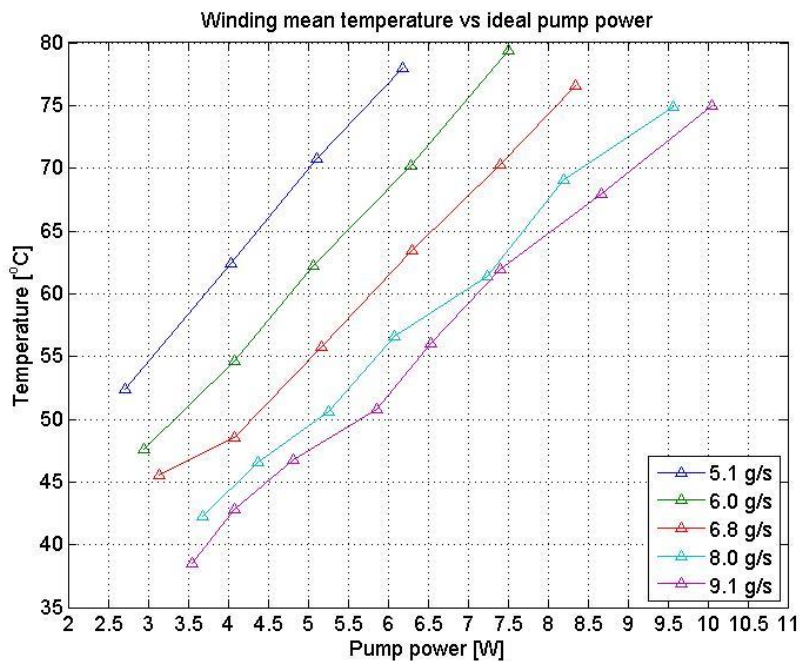
*Fig. 5.3.7. The mean winding temperature plotted against the ideal pump power required for different mass flows for M2.*

As mentioned above the heat losses and absorbed power does not add up as they should in steady state conditions. Even after taking natural heat transfers into account the mean difference is 9% which seems a bit high for the measurements to be reliable. These 9% are believed to be a consequence from a number of factors such as faulty mass flow and temperature readings as well as air leakages in the insulation of the test rig. The plastic frame which holds the winding emits heat radiation that blurs the image from the camera which might influence the temperature readings.
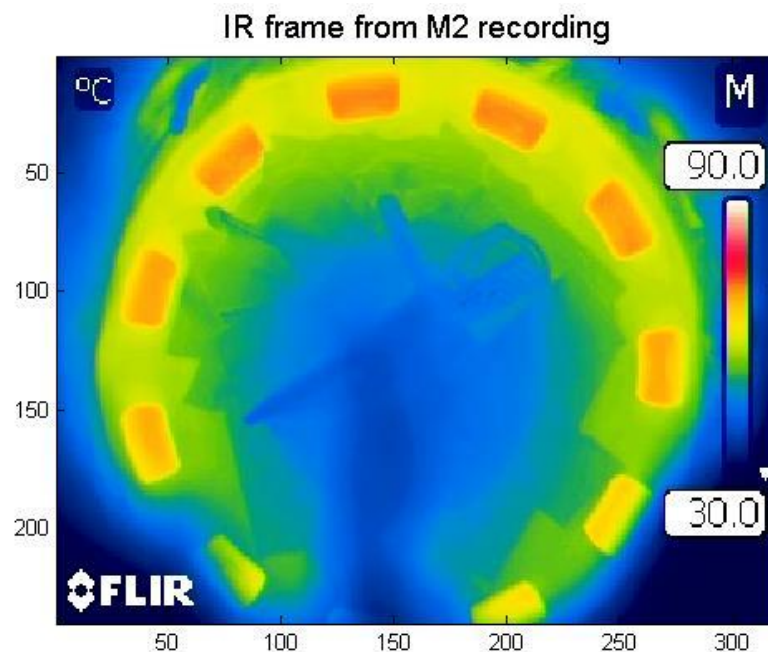
Fig. 5.3.8. A blurry image from the temperature recordings of M2. The focus of the image is correct but the radiation from the plastic frame makes the image blurry.

The factors mentioned degrade the trustworthiness of the measurements executed on winding M2. The lack of time stopped the development of a better test rig. Listed below are things that should be considered for future measurements:

- Recalibrate the flow meter or even buy a proper one.
- New junction end on all thermocouples.
- Paint the plastic frame of the winding, preferably matte black.
- Build a proper test rig to minimize air leakages, preferably lathing a cylindrical casing which fits the winding perfectly like the one used for M1.

5.4 DIRECTED FORCED COOLING

The measurement with the directed forced cooling is made the same way as for the regular forced cooling. The same current densities and similar air flows are used. The increased pressure in the housing affected the flow measurement device, which resulted in that the set points to the air flow differed from the measurements with regular forced cooling. The new set points of the air inlet valve are chosen such that the air flow would end up near the ones used in regular forced cooling. The actual air flows ended up at 5.9, 6.7, 7.4, 8.1 and 8.8 g/s, which correspond to 42, 48, 53, 58 and 63 l/min at 6 bar air gauge pressure. If the reader want to remind him-/herself of how the directed cooling is applied you might want to look at fig. 3.2.3.
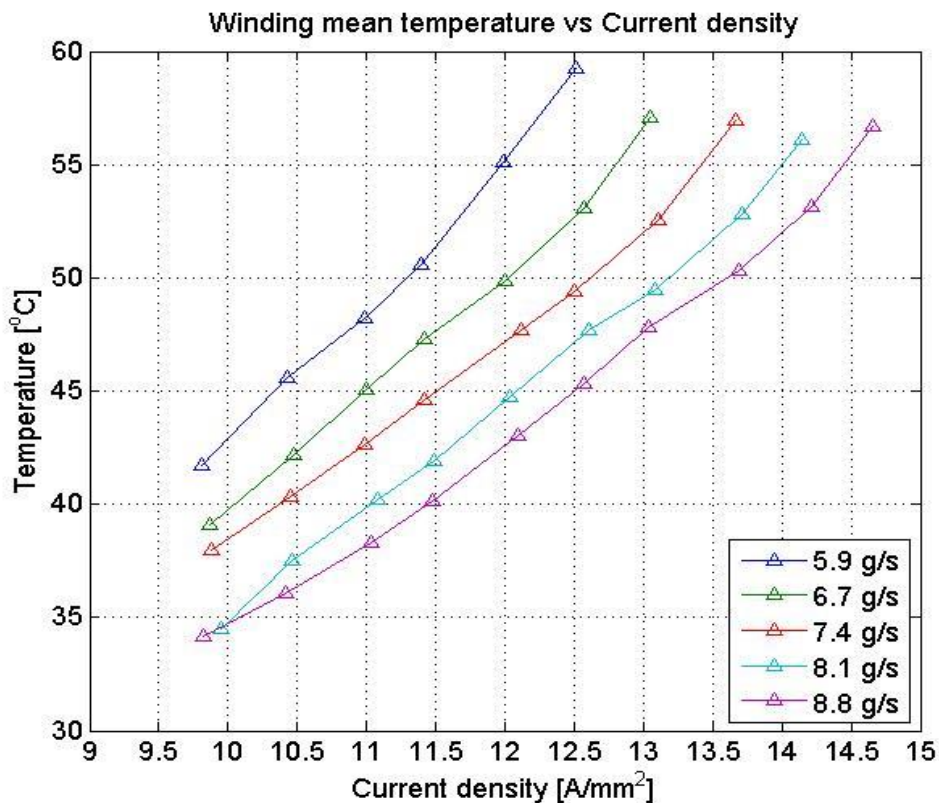
Fig. 5.4.1. The mean winding temperature plotted against the current density for different mass flow rates.

Unfortunately the air flow set points were selected a bit carelessly, giving only two air flows that are comparable to each other, i.e. the blue and green curves. If comparing the results in fig. 5.3.1 and 5.4.1 one notices that the temperatures are slightly higher in the latter. This results in that less added power is required to reach the maximum temperature restriction in the

measurements, i.e. the winding is cooled less with the directed cooling than without it. This will be noticed when comparing results presented in fig. 5.3.2 and 5.4.2.
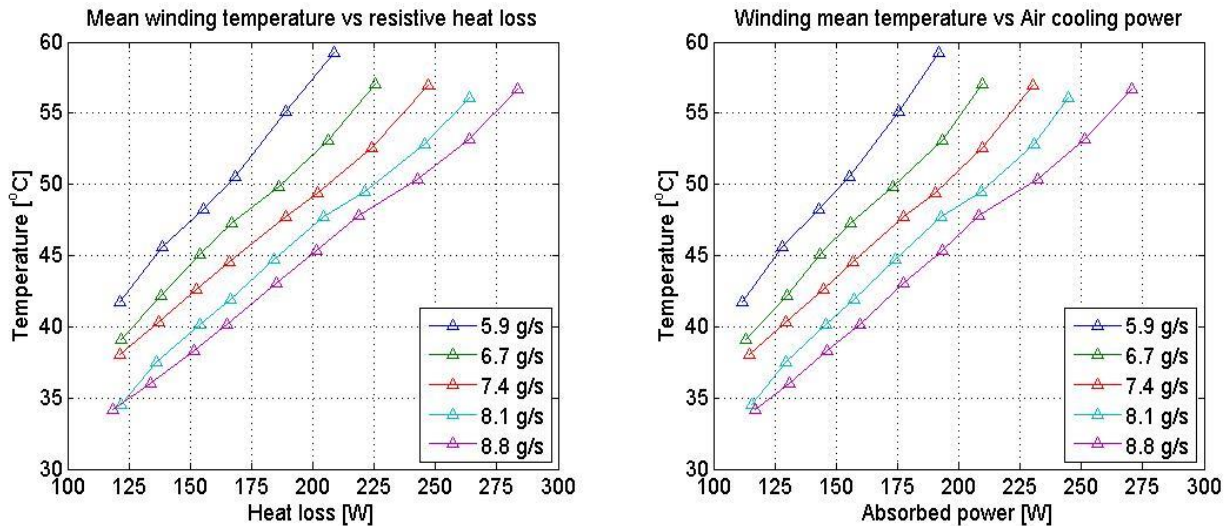
Fig. 5.4.2. The mean winding temperature plotted against the resistive heat loss (left) and air cooling power (right) for different mass flow rates.

It is excepted that the pressure inside the housing would increase since the area which the air could pass through the winding is reduced. Increased pressure drop over the winding is directly correlated to increase in the pump power needed to supply the required air through the winding. Fig. 5.4.3 and 5.3.3 are very similar, meaning that the pressure drop over the winding was not affected to a noticeable degree. But when studying these previously mentioned figures further there is a minor difference in the mean winding temperatures. With the directed forced cooling the temperature are slightly higher than for the regular forced cooling, suggesting that the cooling is not as effective in the both cases even with the mass flow and ideal pump power are almost the same. This means that the pump power should be increased when using directed forced cooling in order to achieve the same performance, i.e. the same winding temperature, as with the regular forced cooling.
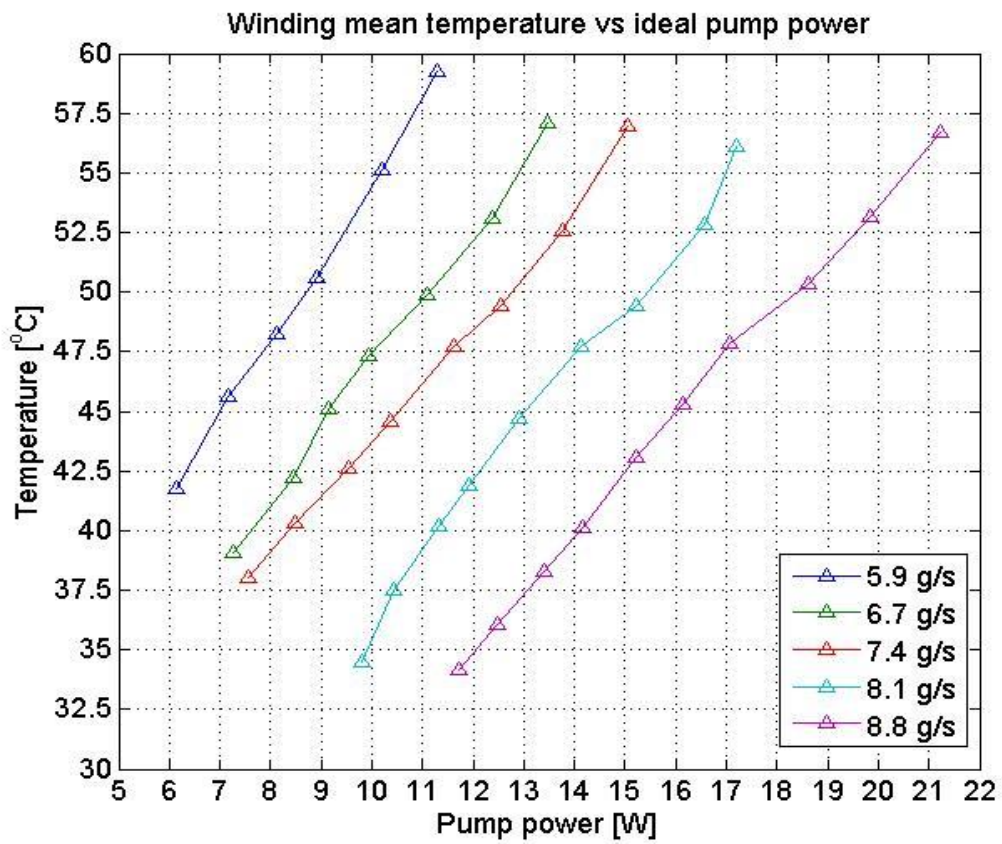
Fig. 5.4.3. The mean winding temperature plotted against the ideal pump power required for different mass flows.

The difference between fig. 5.4.4 and 5.3.4 are quite noticeable. Fig. 5.4.4 suggests that for a specific heat loss there might not be a suitable operation point to which both pump power and winding temperature requirements are met. Taking the same example as for the results in fig. 5.3.4, i.e. study the figures around 190W of added power, there are some similarities between the two for higher temperatures. But if one wishes to cool the winding further the cost in pump power increases more in the directed cooling approach. It is possible that the temperature curves in fig. 5.3.4 would show the same behavior as in fig. 5.4.4, but failed to show this within the range of the measurements.
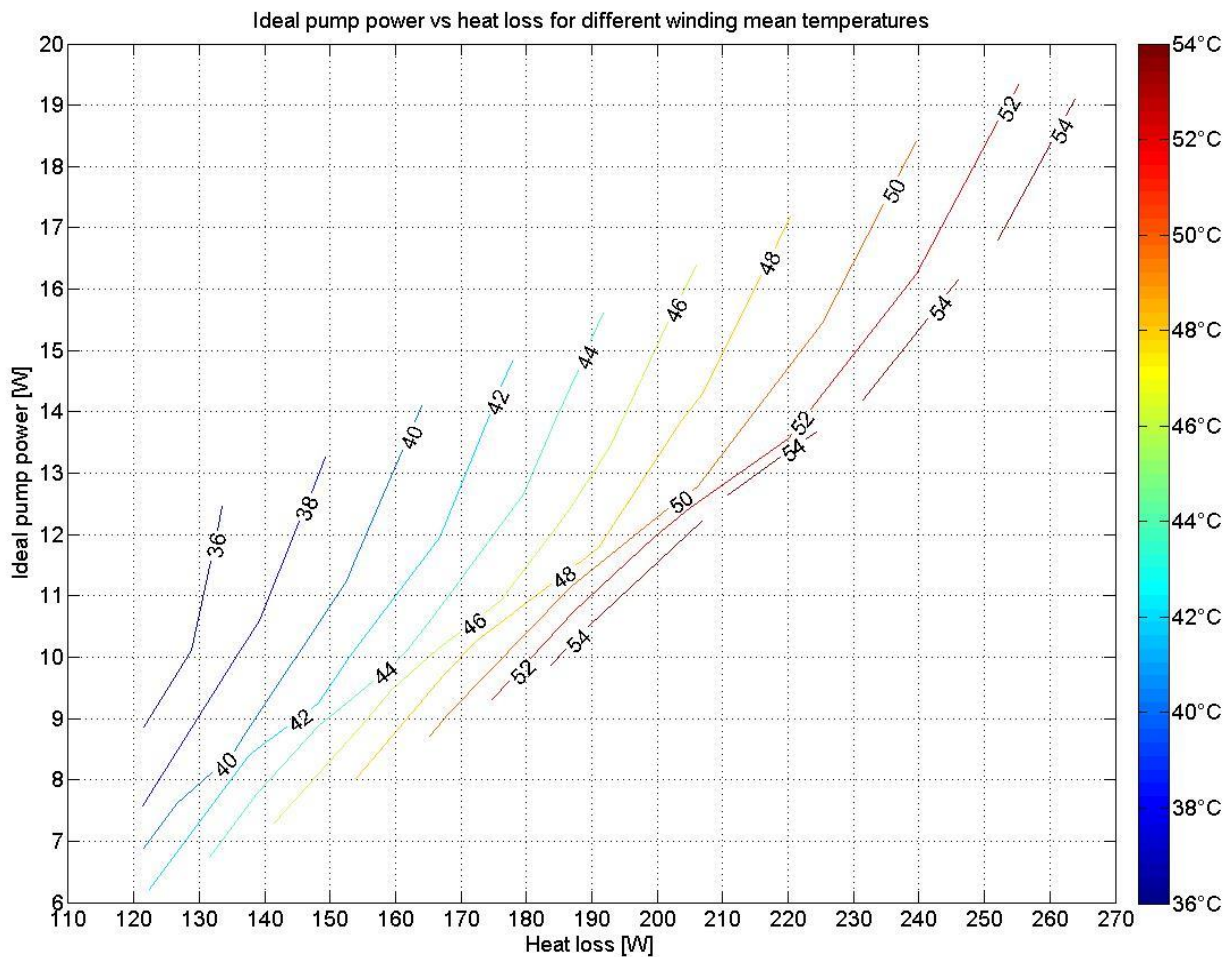
Fig. 5.4.4. The of Ideal pump power against resistive heat loss for different mean winding temperatures.

The first comparison is made between the results from chapter 5.3 "Forced cooling" and an ideal simulation done with the help of the analytical Matlab model which is presented in chapter 4.1. The simulation is ideal with regard to distance between winding layers, meaning that all layers are spaced equally and with the specified width. The recorded values of current density and mass flow from the measurements are used as input to the simulation model.
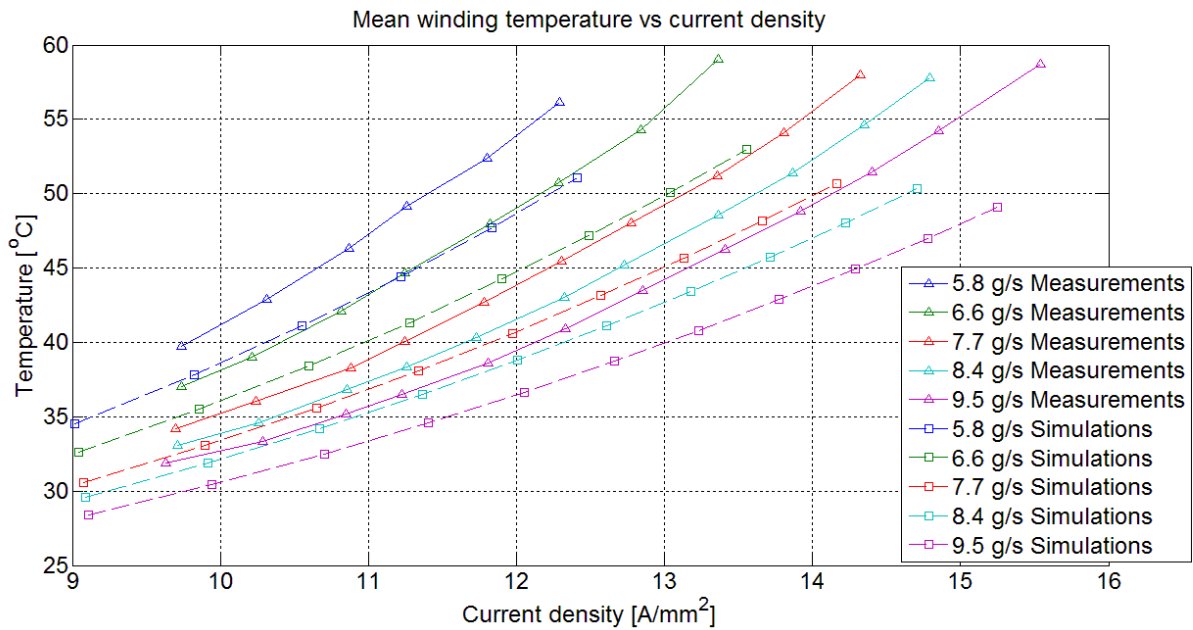

Fig. 5.5.1. Mean winding temperature for different current densities and mass flow rates. Dashed lines with squares represent values from the simulation with evenly spaced winding layers. Solid lines with triangles represent recorded values from the measurement series "Forced cooling".

The mean winding temperatures from the measurement series are higher than the ideal simulated case. This is not strange since the prototype used in the measurements has flaws that the ideal model does not take into account. Figure 5.5.1 show that the simulated and measured results follow the same trend as the current density increase but the simulated winding temperatures are cooler. This tells that the mean convection of the prototype winding is lower than the ideal case and therefore is the winding bound to hold a higher surface temperature in order to dissipate the heat loss energy to the air. From model evaluations (chapter 4.4) one can read about the mean convections sensitivity to unevenly spaced layer turns. The results in figure 5.5.1 indicate that the winding layers of prototype M1 are unevenly spaced and an attempt to describe the magnitude of the error is presented below.

The assembly the prototype laminated winding is made by wind a long conductor plate into a coil. This is done by hand and the precision of the space between winding layers is not always the best. In the prototype M1 the layers closest to the rotor is more tightly wounded than outer layers, the problem has been helped by inserting distances between laminates but the problem still exists in some extent.

Fig. 5.5.2. Illustration of the layer spacing in prototype machine M1.

From figure 5.5.2 one can scent that the inner layers are more tightly winded than the outer ones but the difference is hard to extinguish with the naked eye. Figure 5.5.3 show a thermal image of the same winding piece but with heat losses present, note that the air flow is not turned on in figure 5.5.3.
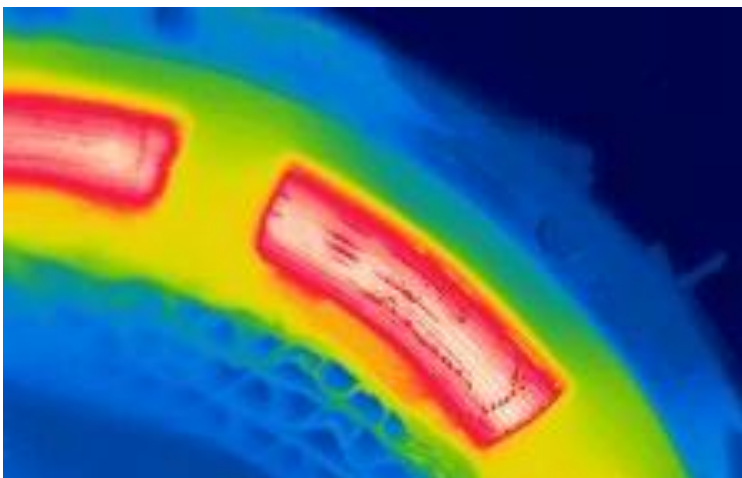
Fig 5.5.3. Thermal image of M1, heat losses are present but mass flow is turned off.

In figure 5.5.3 one can see that the heat is evenly distributed over the whole winding except for the winding turns closest to the casings which are a bit cooler due to the path of the natural cooling (see chapter 2.2). Figure 5.5.4 show the same winding piece under similar circumstances but with a steady stream of forced airflow through it.
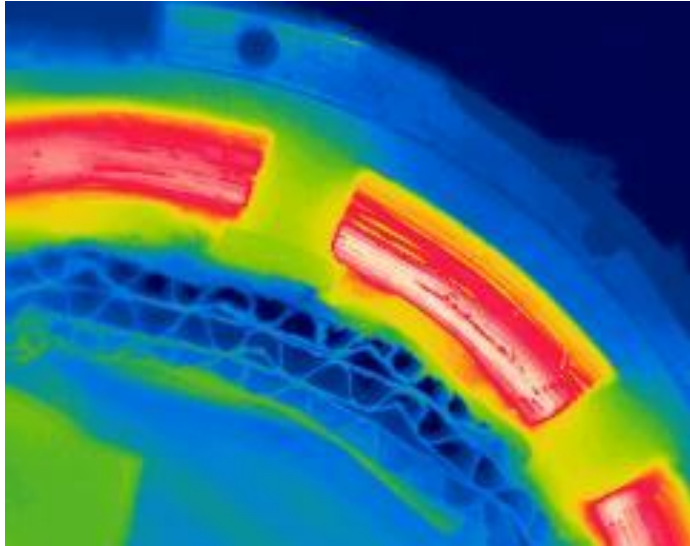
Fig 5.5.4. Thermal image of M1, heat losses and mass flow are present.

In figure 5.5.4 one can see that the winding turns closest to the casing are considerably cooler than the inner turns as the air flow is present. Since the temperature difference is higher with forced air present than without it is the phenomena not only a result from the natural heat paths but also on the fact that more air travels though the outer turns since they have a larger layer spacing. To determine exactly how big a difference in layer spacing there is between laminates are not possible but figure 5.5.5 show a comparison between measured values and simulations using the layer spacing presented in figure 5.5.6.
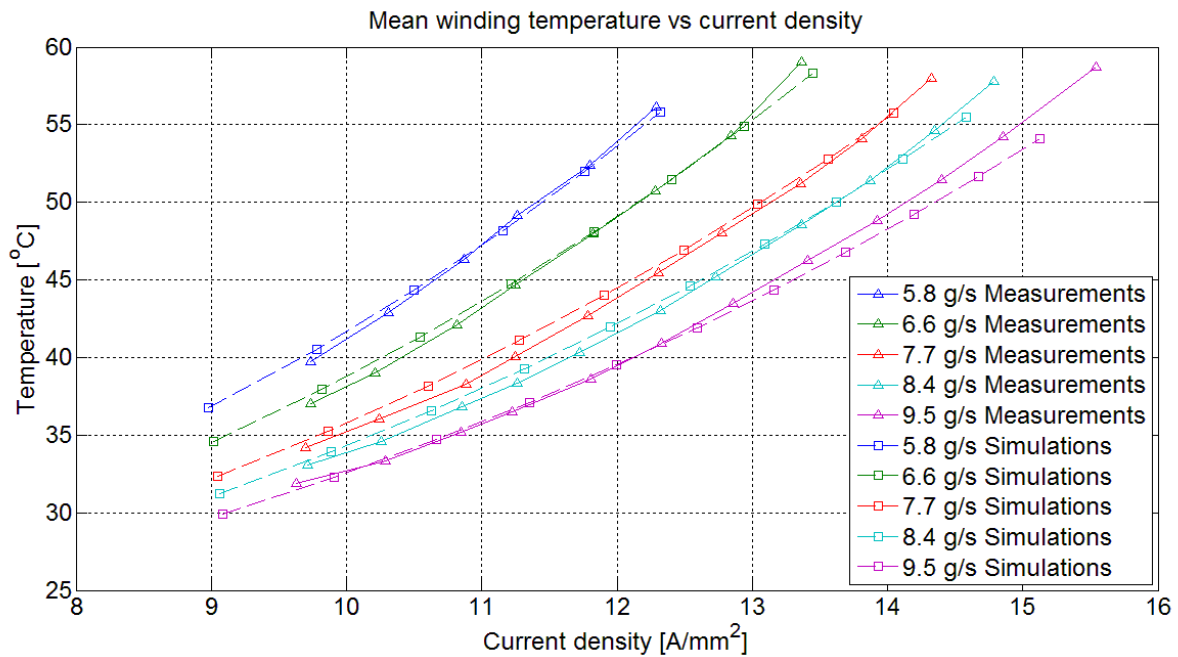
Fig 5.5.5. Mean winding temperature for different current densities and mass flow rates. Dashed lines with squares represent values from the simulation with the layer spacing presented in figure 5.5.6. Solid lines with triangles represent recorded values from the measurement series "Forced cooling".
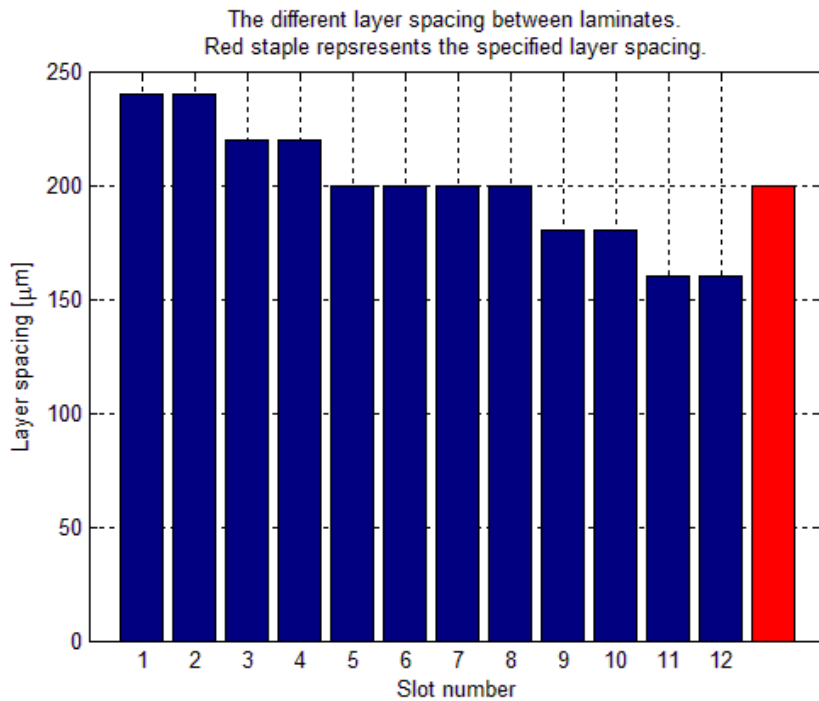
Fig 5.5.6. Illustration of the distance between laminates that is being used in the simulation presented in figure 5.5.5. The red staple represents the ideal case.

The result presented in figure 5.5.5 seems to give a better representation of the performance of prototype M1 than the ideal case. The approximation of the layer spacing used in the simulation (fig 5.5.6) is supported by visual inspection (fig 5.5.2-4).

We cannot exclusively prove that the analytical Matlab model is accurate in every case but the results from this chapter and the theory presented in chapter 2.3 and 4.1 gives us confidence enough to use it when simulating the performance of the three prototype machines M1-3.

6. EVALUATION

The cooling performance of the prototype windings are evaluated for a variety of conductor current densities and winding mean temperature. By controlling the winding mean temperature by altering the air volume flow one can produce cooling maps for the winding. The cooling maps are presented as three coherent maps that show the volume flow, the pressure drop over the winding and the ideal pump power required to maintain the volume flow for different sets of conductor current densities and winding mean temperatures.

Prototypes M2 and M3 are also evaluated in simulated drive cycles with a fictional cooling system in order to see if the machines could be used in a real application.

6.1 COOLING MAPS

To evaluate the cooling performance of the windings cooling maps are made. The cooling maps can be used to determine volume flow, pressure drop and ideal pump power for different conductor current densities for certain winding temperatures. The maps represent only one winding segment, i.e. for a whole machine the ideal pump power and volume flow has to be multiplied with the number of segments used in that machine.

6.1.1 M1

The first prototype (M1) is a generator which is designed to operate at a maximum generated power of 1 kW. The winding was built for educational purposes and is being used during measurements in this thesis. The resistivity that has been evaluated during measurements is used in determining the heat losses from current density, see chapter 5.1.

The cooling performance of M1 has been simulated with the analytical model and is presented in figures 6.1.1 to 6.1.3. In Appendix C figures from the same type of simulation but with an induced layer spacing error are presented.
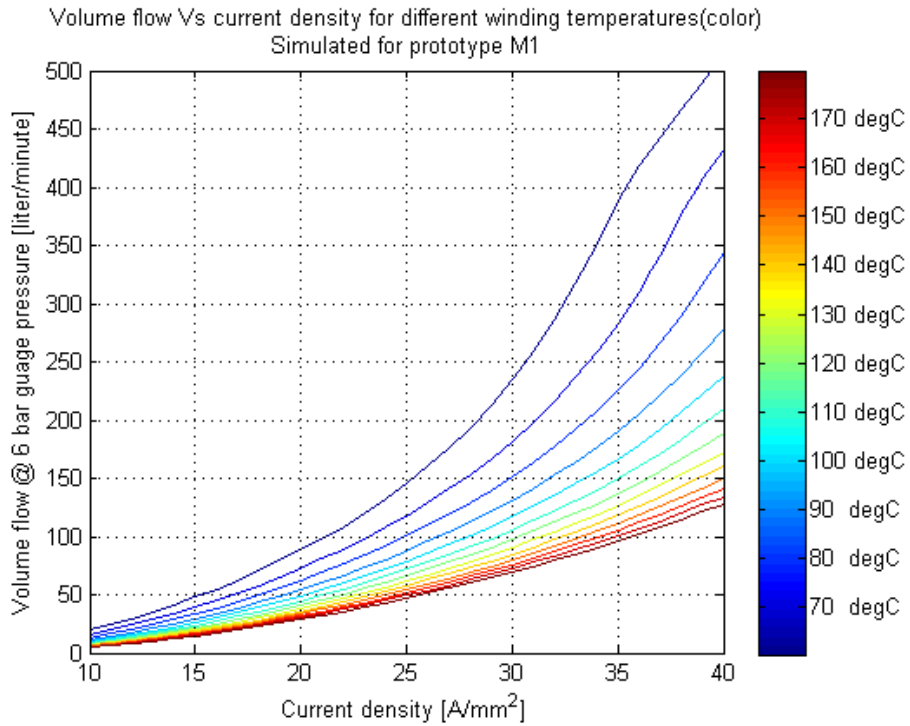
Fig. 6.1.1. The volumetric air flow @ 6 bar gauge pressure that is needed to hold the winding M1 at a certain temperature for different current densities. The temperature curves represent every tenth degree between 40 and 180℃.
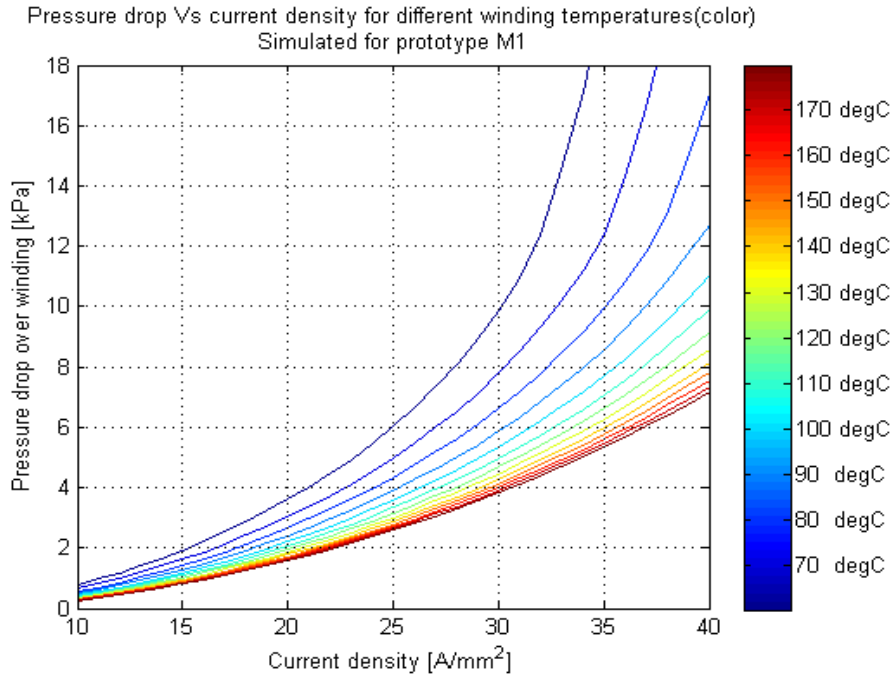
Fig. 6.1.2. Pressure drop over the winding M1 for different current densities and temperature. The temperature curves represent every tenth degree between 40 and 180°C.
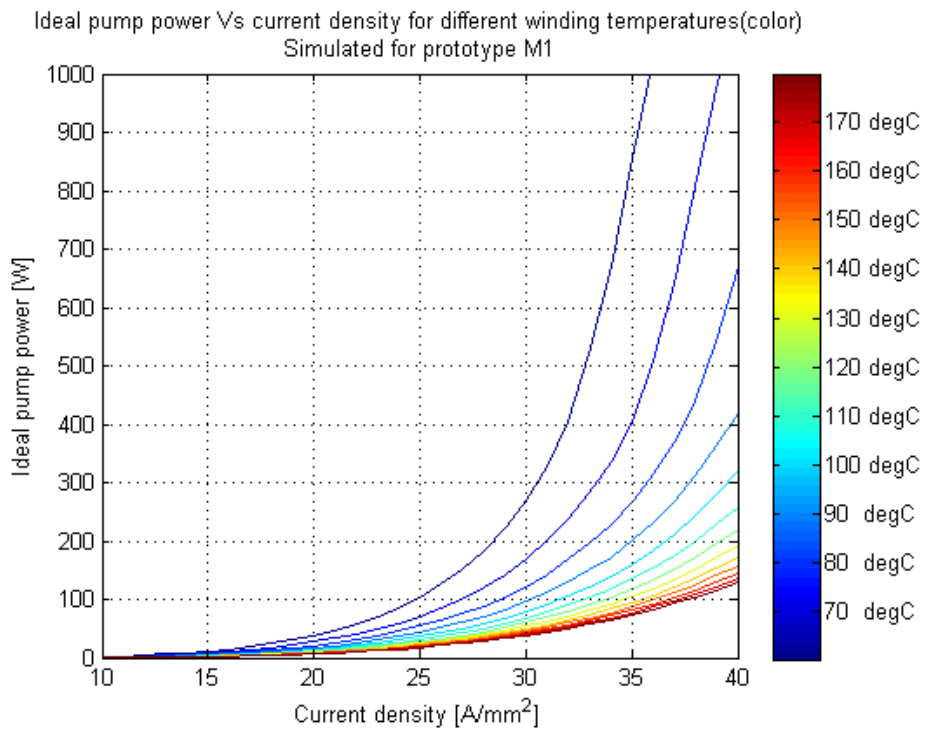

Fig. 6.1.3. Ideal pump power that is needed to cool winding M1 for different current densities and winding temperatures. The temperature curves represent every tenth degree between 40 and 180°C.

6.1.2 M2

The second winding prototype (M2) is going to be used in an electrical wheel chair. The machine which holds M2 is an outer rotor wheel machine and operates at a power of 800 W. The wheel chair has two machines, one for each side and operates at a maximum speed of 20 km/h. Even if the heat development in M2 is low due to the limitations set by the application it is built with laminate technique. The resistivity from chapter 5.2 is used during simulations.

The cooling performance of M2 has been simulated with the analytical model and is presented in figures 6.1.4 to 6.1.6. In appendix C figures from the same type of simulation but with an induced layer spacing error are presented. The results in the cooling maps represent the performance of one winding segment and in M2s case should volume flow and pump power be doubled in order to represent the whole machine.
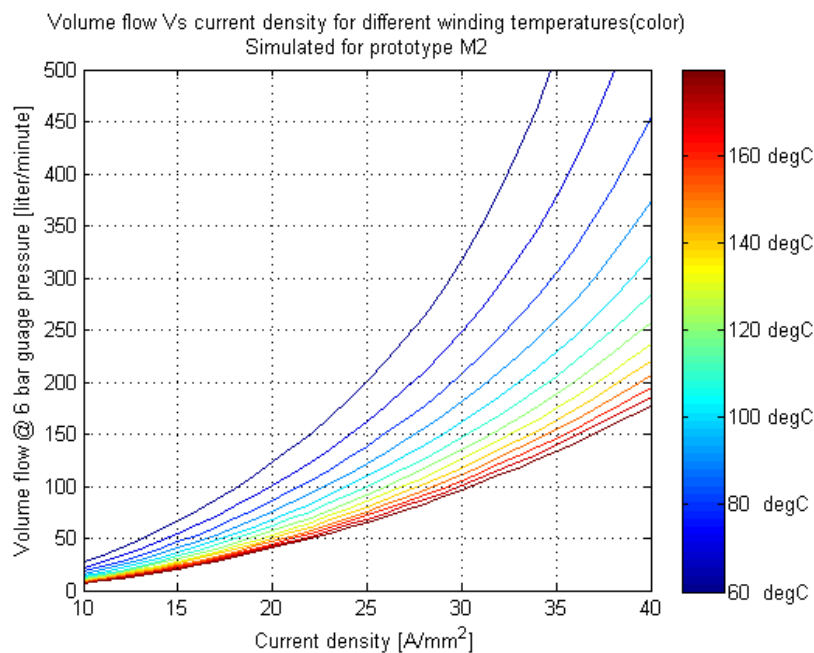
Fig. 6.1.4. The volumetric air flow @ 6 bar gauge pressure that is needed to hold the winding M2 at a certain temperature for different current densities. The temperature curves represent every tenth degree between 60 and 180℃.
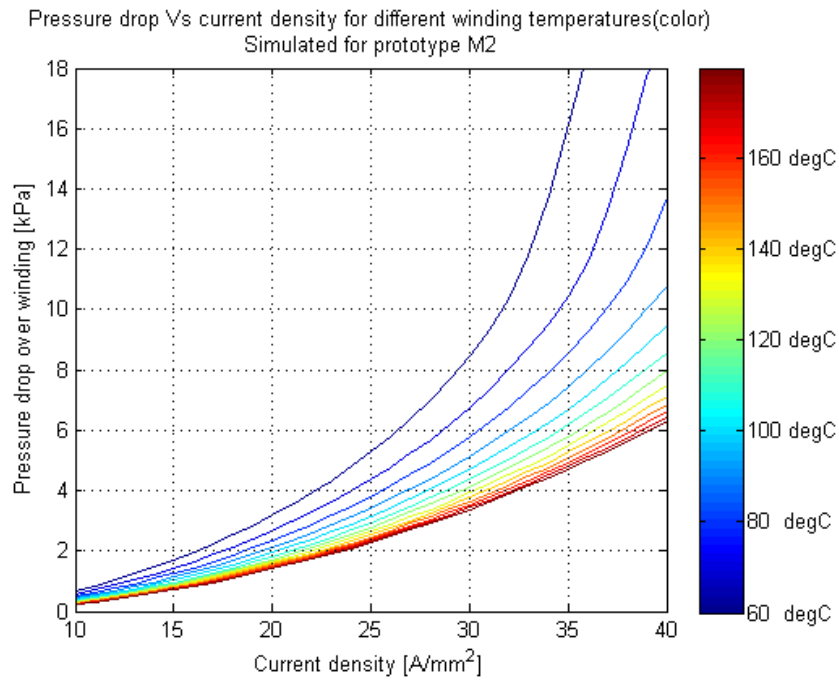
Fig. 6.1.5. Pressure drop over the winding M2 for different current densities and temperature. The temperature curves represent every tenth degree between 60
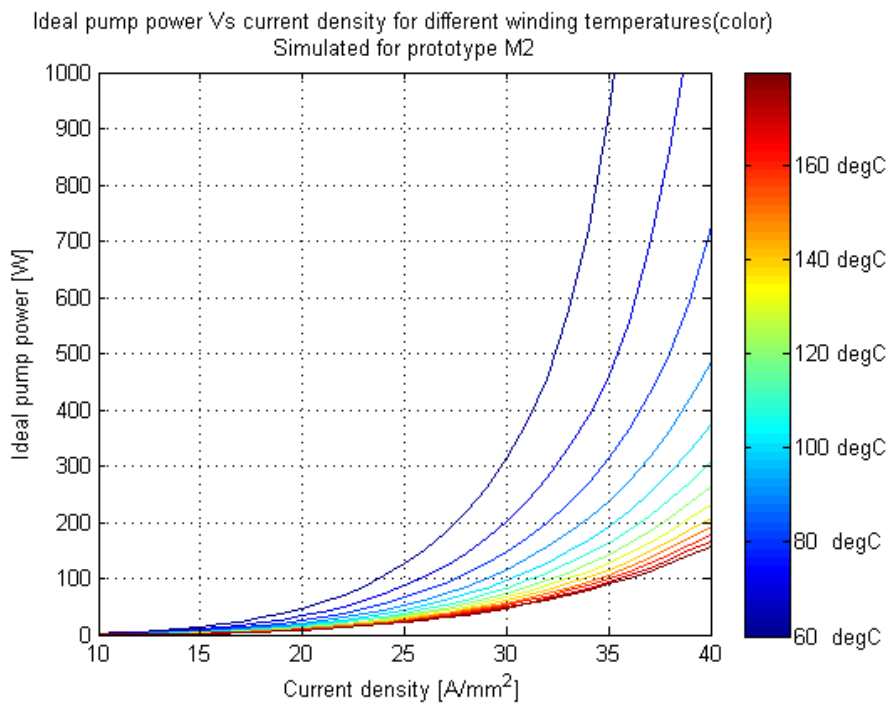
and 180℃.

Fig. 6.1.6. Ideal pump power that is needed to cool winding M2 for different current densities and winding temperatures. The temperature curves represent every tenth degree between 60 and 180℃.

6.1.3 M3

The third winding prototype (M3) is being used in a three phase traction machine. The machine has an intended nominal power of 80 kW and is designed to be used in a city bus.

The cooling performance of M3 has been simulated with the analytical model and is presented in figures 6.1.7 to 6.1.9. In appendix C figures from the same type of simulation but with an induced layer spacing error are presented. The electrical machine M3 is using three winding and therefore the maps representing air flow through the winding and needed pump power (6.1.7 and 6.1.9) a third of the total air flow and pump power needed to cool the whole machine.
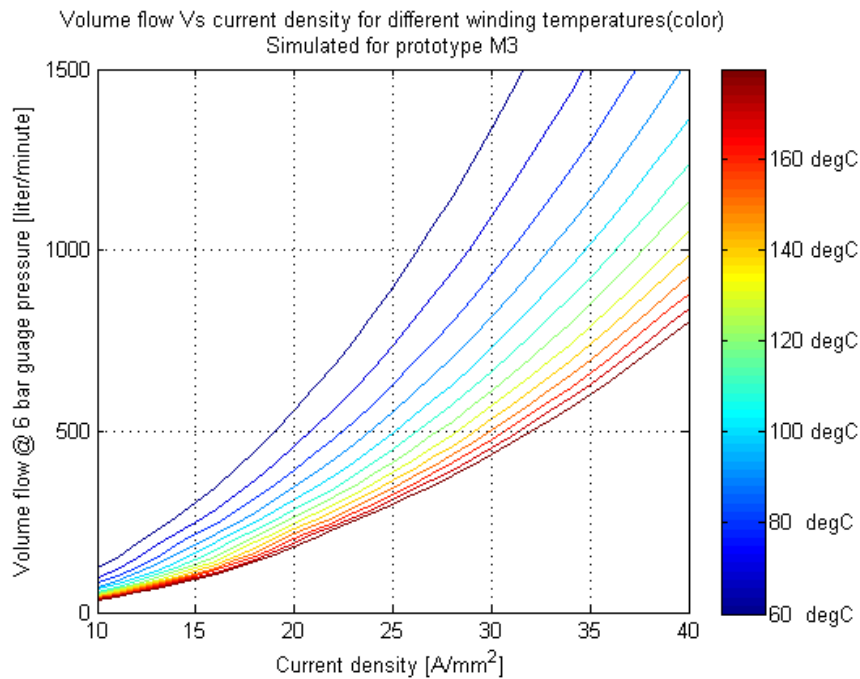
Fig. 6.1.7. The volumetric air flow @ 6 bar gauge pressure that is needed to hold the winding M3 at a certain temperature for different current densities. The temperature curves represent every tenth degree between 60 and 180℃
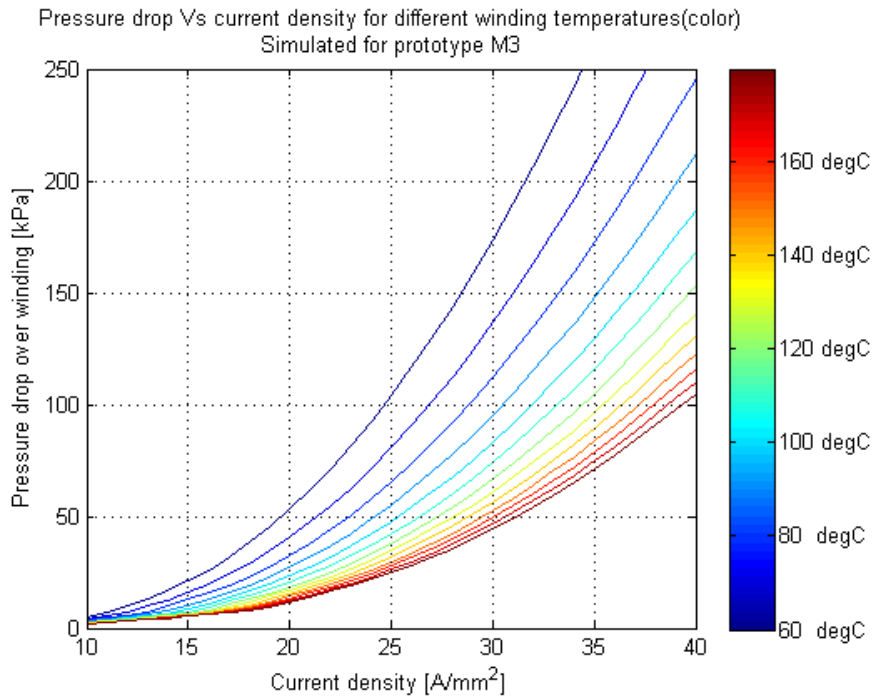
Fig. 6.1.8. Pressure drop over the winding M3 for different current densities and temperature. The temperature curves represent every tenth degree between 60 and 180℃.
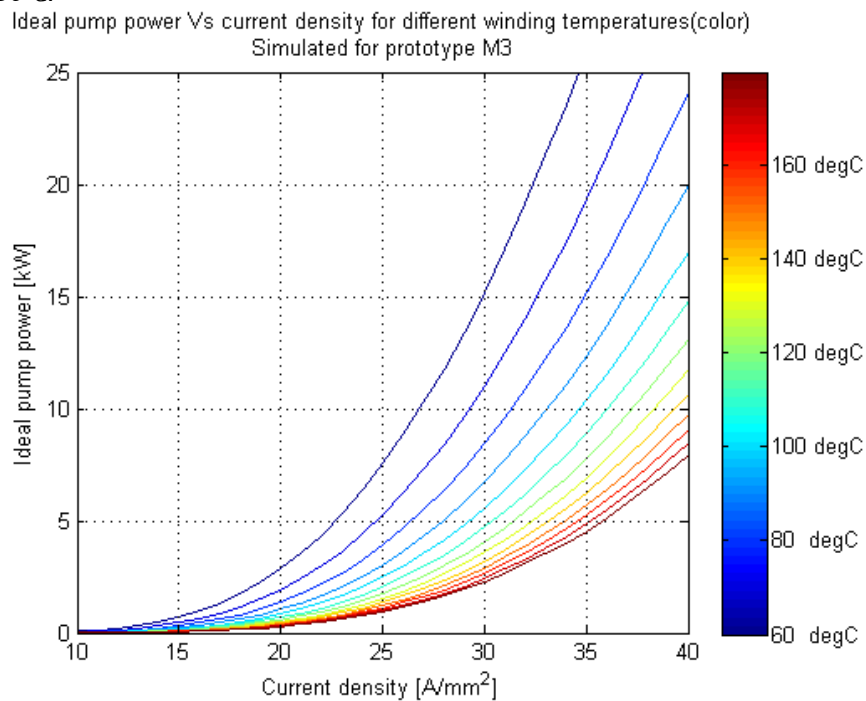
Fig. 6.1.9. Ideal pump power that is needed to cool winding M3 for different current densities and winding temperatures. The temperature curves represent every tenth degree between 60 and 180℃.

6.1.4 IMPLEMENTATION OF COOLING SYSTEM

The cooling maps presented in chapters 6.1.1 to 6.1.3 can be used in order to design a suitable cooling system for each of the prototype machines. Depending on the application different cooling system approaches could be taken, some thought about the implementation of a suitable cooling system for a laminated machine will be discussed below.

In order to force the needed amount of air through the winding one need a pump, compressor or other type of device that is able to create a movement of air. The most obvious design is to use a fan, pump or suction device to move air through the winding. Such a device can be coupled directly in series with the machine i.e. it does not need any intermediate storage and it can run continuously. When using a fan or pump one can move large quantities of air with low energy needs but the cooling system will not be able to withstand high counter pressures. The lack of intermediate air storage is positive since it will reduce energy losses due to pressure changes filling and emptying the storage, it is also negative since an intermediate storage enables the possibility to use more air flow than the pump or fan can deliver during shorter periods.

The pumps or fans ability to withstand counter pressure is very limited and therefore the placement is important in order to minimize unnecessary pressure drops. This also sets a limitation on the machine design since longer machines induce a larger pressure drop in the system. The need of clean air to cool the winding is a problem since the air most definitely needs to be filtered before entering the winding, such filter will induce extra pressure drop in the cooling system. If a laminated machine are to be cooled using a fan or pump one should consider the winding design carefully to minimize the induced pressure drop.

Another approach is to use a compressor which compresses air and stores it in an intermediate tank. The air in the tank can later be used to cool the machine by the use of a valve that regulates the pressure at the outlet of the tank. The compressor system already exists in some extent in buses and trucks since they often use pressurized air to steer brakes, shock absorbers etcetera; that will make the integration of the cooling system easier since it might be possible to connect to an existing compressor and pipe system. The efficiency of the compressor system is less than using a pump or fan since the compressor work at a higher pressure. One will experience losses both when compressing air into the tank and when letting the air out through the valve. The pump on the other hand forces the air directly through the winding and will only experience the loss for compressing air enough to overcome the counter pressure of the winding.

Since the efficiency of the compressor system is relatively low one could use a dual cooling system. The dual system could consist of a machine casing with cooling channels where oil or water could be used; this would be designed to cool the machine during nominal power use. If one need to overpower the machine in order to get fast acceleration or maintain speed during a large uphill one can use the pressurized air cooling system to supercool the machine and for a limited time get a lot more traction power out of it. By combining these two system one would get the ability to supercool the machine during periods of high power and at the same time use a more efficient cooling method during nominal drive.

In order to get a more application oriented evaluation the performance of the machines M2 and M3 are evaluated by simulating the machines as the main propulsion in a drive cycle test. The drive cycle recordings are provided by a Simulink program made by Mats Alaküla, the examiner of this thesis.

6.2.1 M2

M2 is originally designed to power a small vehicle intended as a mean of transportation for the disabled. Due to Swedish law[27] this type of vehicle cannot have a higher power than 1 kW. The heat losses at these power ratings are minimal and the forced air cooling becomes unnecessary. To enhance the effectiveness of applying forced air cooling, M2 is simulated to be the main propulsion in a small Smart Fortwo Cabrio with a power rating of 40 kW.

Fig. 6.2.4. Smart Fortwo Cabrio. Picture retrieved from manufacturers home page.

The compressor used to simulate the cooling system is from Biltema and are able to deliver 118 l/min of air under a pressure of 6 bar. The compressor has a nominal power of 1.1 kW. The compressor cooling system is designed to have a tank of 25 liters with pressurized air at 6bar gauge pressure.

---

[27] [16] [SFS 2001:559. *Lag om vägtrafikdefinitioner.* Stockholm: Näringsdepartementet]

Nominal power	1.1 kW
Tank volume	6 l (25 l)
Flow rate @ 6 bar	118 l
Maximum work pressure	8 bar
Measurements	33 x 26 x 50 cm (l x w x h)
Weight	12 kg

Fig. 6.2.1. Specifications for the compressor retrieved from the manufactures home page. Tank capacity in picture is 6 l, in simulations 25 l.

The cooling efficiency map of machine M2 is not available at this point of time and therefore an efficiency map which fits most 40 kW machines is used as a substitute.
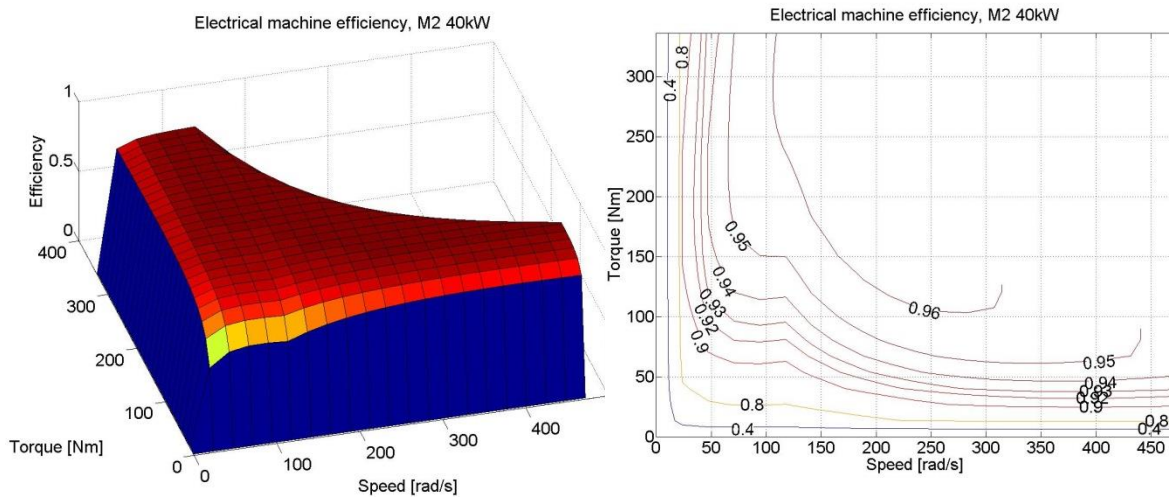
Fig. 6.2.2. Efficiency map used in simulations of prototype machine M2.
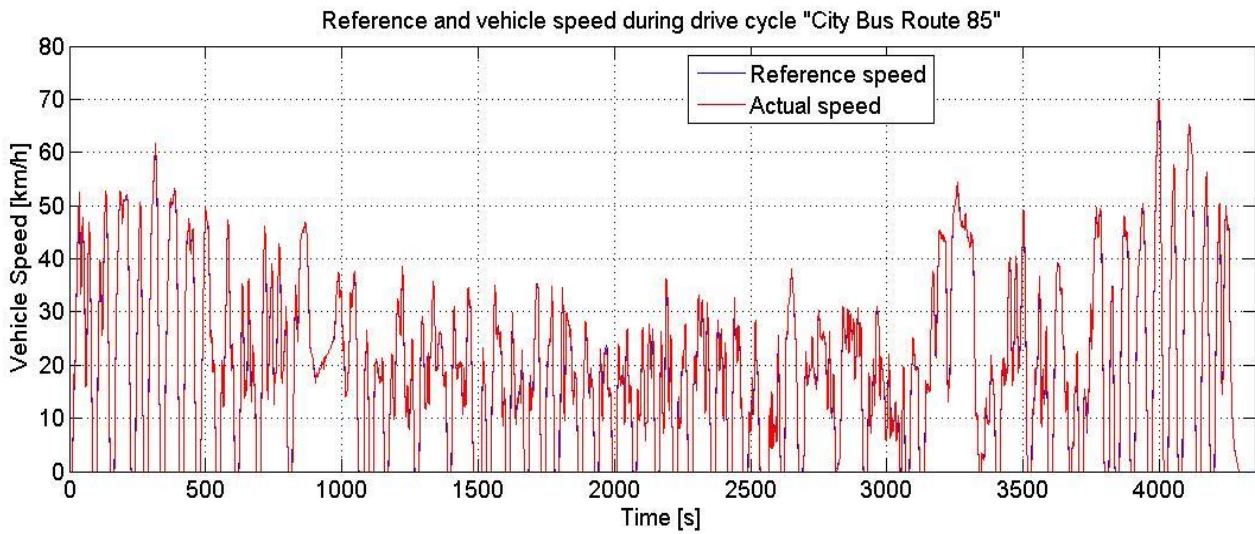
Fig. 6.2.3. The speed and speed reference of the simulated drive cycle for a city bus.

The simulated drive cycle is *City bus route 85* used as analogue to regular city traffic, with red lights at a regular interval. The small car is able to follow the speed reference as seen in figure 6.2.3, i.e. the 40 kW engine is deemed as large enough for this vehicle. The traction power throughout the drive cycle is plotted in figure 6.2.4 together with the heat losses generated in the machine and the power requirements to maintain the cooling system.
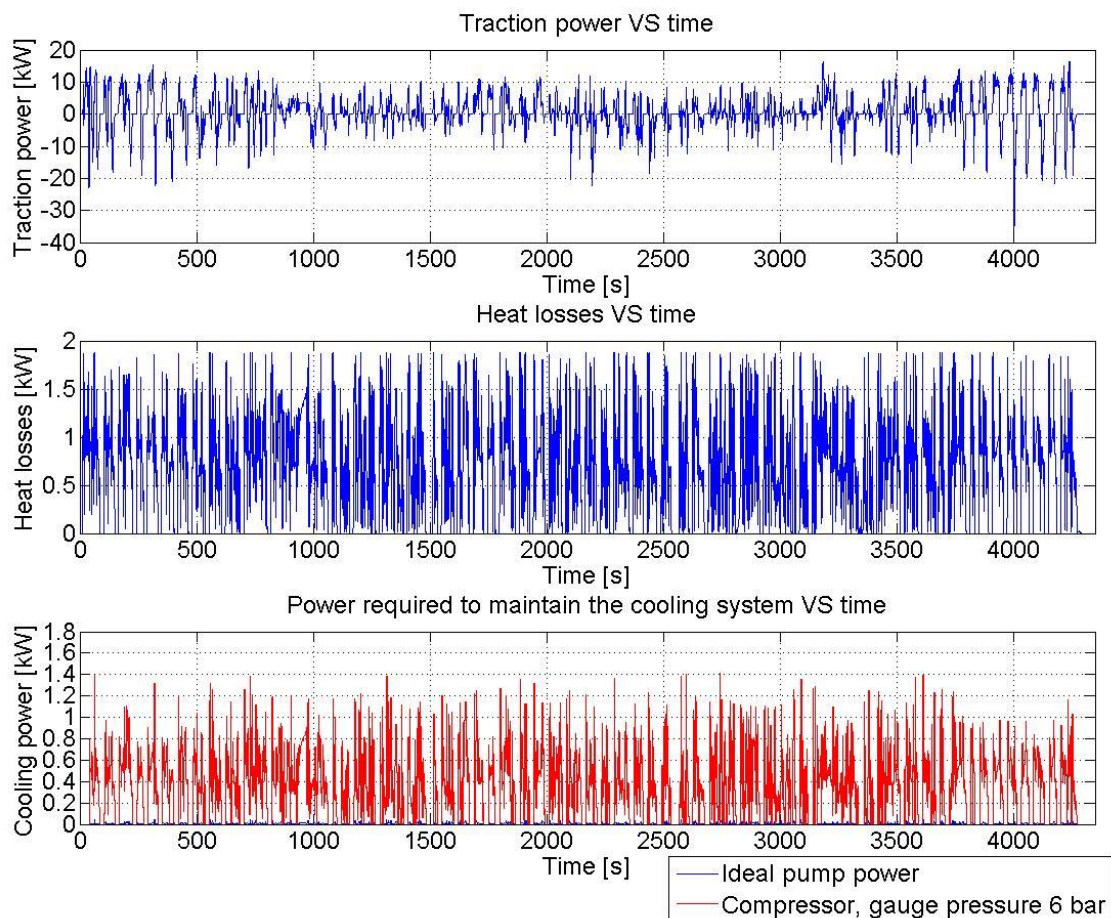
Fig. 6.2.4. The traction power, heat losses and power requirements for the cooling system for the bus during the drive cycle.

The compressor is either on or off, i.e. if the pressure inside the tank decreases under a preset set point the compressor works at full power to fill the tank again before it shuts down. The set point of the compressor on-state is intentionally left at a quite high pressure in order to have reserve if there would be periods when more cooling is required. Fig. 6.2.7 shows the pressure inside the tank during the drive cycle as well as when the compressor starts refueling the air supply. The small air supply is emptied quite quickly, i.e. looking at figure 6.2.7 it seems as the compressor has to work a lot in order to maintain the air supply. But the on/off-duty cycle of the compressor is only 32%.
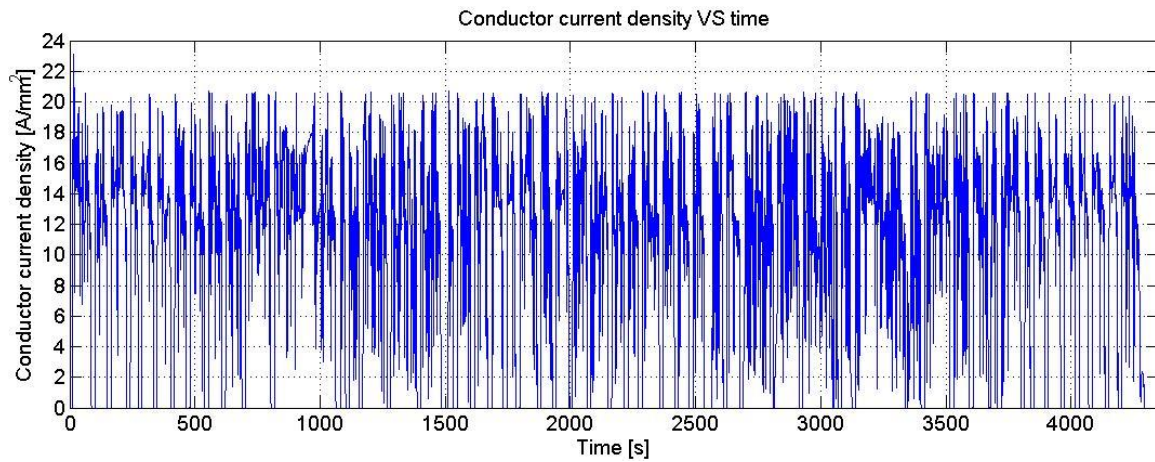
Fig. 6.2.5. Current density vs time.
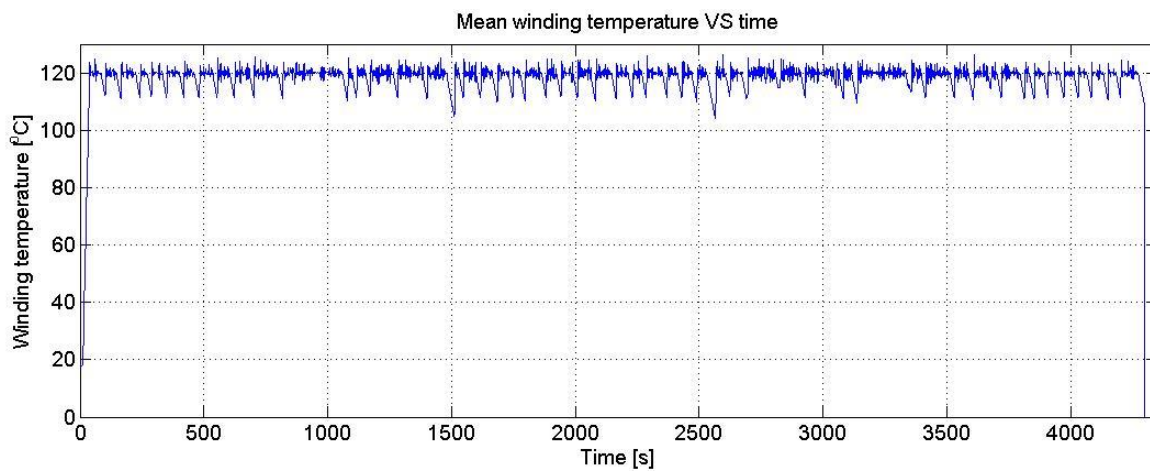
Fig. 6.2.6. The mean winding temperature vs time. The reference temperature is 120℃.
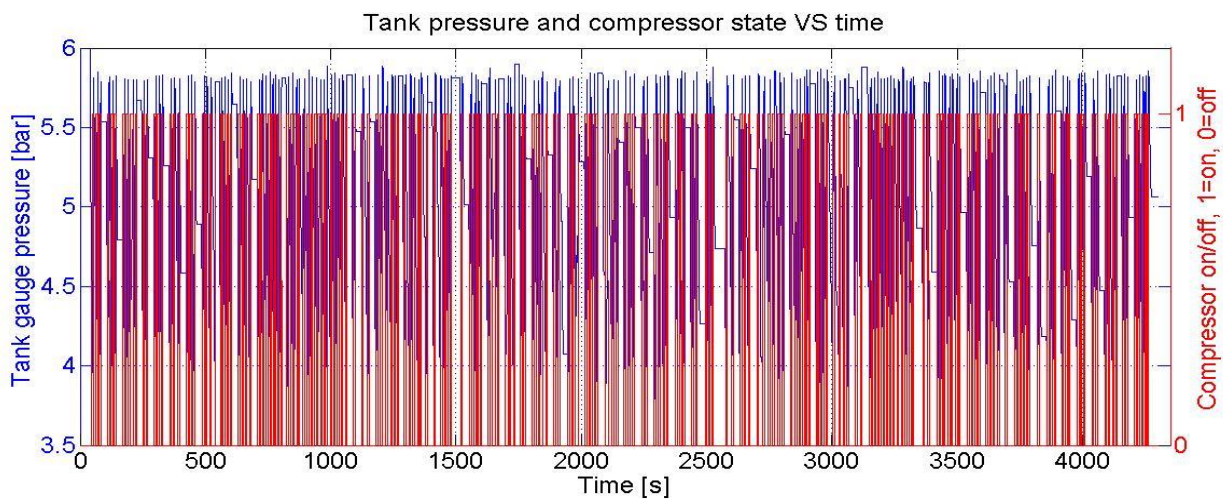
Fig. 6.2.7. Tank pressure and compressor state vs time.
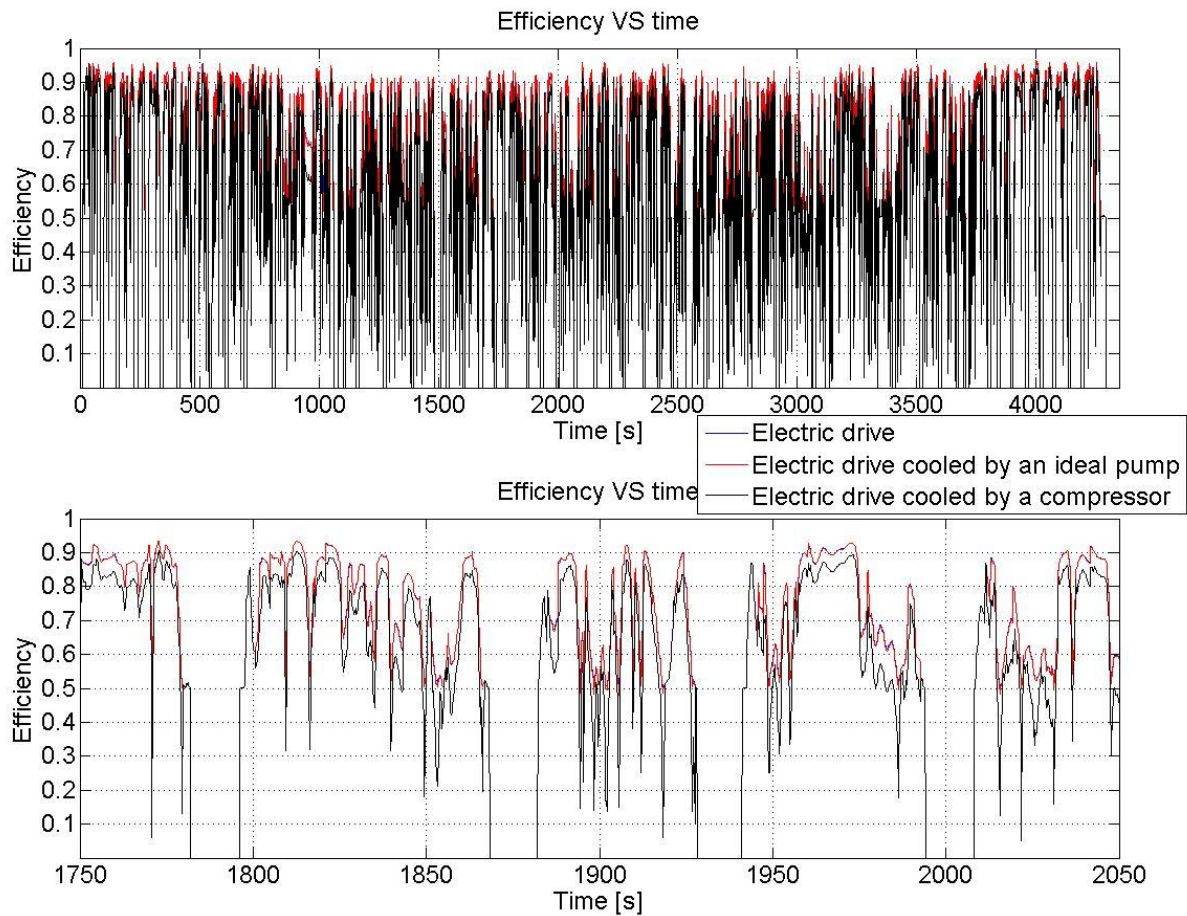
Fig. 6.2.8. Machine efficiency evaluated with and without cooling systems.

Figure 6.2.8 illustrates the instantaneous efficiency for the electric drive, both with and without cooling. The average efficiency for the 3 cases plotted in figure 6.2.8 are 0.6050 (blue line), 0.6037 (red line) and 0.5454 (black line). As seen in the plots the ideal pump or compressor does not degrade the overall efficiency. The larger spikes in the top efficiency plot in figure 6.2.8 are due to that the controller for the mass flow has a lower update rate than that for the traction, i.e. if the machine is at maximum power and the throttle is suddenly released the mass flow controller does not react instantly resulting in a sudden very low efficiency.
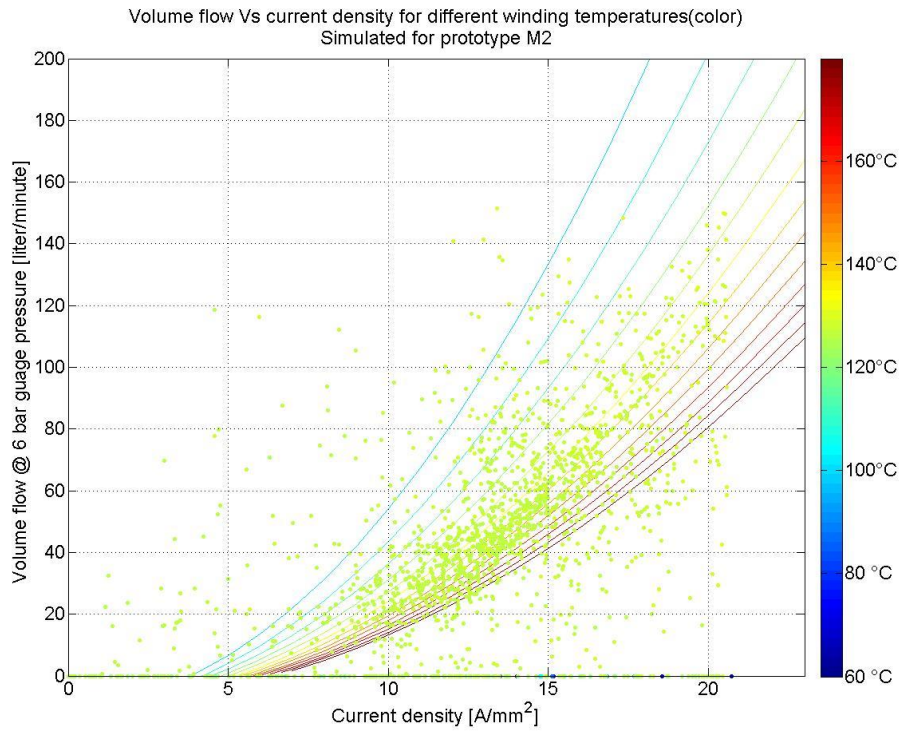
Fig. 6.2.9. Volume flow vs current density for different winding temperatures.
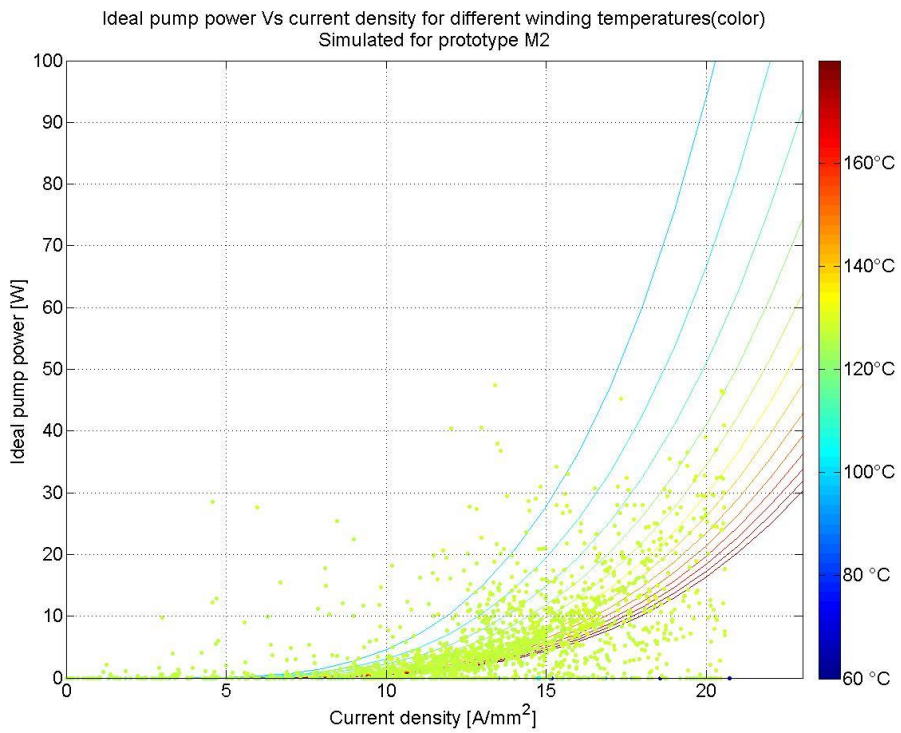
Fig. 6.2.10. Ideal pump power vs current density for different winding temperatures.
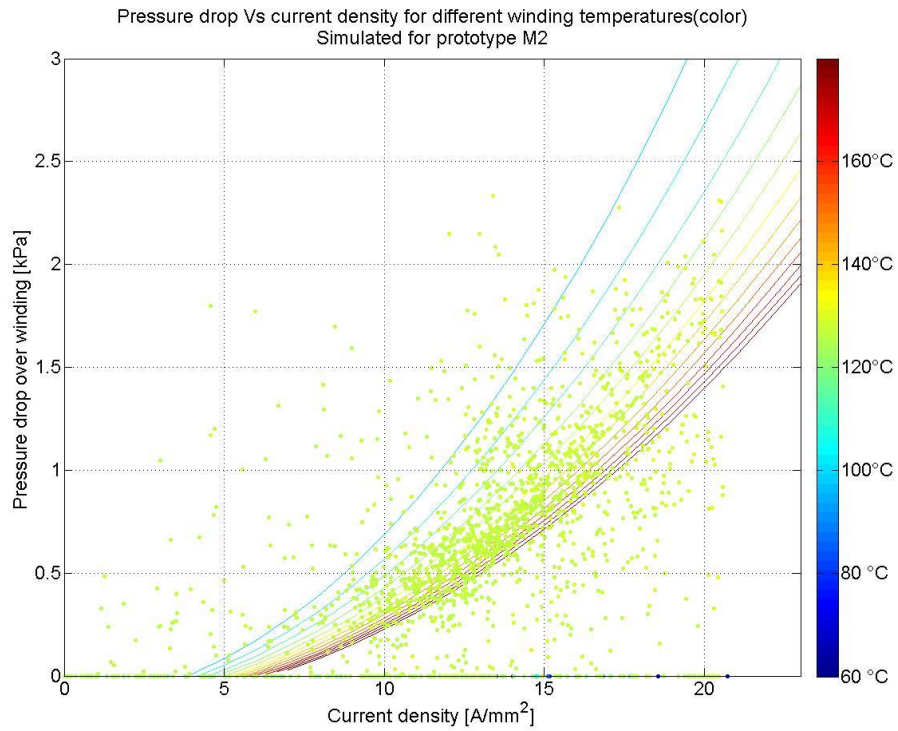
Fig. 6.2.11. Pressure drop over winding vs current density for different temperatures.

The figures in 6.2.9-11 show the mapping of the drive cycle to the different operating points (lime green dots) that the machine experienced during the drive cycle. The operating points have a corresponding value for the ideal pump power, volume flow and pressure drop over the winding. The lime green color of the dots is due to the winding temperature is held at 120℃.

The simulation of the overpowered M2 shows that it is possible to cope with the heat generation without deteriorating the overall efficiency with the added power consumption of the compressor.

6.2.2. M3

M3 is originally design to be used in a city bus. The bus is simulated as a fully electrical and of slide in type, i.e. unlimited electric power. Even though the nominal traction power of prototype M3 is 80 kW it is simulated to run at 200 kW in order to investigate the performance of the cooling system under extreme conditions.

The compressor used to simulate the cooling system is from Esska and are able to deliver 390 l/min of air under a pressure of 7.5 bar. The compressor has a nominal power of 3 kW. The compressor cooling system is designed to have a tank of 400 liters with pressurized air at 6 bar gauge pressure.

Fig. 6.2.12. Specifications of the compressor used in simulations of the cooling system. Retrieved from the manufacture data sheet.

Type	Flow Rate		m³/min	Drive Capacity		Tank	Measurements	Weight
	7,5 bar	10 bar	15 bar	kW	HP	l	B x T x H	kg
RS-COMPACT 3,0	0,39	0,30	0,19	3,0	4,0	–	445 x 1000 x 445 mm	120
RS-COMPACT 4,0	0,54	0,44	0,28	4,0	5,5	–	445 x 1000 x 445 mm	125

The efficiency map used for drive cycle simulations of machine M3 is a combination of the real efficiency map and a general efficiency map of a 200 kW machine. Since the real efficiency map did not include all working points a general efficiency map is used to fill in the blanks in the map. It should also be noted that prototype M3 uses a 6:1 gear ratio which is assumed to be ideal. The torque and speed axis in figure 6.2.13 are scaled according to the gear ratio.
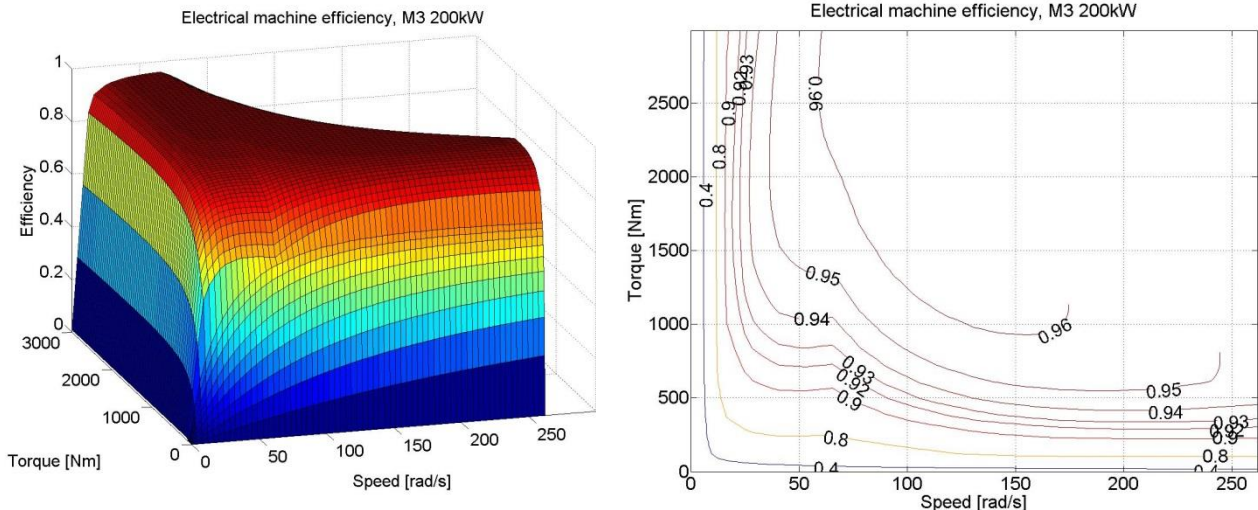
Fig. 6.2.13. Efficiency map used in simulations of prototype machine M3.
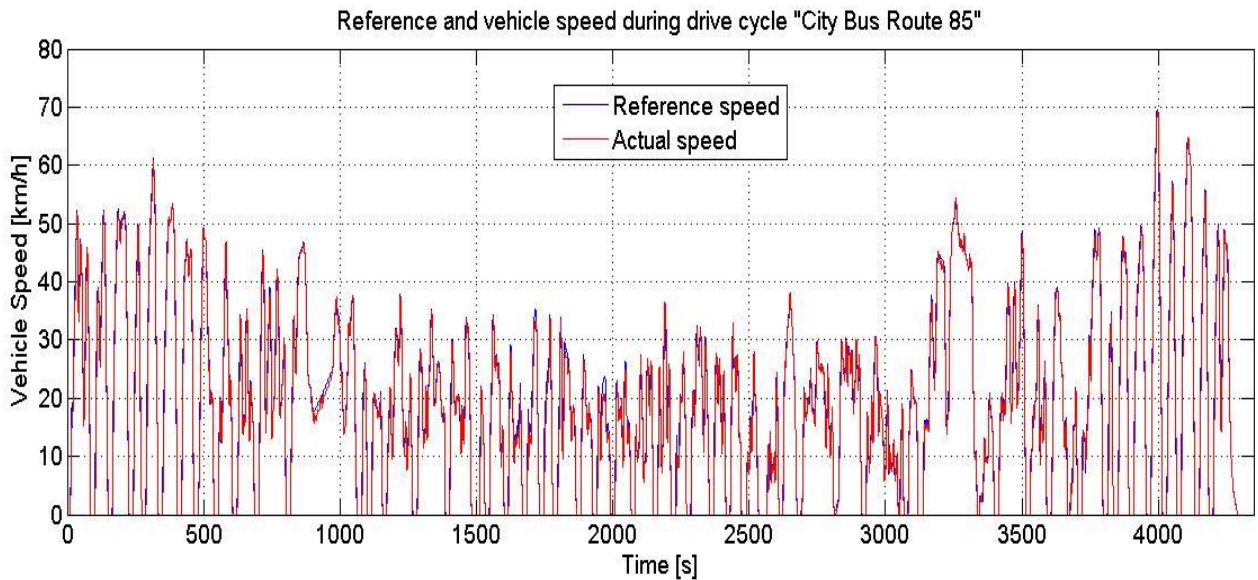
Fig. 6.2.14. The speed and speed reference of the simulated drive cycle for a city bus.

The *City bus route 85* drive cycle is chosen because it is a god analogue for a regular city bus driving both low speeds in city traffic and high speed with long acceleration times as it would on a highroad. Since the vehicle is able to follow the reference speed the machine power of 200 kW is considered enough. The traction power throughout the drive cycle is plotted in figure 6.2.15 together with the heat losses generated in the machine and the power requirements to maintain the cooling system.
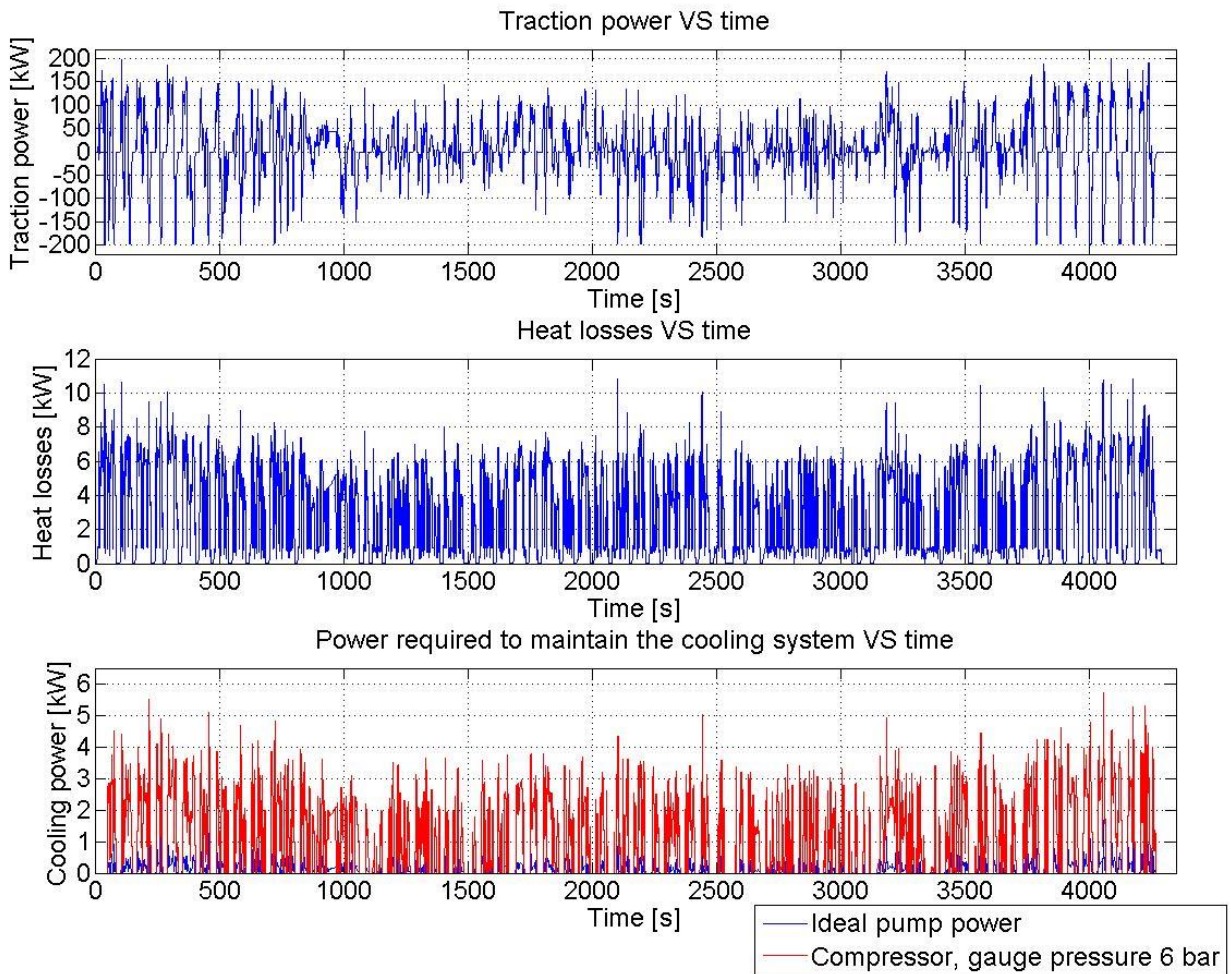
Fig. 6.2.15. The traction power, heat losses and power requirements for the cooling system for the bus during the drive cycle.

The compressor is either on or off, i.e. if the pressure inside the tank decreases under a preset set point the compressor works at full power to fill the tank again before it shuts down. The set point of the compressor on-state is intentionally left at a quite high pressure in order to have reserve if there would be periods when more cooling is required. Fig. 6.2.18 shows the pressure inside the tank during the drive cycle as well as when the compressor starts refueling the air supply. Since the drive cycle has a rather periodic behavior the compressor gets a quite periodic on-off time. The average duty cycle of the compressor is 27.43 %.
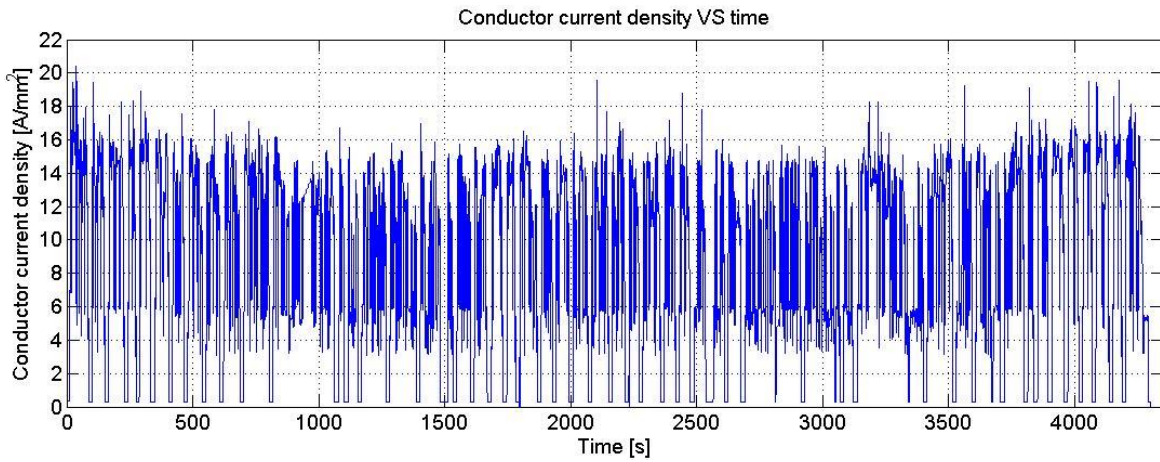
Fig. 6.2.16. Current density vs time.
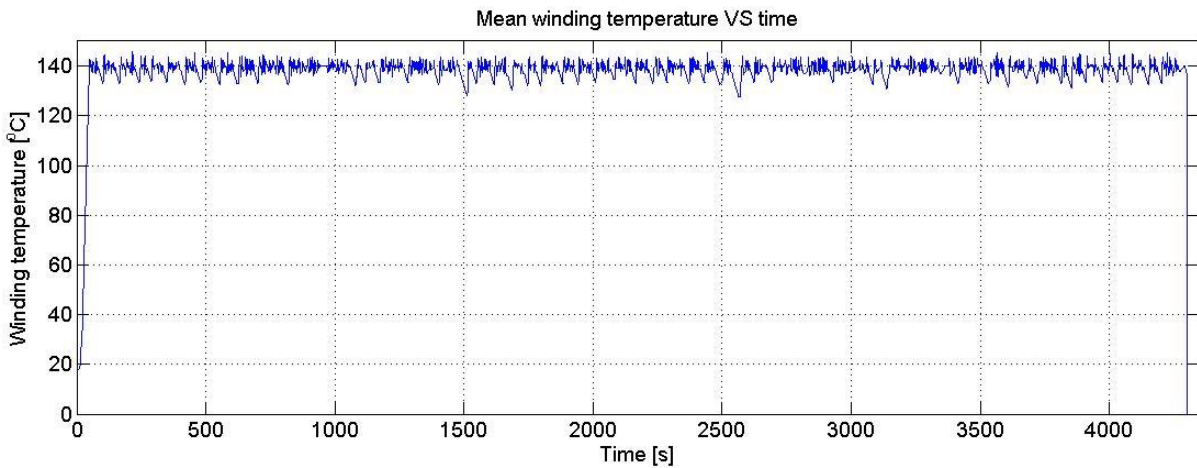
Fig. 6.2.17. The mean winding temperature vs time, the reference temperature is 140°C.
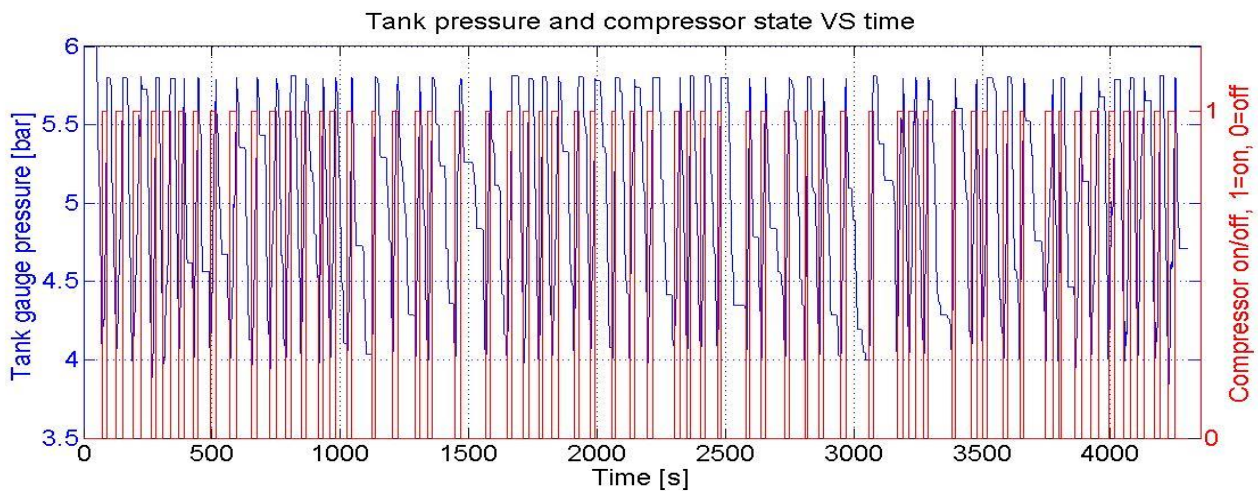
Fig. 6.2.18. Tank pressure and compressor state vs time.

155
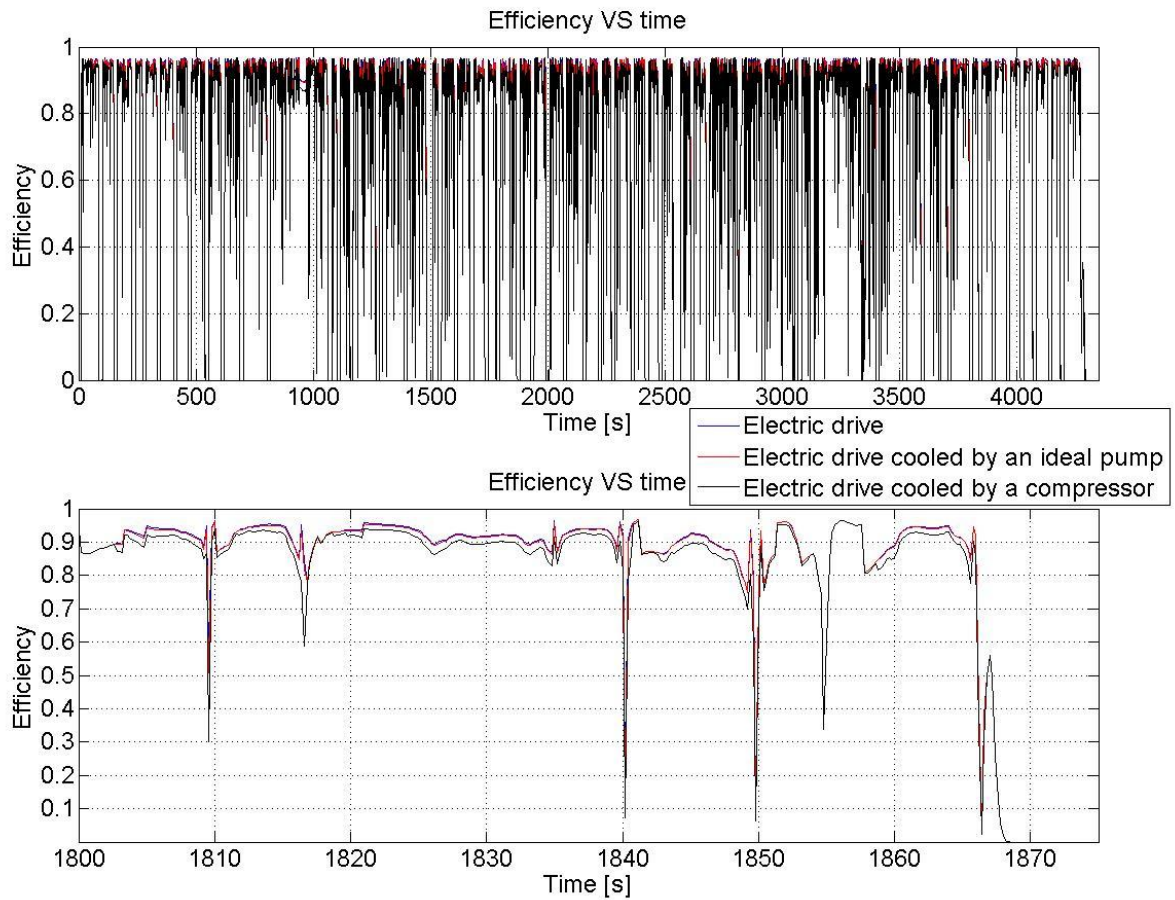
Fig. 6.2.19. Machine efficiency evaluated with and without cooling systems.

Figure 6.2.19 illustrates the instantaneous efficiency for the electric drive, both with and without cooling. The average efficiency for the 3 cases plotted in figure 6.2.19 are 0.7196 (blue line), 0.7178 (red line) and 0.7027 (black line). As seen in the plots the ideal pump or compressor does not degrade the overall efficiency. The larger spikes in the top efficiency plot in figure 6.2.19 are due to that the controller for the mass flow has a lower update rate than that for the traction, i.e. if the machine is at maximum power and the throttle is suddenly released the mass flow controller does not react instantly resulting in a sudden very low efficiency.
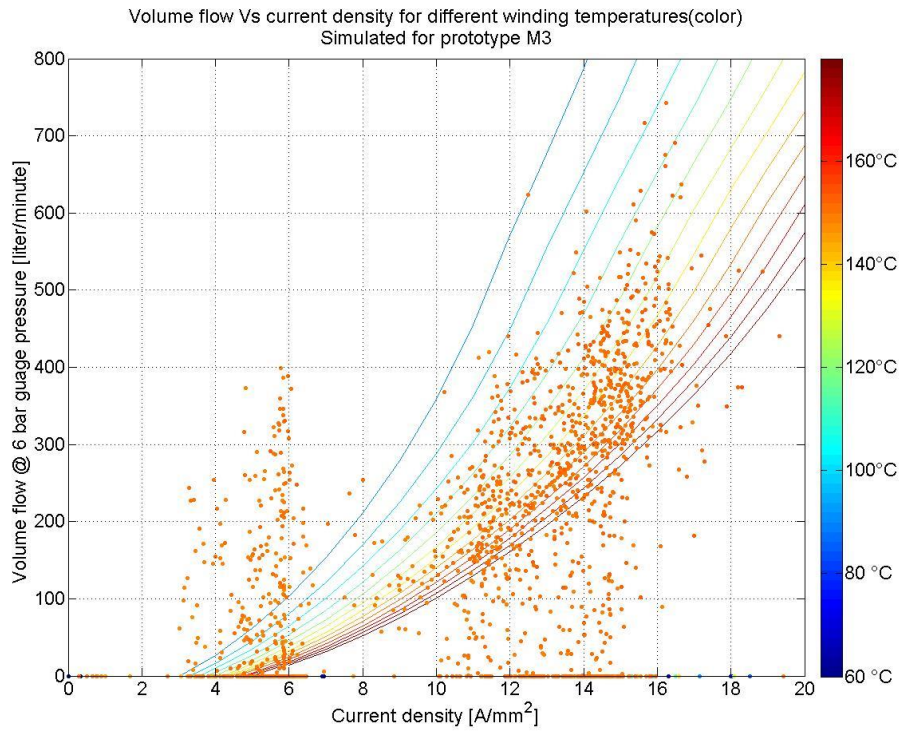
Fig. 6.2.20. Volume flow vs current density for different winding temperatures.
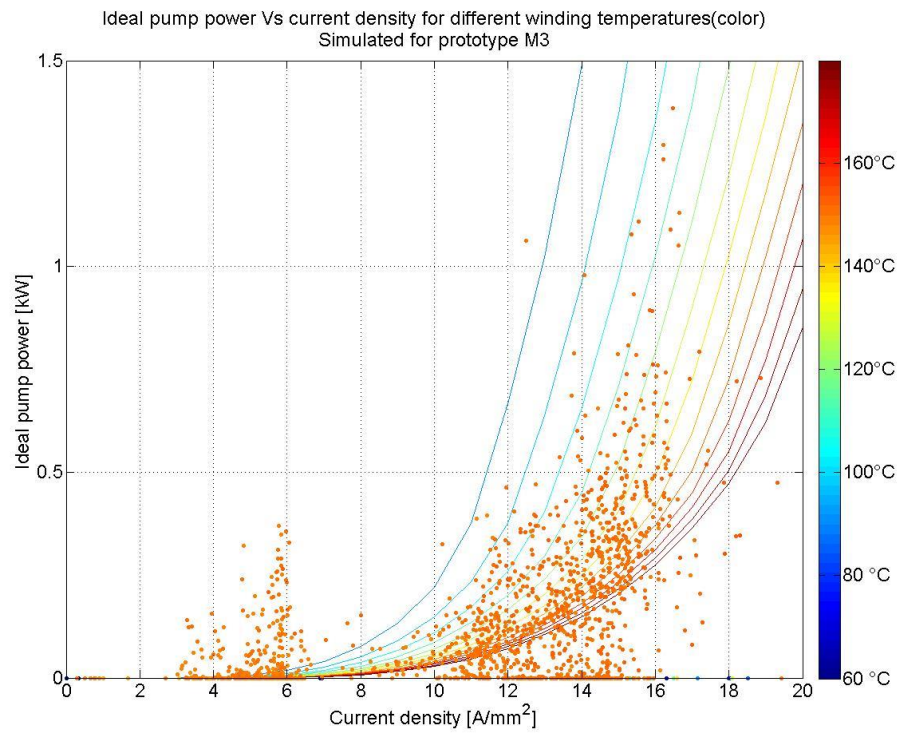
Fig. 6.2.21. Ideal pump power vs current density for different winding temperatures.
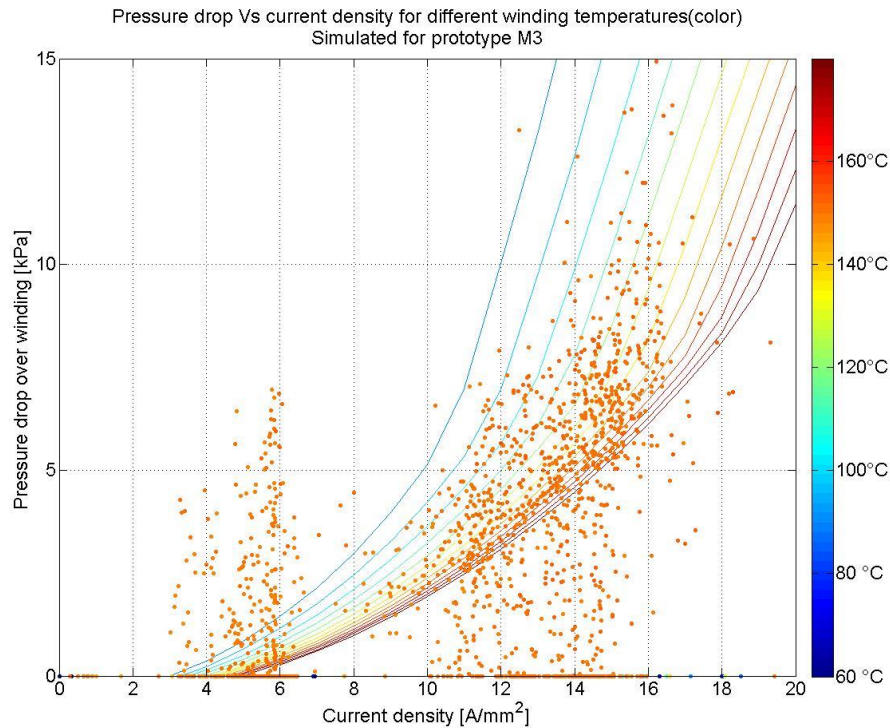
Fig. 6.2.22. Pressure drop over winding vs current density for different temperatures.

The figures in 6.2.20-22 show the mapping of the drive cycle to the different operating points (orange dots) that the machine experienced during the drive cycle. The operating points have a corresponding value for the ideal pump power, volume flow and pressure drop over the winding. The orange color of the dots is due to the winding temperature is held at 140℃.

The simulation of M3 in the drive cycle suggests that the forced air cooling is a feasible solution for counter acting the heat losses. The results from the simulation shows that it is possible to overpower a smaller engine and still be able to cool it without influencing the efficiency.

The overall efficiency is not affected to noticeable degree. For lower traction power heat losses an alternative solution should be considered, such as the traditional oil or water cooled jackets, in addition to the forced air cooling which would only kick in at higher powers.

7 CONCLUSIONS

The results from simulations and measurements show that a laminated winding can withstand significant heat losses in the conductor and remain at a functional temperature as a result of the air cooling between the laminates. The ability to overpower the electrical machine during periods of heavy load results in the use of smaller electrical machines which hold better efficiency during lower loads. One example where the laminated winding could be of great use is in a long haul truck. Let us say that the truck drives at an average power of 150 kW but need to use 350 kW of traction power during a period of few minutes in order to cope with steep hills or large accelerations. Traditionally one would need to put a 350 kW electrical drive in the long haul truck in order to thermally endure the periods of extreme need of traction power. During nominal drive of 150 kW on the other hand the efficiency of the larger machine is less than for example using a machine designed for 200 kW. If one instead uses the laminated technique one could build a smaller machine with optimum efficiency at average driving power need but still be able to deliver the 350 kW needed for the periods of extreme loading due to its exceptional cooling capability.

It is shown during the thesis that the geometry of the winding greatly influences the cooling capability of the laminated winding. Typically axially shorter machines (less than 5 cm) are both less sensitive to uneven layer spacing and induce less pressure drop than its longer counterpart. Another way of reducing the pressure drop over the machine is to reduce the fill factor in the machine but that comes with the cost of a higher heat loss to torque ratio since the current density has to increase in the conductor as the winding volume reduces. If a short design is chosen the most efficient way of cooling the machine is typically by using a fan or suction pump since they are able to move high amounts of air.

If one would go for an axially longer machine design the mechanism delivering air to the winding would have to withstand higher counter pressure. Depending on the application could either a suction pump or a compressor and tank be a good way of delivering the air.

As shown in chapter 4.4.2 the air distribution along the winding turns is greatly influenced by the layer spacing. The cooling performance is also sensitive to air leaks that could appear, for example between outer turn and casing or in the air gap between stator and rotor. This makes the winding sensitive to error margins and could increase the construction cost of the winding. Of course the sensitivity to unevenly spaced turns and leaks is dependent on the application but one should strive to keep good margins and

always simulate for an uneven stack in order to determine which error margins that can be accepted.

The thesis show through simulations and measurements that it is possible to use laminated winding technique in order to enhance the cooling capability and thereby performance of an electrical machine. The possibility to overpower the electrical machine enables the use of smaller and more efficient electrical drives.

7.1 FURTHER WORK

Even if the cooling capability of the laminated winding is thoroughly examined throughout the thesis there are still great deals of further development that can be done. In the following chapter suggestions of things that we think would lead the development of the laminated windings cooling system forward are discussed.

The Matlab model is used as the main simulation tool during the thesis. The model can be used to simulate a large variety of different winding geometrics, drive cycle etcetera but there is nothing that connects the results regarding cooling capabilities with the machine performance, i.e. torque, power, rotational speed etcetera. When parameters regarding winding geometrics is changed to give the best possible cooling performance one will affect other properties of the machine which the model do not take into account. If a model describing the machine performance would be combined with the cooling model one could optimize the overall performance of the combined system instead of as now keeping the two apart.

One of the biggest problems regarding the laminated machine is that the layer spacing is unevenly distributed along the winding turns. As shown throughout the thesis this is a major factor concerning the cooling capability of the winding. Therefore one would need to find a way to keep an even distance between winding turns without blocking the air flow or deteriorate the winding in any other way. One solution which was presented by Mats Alaküla, the examiner of this thesis, is to put small supporting dots on the upper side of the laminates making sure that the layer spacing is kept even. This solution would give enough support for the laminates and at the same time not block the channel in a big extent.
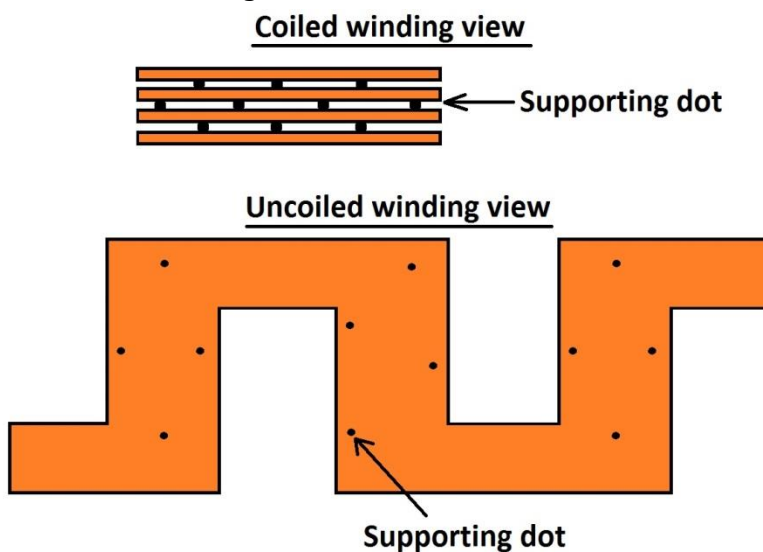
Fig. 7.1.1. Illustration of the supporting dot idea.

When simulating the cooling performance it is decided to use the assumption of even surface temperature along the length of the machine. In a real application this is not true and one will experience a lower temperature at the inlet side of the laminate. This does not impose a problem in shorter machines, but in a longer machine application the temperature difference between the inlet and outlet side of the laminate could be significant. When assuming constant surface temperature one will always design for the highest temperature (the one at the outlet) and therefore the temperature at the inlet will be "unnecessarily" low. By cooling the winding from different direction or change the way air enters the winding one might be able to reduce the temperature differences and thereby get a more efficient cooling.

During the thesis a short investigation of directed cooling was made. The possible improvements of using directed air cooling through a nozzle is that one would not need to insulate the winding in the same extent as one would need in an application where the air is allowed to flow freely through the winding. The air nozzle would have to sit close to the winding stack for this to work but one would not have to insulate the area between stator winding and rotor or the winding and casing. Other positive features is that the air distribution could be steered by for example manipulating the nozzle outlet letting more air out in parts of the stack that is expected to have the highest temperatures, classically the middle turns. The inlet air used to cool the winding would hold a lower inlet temperature using a nozzle due to the pressure drop over it. The negative aspect of using directed cooling would be the increased pressure drop and increased pump power needed to withstand it. The directed cooling approach is something that we think could hold great potential for further development of the laminated windings cooling system.

For the cooling to work one would need an air distribution system that is able to fit in a vehicle and at the same time deliver the requested amount of air. Solving this problem is crucial in order to be able to use the air cooled laminated winding in a real application. One way of solving the problem is to use a compressor and tank for delivering the air. By using a compressor one will get a low efficiency if the cooling system has to be used during nominal drive. In order to get better efficiency of the cooling system one could try to integrate a second cooling system. If the machine would be water/oil cooled during nominal drive and only use the less efficient compressor during stretches of extreme heat losses one would probably get a more efficient overall cooling system.

Due to limitations in the experimental setup the measurements on the windings could not be pushed as far as in the simulations. It would be interesting to see how real measurements would correspond to the simulations at much higher heat losses than the ones that could be achieved in the current test rig. It would also be interesting to see how the forced air cooling would work on a complete machine, i.e. not only a winding segment as was done in this thesis.

8 NOMENCLATURE

A = Area [m²]

C_p = Specific heat capacity [J/kgK]

d = Diameter [m]

D_h = Hydraulic diameter [m]

E = Internal energy [J]

Emf = Electromotive force [V]

F = Force [N]

f = Friction factor [1]

h = Convection [W/m²K]

I = Current [A]

J = Current density [A/m²]

k = Thermal conductivity of fluid [W/mK]

k_r = Absolute roughness [m]

L = Length [m]

Lt = Thermal inlet stretch [m]

Lv = Velocity inlet stretch [m]

ṁ = Mass flow [kg/s]

Nu = Nusselts number [1]

P = Power [W]

p = Pressure [Pa]

Pr = Prandelts number [1]

P_W = Air wetted perimeter [m]

Q = Energy transfer [W]

R = Resistance [Ohm]

R_{air} = Specific gas constant [Nm/kgK] (value for air is 287)[28]

Re = Reynolds number [1]

S = Seebeck coefficient [V/K]

T = Temperature [K]

t = Time [s]

U = Velocity [m/s]

v = Kinematic viscosity [m^2/s]

V = Voltage [V]

W = Work [Nm]

Vol = Volume [m^3]

Vol_{flow} = Volumetric flow [m^3/s]

Z_m = Mean compressibility factor [1] (Is approximated to 1 for air)[29]

α = Resistive temperature coefficient [1/K]

ζ = Specific head loss coefficient [1]

λ = Heat conductivity [W/mK]

ρ = Density [kg/m^3]

φ = Resistivity [Ohm m]

μ = Dynamic viscosity [Pa s]

---

[28] [7] [*Tillämpad termodynamik,* I. Ekroth, E. Granryd, Studentlitteratur 2006, *p. 408*]

[29] [17] [*Perry's chemical engineers' handbook* (6ed). McGraw-Hill. 1984, *table 3-162*]

REFERENCES

[1] *Physics For Scientists and Engineers,* P. A. Tipler, G. Mosca, W. H. Freeman & Co., 2008

[2] *Design of Powder Core Inductors,* H. Skarrie, Lic. Thesis, IEA, 2001

[3] *Värmeöverföring,*B. Sundén, Studentlitteratur, 2006

[4] *Heat and Mass Transfer: A Practical Approach, 3/e*, Y.A Cengel, McGraw-Hill, 2007

[5] *Journal of Heat Transfer*, Y. S. Muzychka, M. M. Yovanovich, ASME, Vol. 126 2004

[6] *A heat transfer textbook,* J.H. Lienhard IV, J.H. Lienhard V, Phlogiston Press, 2008

[7] *Tillämpad termodynamik,* I. Ekroth, E. Granryd, Studentlitteratur 2006

[8] *Applied Mathematics Letters Vol. 24 Issue 8,* D. Brkić, August 2011

[9] *Compressible gas flow,* Pipe flow Calculations, *Retrieved 06-03-2013 at* *http://www.pipeflowcalculations.com/pipe-valve-fitting-flow/compressible-gas-flow.php*

[10] Norsok standard P-001 "Process Design", Edition 5, September 2006, p.9

[11] Absolute Roughness of pipe materials, Native Dynamics, May 26th 2012, Retrieved 06-03-2013 at http://nativedynamics.com.au

[12] Pipe flow wizard v1.12, PipeFlow®, Daxesoft Ltd.

[13] Fluid Mechanics, Binder, R.C. , Prentice-Hall, Inc. (Englewood Cliffs, NJ), 1973

[14] *Temperature Sensors,* The Watlow Educational Series Book Four, Watlow St. Louis, 1995, *retrieved at 2013-05-31 from* *http://www.m-r-c.co.il/Media/Doc/TechnicalInformation/Temp_Measuring1.pdf*

[15] [*Laminated Winding with a Rapid Cooling Capability for Electrical Machines,* C. Högmark, A. Reinap, K. Frogner, M. Alaküla, *International Conference for Inductive and Electromagnetic Components, Systems and Devices including Manufacturing and Processing (INDUCTICA 2012)*, Berlin, Germany, June 26-28, 2012]

[16] SFS 2001:559. *Lag om vägtrafikdefinitioner.* Stockholm: Näringsdepartementet

[17] *Perry's chemical engineer's' handbook* (6ed). McGraw-Hill. 1984, *table 3-162*

APPENDIX A.

ERROR ESTIMATION FROM ASSUMING ISOTHERMAL FLOW THROUGH A PIPE.

Mach number describes the quota between the speed of which a gas is traveling and the speed of sound traveling through the gas as medium.

$$M = \frac{u}{\sqrt{kRT}} \qquad \text{A.1}[30]$$

The relationship between inlet and outlet Mach number can be expressed as a function depending on the length, diameter and friction factor of the channel the air is flowing through; as follows.

$$f\frac{L}{d} = \frac{1}{2k} * \left(\frac{1}{M_I^2} - \frac{1}{M_E^2}\right) - \frac{k+1}{4k} * ln\left(\left(\frac{M_E}{M_I}\right)^2 * \frac{(k-1)M_I^2+2}{(k-1)M_E^2+2}\right) \qquad \text{A.2}[31]$$

If the length, diameter and friction factor of the channel is known one could determine the upstream Mach number for any chosen downstream Mach number. If the diameter is constant along the channel and the speed never exceeds one Mach the air will always have the highest Mach number at the outlet. This states that if the friction factor also is constant along the channel one would have the lowest Mach number and therefore highest pressure and temperature at the inlet or beginning of the channel. The following expressions gives the temperature and pressure difference between two points along the channel, if the Mach number at these points is known. (Point 1 ex. T_1 is upstream of point x)

$$\frac{T_x}{T_1} = \frac{(k-1)M_1^2+2}{(k-1)M_x^2+2} \qquad \text{A.3}[31]$$

$$\frac{p_x}{p_1} = \frac{M_1}{M_x}\sqrt{\frac{T_x}{T_1}} \qquad \text{A.4}[31]$$

---

[30] [7] [*Tillämpad termodynamik,* I. Ekroth, E. Granryd, Studentlitteratur 2006, *p. 408*]
[31] [7] [*Tillämpad termodynamik,* I. Ekroth, E. Granryd, Studentlitteratur 2006, *p. 436-437*]

If the points evaluated for are located at the inlet and outlet of the channel the temperature and pressure differences obtained are bigger than between any other two points along the channel.

If the maximum outlet speed of the air is known one could determine how large effect the temperature change would have on the pressure difference.

For determining the temperature impact on the pressure measurement needed for determining the mass flow through the hose in our application the following data is being used.

- Channel length 8m
- Channel diameter 1cm
- Mean friction factor is determined by Colebrook's equation for any chosen Mach number at the outlet and the absolute roughness of the channel is considered constant at 0.005mm.
- Maximum outlet Mach number of 0.3.
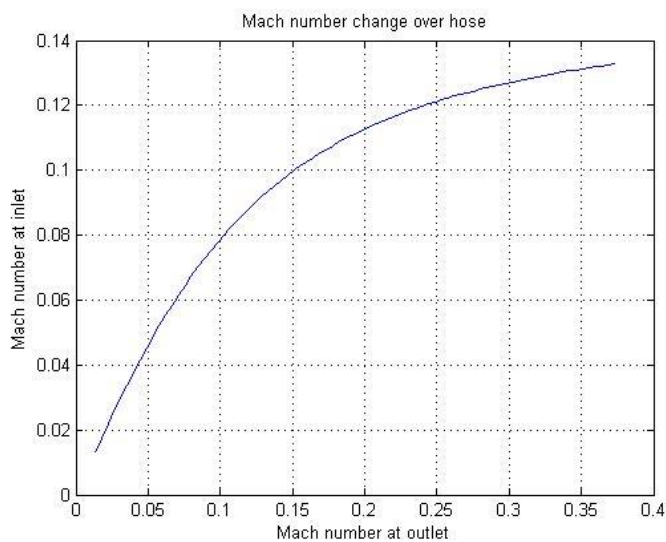
Fig. A.1. Illustration of how the inlet Mach number changes with output Mach number. Note that the friction factor is changing with increasing outlet Mach number because of the increased mass flow rate through the channel.
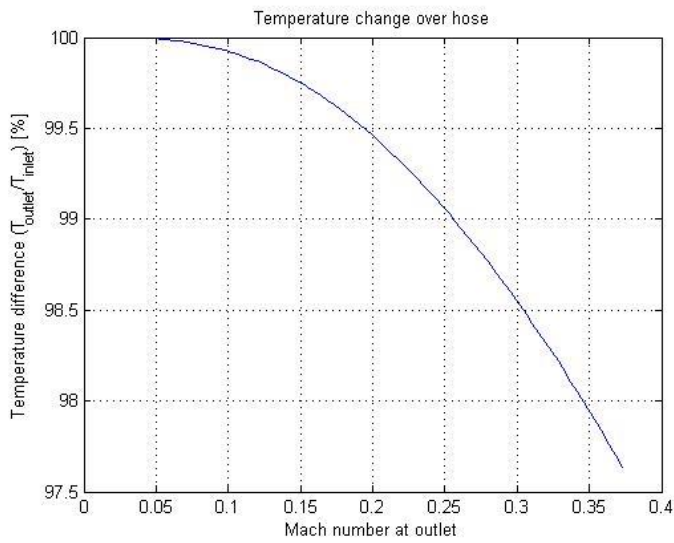
Fig. A.2. Illustration of the percentage quote between outlet and inlet temperature. The temperature drops approximately 1.5% at the maximum flow rate in the application.
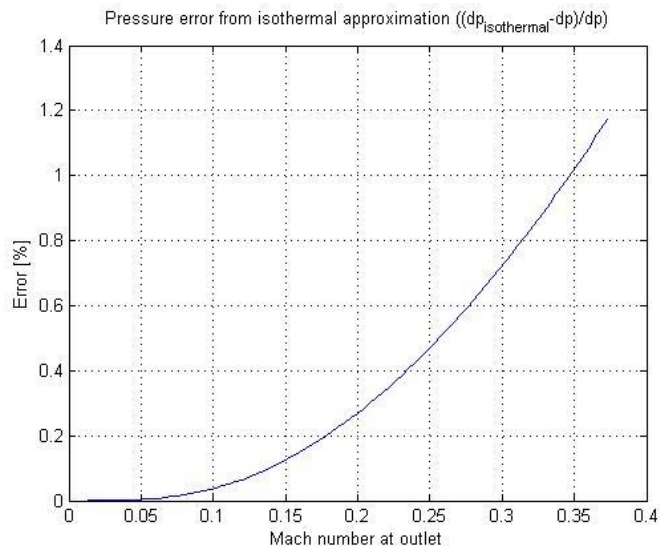
Fig. A.3. Illustration of the percentage pressure difference error from approximating that the process is isothermal. The error is less than 1% at the maximum flow rate in the application.

The figures above give an error estimate of the error one could get when measuring high flow rates. It should be noted that the error margin of one percent is calculated when measuring the pressure difference between the inlet and outlet. In the real application the pressure drop will be measured over a smaller piece of the channel transporting air to the winding, which will reduce the pressure error accordingly.

The reader should also know that the one percent error only shows the error one would get from using the simpler set of equations available when assuming isothermal flow and do not reflect the impact of other sources of error.

The reason for not including the temperature change into the flow meter calculations is that the small accuracy gain is not worth the extra work that had to be put into sorting out a more complex algorithm.

It is on these calculations that the statement of that the mass flows in channels where the Mach number exceeds 0.3 can be considered isothermal without any major loss in accuracy.

APPENDIX B

There were several measurements that took place before the one described in chapter 5. These were made with the intention of study the effects of forced cooling on the winding, but as was learned during the investigation of the measurement results was not really useful in the way that was intended. Instead these results were used to improve the test bench, both in how the measurements were made and how the test object should be improved to require good and trustworthy measurement results.

The results discussed in this B.1 and B.2 is the two larger measurements made before the final ones in chapter 5.3 and 5.4. Of course there were other minor measurements before and in between these measurements, but the results are summarized into the larger measurements.

B.1 FIRST FORCED COOLING MEASUREMENT

B.1.1 TEST EQUIPMENT

Air flow meter: Pitot-Piezometer (see chapter 3.4.4)

Winding temperature measurement: Thermocouples

Modifications to the test object: Spacing between winding turns.

Air flow set points: 200 to 450 l/min in increments of 50 l/min (at atmospheric pressure)

Current density set points: 10 to14 A/mm^2 in increments of 1 A/mm^2

B.1.2 CONCLUSIONS

The main problem noticed during these measurements was the behavior of the air flow meter. The erratic behavior of the flow meter made it hard to predict or verify any measurement results. The flow meter would vary the output for a day to day basis; even though the input at the valve would be the same each day. This led to a redesign of the flow meter.

It was also noticed that the temperature in the winding was not uniformly distributed, i.e. there were spots that had a quite significantly higher temperature than other spots. This led to a redesign in the way the temperature of the winding was measured and monitored.

B.2 SECOND FORCED COOLING MEASUREMENT

B.2.1 TEST EQUIPMENT

Air flow meter: Pressure drop based flow meter (see chapter 3.5)

Winding temperature measurement: 3 thermocouples and the IR-camera.

Modifications to the test object: No new modifications from the earlier measurement.

Air flow set points at the inlet: 30 kPa to 60 kPa in increments of 5 kPa

Current density set points: 8 to 14 A/mm^2 in increments of 1 A/mm^2

B.2.2 FINDINGS

As mentioned in chapter B.1.2 the temperature in the winding is not uniformly distributed, this is shown more illustrative in fig. B.2.1. By using the measurements from the IR-camera it is possible to get a more accurate value of the mean temperature over the winding. It should be noted that during these measurements the IR-camera photage was analyzed with a more primitive manor than that described in chapter 3.7.
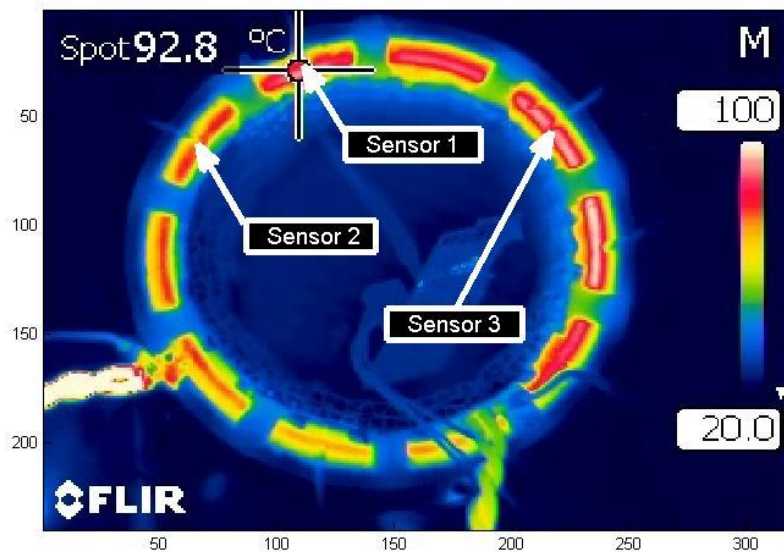
Fig.B.2.1: A frame from the IR-camera recording of the winding during a test, showing the placement of the temperature sensors and illustrating the heat distribution throughout the winding.

From fig. B.2.1 one can see that the hottest spots are in in the middle of the winding. This can be explained by:

1. that the heat in the winding is conducted to the housing, giving a helping hand in the cooling of the winding,

2. that there are larger gaps before the first and after the last winding turn, allowing more cold air to flow through, and

3. uneven spacing in between the winding turns.

The first challenge is not really a problem, the heat dissipated to the housing is not large in comparison to what the air transports away from the winding, and for a complete machine there will still be a housing dissipating some of the heat generated inside. But, as this is an investigation of air cooling through the winding, it is preferable to more accurately know how much is dissipated from the housing for the total heat dissipation to add up.

The second challenge is of course not good since the larger gaps take more of the cooling air than the smaller in between the winding turns. The larger gaps act as bypasses for the air, i.e. letting the air flow through it without taking up as much heat on the way. This results in that the some of the air is actually left unused in the cooling process. It should also be noted that the air may escape from other smaller leakages that is harder to spot. The outer part of where the

winding itself is fixated in has a very good fit around the housing so that the contributed leakages from this should be minimal to none. The inner part of the winding (where the rotor should be placed in the complete machine) has not as good fit as for the outer part; some of the air may escape here.

The third challenge is hard to avoid. There are small distances placed in between the winding turn that gives small uniform layer spacing between each turn, or so was the thought at least. As something larger is placed in between the winding turns they actually push some of the winding turns closer together and hence creating irregular layer spacing. This results in that there is less airflow through the slots with smaller layer spacing which in turn contributes to a higher temperature.

When calculating the air cooling power under the assumption that the air as it exits the winding has the same temperature as the winding, i.e. the calculated mean temperature from the IR-camera photage the result is, to say the least, disappointing. As figure B.2.2 shows the air cooling power exceeds the added power. This cannot be true since it breaks the most fundamental law of thermodynamics, i.e. the law of conservation of energy, and therefore the assumption made earlier has to be rethought.
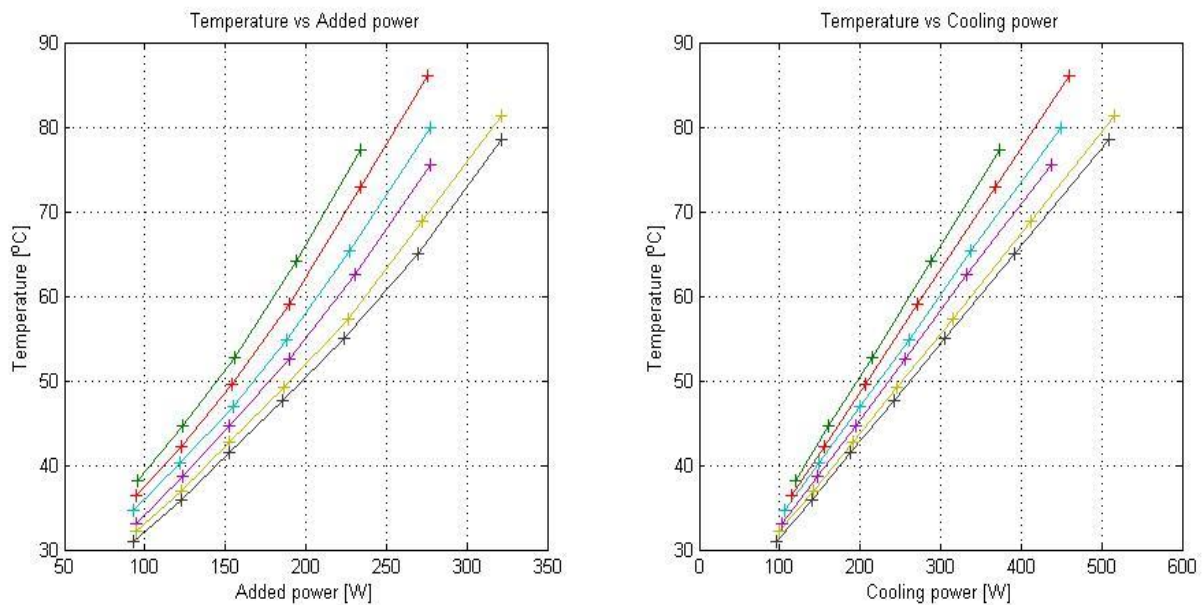
Fig. B.2.2.Shows the mean winding temperature calculated from the IR-camera photage plotted against the added power (left) and air cooling power (right).

175

B.2.3. CONCLUSIONS

These measurements did not give any really usable data that would help in the analyzing the forced cooling of the winding, but several other conclusions were reach that could benefit in future measurements.

The temperature measurement with thermocouple placed in between the winding turns should be avoided if the winding is tightly wound, i.e. if the thermocouple would interfere with the geometry of the winding. Instead a less invasive approach should be considered, such as different possibilities in the placements of temperature sensors or only use the IR-camera if it is possible.

The assumption of the exiting air having the same temperature as the winding was proven to be wrong. This means that for future measurements of the forced cooling the temperature of the air after it has passed through the winding should also be measured.

The larger gaps located before the first and after the last winding turn let large amounts of air through without contributing to the cooling. This was not even considered as a possible source of error before these measurements. This should also be amended to future measurements, not only to improve the cooling but for the sake of being able to more accurately know where the air flows.

APPENDIX C

This appendix include the volume flow, pressure drop and ideal pump power maps for each of the three prototype windings, each representing the worst case layer spacing with an error margin of 10% and 20% respectively. The worst case layer spacing occurs if all small spacing's follow each other i.e. turn 1 to 6 are 10% bigger and turn 7 to 12 are 10% smaller than specified size in a 12 turn machine. Note that the maps represent the performance of one winding segment and therefore the volume flow and pump power has to be multiplied with the number of winding segments in order to represent the performance of the whole machine.

C.1 PROTOTYPE M1
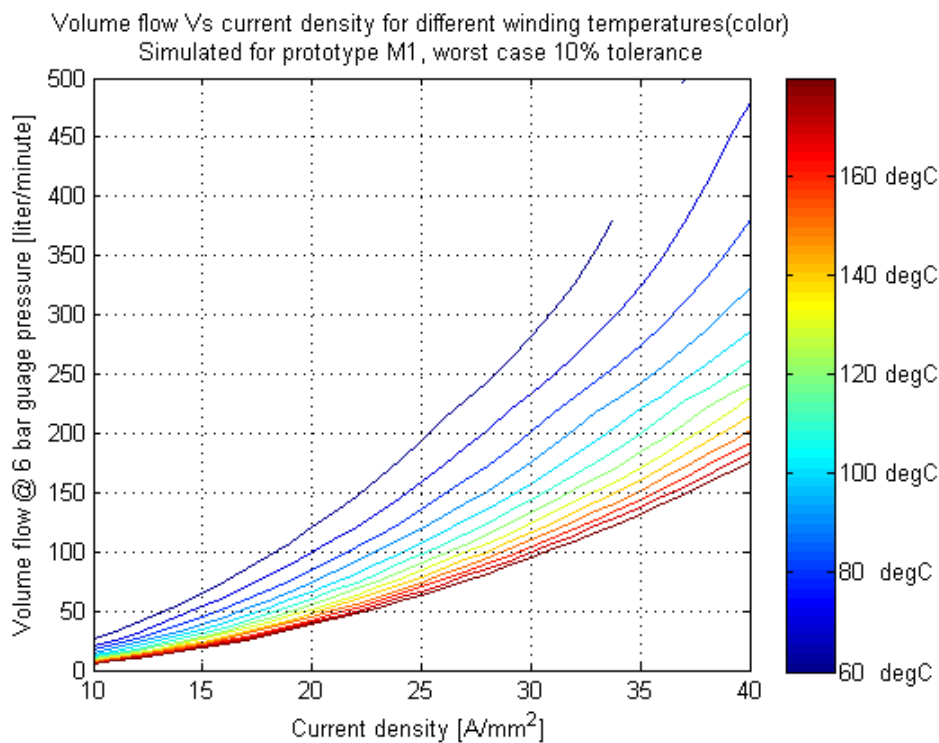
Fig. C.1.1. The volumetric air flow @ 6 bar gauge pressure that is needed to hold the winding M1 at a certain temperature for different current densities. The temperature curves represent every tenth degree between 40 and 180℃. The winding has an induced layer spacing error of 10%.
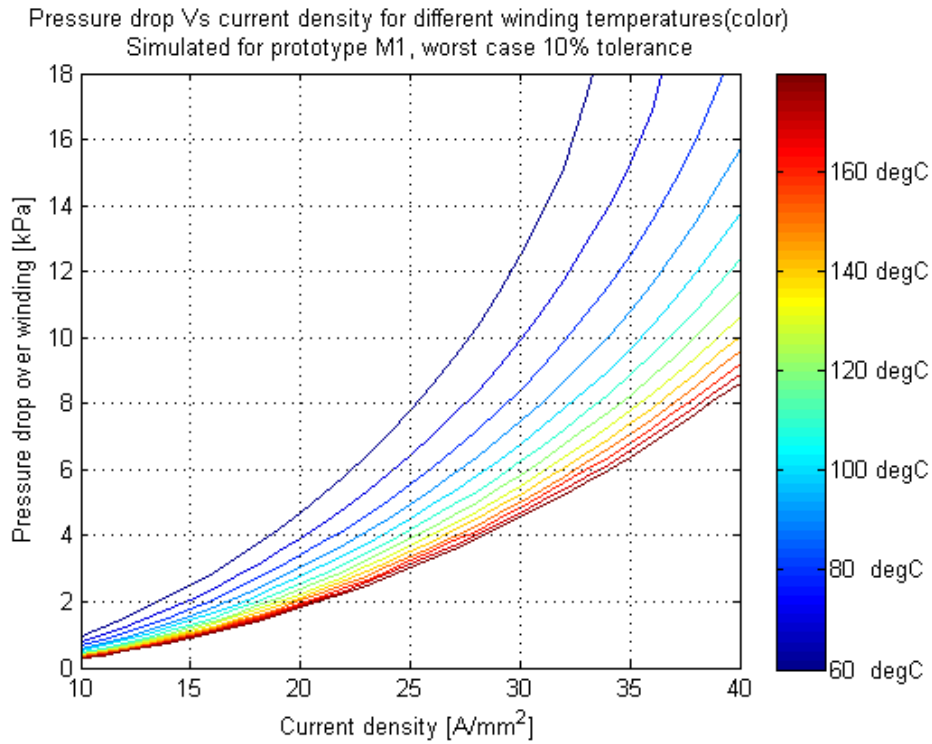
Fig. C.1.2. Pressure drop over the winding M1 for different current densities and temperature. The temperature curves represent every tenth degree between 40 and 180°C. The winding has an induced layer spacing error of 10%.
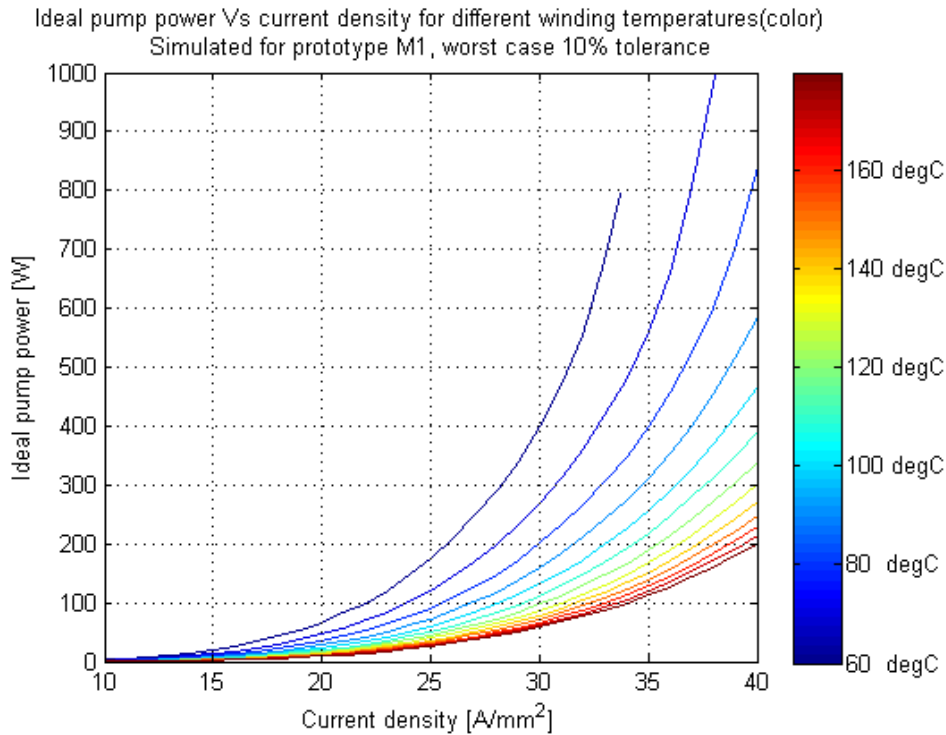

Fig. C.1.3. Ideal pump power that's needed to cool winding M1 for different current densities and winding temperatures. The temperature curves represent every tenth degree between 40 and 180°C. The winding has an induced layer spacing error of 10%.

178
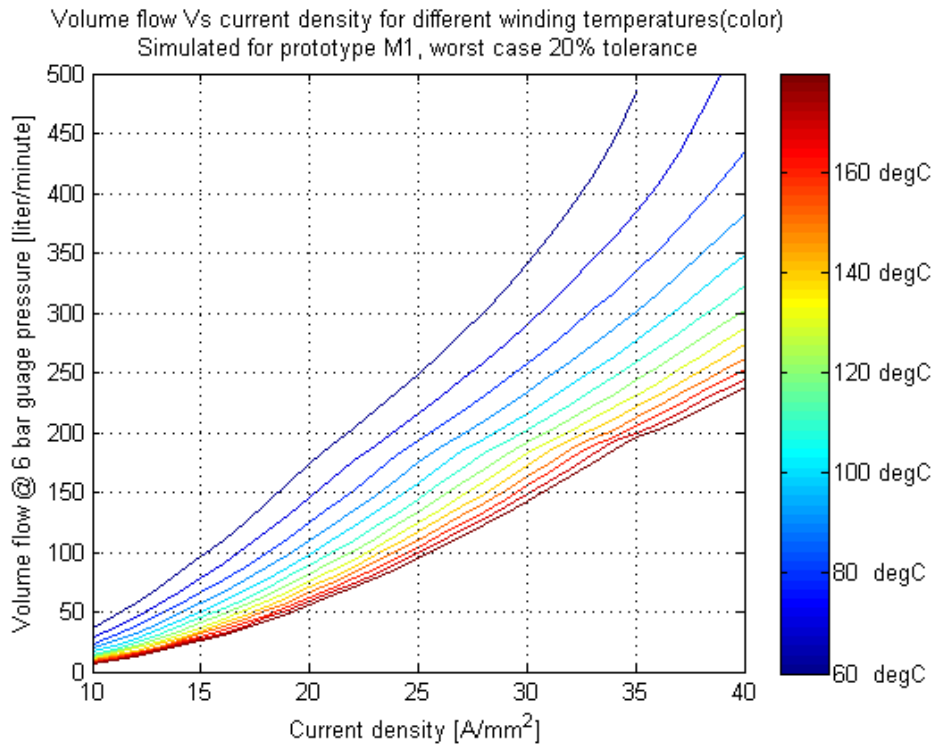
Fig. C.1.4. The volumetric air flow @ 6 bar gauge pressure that is needed to hold the winding M1 at a certain temperature for different current densities. The temperature curves represent every tenth degree between 40 and 180℃. The winding has an induced layer spacing error of 20%.
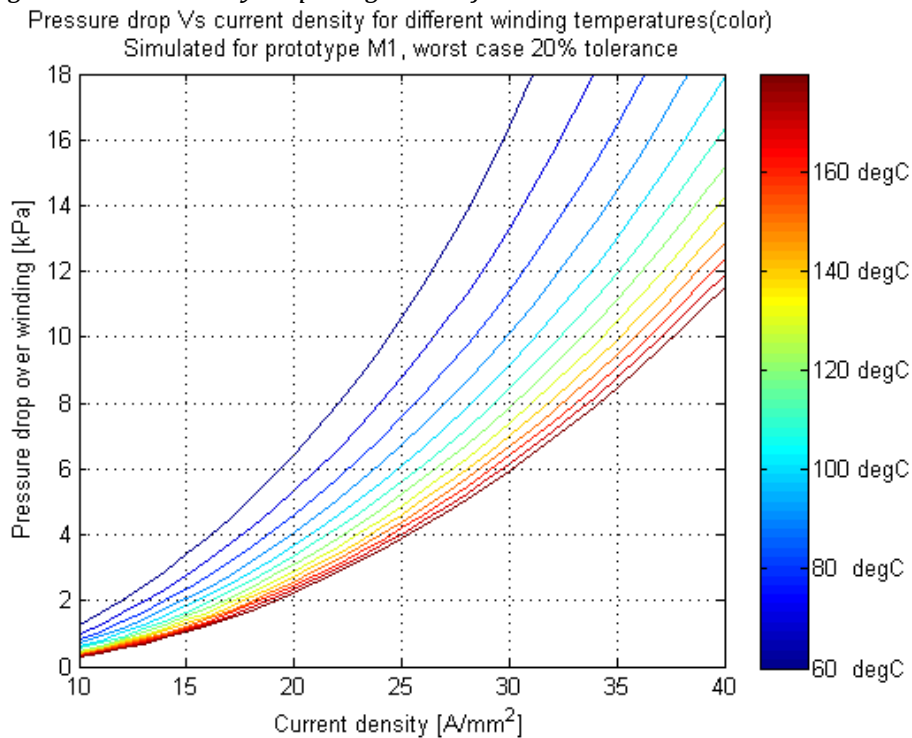

Fig. C.1.5. Pressure drop over the winding M1 for different current densities and temperature. The temperature curves represent every tenth degree between 40 and 180℃. The winding has an induced layer spacing error of 20%.

179
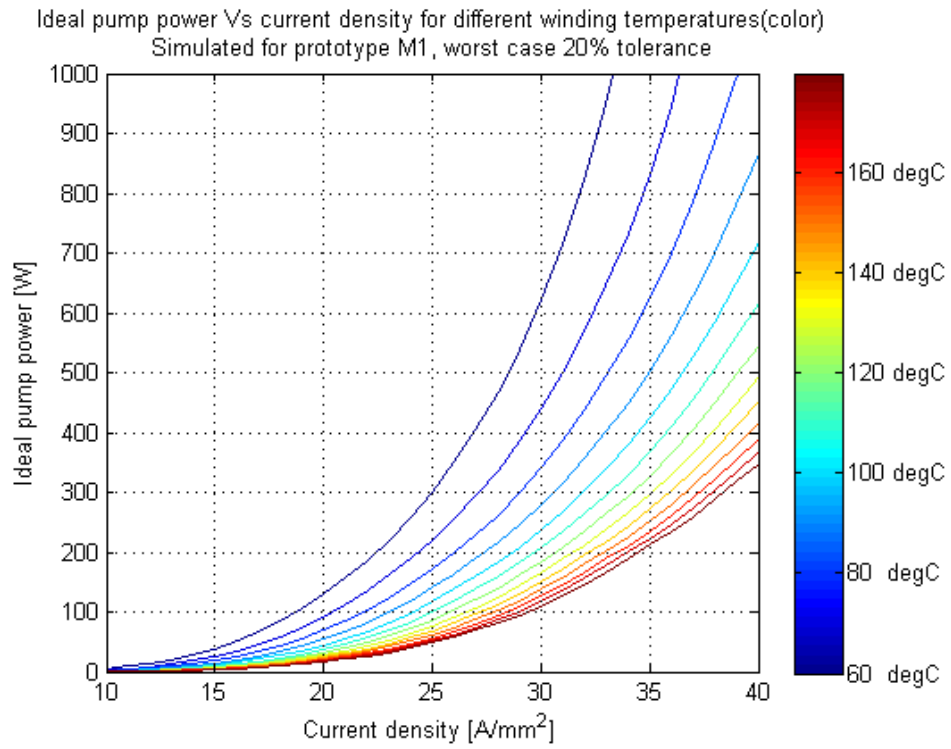
Fig. C.1.6. Ideal pump power that's needed to cool winding M1 for different current densities and winding temperatures. The temperature curves represent every tenth degree between 40 and 180℃. The winding has an induced layer spacing error of 20%
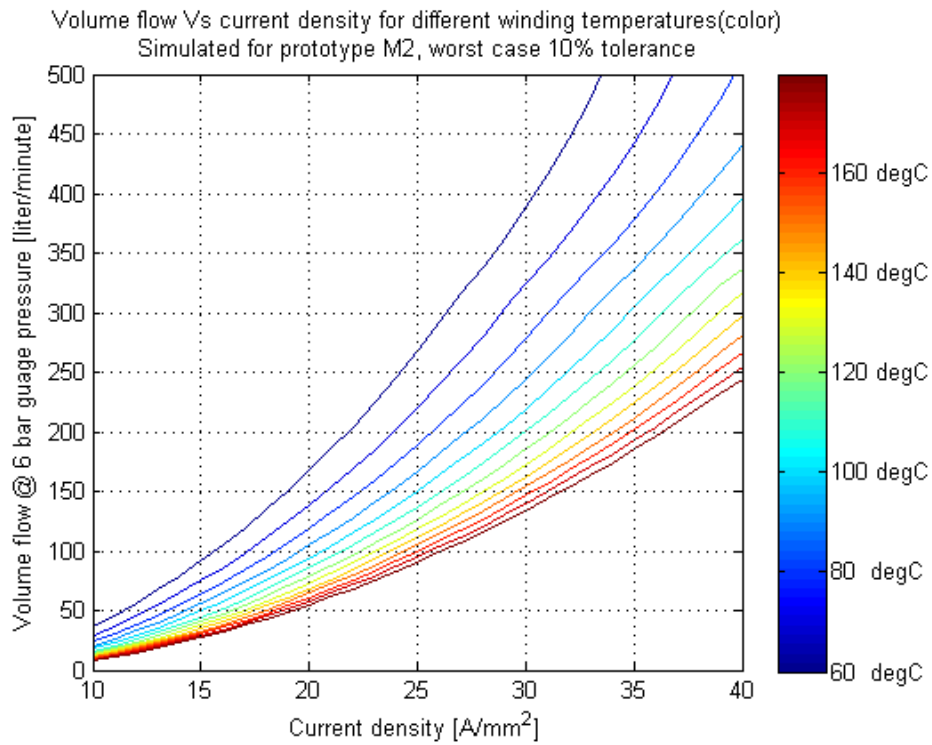
Fig. C.2.1. The volumetric air flow @ 6 bar gauge pressure that is needed to hold the winding M2 at a certain temperature for different current densities. The temperature curves represent every tenth degree between 60 and 180°C. The winding has an induced layer spacing error of 10%.
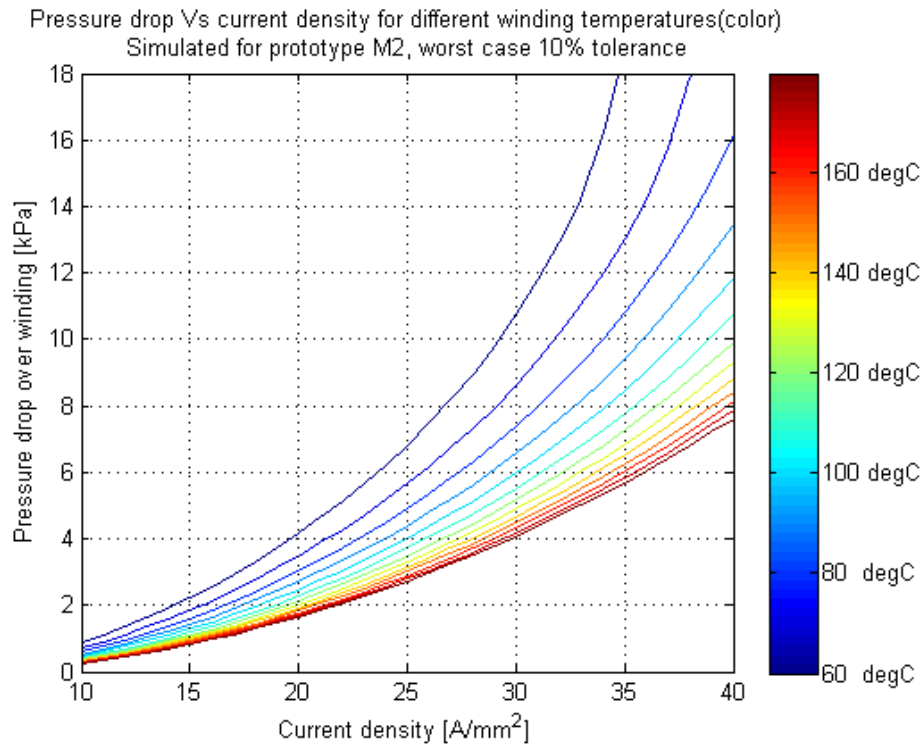
Fig. C.2.2. Pressure drop over the winding M2 for different current densities and temperature. The temperature curves represent every tenth degree between 60 and 180°C. The winding has an induced layer spacing error of 10%.
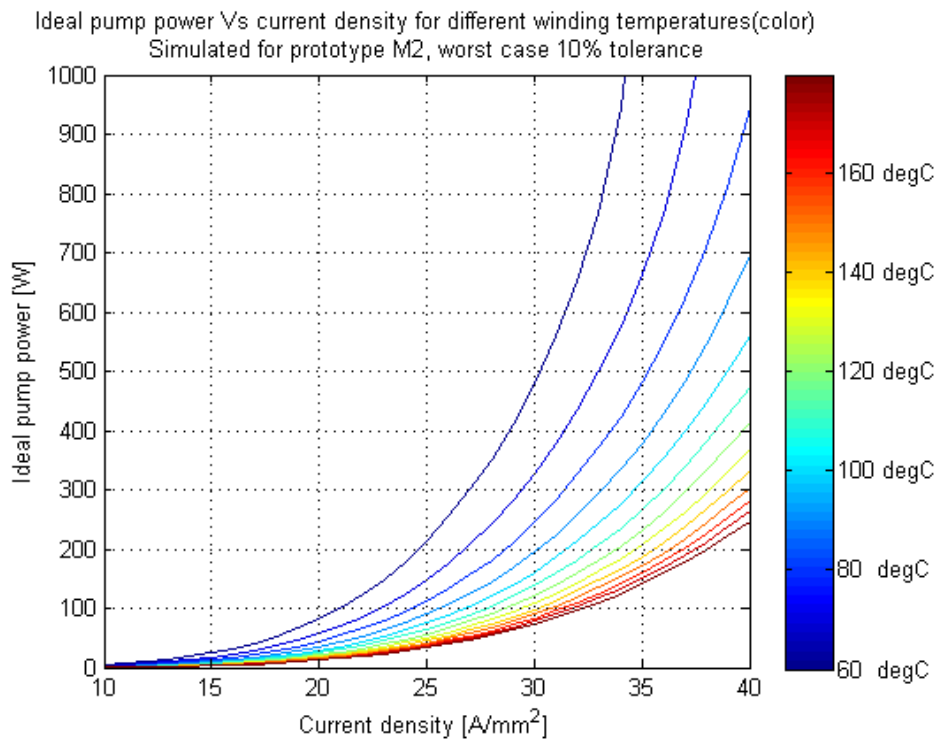
Fig. C.2.3. Ideal pump power that's needed to cool winding M2 for different current densities and winding temperatures. The temperature curves represent every tenth degree between 60 and 180°C. The winding has an induced layer spacing error of 10%.
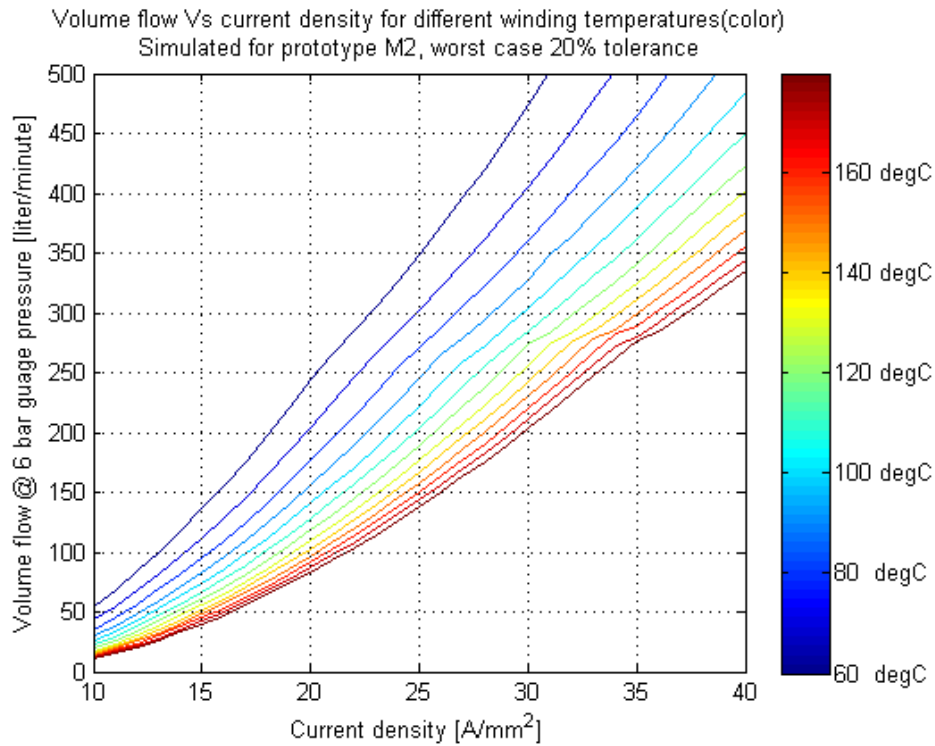
Fig. C.2.4. The volumetric air flow @ 6 bar gauge pressure that is needed to hold the winding M2 at a certain temperature for different current densities. The temperature curves represent every tenth degree between 60 and 180℃. The winding has an induced layer spacing error of 20%.
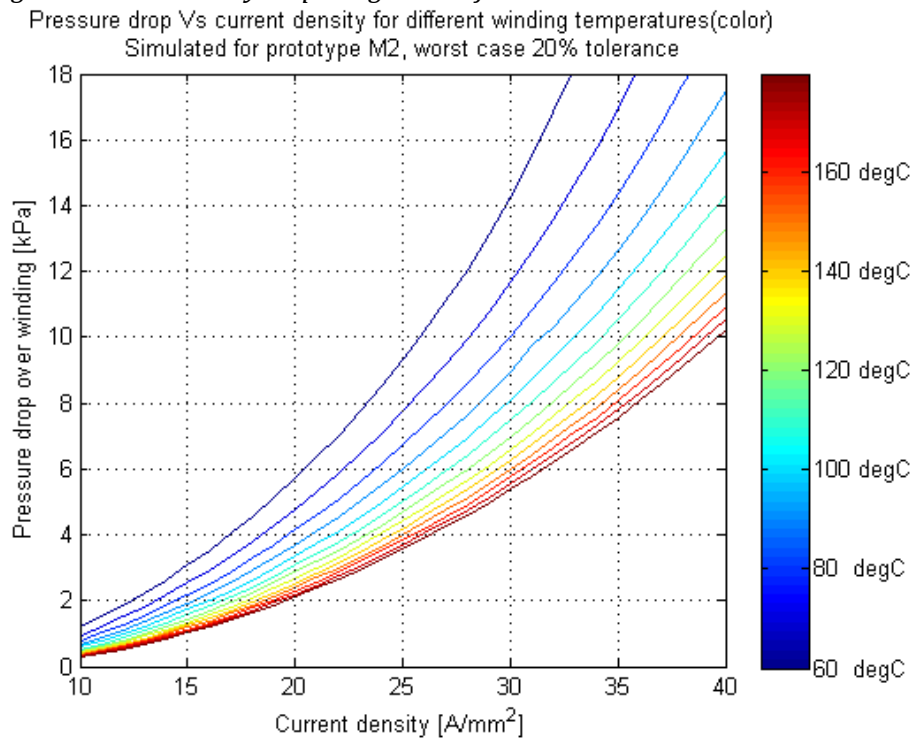

Fig. C.2.5. Pressure drop over the winding M2 for different current densities and temperature. The temperature curves represent every tenth degree between 60 and 180℃. The winding has an induced layer spacing error of 20%.
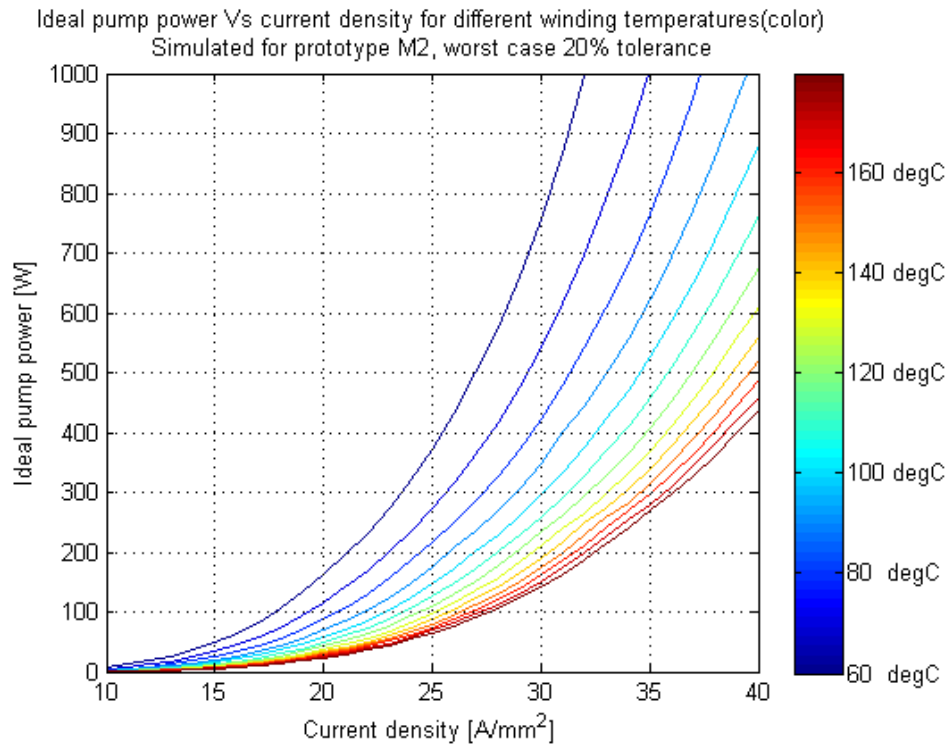
Fig. C.2.6. Ideal pump power that's needed to cool winding M2 for different current densities and winding temperatures. The temperature curves represent every tenth degree between 60 and 180℃. The winding has an induced layer spacing error of 20%
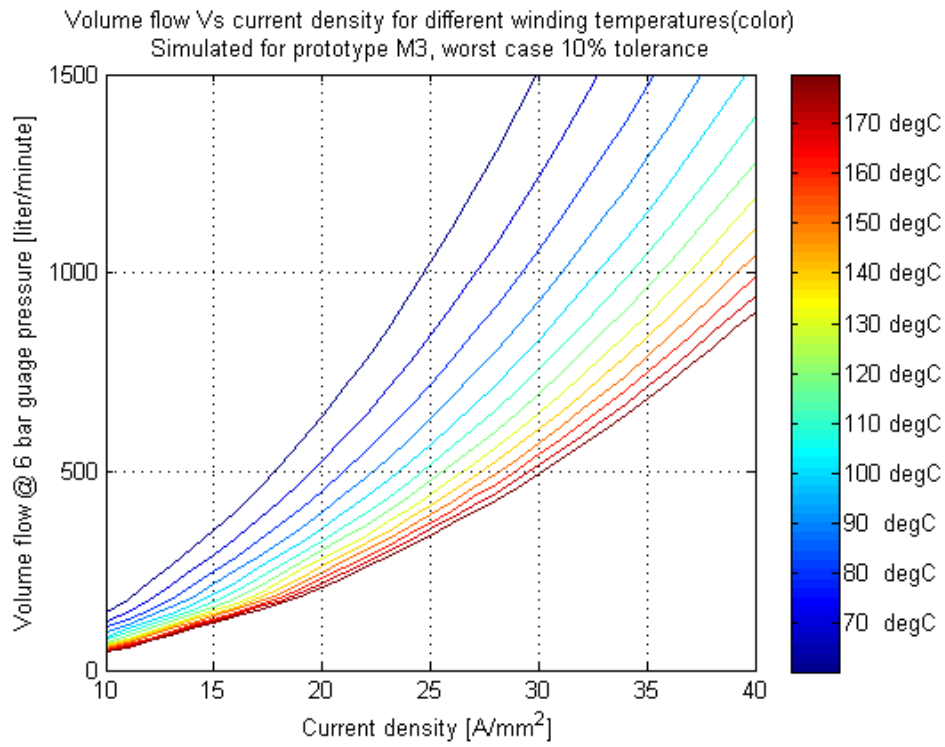
Fig. C.3.1. The volumetric air flow @ 6 bar gauge pressure that is needed to hold the winding M3 at a certain temperature for different current densities. The temperature curves represent every tenth degree between 60 and 180°C. The winding has an induced layer spacing error of 10%.
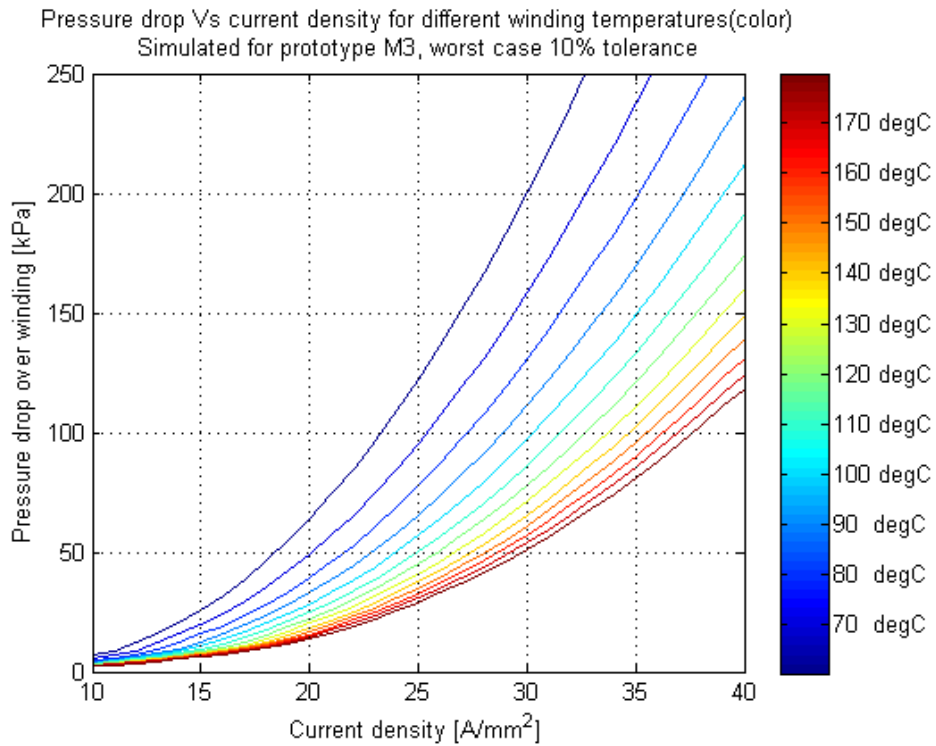
Fig. C.3.2. Pressure drop over the winding M3 for different current densities and temperature. The temperature curves represent every tenth degree between 60 and 180℃. The winding has an induced layer spacing error of 10%.
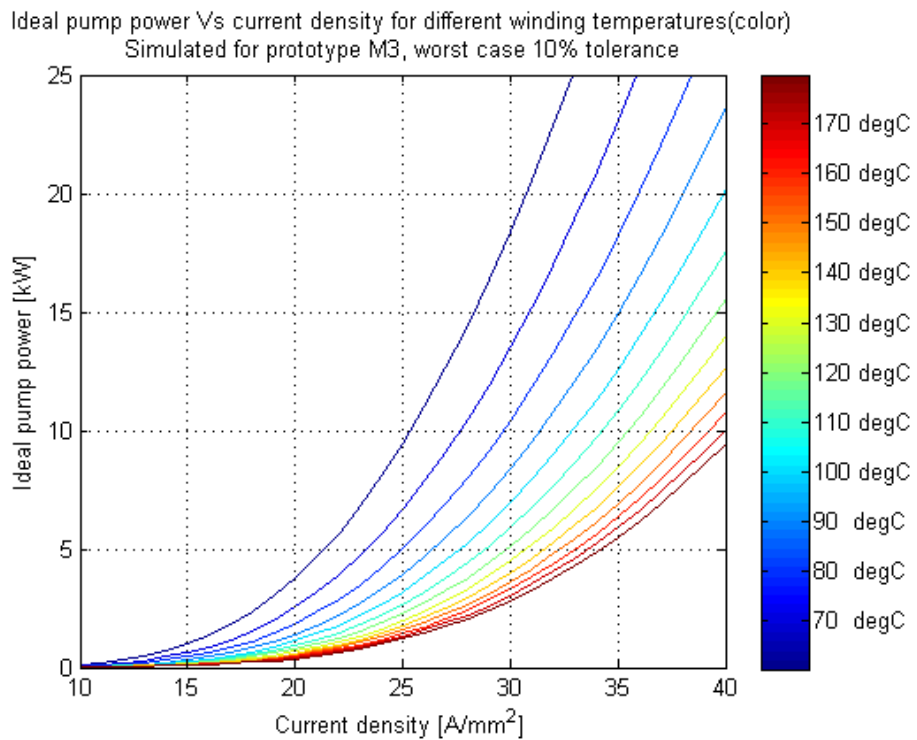
Fig. C.3.3. Ideal pump power that's needed to cool winding M3 for different current densities and winding temperatures. The temperature curves represent every tenth degree between 60 and 180℃. The winding has an induced layer spacing error of 10%.
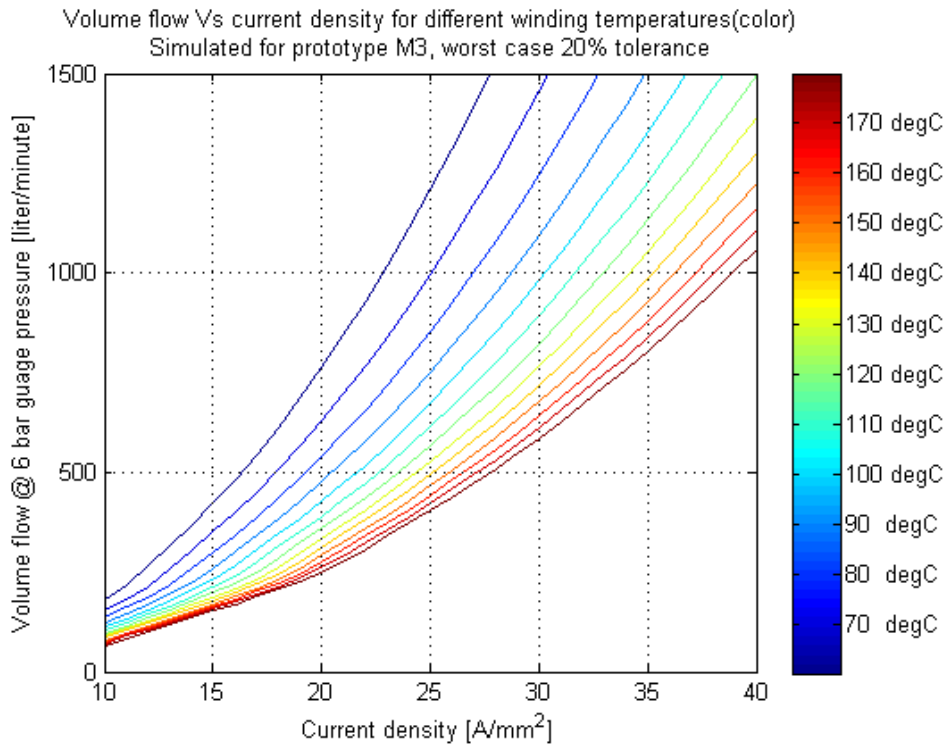
Fig. C.3.4. The volumetric air flow @ 6 bar gauge pressure that is needed to hold the winding M3 at a certain temperature for different current densities. The temperature curves represent every tenth degree between 60 and 180℃. The winding has an induced layer spacing error of 20%.
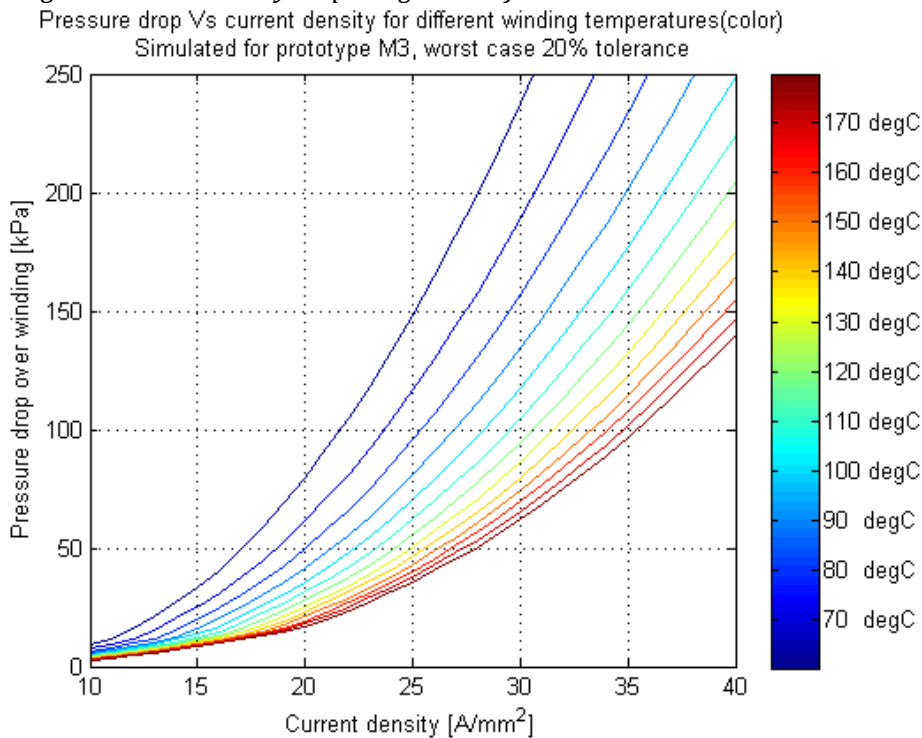
Fig. C.3.5. Pressure drop over the winding M3 for different current densities and temperature. The temperature curves represent every tenth degree between 60 and 180℃. The winding has an induced layer spacing error of 20%.

187
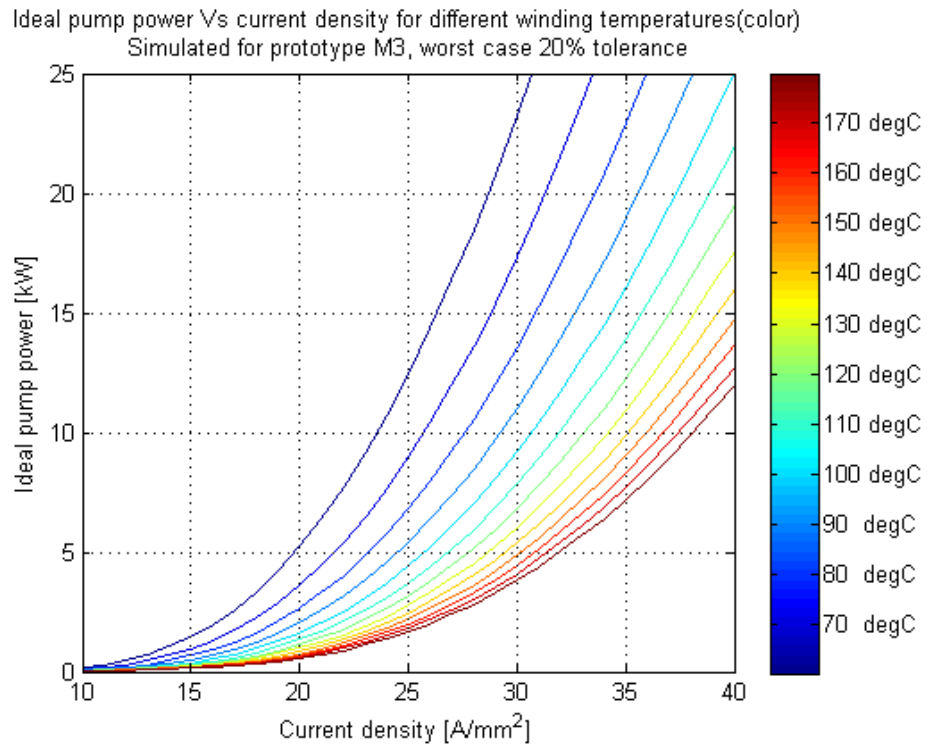
Fig. C.3.6. Ideal pump power that's needed to cool winding M3 for different current densities and winding temperatures. The temperature curves represent every tenth degree between 60 and 180℃. The winding has an induced layer spacing error of 20%

APPENDIX D

This appendix is reserved to the illustration of the test bench. Figure D.1 shows a schematic overview of the test bench. Within that figure are numbers which are referred to later on in the figure texts.
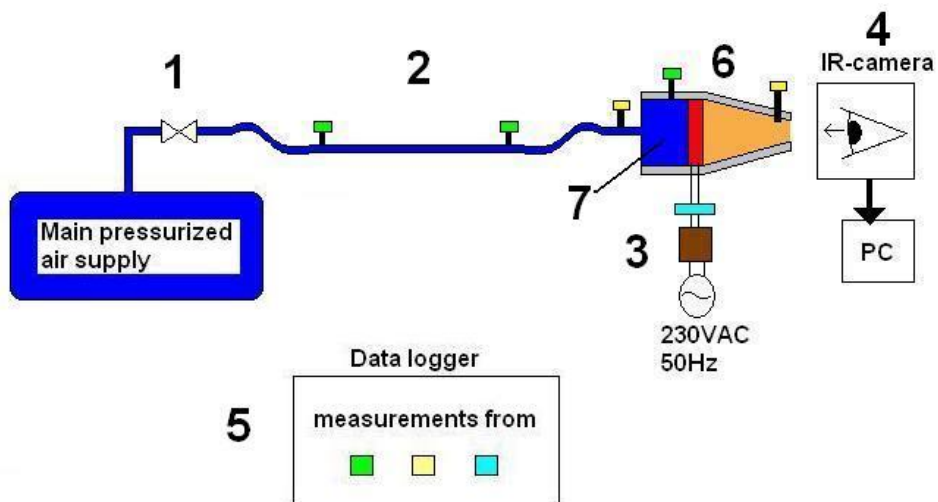


Fig. D.1. The schematic sketch of the test bench.

Fig. D.2. Inlet pressure regulator, number 1 in fig. D.1
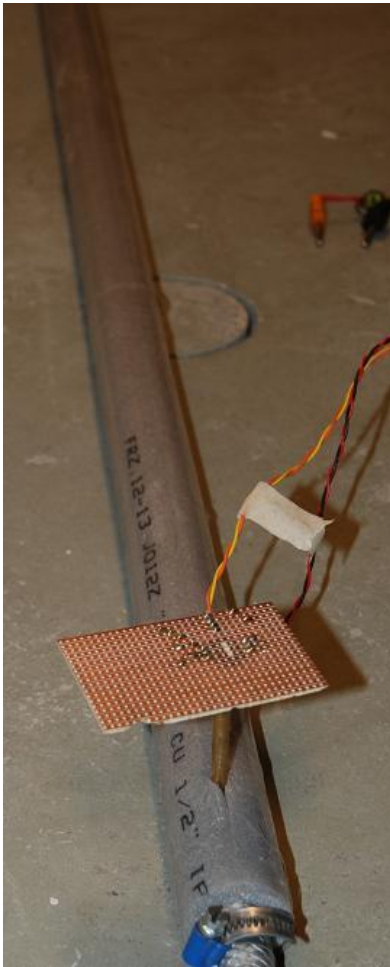
Fig. D.3. The up-stream side of the flow meter, number 2 in figure D.1.
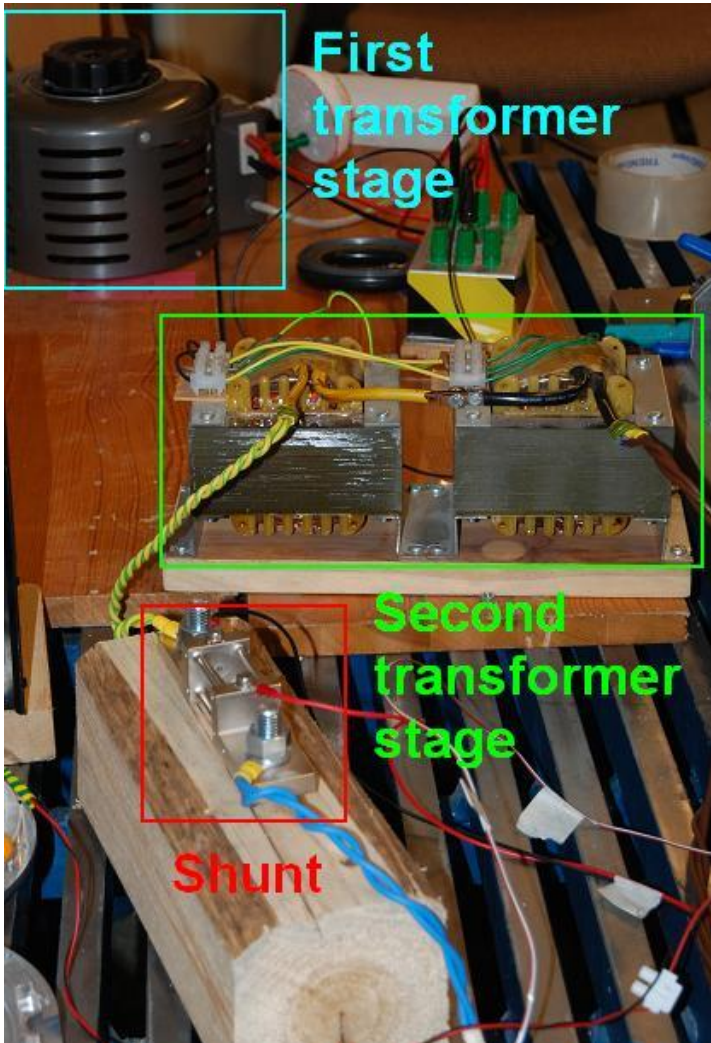
Fig. D.4. The electric circuit that generate the heat in the winding, number 3 in figure D.1.
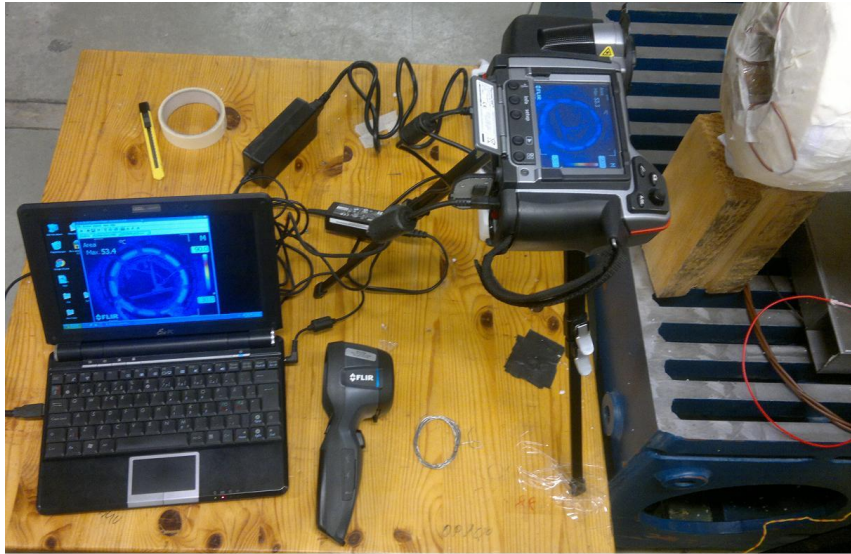
Fig. D.5. The IR-camera with a PC recording the winding temperature, number 4 in figure D.1.

Fig. D.6. Agilent 34972A logging the voltage, current and inlet and outlet temperature, number 5 in figure D.1.
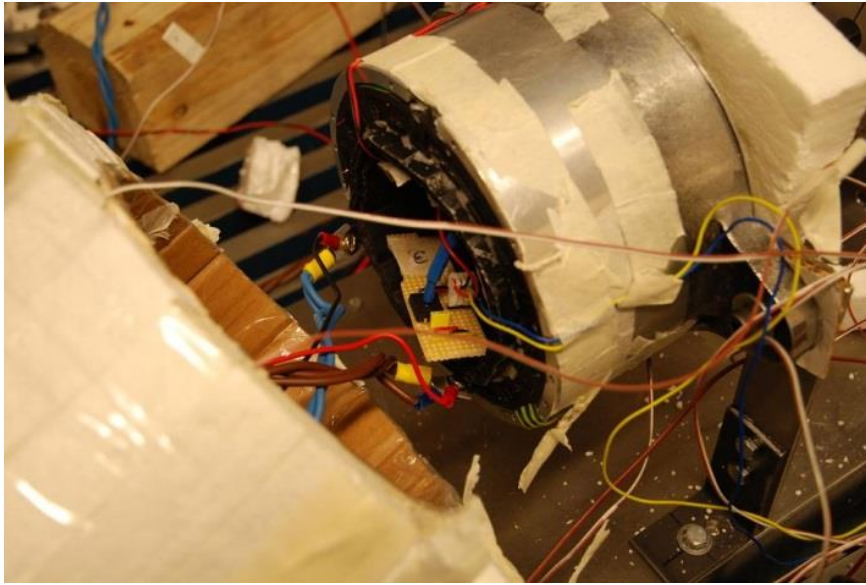
Fig. D.7. The winding as it is being inserted into the funnel.
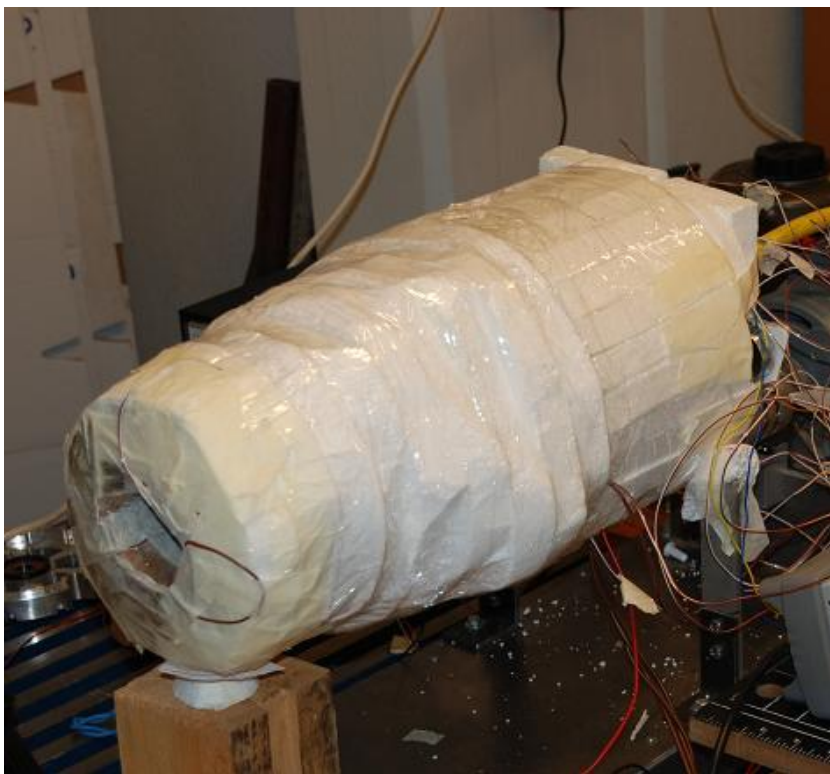
Fig. D.8. The funnel covering the winding, number 6 in figure D.1.
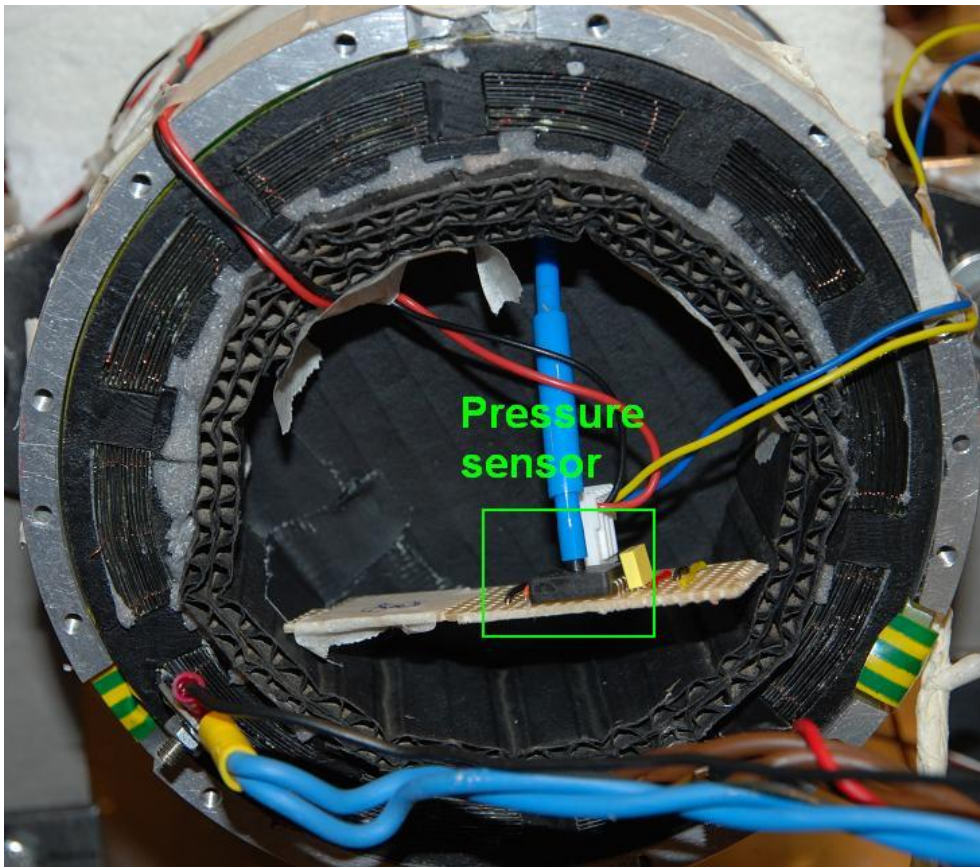
Fig. D.9. The winding inserted into the housing with the pressure sensor attached, number 7 in figure D.1.